IN VITRO AND *IN VIVO* SYSTEMS MECHANOBIOLOGY OF OSTEOARTHRITIC CHONDROCYTES

by

Donald Lee Zignego

A dissertation submitted in partial fulfillment
of the requirements for the degree

of

Doctor of Philosophy

in

Mechanical Engineering

MONTANA STATE UNIVERSITY
Bozeman, Montana

July 2015

ACKNOWLEDGEMENTS

First and foremost I would like to thank my graduate advisor Dr. Ron June who not only provided me with guidance, scientific input, and motivation throughout my research, but forced me to learn subjects far outside my comfort zone. With limited biology experience prior to my doctoral studies, Dr. June continually pushed the limits of my knowledge, which has made me a more well-rounded scientist/engineer. I would like to thank my committee members: Dr. Chris Jenkins for his guidance throughout my academic career as both an undergraduate and graduate student at Montana State University, Dr. Brian Bothner for his critical insight into mass spectrometry, metabolomics, and proteomics, Dr. William Schell for his input with statistical analysis, and Dr. Anthony Hartshorn for his critical input. I would also like to thank Dr. Jonathan Hilmer and Tim Hamerly for their assistance and expertise in the mass spectrometry facility, Betsey Pitts for her assistance using the confocal microscope, Dr. Francisco Blanco at INIBIC for allowing me the opportunity to study in his lab, and all the members of the Blanco Lab especially Dr. Carolina Fernández Costa, Dr. Angel Soto Hermida, Dr. Valentina Calamia, and Lucia Lourido Salas, for their expertise and insight into proteomics. I would also like to acknowledge all of my friends and especially my family for their continual support throughout my academic endeavors. Last but certainly not least I would like to thank all members of the June lab for their help, in particular Aaron Jutila and Sarah Mailhiot.

TABLE OF CONTENTS

1. INTRODUCTION 1

Background 1
Arthritis 4
Osteoarthritis 5
Osteoarthritis Prevalence 6
Osteoarthritis Risk Factors 7
Age 8
Gender 9
Genetics 9
Obesity 10
Trauma 10
Physical Exercise 11
Osteoarthritis Related Costs 11
Biological Structure of Cartilage 13
Extracellular Matrix 15
Articular Chondrocyte and the PCM 16
Mechanotransduction 20
Scientific Studies 23
Metabolomics 28
Mass Spectrometry 29
Liquid Chromatography 31
Normal-Phase Chromatography 33
Reverse-Phase Chromatography 34
Hydrophilic-Interaction Chromatography 35
Hydrophobic-Interaction Chromatography 35
Metabolomic Analysis 36
Proteomics 37
Dissertation Outline 43
Intellectual Merit 46
Broader Impacts 47

2. DEVELOPMENT OF EXPERIMENTAL METHODOLOGY 48

Physiological Characterization of Agarose Hydrogels 48
Introduction 48
Methods 49
Results & Conclusion 52
The Mechanical Microenvironment of High Concentration Agarose for Applying Deformation to Primary Chondrocytes 55

TABLE OF CONTENTS - CONTINUED

Contribution of Authors Page 55
Manuscript Information Page 56
Abstract 57
Introduction 58
Methods 61
Encapsulation of Fluorescent Microspheres in Physiologically Stiff Agarose 61
Mechanical Loading and Confocal Imaging 61
Particle Tracking and Finite Deformation Evaluation 62
Chondrocyte Encapsulation 66
Viability Analysis and Induced Deformations on Primary Chondrocytes 66
Results 67
Discussion 68
Conclusions 73
Candidate Mediators of Chondrocyte Mechanotransduction via Targeted and Untargeted Metabolomic Measurements 76
Contribution of Authors Page 76
Manuscript Information Page 78
Abstract 79
Introduction 80
Materials and Methods 82
Chondrocyte Culture and Encapsulation 82
Mechanical Stimulation 83
Metabolite Extraction 83
Untargeted and Targeted LC-MS 84
Data Processing 85
Data Analysis and Candidate Selection 86
Compound Identification 89
Results 89
Untargeted Metabolomics 89
Targeted Metabolomics 92
Discussion 94
Conclusions 98

3. METABOLOMICS 99

Mechanotransduction in Primary Human Osteoarthritic Chondrocytes is Mediated by Metabolism of Energy, Lipids, and Amino Acids 101
Contribution of Authors Page 101
Manuscript Information Page 102

TABLE OF CONTENTS - CONTINUED

Abstract 103
Introduction 105
Materials and Methods 107
Chondrocyte Culture and Encapsulation 107
Mechanical Stimulation 108
Metabolite Extraction 108
Untargeted and Targeted Metabolomic Profiling 108
Compound Identification and Enrichment Analysis 110
Results 110
Untargeted Analysis 111
Targeted Analysis 115
Discussion 118
Conclusions 124

4. PHOSPHOPROTEOMICS 126

Shotgun Phosphoproteomics Identifies Activation of Vimentin, Ankyrin, Vam6/Vps39-Like Protein in Primary Human Osteoarthritic Chondrocytes after Mechanical Stimulation 128
Contribution of Authors Page 128
Manuscript Information Page 129
Abstract 130
Introduction 132
Materials and Methods 134
Chondrocyte Culture and Encapsulation 134
Mechanical Stimulation 135
Protein Preparation and Extraction 135
Proteolysis, TiO2 Phosphopeptide Enrichment, and Graphite Cleanup 136
Shotgun Phosphoproteomics LC-MS/MS 136
Data Processing 137
Data Analysis and Candidate Selection 138
Results 139
Discussion 146
Conclusions 152

5. *IN VIVO* MODEL 154

Alterations in Joint Metabolomics Following Surgical Destabilization and Exercise in a Novel Cartilage Reporter Mouse Model 156

TABLE OF CONTENTS - CONTINUED

Contribution of Authors Page 156
Manuscript Information Page 157
Abstract 158
Introduction 160
Materials and Methods 162
Animals 162
Luciferase Induction, Imaging and Image Processing 162
Treadmill Running and Surgical Destabilization 164
Joint Harvest and Metabolite Extraction 165
Histology 166
LC-MS Data Processing 166
Data Analysis 167
Results 169
Bioluminescent Analysis. 169
LC-MS Analysis 171
Discussion 174
Conclusions 180

CONCLUSION 182

REFERENCES CITED 187

APPENDICES 217

APPENDIX A: Encapsulation of Chondrocytes in High-Stiffness Agarose Microenvironments for *In Vitro* Modeling of Osteoarthritis Mechanotransduction 218
APPENDIX B: Supplemental Material for Chapter 2 – Development of Experimental Methodology 245
APPENDIX C: Supplemental Material for Chapter 3 – Metabolomics 252
APPENDIX D: Supplemental Material for Chapter 5 – *In Vivo* Model 263

LIST OF TABLES

Table Page

1. Kellgren-Lawrence (K/L) grading scheme for scoring OA. 6

2. Prevalence data from radiographic OA from three US population-based studies in the hands, knees, and hips. 8

3. Pathways and metabolites altered by mechanical loading.. 114

4. Statistically significant changes in metabolites for all five donors..... 116

5. Key signaling pathways determined from pathway over-representation analysis..... 145

S1. Stiffness values from mechanical testing experiments. 231

S2. Mechanically-induced changes in metabolites targeted to central energy metabolism depended on agarose concentration 237

S3. Untargeted metabolites of interest following 15 minutes of dynamic compression in either 4.5% or 2% agarose..... 238

S4. PCM and agarose stiffness measurements..... 240

S5. Average Exx, Eyy, and Exy strains ± SEM for each gel concentration. 248

S6. Cell viability after 24 and 72 hours for primary human chondrocytes.. 249

S7. Candidate mediators of chondrocyte mechanotransduction from the targeted metabolite analysis..... 260

S8. Up-regulated candidate mediators of chondrocyte mechanotransduction. 261

S9. Down-regulated candidate mediators of chondrocyte mechanotransduction. 262

LIST OF FIGURES

Figure Page

1. Healthy vs. diseased knee joint 2
2. Joint types in the human body. 5
3. Principal risk factors for OA. 8
4. Cross sectional diagram of the four zones of articular cartilage. 13
5. The three main components of articular cartilage. 15
6. Young's Modulus values for the ECM and PCM 15
7. Anabolic and catabolic enzymes in cartilage. 19
8. Schematic of tensile, compressive, and shear loads on cells.. 21
9. Simplified schematic of a mass spectrometer 30
10. Schematic of a liquid chromatography (LC) system 32
11. Normal-phase chromatography. 33
12. Reverse-phase chromatography. 34
13. Total ion chromatogram and the corresponding mass spectra. 37
14. Central dogma of modern biology. 39
15. 2D-GE of the proteome mapping of all proteins altered in OA 40
16. Schematic of collision induced dissociation (CID) 42
17. Dissertation workflow 43
18. Agarose hydrogel mold. 50
19. Custom built bioreactor with sub-micron precision 52
20. Equilibrium and dynamic moduli values for 3-5% [w/v] agarose 53
21. Approach for measuring micron-level deformations within agarose gels 63

LIST OF FIGURES – CONTINUED

Figure Page

22. Two-dimensional displacement measurement.. 64

23. Finite deformation Lagrangian strain fields within 4.5% agarose hydrogel. 69

24. Axial displacement and strain as functions of gel position and agarose concentration 70

25. Viability of primary human chondrocytes in high concentration agarose gels after 24 and 72 h..... 71

26. Deformation of primary human chondrocytes in 2.0% and 4.5% agarose 72

27. Schematic of experimental methods for SW1353 cell encapsulation 88

28. Loading-specific differences in untargeted metabolite expression..... 91

29. Dynamic compression results in both accumulation and depletion of untargeted metabolites..... 92

30. Changes in expression of targeted central-energy-related metabolites over from 0-30 minutes of applied compression..... 93

31. Applied compression resulted in distinct untargeted metabolomic profiles for primary OA chondrocytes..... 113

32. Dynamic compression results in both accumulation and depletion of untargeted metabolites..... 114

33. Aging-related chondrocyte mechanotransduction. 116

34. Patient-specific heterogeneity in chondrocyte mechanotransduction 117

35. Loading-induced changes in expression of targeted metabolites specific to central-energy-metabolism..... 120

LIST OF FIGURES – CONTINUED

Figure Page

36. Experimental design in phosphoproteomic study 140

37. Dynamic compression alters phosphoprotein expression in primary OA chondrocytes..... 142

38. Applied compression resulted in distinct untargeted phosphoproteomic profiles for primary OA chondrocytes 147

39. Experimental design and transgenic strategy for mouse with aggrecan-specific bioluminescence 163

40. The combination of exercise and joint destabilization resulted in decreased bioluminescence compared with controls 170

41. Metabolomic profiling captured joint-wide changes induced by the combination of vigorous treadmill running and joint destabilization 172

42. Unsupervised clustering identifies patterns of metabolites differentially regulated by exercise and joint destabilization 175

43. Representative histological images for one mouse from the exercised/destabilized group 177

S1. Agarose stiffness was concentration dependent as determined in stress-relaxation experiments..... 231

S2. Concentration-dependent dynamics of agarose stress-relaxation. 232

S3. Complex agarose stiffness as high as ~225 kPa from cyclical loading experiments 233

S4. Encapsulation of SW1353 chondrocytes in high-stiffness agarose gels resulted in high viability..... 234

S5. Primary human chondrocyte mechanotransduction is affected by agarose concentration 236

S6. Model for studying mechanotransduction in joint disease.. 242

LIST OF FIGURES – CONTINUED

Figure Page

S7. Pilot study to determine confidence interval for bead displacements. 246

S8. Concentration-dependent displacement fields within 4.5% agarose hydrogels. 247

S9. Propagation of displacement errors for axial strain (Eyy) calculation 248

S10. Analysis workflow for quantifying metabolite intensities following LC-MS analysis. 249

S11. Scatter plots of untargeted metabolites 250

S12. Representative chromatograms of targeted metabolites. 251

S13. Experimental design for primary human chondrocyte metabolomic study 257

S14. Two-sample Kolmogorov-Smirnov tests identify significant difference in metabolomic distributions. 258

S15. Age-correlated increases in the number of significant metabolites for donors 1 - 5. 258

S16. Venn-diagram for untargeted metabolomic comparisons. 259

S17. Patterns of distinct metabolite distribution for 37 targeted metabolites common to central energy metabolism. 264

S18. Untargeted Principal Components Analysis 265

ABSTRACT

All cells are subjected to and respond to mechanical forces, but the underlying processes linking the mechanical stimuli to biological responses are poorly understood. In the joints of the body (*e.g.* the knee, hip, etc…) articular cartilage serves as a low friction, load bearing material and is subjected to near-constant mechanical loading. Through excessive loading of the joint, usually caused by obesity or injury, the protective articular cartilage begins to diminish, leading to the progression of osteoarthritis (OA). Osteoarthritis is the most common joint disorder in the world and is characterized by the deterioration of articular cartilage. Determining the link between cartilage deterioration and mechanical loading is one motivation that drove this research. Articular cartilage is composed of a dense extracellular matrix (ECM), a less-stiff pericelluar matrix (PCM), and highly specialized cells called chondrocytes. As the sole cell type in cartilage, chondrocytes are responsible for the healthy turnover of the ECM by creating, maintaining, and repairing the matrix. Multiple lines of evidence suggest chondrocytes can transduce mechanical stimuli into biological signals. The hypothesis for this research is that physiologically pertinent loading of chondrocytes results in a specific set of bio-signals resulting in matrix synthesis. To test this hypothesis, two unbiased, large-scale metabolomic and phosphoproteomic datasets were generated by modeling physiological compressive loading on 3D-embedded chondrocytes. To assess loading-induced changes in metabolites (*e.g.* small molecules representing the functional state of the cell) and proteome-wide patterns of post-translational modifications (*i.e.* phosphorylation), chondrocytes were encapsulated in physiologically stiff agarose, compressively loaded in tissue culture, and analyzed via liquid chromatography – mass spectrometry (LC-MS). The results helped identify global and local biological patterns in the chondrocytes which are a direct result from mechanical loading. In addition, a novel mouse model that expresses cartilage specific bioluminescence was used to assess loading induced changes *in vivo*. The results from the mouse model allowed for *in vivo* validation and integration of the *in vitro* results from the metabolomic and phosphoproteomic results. To my knowledge, such research has never been done, and considerably expands the scientific knowledge of chondrocyte mechanotransduction.

INTRODUCTION

Background

Osteoarthritis (OA) is the most common joint disorder, affecting over 200 million individuals worldwide, ~40 million of them in the United States [1-7]. By the age of 65, approximately 50% of individuals may develop OA. OA is most commonly associated with excessive loading of the aging joint (*e.g.* caused by obesity or injury), leading to deterioration of articular cartilage and joint inflammation (Figure 1). With aging and wear, OA incidence rates increase substantially. In most cases, after the age of 18, humans lose the ability to repair or replace damaged articular cartilage [3]. As the cartilage begins to deteriorate, bone-to-bone contact is imminent, leading to joint stiffness, swelling, and pain. At these articulating regions of the body (*e.g.* the knee), the articular cartilage, and thus articular chondrocytes, are subjected to almost-constant mechanical loading (*e.g.* walking, running, etc…). Repetitive action has been shown to be crucial for joint health, yet excessive loading can lead to OA [8]. Individuals with a history of heavy mechanical work (heavy lifting, bending, etc.) are ~7-fold less likely to have OA at the age of 90 [9], suggesting that long-duration, but sub-injurious, mechanical loading may induce protective biological responses. Therefore, the biological responses of chondrocytes to mechanical loading are extremely important to understanding and improving joint health. Currently, the only treatments for OA, are only partially-effective, and include joint replacement surgery and weight loss. The caveats for these

treatment strategies are (1) they fail to restore healthy cartilage and (2) they are often infeasible or impossible for many patients due to the extreme costs of a joint replacement.

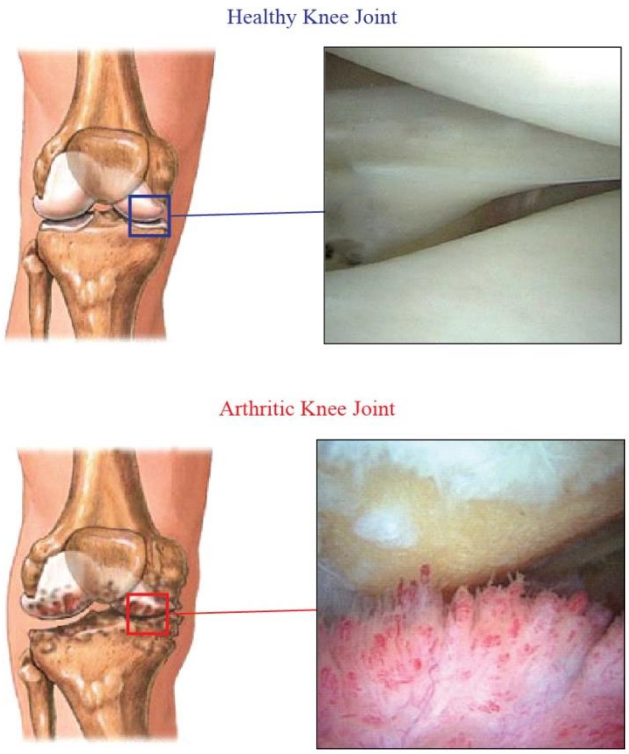

Figure 1. Schematic (top left and bottom left) and actual scoped (top right and bottom right) depictions of both a healthy knee joint (top) and a diseased or arthritic knee joint (bottom).

The overall goal of this research is to develop a comprehensive understanding of the cellular response of the chondrocyte to applied, dynamic compression. Well-controlled data are needed to define the complex, intracellular responses. The objective of these experiments is to determine changes in metabolite and protein phosphorylation profiles for late OA chondrocytes as a function of applied dynamic compression. These studies will test the hypothesis that dynamic compression alters both the metabolite levels

and protein phosphorylation in chondrocytes to promote matrix synthesis. My approach will start by encapsulating chondrocytes in physiologically-stiff agarose, and applying dynamic compression to simulate physiological loading conditions (*i.e.* walking). Immediately following dynamic loading, samples will be flash-frozen in liquid nitrogen and pulverized. Metabolites will be extracted, and identified via liquid chromatography-mass spectrometry (LC-MS) at the MSU Cobre Mass Spectrometry Core Facility. Similarly, proteins will be extracted, digested, and enriched for phosphopeptides prior to quantification via liquid chromatography-mass spectrometry/mass spectrometry (LC-MS/MS). This research generated a well-controlled dataset of the intracellular response to mechanical loading, and helped confirm our hypothesis that dynamic compression induces matrix synthesis in the context of OA.

To my knowledge, such research has never been performed, and considerably advances the scientific knowledge of chondrocyte mechanobiology. Most existing studies focus on individual signaling pathways which have the potential to exclude important data [2]. This research is advantageous since it is unbiased, by not excluding pathways *a priori.* By collecting data on multiple stages (protein phosphorylation and metabolite levels) of the central dogma, this research provides a valuable contribution to basic science in addition to the potential to discover new, therapeutic strategies to combat OA. This research lays a strong foundation for future work in this field, specifically understanding how mechanotransduction plays a role in OA. The results from this study dramatically expands the knowledge and understanding of chondrocyte

mechanotransduction, and may be implemented in treatment strategies and preventative measures for OA.

Arthritis

The term arthritis is derived from the Greek words *arthro*, meaning joint, and *itis*, meaning inflammation. Arthritis is defined as any type of joint disorder that involves inflammation of one or multiple joints in the body. Joint locations include any area of the body were articulation is present, such as the knee, hip, spine, fingers, etc... At these articulating locations, cartilage covers the joints to allow for fluid movement and to prevent bone on bone contact. In the human body, there are six different types of joints that can be affected by arthritis (Figure 2): A pivot joint (the neck between the C1 and C2 vertebrae), a ball-and-socket joint (hip, shoulder), hinge joint (knee, elbow), saddle joint (between the trapezium carpal bone and 1st metacarpal bone), condyloid joint (between radius and carpal bone of the wrist), and a planar joint (between the tarsal bones in the foot).

There are over 100 different types of arthritis, including the most common, osteoarthritis, rheumatoid arthritis, osteoporosis or fibromyalgia, and gout. Each of the specific forms of arthritis attacks the joints differently. Rheumatoid arthritis is an autoimmune disease, or inflammatory disease, in which the individual's immune system actually attacks the tissue in the joints. Rheumatoid arthritis most commonly occurs in the fingers, wrists, and knees and the symptoms normally include deformed and painful joints. Gout, another form of inflammatory arthritis, is characterized by the deposition of uric acid crystals in the joints, and is also characterized by a swollen and tender joint.

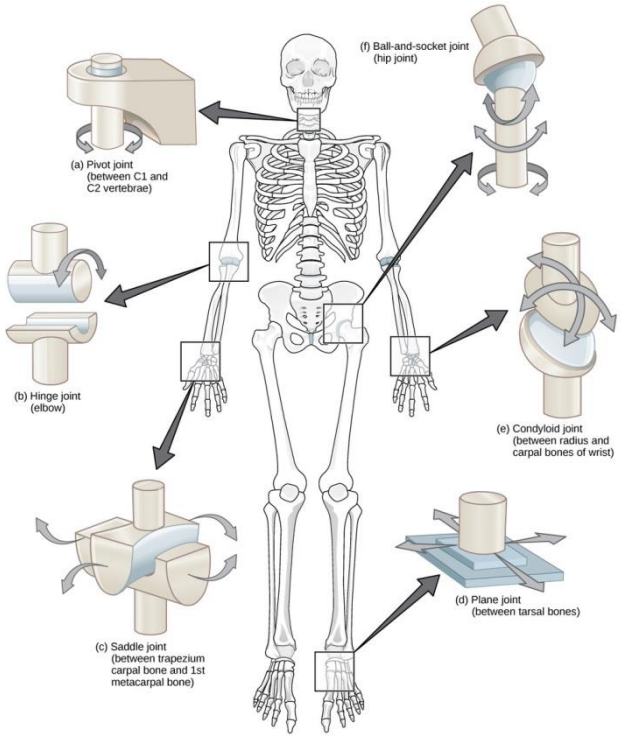

Figure 2. Schematic illustrating the six unique joint types in the human body [10].

The most common form of arthritis is osteoarthritis (OA). OA is not an inflammatory form of the disease, but rather a disease resulting from mechanical "wear and tear."

Osteoarthritis

The word osteoarthritis comes from the Greek words *osteo* meaning bone, *arthro*, meaning joint, and *itis*, meaning inflammation. OA can occur in all of the joints of the body, but most commonly affects the knee, hip, and hands. The disease is characterized by the breakdown of the protective, load-bearing tissue that covers the joint surface, and is usually caused from "abnormal" joint loading (*i.e.* obesity or injury). When the protective cartilage begins to deteriorate, the bones begin to rub on one another. The loss of cartilage significantly hinders joint mobility and the bone on bone contact results in

intense pain, stiffness, and joint inflammation. OA is primarily diagnosed through a medical examination and radiographic images. Radiographic images can be taken of the joint, and the severity of the disease can be assessed to determine if surgical intervention is necessary. The most common form of radiographic characterization to assess the severity of OA is the Kellgren-Lawrence (K/L) grading scheme [11]. The K/L scale scores patients on a scale from 0 – 4 depending on the progression of the disease [12] (Table 1).

Table 1. Kellgren-Lawrence (K/L) grading scheme for scoring OA [13].

Grade OA	Description
0	None - No radiographic features of OA
1	Doubtful - Possible joint space narrowing (JSN) and osteophyte formation
2	Minimal - Definite osteophyte formation with possible JSN
3	Moderate - Multiple osteophytes, definite JSN, sclerosis and possible bony deformity
4	Severe - Large osteophytes, marked JSN, severe sclerosis and definite bony deformity

Osteoarthritis Prevalence. Osteoarthritis is the most common joint disease in the world, and mainly affects individuals over the age of 50. In the United States alone, OA affects 13.9% of the adults over the age of 25, and 33.6% of those over 65 years of age accounting for approximately 40 million of the population [14]. This value has risen from 21 million Americans in 1990, meaning that better understanding this disease is extremely crucial to curtail the rising OA incidence rates. It is quite hard to estimate the exact number of individuals with OA (prevalence), since the symptoms and severity of

the disease can differ greatly, and a true quantitative measure of OA has yet to be determined. There are essentially three ways to assess the prevalence of OA; self-diagnosed OA, clinically defined OA, and radiographically defined OA. Most of the statistical data on OA prevalence in the U.S. are based on radiographically and clinically defined OA. These values are usually considered an underestimate. A recent study done by Lawrence et al., summarized the prevalence data from three US population-based studies: The National Health and Nutrition Examination Survey III (NHANES III), the Framingham Osteoarthritis Study, and the Johnston County Osteoarthritis Project [14]. The NHANES III study assessed the prevalence of knee OA in U.S. adults over the age of 60 years [15]. The Framingham OA Study surveyed ~2600 adults ≥ 26 years of age with knee and hand OA from suburban Boston, Massachusetts [16]. Finally, the Johnston County OA Project surveyed ~3000 African Americans and white adults ≥ 45 years of age with hip and knee OA in a rural county in North Carolina [17]. All individuals in these studies underwent radiographic OA testing. The prevalence rates from these three studies can be seen in Table 2. As aforementioned, prevalence of OA is an extremely difficult measure to quantify. However, from these data on OA incidence rates, risk factors of OA can be determined, such as sex, age, race, etc…

Osteoarthritis Risk Factors. Osteoarthritis is a disease that can manifest from a number of different factors, both endogenous and exogenous. The endogenous risk factors that can predispose an individual to OA include age, gender, race, genetics, and bone density. Exogenous factors that can lead to OA include obesity, injury or trauma,

surgery, and even professional occupation [18]. The most important risk factors of OA include age, gender, genetics, obesity, trauma, and physical exercise (Figure 3).

Table 2. Prevalence data from radiographic OA from three US population-based studies in the hands, knees, and hips [14].

Diseased area, age	Source [ref.]	% with symptomatic OA		
		Male	Female	Total
Hands, ≥ 26	Framingham OA Study [16]	3.8	9.2	6.8
Knees				
≥ 26	Framingham OA Study [16]	4.6	4.9	4.9
≥ 45	Framingham OA Study [16]	5.9	7.2	6.7
≥ 45	Johnston County OA Project [17]	13.5	18.7	16.7
≥ 60	NHANES III [15]	10.0	13.6	12.1
Hips, ≥ 45	Johnston County OA Project [17]	8.7	9.3	9.2

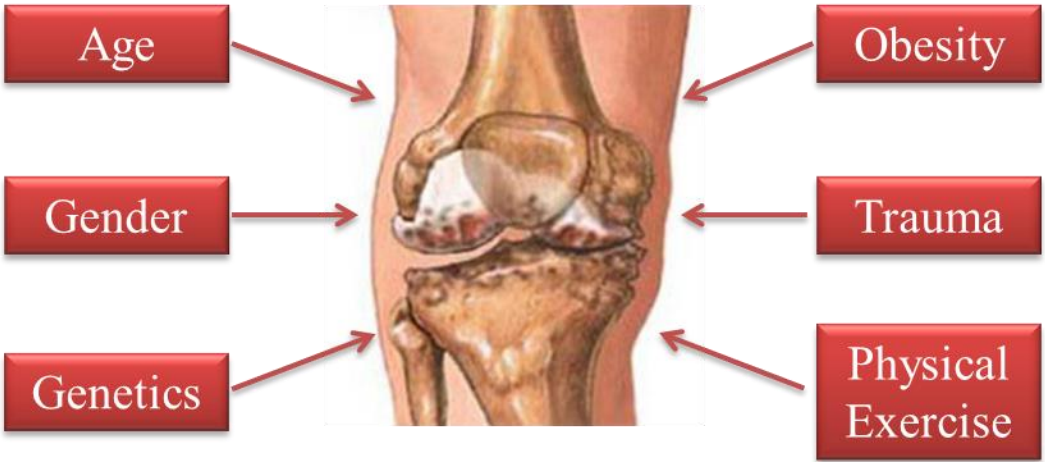

Figure 3. Principal risk factors for OA.

Age. Age is one of the strongest risk factors correlated with OA for all of the joints [14]. The reason being that age is a combination of both biological (aging) and mechanical (excessive loading) factors. Through aging, a number of biological changes take effect: the muscles in the body begin to weaken, along with the bones, cartilage, and

everything holding the joint together. These weakening components create a destabilized joint, which usually results in "abnormal" loading of the joint. This abnormal loading creates heightened and localized states of stress within the joint, which in turn wears out the cartilage more rapidly.

Gender. Gender is also a major risk factor of OA. It is has been shown that women are more likely to have OA than men [11]. Also, women are not just more likely to have OA, but they tend to have a more severe form of OA when compared to men [19]. The higher prevalence of women with OA is thought to be associated with increased hormone levels. Articular chondrocytes have a number of estrogen receptors, and the higher abundances of estrogen in women have been thought to effect the operation of these cells. A recent study has linked estrogen replacement therapy with a decreased risk of developing OA in post-menopausal women [7, 20].

Genetics. Several studies have showed that genetic factors play an important role in the development of OA, including a number of twin and family studies that have revealed a genetic component of OA [21-23]. Growth and differentiation factor 5 (GDF5) is a ligand of the transforming growth factor (TGF-β) family, and encodes for a bone morphogenetic protein (BMP). These BMP's play a critical role in the development of synovial joints, and have been associated with both hip and knee OA [24]. A recent study has also shown a number of genes that play a role in the development of knee OA, including HPB1, COG5, BCAP29, DUS4L, GPR22, and PRKAR2B [25]. These 6 genes play an important role in the development of cartilage as well as regulating chondrocyte

metabolism. If the joint is improperly formed in the development stages, loads cannot be distributed evenly resulting in "abnormal" joint loading, and eventually OA.

Obesity. Obesity has long been linked as the most potent exogenous risk factor of OA, especially of the knee [7]. It has been shown that weight loss in obesity patients, even as little as 10 pounds, can reduce an individual's risk of knee OA up to 50% [26]. Another study showed that weight loss combined with exercise in elders reduced the risk of symptomatic knee OA [27]. In this same study, neither exercise or weight loss alone reduced the risk of knee OA, but rather both were needed to minimize the risk. This emphasizes the potential regenerative effects that exercise has on cartilage and chondrocyte metabolism. Exercise could potentially promote restorative mechanisms in the chondrocytes increase matrix protein synthesis to help rebuild or repair the damaged cartilage. The increased risk of OA in obese individuals is fairly clear. The excessive weight creates a more severe loading scenario for the joint. The joint is easily overloaded which breaks down the protective cartilage covering the bones. If the overloading continues, the cartilage completely deteriorates until ultimately the pain and inflammation of the joint causes the individual to seek medical intervention (usually through a total joint replacement).

Trauma. Analogous to the endogenous risk factor of age, trauma or injury has been linked as one of the strongest exogenous risk factors of OA. Joint injuries that increase an individual's risk of OA include: trans-articular fracture, meniscal tearing requiring meniscectomy (surgical removal of all or part of a torn meniscus), or anterior or

medial cruciate ligament (ACL or MCL) injury [7]. In fact, previous trauma to the knee can increase a man's risk of knee OA up to 5-6 times, and ~3 times for women [16]. The trauma to the joint usually creates a destabilized joint, which results in "abnormal" loading of the joint. As aforementioned, this "abnormal" loading of the joint creates extremely localized stress states to develop, which wears down the cartilage more rapidly when compared to a normal joint.

Physical Exercise. Physical exercise in high-intensity sports has been linked as a risk factor of OA, due to the continual, extreme loading of the joint. Recent studies suggest evidence that elite long distance runners [28] and professional soccer players [29] are at a higher risk of developing knee and hip OA when compared to non-athletes. On the contrary, individuals with a history of heavy mechanical work are ~7-fold less likely to have OA at the age of 90 [3]. Also, in the absence of injury, recreational running or jogging did not increase the risk of OA [30]. This suggests that overloading the joint through excessive exercise can result in the development of OA, but moderate or recreational exercise can improve the health of the joint and can even protect against the development of OA.

Osteoarthritis Related Costs. There is currently no cure for OA, and once the disease progresses (*i.e.* the articular cartilage begins to deteriorate) it usually worsens due to the limited regenerative ability of cartilage. Because OA has no permanent cure, OA is usually treated through weight loss, rest, drugs, and if the disease has progressed too far, joint replacement. The limitations for these treatments are that they are usually

infeasible for most patients due to the extreme costs of a total joint replacement. In the United States, a typical total knee joint replacement costs on average ~$50,000 [31]. Most insurance companies will cover a total knee joint replacement, but for individuals without health insurance, surgical intervention is impossible. In fact, in 2003, total osteoarthritis related costs were estimated to be 128 billion dollars (not including time spent away from work), with direct medical expenditures totaling ~81 billion dollars [32]. Due to the extreme costs and trauma for joint replacement surgery, another treatment plan for OA is essential.

As suggested from a number of studies [3, 9, 30, 33, 34], moderate exercise can actually induce protective mechanisms in cartilage against OA. With that being said, what if exercise could be used as a treatment plan? If early diagnosis of OA was more effective, what if a doctor could prescribe 30 minutes of daily exercise as a treatment option for the patient. Not only would the exercise increase the patient's overall health, it could potentially reduce the patient's risk of developing OA. These are the main questions driving the motivation for this research. Determining the link between mechanical loading and chondrocyte metabolism is extremely important in understanding how these highly specialized cells sense and respond to their mechanical environment. Because OA is considered a whole joint disease, it is important to look at the overall composition of cartilage to observe the interactions between the chondrocytes and their micro-environment and how mechanical loading can alter the functions of these cells.

Biological Structure of Cartilage

Cartilage is a non-vascular, flexible, connective tissue that is found primarily in the joints throughout the human body (*e.g.* the knee, hip, elbow, etc…). Cartilage serves as a protective, low-friction material (cartilage on cartilage coefficient of friction, $\mu \sim 0.001$) at these load bearing surfaces and allows bones to articulate smoothly. In OA instances, when cartilage has deteriorated, the bones begin to rub on each other (bone on bone coefficient of friction, $\mu > 0.3$), which is usually accompanied with extreme pain and inflammation (Figure 1). Cartilage can be classified into three groups: hyaline cartilage, fibrocartilage, and elastic cartilage. The cartilage found primarily in human joints is hyaline cartilage [35]. Articular cartilage can be broken up into four different zones: the superficial zone, the middle zone, the deep zone, and a region of calcified cartilage (Figure 4) [36].

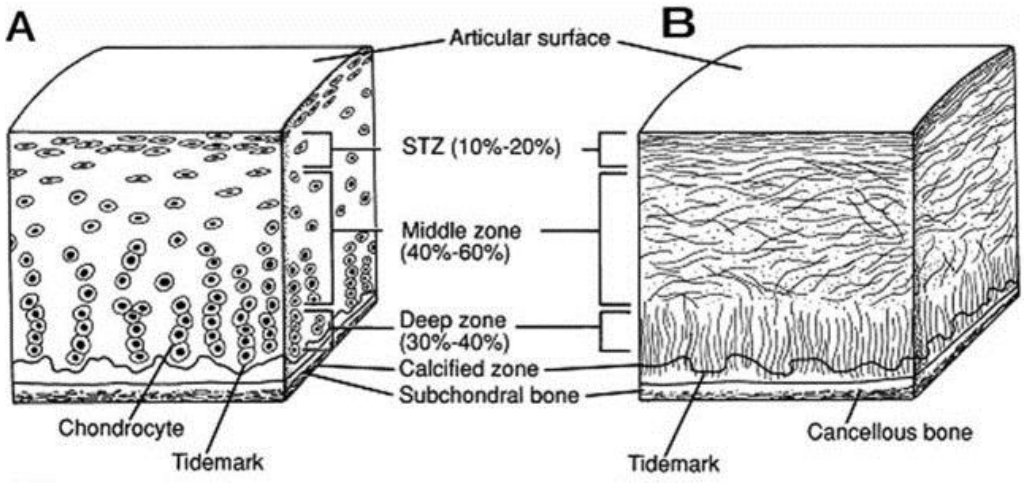

Figure 4. Cross sectional diagram showing the cellular (A) and collagen fiber (B) organization in the four zones of articular cartilage [37].

The outermost surface of the cartilage, the superficial or tangential zone, accounts for approximately 10 to 20 percent of the cartilage thickness. The superficial zone contains the highest concentration of type II collagen fibers, which are oriented parallel to the surface of the joint. As we move further from the surface, the amount of type II collagen fibers decreases in each zone. The next zone is the middle zone (~60% of the cartilage thickness). In the middle zone, the collagen fibers are more randomly oriented most of them at a 45° angle with respect to the articular surface. Following the middle zone is the deep zone. The deep zone accounts for approximately 20-30 percent of the cartilage thickness, with collagen fibers oriented perpendicularly to the articular surface. The final zone contains calcified cartilage, which is in direct contact with subchondral bone. Calcium salts begin to develop in the matrix and this region provides the needed bone to cartilage interface [36]. If we compare the constitution and orientation of type II collagen fibers in cartilage to a standard carbon fiber composite material, we see many similarities. The collagen fibers in the superficial zone are oriented parallel to the articular surface (0° layup in a composite), which provide cartilage the ability to resist various tensile and shear loads. Next, we see the collagen fibers oriented at a 45° angle with respect to the articular surface, providing the cartilage with the ability to resist shear and compressive loading that the joint might encounter. Finally, we have the deep zone, where the fibers are oriented perpendicular to the articular surface (90° layup), and provide the joint the ability to resist compressive loading. This unique layered structure provides the cartilage with its exceptional mechanical properties and the ability to handle a wide array of loading scenarios.

When looking at the composition (micro-scale level) of cartilage, there are three main components: The extra cellular matrix (ECM), the pericelluar matrix (PCM) and the sole cell type in cartilage, articular chondrocytes (Figure 5).

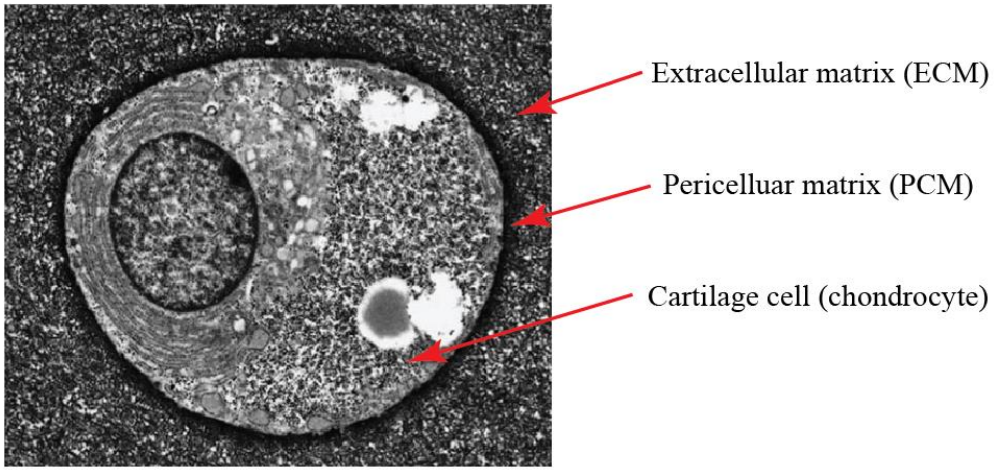

Figure 5. The three main components of articular cartilage: The extracellular matrix (ECM), the pericelluar matrix (PCM), and the chondrocyte.

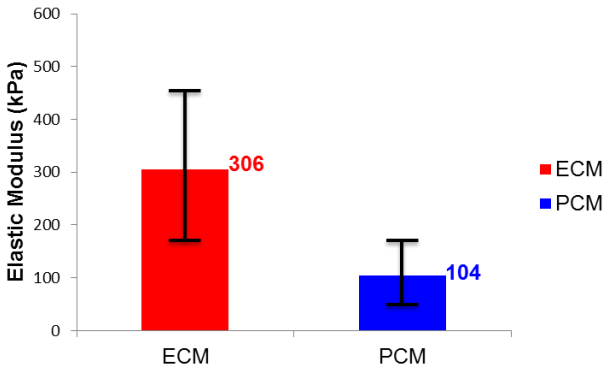

Figure 6. Young's Modulus values for the ECM (red) and PCM (blue), respectively.

Extracellular Matrix. The ECM is a relatively stiff, matrix material (elastic modulus, E_{ECM} = 306 ± 133 kPa) that surrounds the less stiff PCM (E_{PCM} = 104 ± 51 kPa)

(Figure 6). The ECM provides a physical microenvironment for the chondrocytes to exist in. The ECM is composed primarily of water, collagen, and proteoglycans, and is responsible for the transmission of various biological signals to the chondrocytes which affects cell proliferation (growth), cell differentiation (less specialized cell becoming more specialized), and cell apoptosis (death). The ECM accounts for approximately 80% of the total wet weight of cartilage [37]. Within the ECM, collagen accounts for 60% of the dry weight making it the most abundant macromolecule. Collagen is classified into "types" (*i.e.* type I, II, III, IV, etc…). Type II collagen represents ~95% of the collagen found in the ECM and provides the ECM with exceptional strength and resistance to a variety of mechanical loads (*i.e.* tensile, shear, etc…). The second most abundant molecules found in articular cartilage are proteoglycans. Proteoglycans are heavily glycosylated protein monomers and the most significant proteoglycan is aggrecan. Aggrecan interacts with hyaluronan to form long polymer chains that interlace with the collagen fibers. Both aggrecan and hyaluronan are extremely hydrophilic molecules, which allow them to easily bind with water molecules. From a mechanical standpoint, the aggrecan, hyaluronan and water molecules help fill the voids between collagen fibers (similar to epoxy in a composite material) allowing the cartilage the ability to resist high compressive loads. In direct contact with the ECM are the PCM and articular chondrocytes.

Articular Chondrocyte and the PCM. The sole cell type found in articular cartilage is the chondrocyte. These cells play an extremely important, metabolically active role in synthesizing, maintaining, and repairing the ECM. Chondrocytes only

constitute to about 2-5% of the total volume in articular cartilage [38]. Similarly to the ECM collagen fibers, chondrocytes vary in shape and size depending on where they are located throughout the cartilage (Figure 4A). Chondrocytes in the superficial zone (the outermost zone) tend to be flatter and smaller in size than cells in the deeper regions of cartilage. Chondrocytes are an extremely slow proliferating cell type, and in some cases may not proliferate at all [34]. This low or even non-existent proliferation rate is one of the reasons cartilage has such a narrow capacity for healing in response to injury. The limited ability of cartilage to repair itself indicates that chondrocyte metabolism plays a functional role in maintaining the overall health of the articular cartilage.

Metabolism is defined as the management of material and energy resources utilized by a cell that allow organisms to grow, reproduce, maintain their structures, and respond to their environments [39]. In articular cartilage, chondrocyte metabolism involves both anabolic and catabolic processes. For chondrocytes, the anabolic process usually involves the synthesis and production of ECM and PCM molecules through secretions of various enzymes such as growth factors, cytokines, and protease inhibitors [40-42]. In cartilage, the most common growth factors are fibroblast growth factor family (FGF), insulin-like growth factor family (IGF), transforming growth factor family (TGF-β), and bone morphogenetic proteins (BMPs). The most common anti-inflammatory cytokines in cartilage include interleukin 4, 10, 13, and 1Ra (IL-4, IL-10, IL-13, and IL-1Ra). These cytokines and protease inhibitors are enzymes that are secreted by the cells that help block proteolysis in the cells. Proteolysis is defined as the breakdown of proteins into peptides or amino acids, and in chondrocytes, specific

proteases (*e.g.* MMPs) breakdown the proteins that make the ECM and PCM, and have been associated with OA [43]. These degradative processes are known as catabolic processes.

The most common proteases found in cartilage that are responsible for the breakdown of ECM and PCM molecules (such as collagen, proteoglycans, and fibronectin [44]), are matrix metalloproteinase (MMPs). MMPs have not only been found to degrade collagen, but have also been known to degrade aggrecan by cleaving the Asn341~Phe342 bond in aggrecan [45] . MMPs include MMP-1, -2, -3, -7, -9, and -13. Another family of catabolic enzymes that have been known to degrade ECM molecules are the Adamalysin with Thrombospondin Motifs (ADAMTS) family (also known as aggrecanase [45]). ADAMTS include ADAMTS-1, -4, -5, and -11.

Because chondrocytes are the sole cell type in cartilage, they must maintain a delicate balance both the anabolic and catabolic processes (Figure 7). A number of molecules involved in both the anabolic and catabolic processes of cartilage can be seen in Figure 7 (note this list is not comprehensive). When in balance, the chondrocytes can secrete catabolic enzymes to degrade old matrix molecules, and then replace them with new molecules by initiating an anabolic response. This harmonic balance allows for healthy turnover rates of the ECM and PCM, and keeps the cartilage functioning properly. However, during aging or in diseased (OA) conditions, the equilibrium is disrupted, and the catabolic (degradative) process dominates.

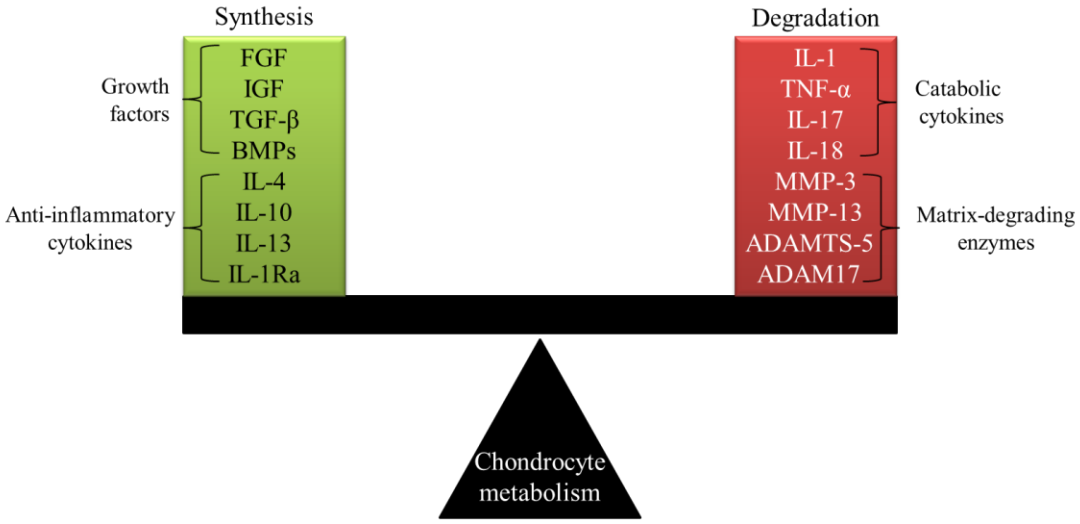

Figure 7. Anabolic and Catabolic Enzymes in Cartilage. The delicate balance between the anabolic and catabolic processes in cartilage. The molecules on the left (green) are involved in the anabolic process or synthesis of matrix (ECM and PCM molecules). The molecules on the right (red) are involved in the catabolic or degradative processes of the matrix in cartilage. Note, this list does not include all of the molecules known to be involved in the anabolic or catabolic processes of cartilage.

As aforementioned, articular cartilage is avascular, meaning chondrocyte metabolism is heavily dependent on glycolysis [46]. In light, ATP is created in either the TCA (citric acid cycle) or in glycolysis, and energy is released when ATP (adenosine triphosphate) is broken down into ADP (adenosine diphosphate). In the presence of oxygen, the TCA cycle is the primary metabolic pathway used by cells to create ATP. On the contrary, in the absence of oxygen or in low levels of oxygen, glycolysis is the dominating pathway. Due to the low oxygen levels found in cartilage (ranging from 10% at the surface to <1% in the deep layers), the majority of the chondrocyte's energy utilization come almost exclusively from glycolysis [46]. Glycolysis is a metabolic pathway where extracellular glucose ($C_6H_{12}O_6$) is broken down into pyruvate ($CH_3COCOO^- + H^+$) through a number of metabolic reactions. Throughout glycolysis,

ATP is broken into ADP, which gives the cells the energy they need to maintain and repair their own individual microenvironment. Due to the low density of chondrocytes in cartilage, each chondrocyte is responsible for its immediate surroundings and very rarely do chondrocytes form cell-to-cell contacts for signal transduction and intercellular communications [37].

Surrounding each chondrocyte is a thin membrane known as the pericelluar matrix (PCM). The PCM plays an important role in that it provides an interface between the stiff ECM and the more compliant chondrocytes [47]. As seen in Figure 5, the PCM is in direct contact with both the ECM and chondrocyte as seen by the darker black ring surrounding the cell. It is believed that the PCM serves as a transducer of physical signals within the chondrocyte's microenvironment, therefore playing a very important role in chondrocyte mechanotransduction and thus the overall metabolism of cartilage [48].

Mechanotransduction

Mechanotransduction describes the processes by which cells convert mechanical stimuli into biochemical responses [49]. It is well known that cells can convert a mechanical input into a biological signal, but the underlying processes remain unclear [50]. An example of mechanotransduction, one in which we have all experienced, is touching a hot plate. When we touch the hot plate (heat is the mechanical stimuli), our cells on the surface of our hand translate the stimuli into a biochemical signal (we recognize this as pain). This signal informs us to quickly remove our hand to prevent injury. The process of mechanotransduction provides cells the unique ability to adapt to

their physical environment [51]. As one could imagine, the heavily-loaded joint surfaces of our bodies (*i.e.* knees, hips, etc...) provide a very specialized physical environment for chondrocytes to live in. At these locations, the articular cartilage, and thus the chondrocytes, are exposed to near-constant mechanical loading including compressive, tensile, and shear loads (Figure 8). In fact, during normal, sub-injurious human activities (*i.e.* walking, jumping, running, etc.) cartilage is subjected to millions of loading cycles with *in vivo* compressions as large as 20% [52-54].

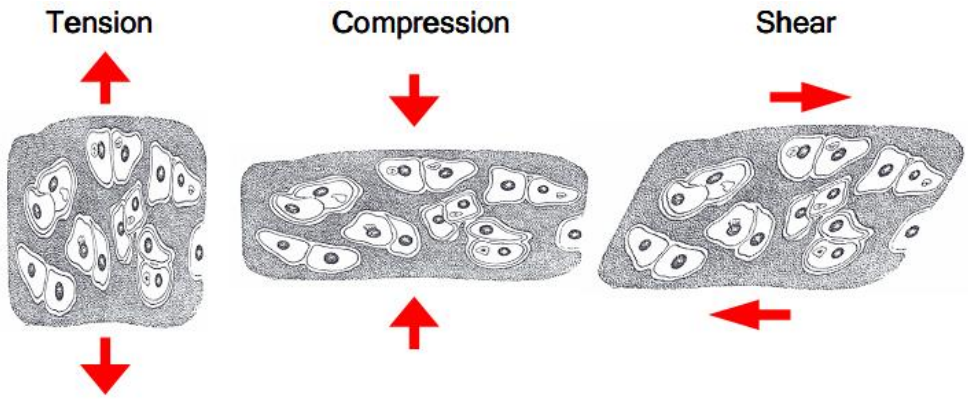

Figure 8. Schematic of tensile, compressive, and shear loads on cells. The process in which cells convert mechanical stimuli into biological signals is known as mechanotransduction.

The average human gait has been measured to be at approximately 1 Hz, meaning during a 1 hour walk, each knee joint is loaded 1800 times with contact pressures as high as 5-6 MPa from forces up to 10 times the individual's body weight [55]. Physiological loading conditions such as running or jumping can produce substantially increased loading rates (as high as 140 Hz) with contact pressures up to 18 MPa [56]. Joint motion

and variable loads are important to maintain normal articular cartilage function and health, yet excessive loading can result in OA [8, 57].

The threshold between healthy joint loading and unhealthy loading is an extremely fine line, and remains to be highly controversial. Joint loading under physiologic conditions (*i.e.* healthy joint loading) has been shown to have no adverse effects on cartilage or other joint tissues, and clinical studies even suggest exercise in osteoarthritic patients [58]. In fact, a study in the Netherlands showed that people with a history of heavy mechanical loading had a 7.2 less likely of a chance to get OA than people without a history of heavy mechanical work [3]. This study suggests that joint loading can potentially promote protective mechanisms against OA. Unhealthy joint loading, also classified as "abnormal" joint loading, is most commonly a direct result from obesity, trauma, overuse, immobilization, and joint instability [55]. Obesity is strongly linked with OA, and studies have shown that a decrease of ~10 lbs. of body weight in obesity patients can decrease the risk of OA up to 50% [26, 59]. Joint stability issues are also a common precursor to OA, and a number of models have been developed and validated to show how joint destabilization promotes OA [60, 61]. A number of other studies have shown how these abnormal loading conditions play an important role in the onset of OA, yet the underlying biomechanical processes that cause this still remains unclear. In order to determine whether or not joint loading can be used as an effective therapeutic strategy in combating or preventing OA, chondrocyte mechanotransduction needs to be heavily explored in the scientific community.

Scientific Studies

Cartilage experiences a variety of *in vivo* loading mechanisms. Due to the difficulty of studying human articular cartilage *in vivo*, scientists have developed a number of *in vitro* studies to explore cartilage mechanics and chondrocyte mechanotransduction. Plus, who really wants to give up their healthy knee in the name of science? Two approaches are commonly used in the scientific community in studying these topics. The first method is removing cartilage samples surgically from animals (*i.e.* mice, rats, bovine, etc…) or human donors (*i.e.* joint replacement), and then mechanically stimulating the entire tissue. This approach is most commonly used in studying cartilage mechanics/behavior as well as characterizing ECM and PCM material properties on macro-scale, micro-scale, and nano-scale levels [47, 62-66]. The second approach involves studying the chondrocytes themselves. Chondrocytes are most commonly obtained by harvesting cartilage from an animal or human donor joint, and then digesting the cartilage (usually in in collagenase, an enzyme that breaks down the peptide bonds in collagen). After digestion, the cells can be removed, cultured, mechanically stimulated, and their biological outputs observed. Most chondrocyte mechanotransduction studies generally involve encapsulating the cells in some sort of hydrogel, creating a 3D microenvironment in which they may be studied. A variety of hydrogels are utilized in creating these 3D cell suspensions, such as photo cross-linked polyethylene glycol [43], self-assembling peptides [67], alginate [68], and agarose [69, 70]. Agarose hydrogels are of particular interest because the stiffness can be manipulated to match the stiffness of cartilage PCM [71] without potential complications of UV photo-crosslinking (*e.g.*

induction of the DNA damage response [72]). Currently, most existing studies utilize 3D microenvironments (*e.g.* agarose or alginate) for cell encapsulation with a much lower stiffness (< 5 kPa) than the cartilage pericelluar matrix (25-200 kPa) [47, 73]. These lower stiffness gels don't appropriately emulate the microenvironment that the actual *in vivo* chondrocytes reside in. By utilizing higher stiffness gels that match the mechanical properties of the PCM, the chondrocyte mechanotransduction studies will more effectively simulate the physiological environment of the *in vivo* chondrocyte.

To emulate physiological loading conditions for *in vitro* mechanotransduction studies, dynamic stimulation is often applied with matched load amplitudes and frequencies similar to the human gait (both walking and running). To simulate walking *in vitro*, cartilage explants or 3D cell cultures can be subjected to low levels of oscillatory strain with frequencies less than 5 Hz. Higher frequencies and strains can be used to emulate running or jumping. It has been shown that dynamic, mechanical stimulation has both an anabolic and catabolic effects on articular cartilage [43]. As aforementioned, an anabolic process is defined as the synthesis of larger molecules from smaller units, which requires energy. In eukaryotic cells, this energy is usually harvested by the hydrolysis of ATP. On the contrary, a catabolic process is defined as breakdown of larger molecules into smaller units, which often releases energy. In regards to chondrocytes, an anabolic process can be characterized by the synthesis of PCM and ECM molecules, and a catabolic process would be the breakdown of these molecules. In healthy tissue, resident chondrocytes maintain the cartilage by remodeling the tissue with a good balance

between these two processes, which lead to a healthy turnover rates for the PCM and ECM [43, 74].

Exogenous dynamic compression has been shown to substantially alter chondrocyte metabolism in both an anabolic and catabolic manner, but the balance between matrix synthesis and matrix degradation is not yet fully understood [75, 76]. Dynamic loading performed directly on cartilage samples has been shown to increase [^{35}S] sulfate and [^{3}H] proline uptake which is a strong indication of proteoglycan and protein biosynthesis [77]. Proline is of significance, since it has been found to be a marker in the synthesis of the ECM. Proline is a non-essential amino acid, and is incorporated with the synthesis of collagen inside the cells cytoplasm. Note that a non-essential amino acid can by synthesized within the body, whereas an essential amino acid cannot be synthesized within the body and must be supplied externally. Changes in proline levels could potentially be associated with the synthesis or breakdown of collagen.

Short duration dynamic compression (as little as 5 minutes) as shown to induce phosphorylation of multiple enzymes, such as MAPK and SEK [78, 79], Akt [80], ERK -1 and -2 [81-83], and Rho kinase [84]. MAPK (mitogen-activated protein kinases) and ERK (extracellular signal-regulated kinases) pathways are heavily involved in extracellular stimulation, and have been hypothesized to regulate anabolic and catabolic changes of chondrocytes [76]. Dynamic compression has also been shown to promote Smad2 phosphorylation [85], gene expression of MMP-13 [86], which is the marker for

catabolic changes in the ECM, alter Superficial Zone Protein expression [87], induce transcription of ECM genes [9], and activate Rho kinase and RhoA [84].

Rho kinase (ROCK) and RhoA (Ras homolog gene family, member A) are proteins which are heavily involved in regulating the shape and movement of cells through the actin cytoskeleton [84]. Cell shape and size is extremely important when dealing with chondrocytes. As aforementioned, chondrocytes vary with shape and size throughout the layers of cartilage (from the superficial tangential zone to the deep zones). Chondrocytes in to the outer zones tend to be flatter and smaller and generally have greater density than that of the cells in the deeper zones of the matrix [37] (Figure 4B). These flatter, denser cells are better for handling the intensive loads seen at the joint surface and are designed to protect the deeper zones. As we move deeper into the matrix, the cells become more rounded in shape and less dense. The cells in the deeper zones (more rounded cells) have been associated with an increase in cartilage matrix production [88]. Cell shape has been shown to be dependent on the cytoskeleton as well as interactions with the extracellular matrix [89]. Where ROCK and RhoA come into play is that they both play a central role in actin cytoskeleton dynamics, which as mentioned above, affects the shape and size of the cell. Studies show that by inhibiting ROCK cells become more rounded, which increases in cartilage matrix synthesis [84].

Many experimental studies have also been performed on OA tissues. The material properties of articular cartilage, mainly Young's modulus, are derived almost extensively from the ECM [62]. The ECM has a much greater stiffness than that of the PCM (~3X), and dominates the overall stiffness of cartilage. It has been shown that the

PCM and ECM in OA cartilage is significantly less when compared with healthy cartilage [62, 90]. In fact, decreases in both ECM and PCM moduli have been reported as large as 45% and 30% respectively [62]. The catabolic activity of chondrocytes increases significantly in OA joints, which results in a decrease in cartilage matrix production [91]. A recent study was performed to compare changes in gene expression of chondrocytes in OA cartilage to normal cartilage [92]. Significant gene expression changes occurred in the OA cartilage. OA cartilage explants have also been found to express p53R2, a tumor suppressor protein. When this protein was inhibited, an increase in Akt phosphorylation was observed [93]. Akt is a protein of the kinase family, whose role is primarily involved in cell proliferation. This may suggest that if the p53R2 protein is suppressed, then cell proliferation may increase.

These studies demonstrate the sensitivity of chondrocytes to mechanical loading and indicate that a complete understanding chondrocyte mechanotransduction remains to be determined. Many of current scientific studies primarily focus on individual signaling pathways, which have the potential to exclude important data or findings. Also, many of these studies utilize 3D cell constructs with a much lower stiffness than the cartilage PCM, which does not accurately emulate the physiological environment of the chondrocytes. Because the exact mechanisms of how chondrocytes sense and respond to mechanical deformation is not yet fully understood, it is important to study chondrocyte mechanotransduction in an unbiased manner, meaning looking at the entire picture and not excluding pathways *a priori*.

Metabolomics

Metabolomics, as the name suggests, is the comprehensive analysis of metabolites or small molecules in a biological system [94]. Metabolomics is the study of metabolite profiling, and has been adapted into many fields such as pharmaceutics, clinical diagnostics, etc… The metabolome (analogous to the proteome for proteins, and the genome for genetics), is defined as the set of small-molecules found within a biological sample including substrates, co-factors, and many other molecules [95]. The metabolome can be viewed as a collection of state variables describing the cellular phenotype [96]. Metabolomics studies the metabolites of a biological system which are direct products of cellular metabolism. Metabolites give insight on functional readout of the cellular state, essentially a snapshot of the physiology of the cell. Unlike genes and proteins, metabolites serve as direct signatures of biochemical activity which are easier to correlate with phenotype [96].

Metabolomics can be used for metabolite profiling in two basic approaches: targeted metabolomics, and untargeted metabolomics. Targeted metabolomics refers to the method of looking at a predefined, specified list of metabolites after a sample is run. Targeted metabolomics typically focus on one or more related pathways of interest and are usually driven by a specific biochemical question or hypothesis [96]. For example, in chondrocytes, metabolism is heavily driven by glycolysis. So, by studying the specific metabolites in the glycolytic cycle, one could gain a wealth of knowledge regarding the energy re-localization of the chondrocytes. Untargeted metabolomics is just the opposite. An untargeted approach aims to study global metabolite levels under various

conditions, with the potential to discover new cellular pathways to biological mechanisms [96].

With the increasing advances in technology, metabolomics is now becoming a widely used and powerful method for studying many of nature's biological foundations. Mass spectrometry (MS) and liquid chromatography (LC) are the most common engineering tools used in metabolomics, and are often coupled together (LC-MS) to give an abundance of information about the sample. Recent developments in LC-MS have enabled scientists to rapidly measure thousands of metabolites simultaneously from only minimal amounts of samples [97]. Mass spectrometry has been described as the smallest scale in the world since it measures the masses of individual molecules. A mass spectrometer actually measures a mass-to-charge ratio (denoted m/z), but masses are easily backed out since the charge state is usually known.

Mass Spectrometry. A mass spectrometer can be broken down into four basic components (Figure 9): a sample inlet, an ionization source, a mass analyzer, and an ion detector [98]. All mass spectrometers incorporate these four components, even though the processes can vary from instrument to instrument.

The sample is introduced through the sample inlet (Figure 9A), which can be done so in a couple of different ways; direct insertion and direct infusion. Direct insertion methods involve the physical insertion of the sample into the mass spectrometer, usually via a slide or sample plate. The most common type of instrument that utilizes direct insertion methods is a matrix assisted laser desorption ionization (MALDI) mass spectrometer. One main advantage of direct insertion over direct infusion, is that it can

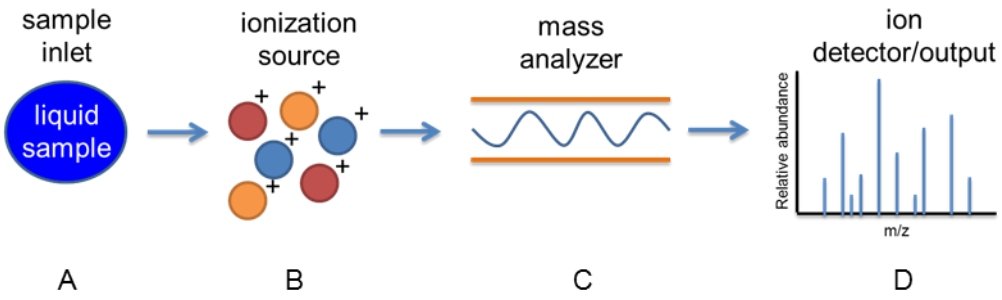

Figure 9. Simplified schematic of a mass spectrometer. Usually the liquid sample going to the ionization source comes from the output of some sort of chromatographer. Usually, mass spectrometers are coupled to a liquid chromatographer (*i.e.* LC-MS).

be used to analyze whole tissue samples (*i.e.* sample does not need to be in solution). Direct infusion methods require samples to be in solution, and utilize capillary columns to introduce small amounts of sample into the mass spectrometer. These columns (typically liquid chromatography (LC) columns) are used to separate the solution into its different components prior to sending it through the mass spectrometer. Quite often mass spectrometry and liquid chromatography are coupled together, as denoted by LC-MS. Once the sample is in the MS, it is ionized using a high powered ionization source (Figure 9B). There are many different ionization methods (MALDI, electrospray ionization (ESI), etc…), but the purpose of each is the same; adding a charge to a neutral molecule (*i.e.* ionizing the molecule). ESI is often the ionization source when coupling LC-MS since it can handle the continuous flow of sample from the LC. Once ionized or charged, the molecules are electrically propelled through the mass analyzer (Figure 9C). Mass analyzers also vary across the board, but their main purpose is to separate the ions according to their specific m/z values. Mass analyzers include quadrupoles, quadrupole ion traps, time-of-flight (TOF), and quad time-of-flight (Q-TOF), and each varies in

performance with respect to speed, accuracy, and resolution. Once the ions are analyzed through the mass analyzer, they ultimately reach an ion detector (Figure 9D), where the ion energies are converted into electrical signals. Note this is simply an extremely brief overview on mass spectrometers, and merely scratches the surface of their descriptions.

Liquid Chromatography. Liquid chromatography (LC) is an analytical chemistry technique that is used to separates the various components of a mixture [99]. Liquid chromatography first came about in the early 1900s, and the word chromatography comes from the Greek words *chroma*, meaning color, and *graph*, meaning writing [100]. The most common and most powerful form of liquid chromatography involves passing the sample through a column which is filled with tiny particles, or packing material. This is known as the "stationary phase". On the contrary, the solvent that passes through the column is known as the "mobile phase." A liquid chromatographer can be broken down into a few main components (Figure 10).

First, the column is usually conditioned or washed using the mobile phase. This preps the column to receive the sample. Depending on the type of sample, different types of columns can be used along with different solvents (mobile phase). The sample is then injected or loaded onto the column, where it binds to the stationary phase. The column is then washed by pumping the mobile phase through it. Then, depending on the sample, the mobile phase is adjusted causing the molecules to elute (come off the column). Normally, the mobile phase is composed of two or more solvents, and the amount of each solvent can be adjusted depending on the sample type. For example, if the sample is

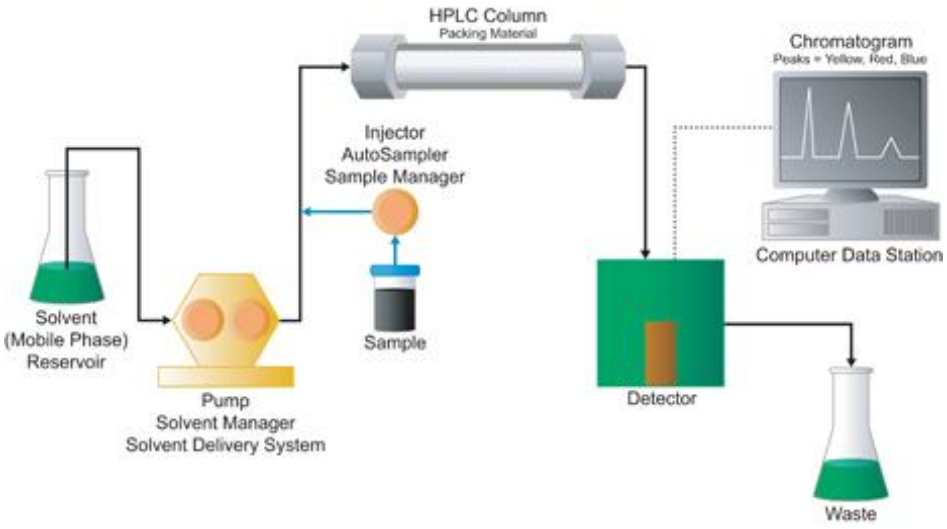

Figure 10. Schematic of a typical liquid chromatography (LC) system [100].

extremely hydrophobic (water-hating/non-polar), then a typical mobile phase will include water and some type of organic solvent (usually acetonitrile or methanol). In this scenario, the water attracts the hydrophilic molecules, or the molecules that bind weakly to the stationary phase, and they will elute first. The amount of acetonitrile in the mobile phase is then increased using a solution gradient (adjusting the amount of water and acetonitrile with respect to time), which out-competes the hydrophobic molecules, or molecules that were strongly bound to the stationary phase, causing them to elute later. As a result of the different hydrophobic and hydrophilic interactions of the molecules, the sample components separate out into discrete fractions, allowing them to be analyzed separately. These discrete fractions elute from the column and pass through a detector which records the chromatogram.

With the rise in technology and the advances in instrumentation, chromatographic methods have increased dramatically. These advances allow samples to be pumped with

greater pressures through columns with much higher stationary phase densities, which significantly increases the resolution, speed, and sensitivity of the system. These liquid chromatography systems are called high-performance liquid chromatography (HPLC) and ultra-performance liquid chromatography (UPLC). Most LC systems in today's research society are either HPLC or UPLC systems.

The most widely used chromatographic methods in metabolomics and proteomics are normal-phase chromatography (NPC), reverse-phase chromatography (RPC), hydrophilic-interaction chromatography (HILIC), and hydrophobic-interaction chromatography (HIC).

Normal-Phase Chromatography. In normal-phase chromatography the stationary phase of the column is extremely polar and the mobile phase is non-polar (Figure 11). Typical stationary phase media of NPC includes silica or other organic molecules and mobile phases include solvents such as hexane or other nonpolar solvents.

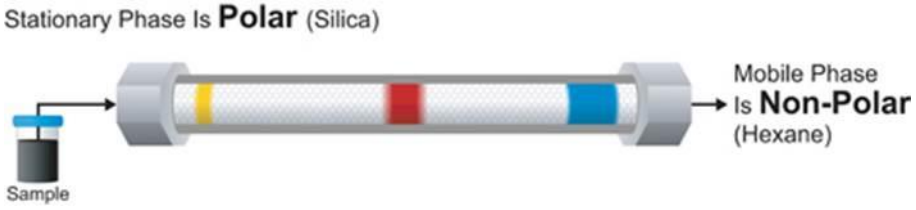

Figure 11. Normal-phase chromatography [99].

In Figure 11, the sample is injected into the column. The polar stationary phase binds the more polar molecules (yellow band) much stronger than the more nonpolar molecules (red and blue bands). When the nonpolar mobile phase is pumped through the

column, it attracts the more nonpolar molecules (blue band), which makes them move faster through the column and elute quicker. Based on the polarity of each of the molecules, they will elute at their own specific time allowing them to be resolved independently.

Reverse-Phase Chromatography. Just the opposite of normal-phase chromatography is reverse-phase chromatography. In reverse-phase chromatography the stationary phase of the column is extremely nonpolar and the mobile phase is polar (Figure 12). Typical stationary phase media of RPC includes octadecyl carbon chain (C18)-bonded silica and mobile phases include mixtures of water and other organic solvents, such as acetonitrile.

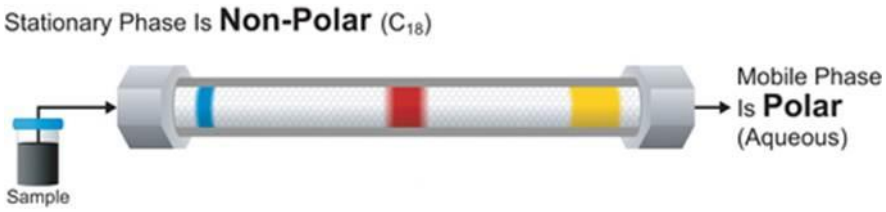

Figure 12. Reverse-phase chromatography [99].

To better describe RPC, the same sample as in Figure 11 is injected into the column. In this case, the most strongly retained molecules are the nonpolar molecules (blue band), and the more polar molecules (yellow band) move quicker through the column, and elute much sooner. The stationary, nonpolar phase retains the nonpolar molecules and the polar mobile phase attracts the more polar molecules (like polarities attract). RPC is more commonly used than NPC, because it is more reproducible and can

be applied to a broader range of applications. RPC accounts for approximately 75% of all HPLC methods [100].

Hydrophilic-Interaction Chromatography. Hydrophilic-interaction chromatography or HILIC is a type of normal-phase chromatography since it uses a polar stationary phase and a nonpolar mobile phase. Typically, with HILIC, the mobile phase is adjusted throughout the run. First, a very nonpolar solvent (100% organic) is used to elute the nonpolar molecules from the column. Then, water (an extremely polar solvent) is mixed in with the mobile phase, starting at low concentrations, and increasing until the mobile phase is 100% water. By increasing the amount of water in the mobile phase, the polar molecules that are bound to the stationary phase are out –competed by the water, and thus are eluted. The process of adjusting the ratio of the mobile phase throughout the course of the run is called a gradient separation.

Hydrophobic-Interaction Chromatography. Hydrophobic -interaction chromatography, or HIC, is a type of reverse-phase chromatography. HIC uses a nonpolar stationary phase and a polar mobile phase, and is usually used to separate larger molecules, such as proteins. Proteins by nature are extremely hydrophobic molecules, meaning they are not attracted to water. When the samples are injected into the column, the hydrophobic stationary phase binds the hydrophobic molecules. The column is then washed with a hydrophilic or aqueous mobile phase. The amount of hydrophobic or organic solvent in the mobile phase is then increased, which out-competes the

hydrophobic molecules that are bound to the stationary phase. The molecules are then eluted in order of increasing hydrophobicity.

Metabolomic Analysis. An output from an LC-MS run gives an abundance of information. Directly from the LC, a total ion chromatogram (TIC) is produced when the sample reaches the detector, which displays relative abundance, or intensity values on the vertical axis and elution time (usually in minutes) on the horizontal axis (Figure 13A). A TIC displays the abundance of sample at any time throughout the LC-MS run. The elution time is defined as the time when the samples elute off of the column and then enter the into the ionization source of the MS. Each elution time point in the TIC corresponds with a specific mass spectrum for the compounds eluting at that specific time, hence why LC-MS runs generate so much data. The mass spectra give the intensity of the signal (unit less) on the vertical axis, and the mass to charge (m/z) ratios along the horizontal axis (Figure 13B).

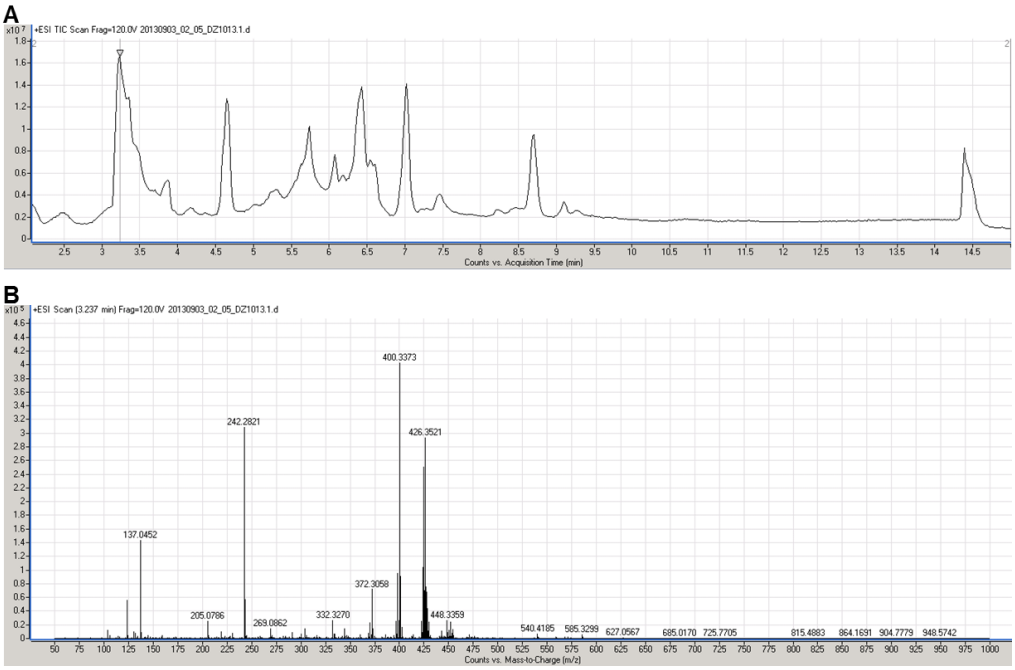

Figure 13. (A) Total ion chromatogram (TIC), and the (B) corresponding mass spectra for the sample that is eluted at ~3.25 minutes. For this figure, the sample is processed through the liquid chromatographer (LC) from ~2 minutes until ~15 minutes. For the TIC, the x-axis represents elution time and the y-axis the intensity of the signal. As the sample elutes from the LC, it goes directly into the ionization source (ESI) of the mass spectrometer (MS). For each elution time, we get a corresponding mass spectra, which gives us the individual mass to charge (m/z) ratios (x-axis) and their representative intensity (y-axis).

Proteomics

Proteomics is defined as the large-scale study of proteins. Again, analogous to the genome (the study of genetics) and the metabolome (the study of metabolomics), the proteome is defined as the entire set of proteins that are expressed by the genome, cell, tissue or organism at a certain time [101]. In mammalian cells, proteins are created from DNA (through many complicated processes), which is commonly referred to as the central dogma of modern biology Figure 14. DNA (deoxyribonucleic acid), is a molecule that encodes the genetic instructions used in the development and functioning of all living

organisms, and in eukaryotic organisms most of the DNA is stored within the cell nucleus (Figure 14A) [102]. According to the central dogma of modern biology, DNA is transcribed into messenger ribonucleic acid (mRNA) (Figure 14B), which is a single stranded copy of the gene. This process is commonly known as transcription. mRNA is then translated into long strings of amino acids in the cell's cytoplasm by ribosomes, and eventually become proteins, in a process called translation (Figure 14C). Each protein serves a unique purpose, and are considered the building blocks and workers of our cells. After translation (post-translation), proteins can be subjected to an array of chemical alterations, which can affect the protein's function. These changes are called post-translational modifications. An important post-translation modification in studying proteomics, in which a phosphate group is added to an amino acid (most commonly serine and threonine) is known as protein phosphorylation [103]. Protein phosphorylation gives insight of specific signaling pathways that could potentially reflect changes in protein activity. Phosphoproteomics is aimed at determining these specific phosphorylated proteins in a cell under some response.

The field of proteomics is awakening more interest in the scientific community, mainly in part to the Human Genome Project (HGP). In the 2003, the National Human Genome Research Institute (NHGRI) announced the successful sequencing of the human genome [104]. After the human genome was successfully sequenced, it was important to understand the relationships between gene expression and the biological functions of the cells. Understanding this important relationship is only possible through the study of the proteins. In most organisms, the genome is more or less static in all of their cells.

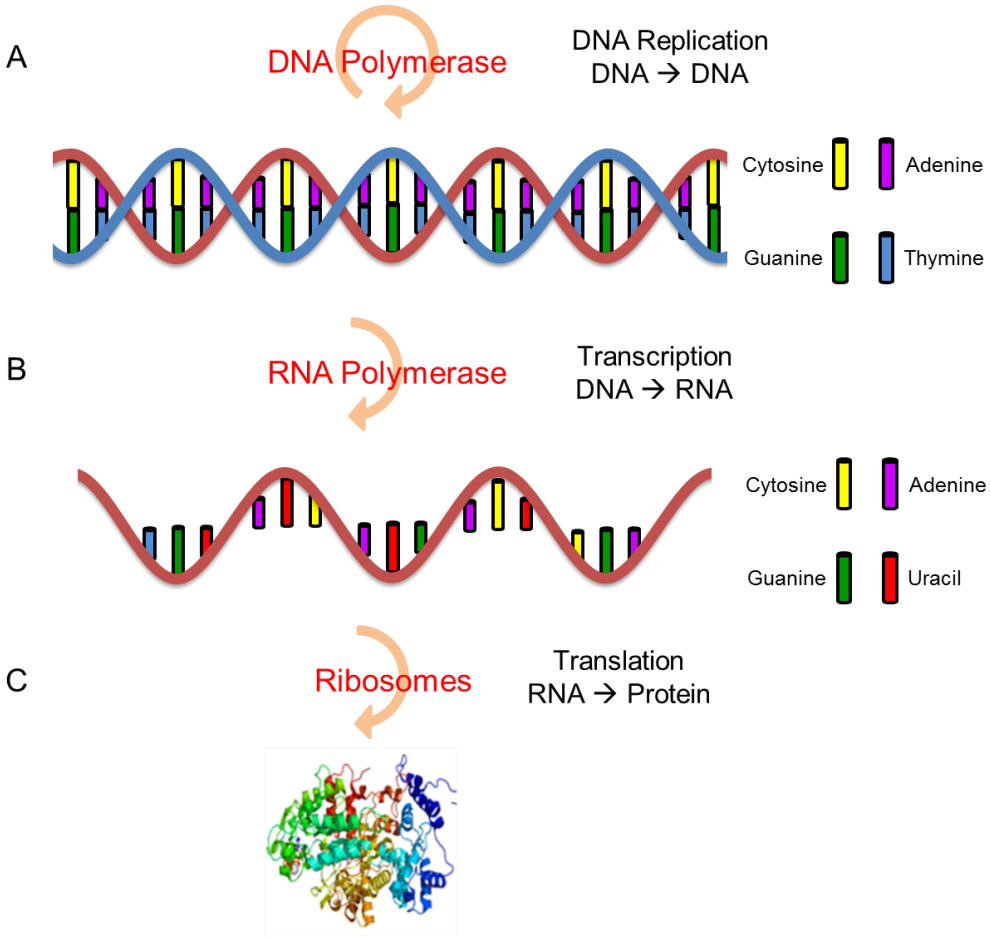

Figure 14. Central dogma of modern biology.

However, the proteome of the cells is highly dynamic, and the functions of the individual proteins can change dramatically in response to their environment, stress, physiological conditions, etc… These factors significantly increase the complexity in studying proteomics; however studying these dynamic characteristics of proteins has an advantage over studying genomics in that it gives more insight into the physiology of the cell. Proteomics is similar to metabolomics (but on a slightly longer time scale), in that it paints a picture of what a cell is doing at a given instant in time.

The breakthrough in proteomics has risen in part to important technological advancements in the past few decades. The first major breakthrough came about in 1975, which was two-dimensional gel electrophoresis (2D-GE) [105]. 2D-GE is used to analyze proteins by first separating them in one-dimension (1D-GE) by their mass. The proteins are then further separated in a second-dimension according to their isoelectric point. A typical 2D-GE gel can be seen in Figure 15.

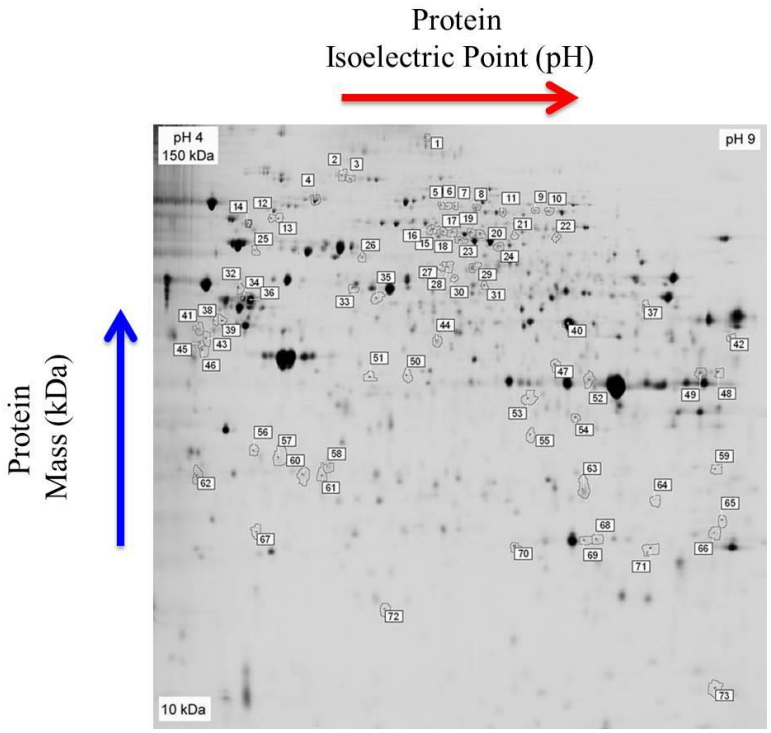

Figure 15. 2D-GE showing the proteome mapping of all of the proteins altered in OA [106]. Each black dot represents in an individual protein. Proteins are separated by increasing mass (kDa) in one-dimension, and by increasing isoelectric point (pH) in the second-dimension.

The second major breakthrough in the study of proteomics was mass spectrometry. Initially, and even currently, both techniques (2D-GE and mass spectrometry) are combined in the study of proteomics. First, the proteins are separated

in the 2D-GE, and then are analyzed and identified using mass spectrometry. The downside to this type of analysis is it is very labor and time extensive. However, with rise of technology, the sensitivity and speed for identifying and sequencing the proteins has improved dramatically. Usually, in mass spectrometry based proteomics analysis, sample preparation requires the proteins to be enzymatically digested using a proteolyzing enzyme, such as trypsin. Trypsin is a serine protease whose main function is in the hydrolyzing of proteins (breakdown of proteins in to smaller fragments called peptides). Trypsin hydrolyzes or cleaves the peptide bonds typically at the carboxyl sites of either the amino acids, lysine (Lys) or arginine (Arg) [107]. This digestion process is usually part of the sample preparation steps, and usually takes around 12 to 16 hours to completely digest the protein samples. Once the sample has been digested it can be analyzed using liquid chromatography and mass spectrometry (with fragmentation).

Liquid chromatography and mass spectrometry (with fragmentation) is typically denoted as LC-MS/MS. LC-MS/MS is typically used in proteomics analysis, and protein identification is only made possible through the information gained from the fragmented peptides. Fragmentation is usually performed by injecting an inert, collision gas (usually nitrogen) into the flight path of the charged, precursor ions, which is known as collision induced dissociation (CID) (Figure 16) [108].

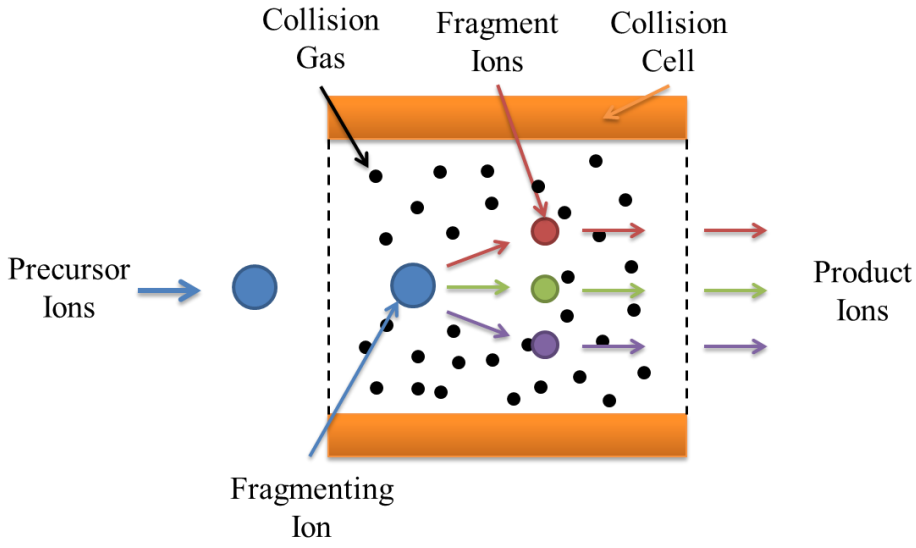

Figure 16. Schematic of collision induced dissociation (CID) used in an LC-MS/MS.

After fragmentation, the fragmented peptides reach the detector and the signal is recorded. Each of the fragmented peptides give important information regarding the amino acid sequence of the particular peptide. Since trypsin (or another proteolyzing enzyme) always cleaves proteins at specific amino acid sites, this information can be used to reconstruct the peptides and assist in identification. To identify the peptides, the m/z fragmentation data is compared with *in silico* fragmentation spectra databases. This process is known as peptide mass fingerprinting [109]. Finally, protein identification is accomplished by comparing the peptide mass fingerprinting data to *in silico* digestion data from proteomic databases [110-112].

Dissertation Outline

The over-arching goal of the research described in this dissertation is to better understand the chondrocyte response to applied, mechanical compression, and whether or not mechanical loading can be used as a potential therapeutic for treating or preventing osteoarthritis. To determine the effects of mechanical loading on chondrocytes, the biological outputs were analyzed utilizing novel *in vitro* and *in vivo* models. To my knowledge, such approaches have never been used to study chondrocyte mechanotransduction, and this research lays a strong foundation for future work in this field. The research in this dissertation is partitioned into four unique parts (Figure 17).

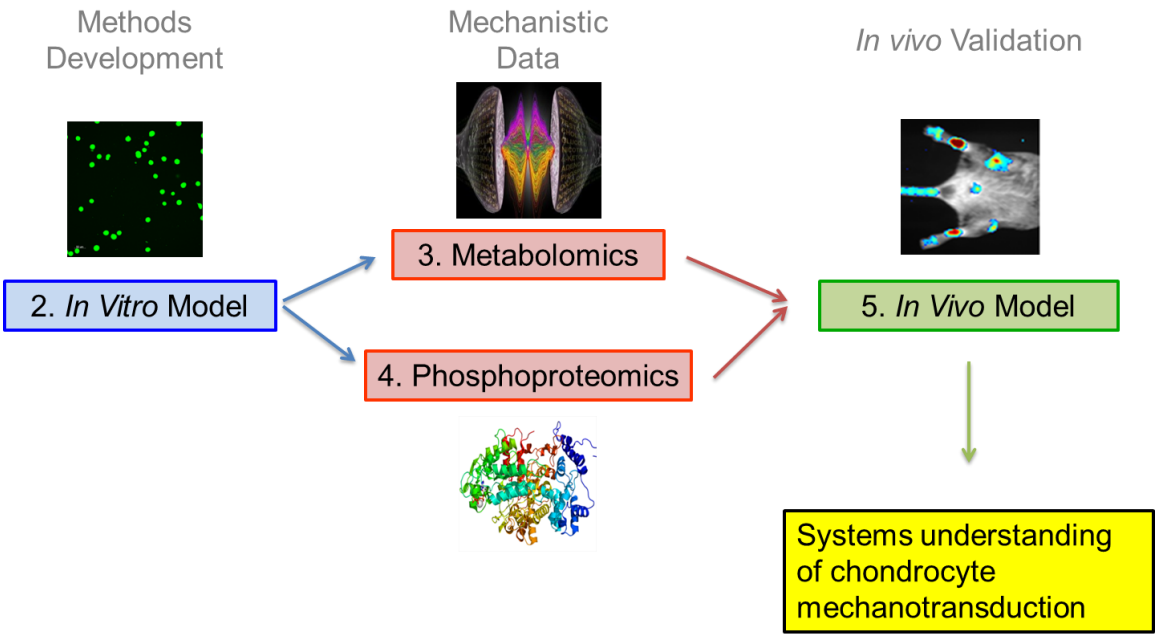

Figure 17. Dissertation workflow. (1) Methods development for the *in vitro* models used for the (2) metabolomics and (3) phosphoproteomics studies. Finally, the (4) *in vivo* model allows for integration and interpretation of the *in vitro* results. All of Chapters combined will help answer will provide a systems understanding of chondrocyte mechanotransduction.

Because chondrocytes are a very specific cell type, and the environment they reside in is highly specialized, controlling the environmental factors for the experiments were extremely important. The second chapter of this dissertation (Figure 17), builds off of previous work [113], and expands the characterization and development of the experimental methodology for the *in vitro* studies (metabolomics and phosphoproteomics). To emulate the physiological loads and environment seen by chondrocytes, a bioreactor (mechanical loading device) was needed, capable of applying well defined static and dynamic loads, as well characterizing the material properties of agarose for physiological, 3D cell constructs [114]. Once completed, it was necessary to characterize the strain homogeneity in the agarose constructs (hydrogels) under applied loading [115]. To ensure the biological outputs of the chondrocytes in response to loading were valid, the deformation, or strain, seen by each cell needed to be the same. After validating the strain homogeneity in the gels, the next step was to determine the viability of chondrocytes in the high-stiffness agarose hydrogels. Following viability assessment, it was necessary to validate that the chondrocytes were capable of being deformed in the hydrogels. The final step of the experimental methodology, was to perform initial metabolomic studies using human SW1353 chondrosarcoma cells embedded physiologically stiff agarose at time intervals of 0, 15, or 30 minutes [116]. Once completed, this *in vitro* model could be applied to explore the mechanosensitive mechanisms in primary human OA chondrocytes.

Following the development of the *in vitro* methodology, the mechanistic data sets (both metabolomics and phosphoproteomics) were developed and generated. The third

chapter of this dissertation delves into the metabolomics studies on mechanically stimulated chondrocytes that were harvested from 5 patients with grade IV OA. The objective of Chapter 3 is to quantify changes in the metabolome for primary human chondrocytes in response to physiological dynamic compression. In this objective, primary human chondrocytes were encapsulated in physiologically stiff agarose, dynamically stimulated with physiological loading values, immediately flash-frozen in liquid nitrogen post-loading and pulverized. Metabolites were extracted and quantified via liquid chromatography-mass spectrometry (HPLC-MS) at the MSU Cobre Mass Spectrometry Core Facility. The objective was to analyze metabolite changes in chondrocytes in direct response to short-duration mechanical compression (0, 15, and 30 minute stimulation). Both untargeted and targeted approaches were used to quantify changes in metabolite levels. The results from this study provided both a global (untargeted) and a more focused (targeted) understanding of the metabolic changes in chondrocytes under mechanical compression.

Similarly, Chapter 4 looks at the same grade IV OA patients but in a phosphoproteomics approach. The objective of this chapter was to quantify protein phosphorylation profiles of primary chondrocytes in response to physiological dynamic compression. Using methods from Chapter 2, and an experimental design similar to Chapter 3, I assessed proteome-wide phosphorylation patterns in chondrocytes as a function of dynamic loading. However, once samples were finished being loaded and flash frozen, proteins were extracted, digested, enriched for phosphopeptides, and then quantified via tandem liquid chromatography-mass spectrometry/mass spectrometry

(HPLC-MS/MS). The results from this study provided a quantification of protein phosphorylation patterns in response to a time course of physiological dynamic compression.

The objective for the final Chapter of this dissertation was to develop novel methods for quantifying changes in cartilage in response to *in vivo* dynamic, mechanical loading on cartilage reporter mice. This Chapter helped validate the *in vitro* results in Chapters 3 and 4 by comparing metabolites with macro-scale imaging obtained in the context of an exercise-induced mouse loading model. This objective was aimed to develop novel methods for studying *in vivo* chondrocyte mechanobiology. Utilizing these novel transgenic mice that express cartilage specific bioluminescence, *in vivo* cartilage quantification was made without mouse euthanization. Two sets of mice were compared in these study; un-exercised, control mice and exercised mice. A custom-built mouse treadmill was used to exercise mice once a day for 30 minutes over a 2 week time span. Un-exercised mice were used as controls to compare cartilage amount against the exercised mice. Following the experimental time course, all of the mice were imaged and then euthanized prior to full-joint, metabolomic analysis. The results allowed for *in vivo* validation and integration of the *in vitro* results from Chapters 3 and 4.

Intellectual Merit

This research substantially expanded the scientific knowledge of chondrocyte mechanobiology (the science of how cartilage cells sense and respond to mechanical loads). To my knowledge, metabolomics, phosphoproteomics, and our *in vivo* mouse

model have not been previously used to study chondrocyte mechanotransduction. This unique approach laid a solid foundation of data for a systems understanding of chondrocyte responses to compressive, mechanical loading. Currently, the only effective OA treatments are surgical, and there are no pharmacological interventions with proven efficacy. This dissertation laid the groundwork to explore specific signaling pathways that could potentially promote loading-induced matrix synthesis. This knowledge could lead to the discovery of new therapeutics to help repair damaged or degenerated cartilage based on mechanical loading. These therapeutic strategies could lead to ground breaking clinical progress in combating the most prevalent joint disorder, osteoarthritis.

Broader Impacts

The successful completion of this dissertation considerably advanced our knowledge of cellular mechanobiology. Currently, most studies focus on individual signaling pathways which have the potential to exclude important data [9]. This research was novel and advantageous since it removes bias, by not excluding pathways *a priori*. By using an unbiased approach, I was able to identify compression-induced changes in levels of metabolites and proteins which were not known. Since the number of mechanosensitive pathways remains unknown, a conservative estimate is that this project increased the known number by a substantial amount. This research provided a valuable contribution to basic science in addition to the potential to discover new, therapeutic strategies to combat OA.

DEVELOPMENT OF EXPERIMENTAL METHODOLOGY

As aforementioned, the research performed in this dissertation is extremely novel. Due to the fact that minimal work has been done in this field, a lot of the experimental methodologies needed to be developed, validated, and optimized. The main objective of Chapter 2 was to develop and optimize the *in vitro* methods used for Chapters 3 and 4. These objectives included (1) characterizing the stiffness properties (Young's Modulus) for various concentrations of agarose hydrogels, (2) evaluate the spatial homogeneity in physiologically stiff agarose under applied compression, (3) determine the feasibility of encapsulating primary human chondrocytes in physiologically stiff agarose, and assess viability of the cells after 24 and 72 hour time points, and (4) quantify metabolite changes in SW1353 chondrocytes in response to physiological, dynamic compression.

Physiological Characterization of Agarose Hydrogels

Introduction

The biological responses of chondrocytes in response to mechanical loading are crucial in understanding how chondrocytes sense and respond to various mechanical cues. To model *in vivo* mechanotransduction studies on chondrocytes, the first goal was to create a physiologically stiff microenvironment for *in vitro* testing. The first milestone was to characterize the material properties for agarose with matched stiffness values to human PCM. A majority of the material characterization was performed by Aaron Jutila for his Master's dissertation [113], but an equal contribution was made by the author and Aaron in developing our 3D, agarose model. The results from this work laid the initial

building blocks for this entire project. It was determined that the agarose concentrations that best matched the human PCM ranged between 3% and 5% (w/v). This is a significant finding because current studies utilize a much lower stiffness for chondrocyte encapsulation (1.5-3% w/v agarose concentration) which could greatly affect chondrocyte mechanotransduction experiments [117-119]. By using a more representative stiffness (3-5% w/v agarose concentration) for chondrocyte mechanotransduction studies, we can more accurately model physiological loading scenarios.

Methods

Agarose hydrogels were prepared by dissolving low-gelling-temperature agarose (Sigma: Type VII-A A0701), in PBS at 1.1X of desired hydrogel concentration. For example, for 4% (w/v) final concentration, agarose was initially mixed at 4.4% (w/v). Concentrations tested were 3, 3.5, 4, 4.5, and 5 (%w/v). After approximately 5 minutes, the dissolved agarose was diluted to 1X with PBS (40°C). Note that this procedure is readily applied to encapsulating cells [120, 121]. Once the entire agarose solution was equilibrated to ~40°C, the agarose was cast in an anodized aluminum mold (Figure 18). The mold produced cylindrical samples with heights of 12.7 ± 0.1mm and diameters of 7.0 ± 0.1mm (aspect ratio, h/r = 3.6). This specific sample geometry was selected to provide spatially homogeneous strain fields under uniaxial deformations [122]. When gels solidified (after ~5 min.), gels were removed and stored in PBS at 4°C for 1-2 days prior to testing consistent with standard mechanotransduction protocols [123, 124].

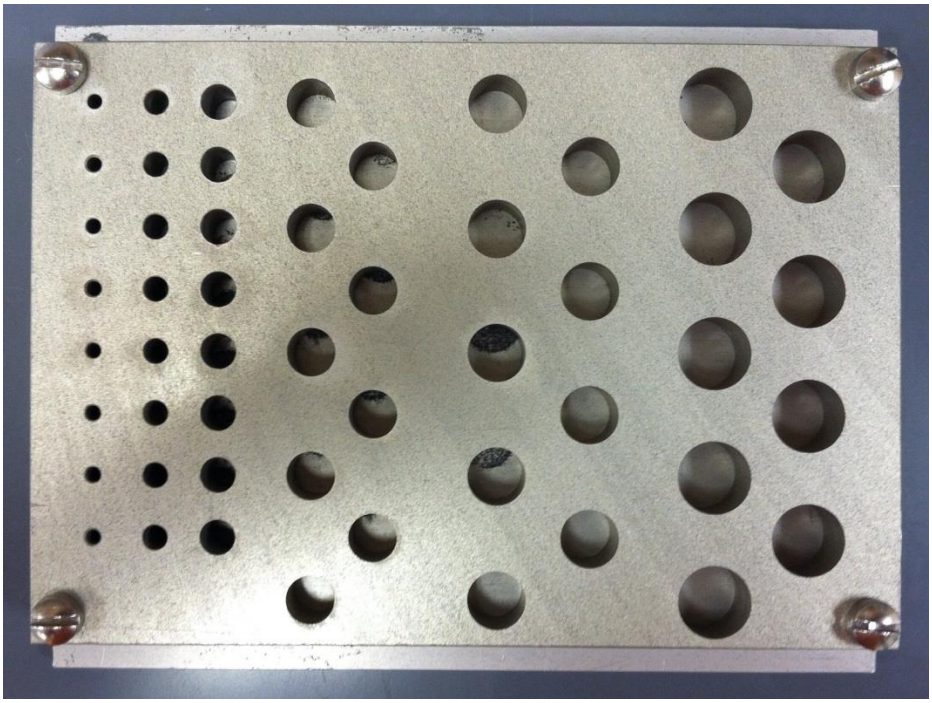

Figure 18. Agarose hydrogel mold. Gel dimensions were approximately 12.7 mm tall by 6.5 mm wide.

Samples were removed from the fridge, equilibrated in PBS at 37°C for 30 minutes, and tested on a custom-built bioreactor [113] (Figure 19A). The bioreactor was designed to allow for testing in an incubator under tissue culture conditions (humidified 5% CO2 atmosphere and operating temperature of 37°C). Samples were loaded vertically in polysulfone cups and completely covered in PBS to prevent dehydration of the samples during testing. The polysulfone cups were loaded into the trays of the bioreactor, which sat on top of a load cell (Futek) to give force feedback during testing. The forcing platens of the bioreactor were loaded until sample contact was made, as visualized from a measured load change (~0.089 N). The sample was allowed to relax for approximately 10 minutes before mechanical stimulation. For all tests, both

displacement and load data was measured. Displacement data was measured using a laser displacement sensor (Acuity AR200-6), and load was measured using a 10lb. capacity load cell (Futek).

For the stepwise stress-relaxation tests, the samples were subjected to 4 steps of 4% compressive, Lagrangian strain [113]. Each strain step was held for 90 minutes. Both dynamic and equilibrium moduli values were calculated by performing linear regression on their appropriate stress and strain values over the 4 deformation steps. This was performed for the entire range of agarose concentrations with n = 5 samples for each. To test the hydrogels, our custom-built bioreactor with sub-micron precision was used [113] (Figure 19A). Stepwise stress-relaxation tests were used to characterize the dynamic and equilibrium moduli of a visco-elastic material by applying a prescribed strain level and holding it constant over a period of time. The strain is then increased, held constant and repeated "n" number of times (Figure 19B). When the strain is applied, the resulting stress in the material has an initial response (dynamic), and relaxes exponentially over time to an equilibrium position (Figure 19C). The dynamic modulus is characterized from the initial dynamic response (peak stress value divided by associated strain value), and the equilibrium modulus is characterized by the material's equilibrium stress value divided by associated equilibrium strain value.

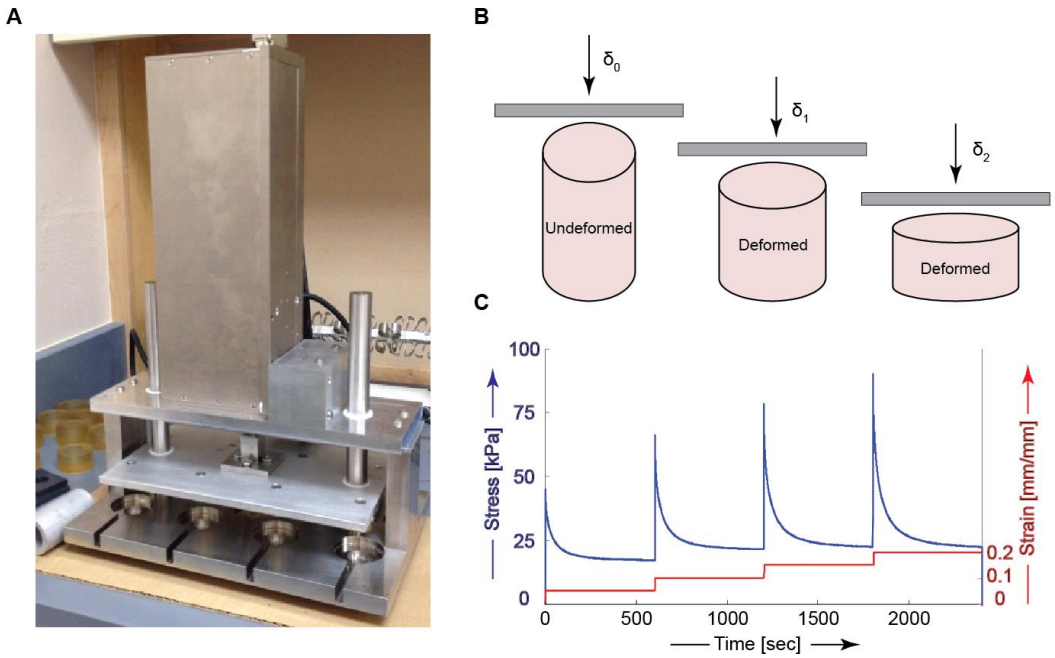

Figure 19. (A) Custom built bioreactor with sub-micron precision [113]. This bioreactor is capable of applying static and dynamic compression to up to 9 samples simultaneously. For agarose stiffness characterization, (B) step relaxation tests were performed by incrementally compressing the samples and (C) computing stress and strain values from experimentally determined displacement and load values.

For all tests, a low-gelling temperature (Sigma: Type VII-A A0701) was used. A low-gelling temperature agarose was selected to allow for encapsulation of chondrocytes without killing the cells (encapsulation had to be performed <37°C). The gelling temperature of the agarose refers to the temperature at which the agarose changes from an aqueous solution into a gelatin state upon cooling. For the agarose hydrogels, a range of concentrations were tested (3-5% w/v), and their appropriate moduli determined.

Results & Conclusion

Stepwise stress-relaxation results show an increasing trend of agarose stiffness with respect to agarose concentration (Figure 20). Equilibrium moduli were 18.9 ± 0.77

kPa, 26.0 ± 1.58 kPa, 34.3 ± 1.65 kPa, 35.7 ± 0.95 kPa, and 42.0 ± 2.88 kPa for agarose concentrations of 3, 3.5, 4, 4.5, and 5% (w/v), respectively. Dynamic moduli were determined to be of 39.4 ± 4.5 kPa, 52.3 ± 1.9 kPa, 64.4 ± 3.1 kPa, 55.5 ± 3.5 kPa, and 78.4 ± 3.2 kPa for the range of agarose gels, respectively. A significant relationship between the calculated stiffness values and the gel concentration (dynamic, $r = 0.78$, $p < 0.001$, and equilibrium $r = 0.91$, $p < 0.001$) was determined.

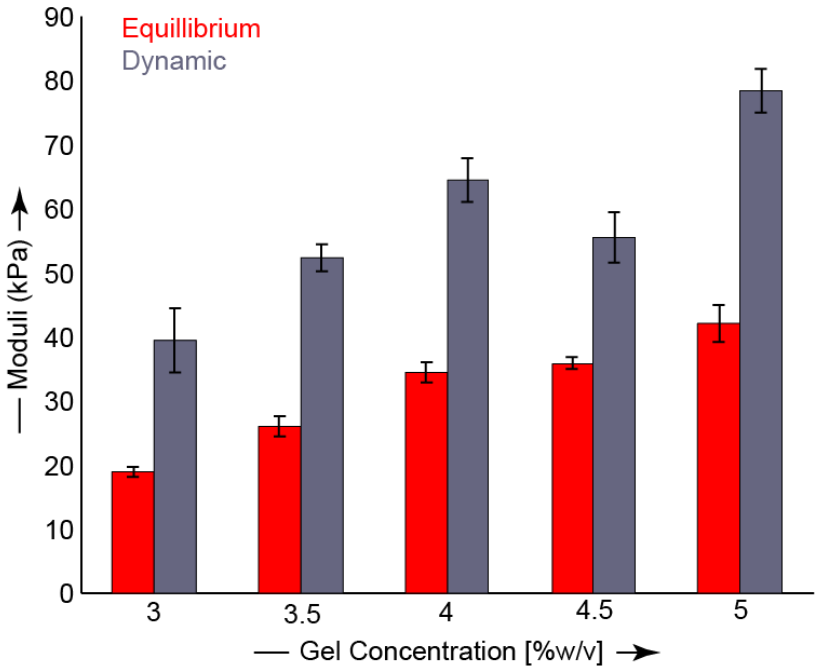

Figure 20. Equilibrium (red) and dynamic (gray) moduli values for 3-5% [w/v] agarose. Modulus value (kPa) is given on the vertical axis and increase gel concentration on the horizontal axis [113].

The dynamic modulus can be thought of as the materials initial, elastic response/stiffness to a rapidly induced mechanical deformation. The equilibrium modulus is the materials stiffness in response to a more relaxed, slower induced deformation. Recalling our goal of creating a physiologically stiff environment for

chondrocyte encapsulation, we find that 3-4% agarose provides a stiffness perfect for modeling OA PCM (~25 kPa), and 4.5-5% agarose provides a stiffness matched to healthy PCM (~40 kPa). This is a significant finding because current studies utilize a much lower stiffness for chondrocyte encapsulation (1.5-3% w/v agarose concentration) which could greatly affect chondrocyte mechanotransduction experiments [117-119]. By using a more representative stiffness (3-5% w/v agarose concentration) for chondrocyte mechanotransduction studies, we can more accurately model real life loading scenarios. This research was published in the Annals of Biomedical Engineering in November, 2014 [114]. The work in this publication was a joint effort between the author and Aaron Jutila, and can be seen in APPENDIX A**.**

Following the material property characterization for the agarose hydrogels, the next goal was to assess the strain homogeneity of the hydrogels under applied deformation. It was necessary to validate the homogeneity of the mechanical deformations in the agarose hydrogels for the chondrocyte mechanotransduction studies (Chapters 3 and 4). Because these two *in vitro* studies are looking into the metabolomic and phosphoproteomic profiles of the chondrocytes in response to mechanical loading, the deformations applied to each of the individual, encapsulated cells needed to be similar. If the applied deformations were not similar, then the biological outputs of the chondrocytes could be a result of the inhomogeneous mechanical loading. However, if the deformations were similar, then the differences in results could signify loading induced changes within the cells.

THE MECHANICAL MICROENVIROMENT OF HIGH CONCENTRATION AGAROSE FOR APPLYING DEFORMATION TO PRIMARY CHONDROCYTES

Contribution of Authors and Co-Authors

Author: Donald L. Zignego[1]

Contributions: Acquired, analyzed, and interpreted the data. Drafted and wrote the manuscript.

Co-Author: Aaron A. Jutila[1]

Contributions: Interpreted data and revised the manuscript.

Co-Author: Martin K. Gelbke[2]

Contributions: Acquired samples and reviewed the manuscript.

Co-Author: Daniel M. Gannon[2]

Contributions: Acquired samples and reviewed the manuscript.

Corresponding Author: Ronald K. June[1,3]

Contributions: Designed the study, analyzed and interpreted the data, and wrote the manuscript.

[1]Department of Mechanical and Industrial Engineering, Montana State University, Bozeman, MT 59717-3800, USA

[2]Bridger Orthopedic and Sports Medicine, Bozeman, MT 59715, USA

[3]Department of Cell Biology and Neuroscience, Montana State University, Bozeman, MT 59717-3800, USA

Manuscript Information Page

Donald L. Zignego, Aaron A. Jutila, Martin K. Gelbke, Daniel M. Gannon, and Ronald K. June.
Journal of Biomechanics
Status of Manuscript:
___ Prepared for submission to a peer-reviewed journal
___ Officially submitted to a peer-reviewed journal
___ Accepted by a peer-reviewed journal
_X_ Published in a peer-reviewed journal

Publisher: Elsevier for the American Society of Biomechanics
Issue: June 27th, 2014, Vol. 47, Issue 9, Pages 2143-2148

Abstract

Cartilage and chondrocytes experience loading that causes alterations in chondrocyte biological activity. *In vivo c*hondrocytes are surrounded by a pericellular matrix with a stiffness of ~25-200 kPa. Understanding the mechanical loading environment of the chondrocyte is of substantial interest for understanding chondrocyte mechanotransduction. The first objective of this study was to analyze the spatial variability of applied mechanical deformations in physiologically stiff agarose on cellular and sub-cellular length scales. Fluorescent microspheres were embedded in physiologically stiff agarose hydrogels. Microsphere positions were measured via confocal microscopy and used to calculate displacement and strain fields as a function of spatial position. The second objective was to assess the feasibility of encapsulating primary human chondrocytes in physiologically stiff agarose. The third objective was to determine if primary human chondrocytes could deform in high-stiffness agarose gels. Primary human chondrocyte viability was assessed using live-dead imaging following 24 and 72 hours in tissue culture. Chondrocyte shape was measured before and after application of 10% compression. These data indicate that (1) displacement and strain precision are ~1% and 6.5% respectively, (2) high-stiffness agarose gels can maintain primary human chondrocyte viability of >95%, and (3) compression of chondrocytes in 4.5% agarose can induce shape changes indicative of cellular compression. Overall, these results demonstrate the feasibility of using high-concentration agarose for applying *in vitro* compression to chondrocytes as a model for understanding how chondrocytes respond to *in vivo* loading.

Introduction

Osteoarthritis (OA) is the most common joint disorder, affecting over 100 million individuals [6]. OA is most commonly associated with excessive loading of aging joints (*e.g.* caused by obesity or injury), leading to deterioration of articular cartilage and joint inflammation. Articular cartilage is located at the surfaces of joints, and serves as a low-friction material between bones. Articular cartilage is composed of articular chondrocytes (cartilage cells), the pericelluar matrix (PCM), and the extracellular matrix (ECM) [125]. In these regions of the body (*e.g.* the knee), the articular cartilage, and thus articular chondrocytes, are subjected to almost-constant mechanical loading (*e.g.* walking, running, etc…). Repetitive action is crucial for joint health, yet excessive loading can lead to OA [8]. Individuals with a history of heavy mechanical work (*e.g.* heavy lifting) are ~7-fold less likely to have OA at the age of 90 [3], suggesting that long-duration, but sub-injurious, mechanical loading may induce protective biological responses. Therefore, understanding the biological responses of chondrocytes to mechanical loading are extremely important to improving joint health. These data emphasize the need for development of fundamental knowledge regarding how chondrocytes and other joint cells sense and respond to mechanical loads, a process defined as mechanotransduction [49]. This paper characterizes the deformational environment of a stiff 3D hydrogel for use in cartilage mechanotransduction studies.

Exogenous dynamic compression can substantially alter chondrocyte metabolism in both an anabolic and catabolic manner, but the balance between matrix synthesis and matrix degradation is not yet fully understood [75, 76]. Dynamic compression can

induce phosphorylation of multiple enzymes, including MAPK and SEK [78, 79], Akt [80], Erk -1 and -2 [81-83], and Rho kinase [84]. Additionally, exogenous loading can alter Superficial Zone Protein expression [87], induce transcription of ECM genes [9], and activate RhoA [84]. Cyclic dynamic compression can promote Smad2 phosphorylation [85], gene expression of MMP-13 [86], which is the marker for catabolic changes in the ECM, and increases in ATP release [126]. These studies demonstrate the sensitivity of chondrocytes to mechanical loading and indicate that a complete understanding chondrocyte mechanotransduction remains to be determined.

A variety of hydrogels have been utilized including photo cross-linked polyethylene glycol [43], self-assembling peptides [67], alginate [68], and agarose [69, 70]. Most existing studies utilize 3D microenvironments (*e.g.* agarose or alginate) for cell encapsulation with a much lower stiffness (< 5 kPa) than the cartilage pericelluar matrix (25-200 kPa) [47, 73]. Agarose hydrogels are of particular interest because the stiffness can be selected to match the stiffness of cartilage PCM [71] without potential complications of UV photo crosslinking (*e.g.* induction of the DNA damage response [72]). This study characterizes the deformational environment of high-stiffness (~35 kPa) agarose gels. To our knowledge, chondrocyte mechanotransduction studies have never been performed using agarose with PCM stiffness.

Cartilage experiences a variety of *in vivo* loading. The motivation for this study is to characterize the micro-level deformation fields in a physiologically stiff, 3D culture environment, to study how chondrocytes sense and respond to mechanical loading. Using a bioreactor capable of applying sub-micron precision, displacement-controlled

loading to agarose hydrogels during confocal microscopy, this study describes (1) the cellular-level deformation fields in agarose hydrogels under mechanical compression, (2) the encapsulation of primary human chondrocytes in agarose hydrogels with stiffness matched to human PCM (25-200 kPa) [47, 114, 127], and (3) the ability to apply uniform compression to embedded cells.

To minimize experimental variability when applying *in vitro* loads to 3D chondrocyte cultures, applied deformations must be spatially homogeneous throughout the hydrogels to avoid spatially-distinct mechanical stimuli. The first objective of this study was to analyze the spatial variability of applied mechanical deformations in physiologically stiff agarose on cellular and sub-cellular length scales. Fluorescent microspheres were used as fiducial markers within agarose hydrogels, which were compressed uniaxially during confocal imaging. Microsphere positions were tracked with 2D-Cartesian coordinates over a range of ~250 μm. These data were used to calculate the displacement and strain fields at multiple locations with spatial resolution of ~5 μm.

The second objective was to assess the feasibility of encapsulating primary human chondrocytes in physiologically stiff agarose, and the third objective was to determine if primary human chondrocytes could deform in high-stiffness gels. Primary chondrocytes were isolated from discarded joint replacement tissue and encapsulated in agarose, and viability was assayed via live-dead staining. The results of this study indicate that (1) applied deformations have minimal spatial variability and strain bias, (2) primary chondrocytes can maintain high viability through 72 hours, and (3) human chondrocytes

can be deformed in physiologically stiff agarose. Future studies may use this system to elucidate cellular mechanisms of chondrocyte mechanotransduction.

Methods

Encapsulation of Fluorescent Microspheres in Physiologically Stiff Agarose. Agarose hydrogels were prepared by dissolving low-gelling-temperature agarose (Sigma: Type VII-A A0701), in PBS at 1.25X of desired hydrogel concentration. For example, for 4% (w/v) final concentration, agarose was initially mixed at 5% (w/v). Fluorescent microspheres (Molecular Probes: Constellation Microspheres, diameter 1-5μm) were added to the agarose (~40°C and 25% w/v) to reduce to the final, desired agarose concentration. Microspheres were vigorously vortexed to distribute them evenly throughout the liquid hydrogel. Gels were then cast in an anodized aluminum mold at 23°C, which produced cylindrical hydrogels with a height of 12.7 ± 0.1 mm and diameter of 7.0 ± 0.1mm (aspect ratio 3.62). The sample geometry was selected to provide uniaxial deformations consistent with spatially homogeneous strain fields [122]. Agarose concentrations were 3, 3.5, 4, 4.5, and 5% (w/v) based on previous stiffness data with n=3 replicates for each concentration [128]. Gels were removed from the mold after 5 minutes and stored in PBS at 4°C until testing.

Mechanical Loading and Confocal Imaging. Samples were bisected longitudinally and placed into the loading tray of a custom-built loading device (Figure 21A & B) mounted to an upright confocal microscope (Leica SP5). The device delivers high-precision compression via displacement control to the hydrogel samples and is

capable of applying displacements from 12.7 μm to 12.7 mm. These displacements can be delivered over a range of speeds as low as 12.7 μm / s and as fast as 12.7 mm / s. The loading platen was moved until contact with the gel was achieved as defined visually through the microscope. 50 mL of 0.15 M PBS was then added to the tray to maintain gel hydration. This preloading process required ~5 minutes to complete. The objective (0.9 NA water objective with x-y resolution of 200 nanometers and z resolution of 600 nanometers) was lowered into the PBS and the fluorescent beads were viewed using TRITC fluorescence (excitation: 547nm, emission: 572nm). Samples were compressed serially for a total of 20 steps at 25.4μm increments followed by a 3 minute relaxation period to accommodate agarose stress-relaxation. Six unique locations (Figure 21C) were tested in each gel to evaluate the spatial homogeneity in the hydrogels.

Particle Tracking and Finite Deformation Evaluation. Following confocal imaging, datasets were input into imaging software (Imaris, Bitplane, South Windsor, CT) for image processing and particle tracking. Each dataset included a 3-dimensional image of the gel for every loading step (20 images total) which was projected onto 2D for further analysis (Figure 22). Images were thresholded and particles (fluorescent microsphere) were tracked over 20 time steps giving a unique x, y, and z location for >90% of particles at each time step using Imaris software. About 600 particles (range 400-800) were tracked in each gel over the course of the applied compressive deformations.

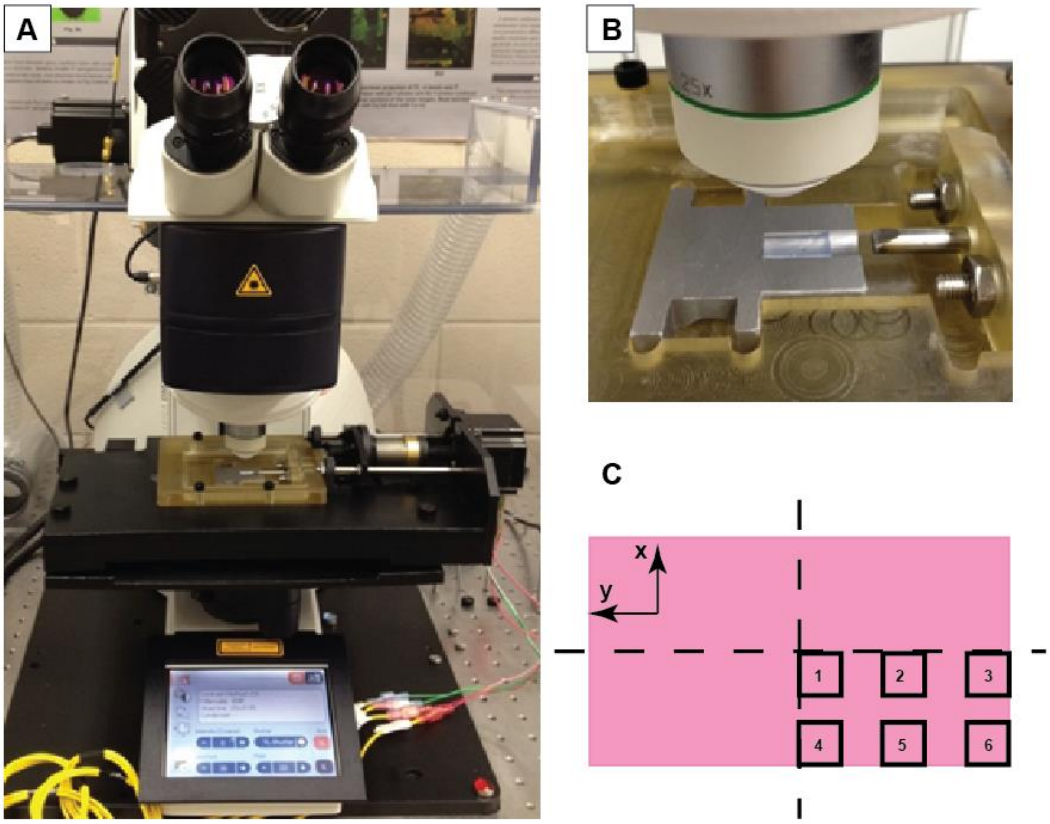

Figure 21. Approach for measuring micron-level deformations within agarose gels. (A) Custom-built loading machine for applying controlled displacements to soft biological samples. (B) This device was designed to be mounted on the platform of an upright confocal microscope and be capable of viewing bisected hydrogel samples using fluorescence imaging techniques. Actuation is provided by a linear stepper motor (Haydon Kerk K57H43-3.25-081ENG, Waterbury, CT). (C) Spatial sampling protocol. Six images (1-6) were taken of each gel during compression to evaluate the spatial homogeneity of the induced deformations. These sampling locations are based on the symmetry of the boundary conditions assuming frictionless contact. Compression was applied in the positive y-direction.

Particle displacements were calculated directly from the position data. Displacements were then input into Matlab to calculate finite deformations and strains using previously-validated techniques [129, 130]. Displacement field smoothing was performed on all displacement data according to common methods [131]. In order to

minimize the amplification of errors we incorporated a Gaussian smoothing filter into our data processing.

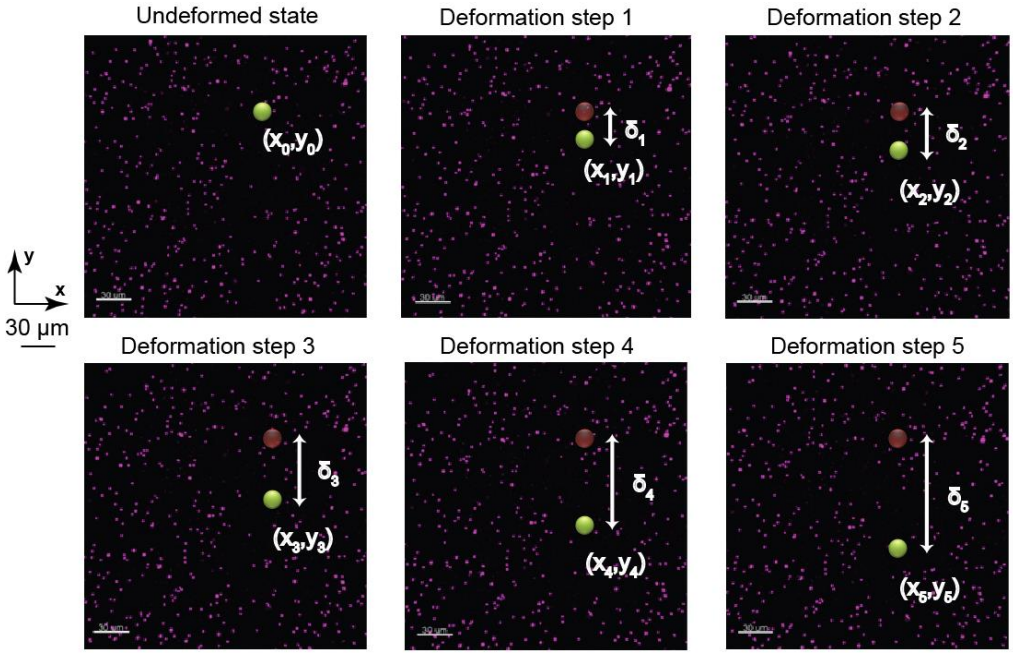

Figure 22. Two-dimensional displacement measurement. Bead displacements, δ, were measured by automated tracking of ~500 beads in each field of view. Displacements were calculated from particle (bead) positions after each displacement step. Final displacement steps were used to evaluate the spatial homogeneity for each gel location. A total displacement of 508 µm was applied to each gel in increments of 25.4 µm followed by 3 minutes of stress-relaxation prior to imaging. Gels were excited using TRITC fluorescence and images recorded after each loading step. Scale bar is 30 µm.

We applied a 5 x 5 box-sized Gaussian filter to the displacement data with 100 iterative smoothing cycles prior to evaluation of the strain fields. To assess the potential for displacement measurement error to propagate, we added random noise to our displacement measurements prior to strain calculation. Green-Lagrangian finite strain values were derived directly from displacement data as follows:

$$E = \frac{1}{2} \cdot (F^T F - I)$$

Where I is the identity matrix and the deformation tensor F is defined as:

$$F = \frac{\partial x_t}{\partial x_0}$$

At a fixed time t the deformation gradient is a function of the actual position vector x_t and the initial position vector x_0.

The calculated deformation variables were: displacements in the direction of loading (Uy), displacements perpendicular to loading (Ux), finite strains in the direction of loading (Eyy), finite strains perpendicular to loading (Exx), and finite shear strains (Exy). Note that z-displacements were not measured in this study. Due to the high density of particles in each image required for the high spatial resolution, the particle tracking software occasionally identified incorrect particles for tracking (*e.g.* in a particular displacement step, particle A was obscured by particle B resulting in missing displacement data for particle A in this step.) These errors presented themselves as abnormally large or small displacements when comparing against the entire displacement dataset. An 85% confidence interval for bead displacement was used to mitigate these random errors. The average displacement value at the final loading step was calculated, and displacements that were outside of 1.44 standard deviations were discarded. This process was selected based on a pilot study which determined the coefficient of determination (R2) as a function of the confidence interval for displacement processing. This study found that a confidence interval of 85% achieved the R2 value to be expected for calculation of finite Lagrangian strain based on the observed deformation gradients (Supplemental Figure 7).

Chondrocyte Encapsulation. Primary human chondrocytes were embedded in agarose of varying concentrations. Chondrocytes were harvested from discarded joint replacement cartilage from human donors (Informed consent obtained under an IRB-approved human subjects exemption), digested in Type IV collagenase (2 mg/mL for 12-14 hrs. at 37°C), and then cultured in DMEM with 10% fetal bovine serum and antibiotics (10,000 I.U./mL penicillin and 10000 μg/mL streptomycin) in 5% atmospheric CO2. For encapsulation, cells were trypsinized, counted, and re-suspended in media at 11X. Agarose was autoclaved and prepared as described above. The cell-suspension was added to the agarose with gentle vortexing to distribute the cells throughout the liquid hydrogel. Gels were subsequently cast for 5 minutes at 23°C. Cell-seeded agarose constructs were removed from the molds and placed in tissue culture for 24 and 72 hours prior to viability analysis.

Viability Analysis and Induced Deformations on Primary Chondrocytes. To assess the feasibility of the encapsulation process, we assessed viability using standard methods [132]. Cells were incubated in 8 μM calcein-AM and 75 μM propidium iodide for 30 min. at 37 °C. Following incubation, constructs were examined by confocal microscopy for calcein-AM fluorescence (excitation: 496 nm, emission: 516 nm) indicating live cells via intracellular thioesterase activity and propidium iodide fluorescence (excitation: 536 nm, emission: 617 nm) indicating dead cells via DNA binding indicative of compromised plasma membranes. Confocal images were acquired from 6 positions (Figure 21C) within each hydrogel to assess potential spatial variability in cell viability. To determine if deformations could be induced on embedded primary

chondrocytes, hydrogels were compressed uniaxially using the loading device described above. Constructs were compressed to 10% strain over 1 minute. Stress-relaxation was allowed to proceed for 10 minutes prior to confocal imaging. Uncompressed control images (aspect ratio width/height = 1) were used to compare against compressed images (10% axial compression).

Results

The spatial homogeneity of each gel concentration was evaluated by comparing the final loading step displacement and strain values at six unique locations in each gel. For each gel concentration we found displacement and strain fields with minimal variability from all six gel locations (Figure 23,

Figure 24, & Supplemental Figure 8). Axial finite strains, (Eyy) were 2.01 ± 0.08, 1.65 ± 0.11, 1.33 ± 0.10, 1.11 ± 0.08, and 0.98 ± 0.07 for 3, 3.5, 4, 4.5, and 5% agarose, respectively (Figure 23A,

Figure 24B, & Supplemental Table 5). Transverse finite strains (Exx) and shear strains (Exy) were minimal for all agarose concentrations (Figure 23B and C, Supplemental Table 5). Error analysis indicated that the observed displacement precision resulted in errors in Eyy strain of ~1% (Supplemental Figure 9). We found high viability which was independent of spatial position, indicating a homogeneous distribution of viable cells (Figure 25, Supplemental Table 6). All average viability measures were ≥ 96.2%. Deformations were applied to agarose constructs containing embedded primary chondrocytes. Cellular geometry was identified with Calcein AM fluorescence, and compressed images showed the cross sections of uncompressed cells to be circular

(width/height of 1.00 ± 0.00) and the compressed cells to be ellipsoidal (Figure 26). Cells in 4.5% agarose exhibited greater deformation than cells in 4.5% agarose as quantified by the aspect ratio of chondrocyte width to height ($p < 0.001$. 2%: 1.07 ± 0.06. 4.5%: 1.28 ± 0.04.). For chondrocytes in 4.5% agarose, the coefficient of variation of the aspect ratio was 3.1% indicating the uniformity of applied compression to the embedded cells.

Discussion

The objectives of this study were to (1) assess the spatial variability of mechanical deformations in physiologically stiff agarose on a sub-cellular length scale, and (2) determine if it is possible to encapsulate live primary human chondrocytes in physiologically-stiff agarose, maintain viability, and induce deformations on the embedded cells. We determined the spatial homogeneity in each gel by assessing displacements and strains at six spatial locations in each gel over an array of pre-determined agarose concentrations (3-5% w/v) which result in stiffness values in the range of the human PCM [47, 114, 127].

When computing strain fields from experimental data, noise is capable of skewing results and requires preliminary filtering of the displacement data [129]. In this study, displacements were calculated directly from individual particle locations within the hydrogels during the twenty steps of applied compression. Displacements at each step were calculated with respect to the undeformed particle locations of the first loading step. A 5x5 box-sized Gaussian filter was applied to the displacement data in order to increase the precision of the calculated strain fields [131].

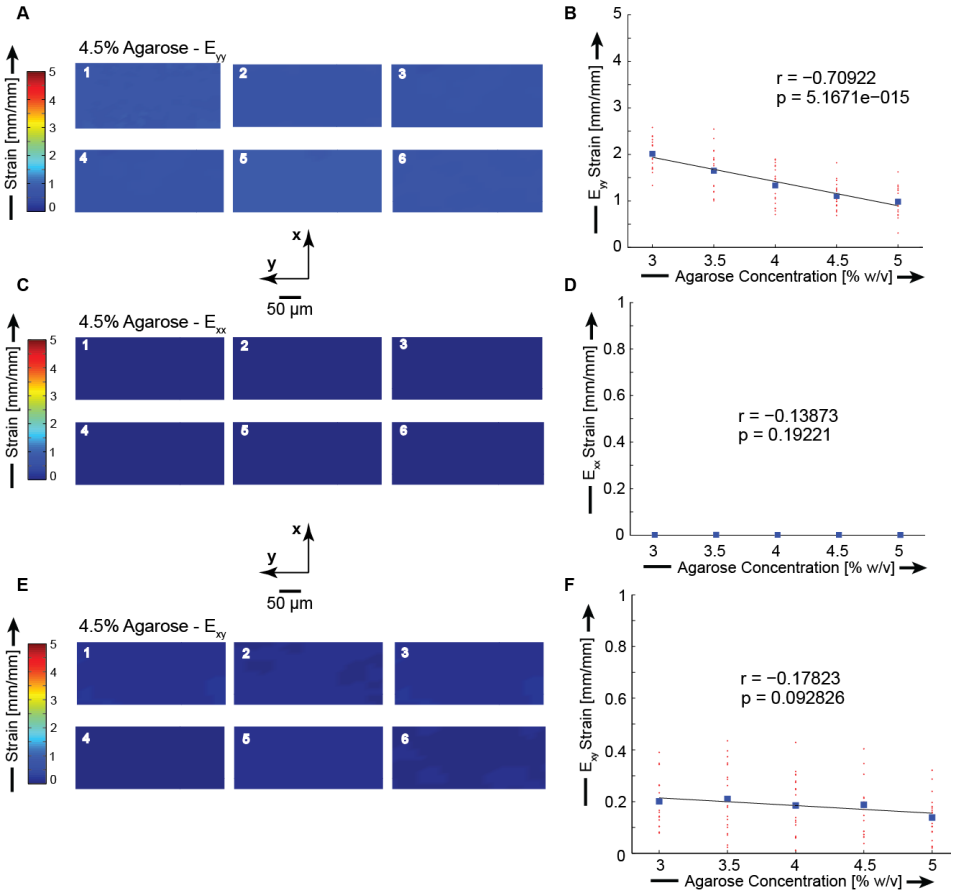

Figure 23. Finite deformation Lagrangian strain fields within 4.5% agarose hydrogel. Strains were calculated using a finite deformation code in Matlab [129]. The axial (Eyy), transverse (Exx), and shear (Exy) strain fields for 4.5% agarose are plotted. Axial strains were calculated to be 1.11±0.08 [mm/mm]. Transverse strains were calculated to be 0.01±0.00 [mm/mm]. Shear strains were calculated to be 0.18±0.02 [mm/mm]. (A) Representative axial strain image Eyy. (B) Axial strain Eyy as a function of agarose concentration. (C) Representative transverse strain Exx. (D) Transverse strain Exx as a function of concentration. (E) Representative shear strain Exy. (F) Shear strain Exy as a function of concentration.

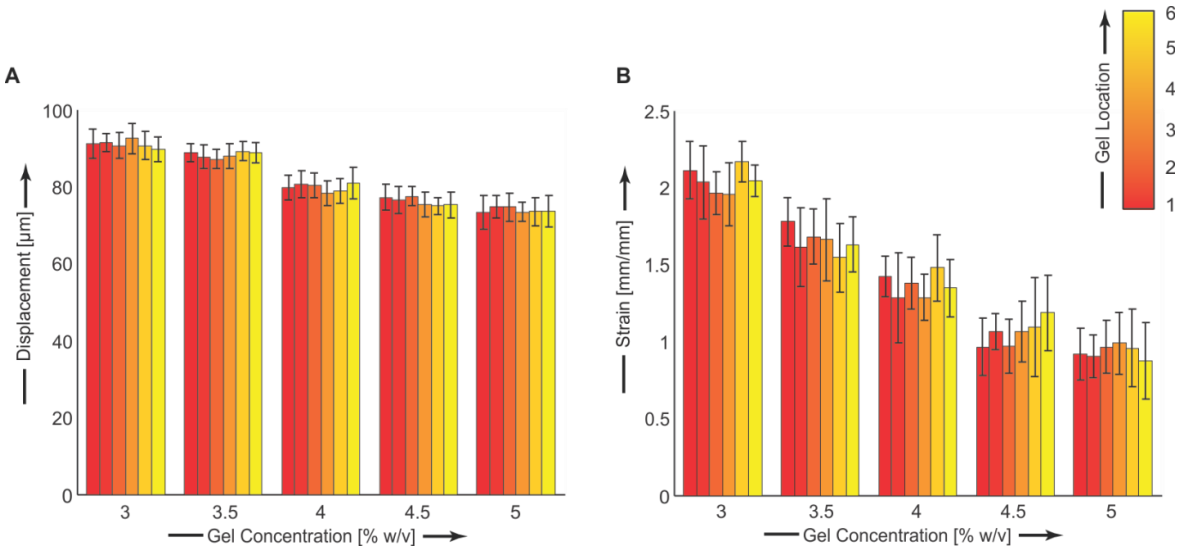

Figure 24. Axial displacement (A) and strain (B) as functions of gel position and agarose concentration. We found a significant relationship for Uy ($r=-0.8466$ and $p<0.001$) and Eyy ($r=-0.71$ and $p<0.001$) between agarose gel concentration and bead deformations, and indicating that the stiffer, higher-concentration gels resulted in smaller bead displacements and strains, as expected. Locations as defined in Figure 21C.

Once the data was filtered, it was input into a finite deformation code in Matlab for strain field calculation [129]. The finite deformation code utilizes a 2D-continuum mechanics approach where Green-Lagrange strain fields are calculated from discretely sampled displacement fields. The code calculates the finite deformation tensor, F, and the Green-Lagrange strain tensor, E, from experimental particle position data. The random spacing of the beads may induce error into the in the strain calculation because larger distances between neighboring particles, will result in larger discretization error. While this may affect the magnitude of the strain values, the objective of this study was to evaluate the homogeneity of the displacement and strain fields, and this error was mitigated by the displacement field smoothing prior to strain calculation.

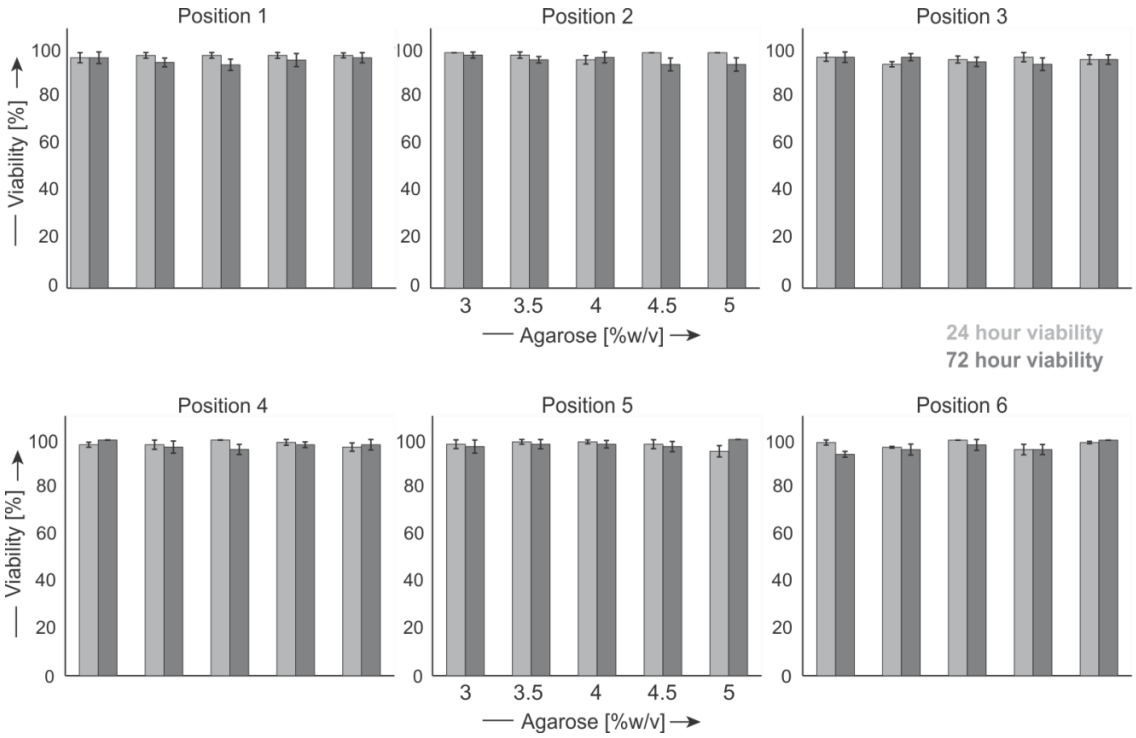

Figure 25. Viability of primary human chondrocytes in high concentration agarose gels after 24 and 72 h. Primary human chondrocytes were harvested from joint replacement tissue (Bridger Orthopedic, Bozeman, MT), digested in Type IV collagenase (2 mg/mL for 12–14 h. at 37 °C), cultured, encapsulated in physiologically-stiff agarose (3–5% w/v), and assessed for viability after 24 and 72 h using confocal microscopy. Live cells were identified with Calcein AM fluorescence (ex. 497 em. 516) and dead cells with propidium iodide fluorescence (ex. 537 em. 617). All six gel locations were imaged showing minimal variability in cell viability throughout the gel. Average viability was >97% and >95% for 24 and 72 h time periods, respectively.

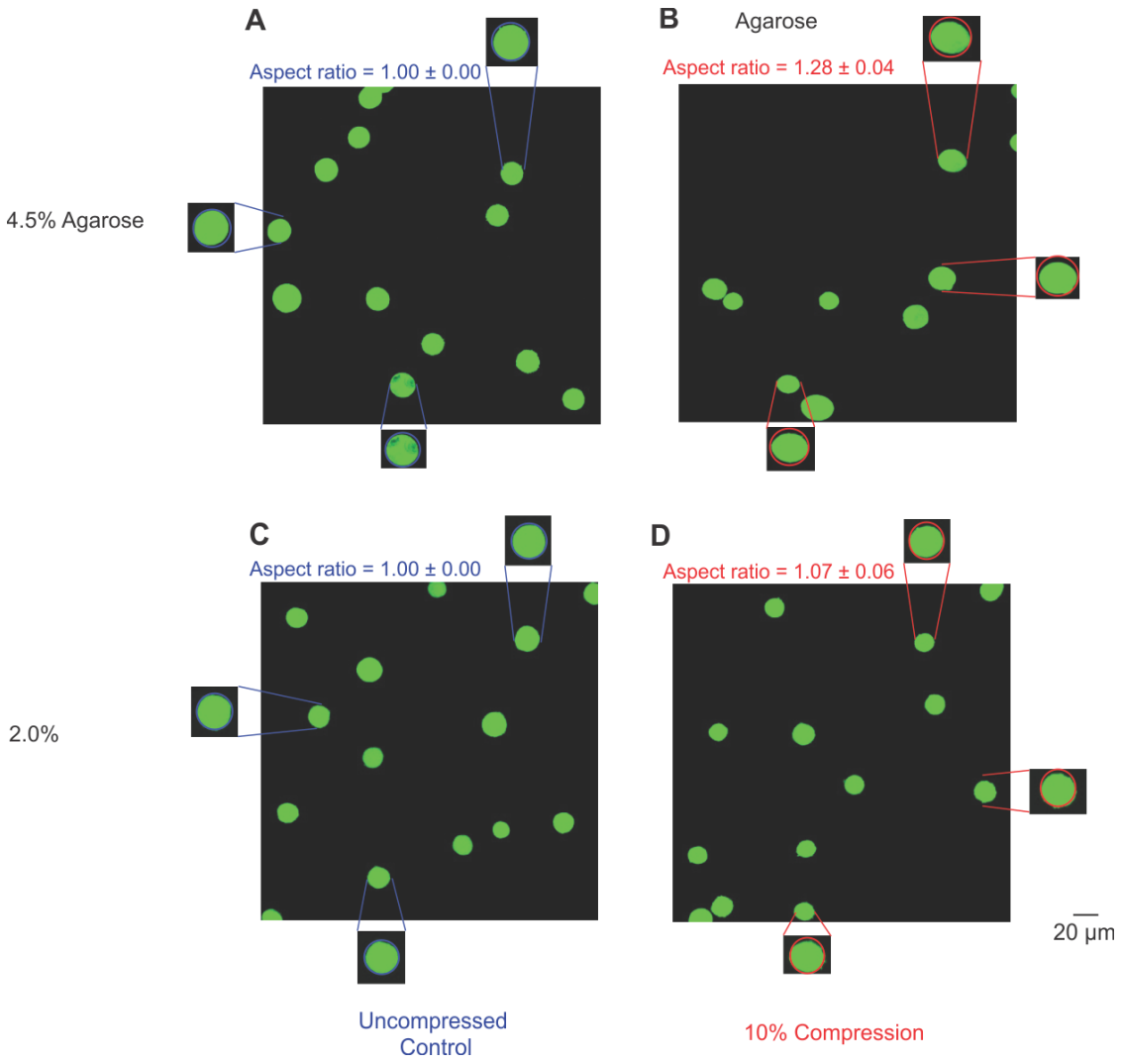

Figure 26. Deformation of primary human chondrocytes in 2.0% and 4.5% agarose. To examine deformations to chondrocytes in typical stiffness (2.0%) and high stiffness (4.5%) agarose, primary human chondrocytes were cast into agarose hydrogels, equilibrated in culture for 72 h, and imaged before and after a 10% nominal compression. Deformations were quantified via the aspect ratio (width/height). Aspect ratios were significantly greater following 10% compression in 4.5% agarose compared with 2.0% ($p<0.001$). Left panels (A and C) show representative uncompressed images. Right panels (B and D) show images following 10% nominal compression. Top row (A and B) shows data for 4.5% agarose. Bottom row (C and D) shows data for 2.0% agarose. A total of n~150 cells were measured for aspect ratio in each condition.

Conclusions

These data demonstrate the ability to apply compressions to physiologically stiff agarose hydrogels with absolute displacement precision of ~1% and absolute strain precision of ~6.5% (*e.g.* application of nominal 10% strain would result in strains between 9.35 and 10.65%). This minimal variability in displacement and strain fields between different spatial locations in each gel implies spatial homogeneity and demonstrates the utility of using this system to apply well-defined strains to primary human chondrocytes and other cells to study cellular mechanotransduction. This study also demonstrated the feasibility of encapsulating primary human chondrocytes in physiologically stiff agarose gels while maintaining high viability. Finally, this study found that 4.5% agarose was capable of physically deforming primary human chondrocytes. These results provide a robust methodological foundation for future studies investigating how chondrocytes respond to mechanical cues: using this system, we can now apply a uniform mechanical stimulus which is necessary to minimize biological variability when dissecting mechanisms of mechanotransduction.

Acknowledgements

The authors thank Professor Marc Geers from Eindhoven University of Technology, The Netherlands, for providing his custom strain computation code and Ms. Betsey Pitts, Montana State University, Center for Biofilm Engineering, for assistance with the confocal imaging. This work was funded by NIH P20 GM103394 and startup funds from Montana State University, Vice President for Research.

Role of Funding Source

The funding source was not involved in study design or performance.

Conflict of Interest

The authors have no conflict of interest regarding this work.

References

See REFERENCES CITED.

After successfully validating the homogeneity of the mechanical deformations in the agarose hydrogels, the next step was to validate the feasibility of measuring differences in the chondrocyte metabolome in response to applied, dynamic loading. To perform these studies, SW1353 chondrosarcoma chondrocytes were encapsulated in physiologically stiff agarose, and were subjected to various lengths of cyclical, mechanical compression. Then following compression, metabolites were extracted and analyzed via LC-MS. The reason for using SW1353 cells is that they are an extremely fast proliferating chondrocyte cell line, and they are extremely hardy. If the metabolite profiles were not observed in the SW1353 cells, then measurements on a primary chondrocytes (cells harvested from human tissue) would be extremely difficult.

CANDIDATE MEDIATORS OF CHONDROCYTE MECHANOTRANSDUCTION VIA TARGETED AND UNTARGETED METABOLOMIC MEASUREMENTS

Contribution of Authors and Co-Authors

Author: Donald L. Zignego[1,*]

Contributions: Acquired, analyzed, and interpreted the data. Drafted and wrote the manuscript.

Author: Aaron A. Jutila[1,*]

Contributions: Acquired, analyzed, and interpreted the data. Drafted and wrote the manuscript.

Co-Author: Bradley K. Hwang[1]

Contributions: Interpreted data and reviewed the manuscript.

Co-Author: Jonathan K. Hilmer[2]

Contributions: Interpreted data and reviewed the manuscript.

Co-Author: Timothy Hamerly[2]

Contributions: Interpreted data and reviewed the manuscript.

Co-Author: Cody A. Minor[1]

Contributions: Interpreted data and reviewed the manuscript.

Co-Author: Seth T. Walk[3]

Contributions: Performed ordination analysis on data and reviewed the manuscript.

Corresponding Author: Ronald K. June[1,4]

Contributions: Designed the study, analyzed and interpreted the data, and wrote the manuscript.

Contribution of Authors and Co-Authors – Continued

[1]Department of Mechanical and Industrial Engineering, Montana State University, Bozeman, MT 59717-3800, USA

[2]Department of Chemistry and Biochemistry, Montana State University, Bozeman, MT 59717-3800, USA

[3]Department of Immunology and Microbiology, Montana State University, Bozeman, MT 59717-3800, USA

[4]Department of Cell Biology and Neuroscience, Montana State University, Bozeman, MT 59717-3800, USA

[*] Authors made equal contributions to this work.

Manuscript Information Page

Donald L. Zignego, Aaron A. Jutila, Bradley K. Hwang, Jonathan K. Hilmer, Timothy Hamerly, Cody A. Minor, Seth T. Walk, and Ronald K. June
Archives of Biochemistry and Biophysics
Status of Manuscript:
___ Prepared for submission to a peer-reviewed journal
___ Officially submitted to a peer-reviewed journal
___ Accepted by a peer-reviewed journal
_X_ Published in a peer-reviewed journal

Publisher: Elsevier for the Archives of Biochemistry and Biophysics
Issue: March 1st, 2014, Vol. 545, Pages 116-123

Abstract

Chondrocyte mechanotransduction is the process by which cartilage cells transduce mechanical loads into biochemical and biological signals. Previous studies have identified several pathways by which chondrocytes transduce mechanical loads, yet a general understanding of which signals are activated and in what order remains elusive. This study was performed to identify candidate mediators of chondrocyte mechanotransduction using SW1353 chondrocytes embedded in physiologically stiff agarose. Dynamic compression was applied to cell-seeded constructs for 0-30 minutes, followed immediately by whole-cell metabolite extraction. Metabolites were detected via LC-MS, and compounds of interest were identified via database searches. We found several metabolites which were statistically different between the experimental groups, and we report the detection of 5 molecules which are not found in metabolite databases of known compounds indicating potential novel molecules. Targeted studies to quantify the response of central energy metabolites to compression found a transient increase in the ratio of NADP+ to NADPH and a continual decrease in the ratio of GDP to GTP, suggesting a flux of energy into the TCA cycle. These data are consistent with the remodeling of cytoskeletal components by mechanically induced signaling, and add substantial new data to a complex picture of how chondrocytes transduce mechanical loads.

Introduction

The field of cellular mechanotransduction seeks to identify mechanisms by which cells respond to their mechanical loading environments. Mammalian cells have the ability to respond to a variety of loads by altering signaling pathways in a diverse set of cells and tissues [87, 133-135]. These and other studies demonstrate the ability of mammalian cells to respond to exogenous mechanical loading. However, knowledge of the mechanisms by which cells sense and respond to loading remains incomplete.

Articular cartilage is the smooth tissue lining the surfaces of articulating joints (*e.g.* knee) which deforms during physiological activity [136, 137]. Articular chondrocytes, the cells of articular cartilage, respond to applied loading via multiple pathways, including activation of GTPase signaling via Rho-A and ROCK [123, 138]. Osteoarthritis (OA) is a major medical problem that involves deterioration of articular cartilage [139], and osteoarthritic chondrocytes demonstrate differences in mechanotransduction compared with healthy chondrocytes. For example, cyclical strain reduces AKT phosphorylation in OA chondrocytes [93], and OA chondrocytes fail to produce sulfated glycosaminoglycans (sGAG) in response to load whereas normal chondrocytes exhibit loading-induced increases in sGAG production [140]. In the present study, we provide high-dimensional data regarding changes in expression levels and flux of thousands of metabolites (*i.e.* cytosolic molecules smaller than ~1000 Da) in response to highly controlled compression of SW1353 chondrocytes [141].

Chondrocytes within articular cartilage are surrounded by a pericellular matrix (PCM) which is composed primarily of Type VI collagen and other proteins [142-144].

The chondrocyte PCM has a stiffness of ~25-200 kPa [47] which is diminished in OA [62]. Previous studies of chondrocyte mechanotransduction have utilized various three dimensional culture methods [43, 67, 68, 70, 145] most with stiffness values of 5-10 kPa or less, which are markedly lower than those present in the human pericellular matrix [47, 62]. The present study sought to build on previous methodology [146, 147] by using high concentrations of agarose to support the chondrocytes and form a high-stiffness gel capable of applying physiological deformation to chondrocytes.

Previous research indicates that central energy metabolism is altered both in inflammation and OA, including the balance between glycolysis and oxidative phosphorylation [148, 149]. Energy metabolism may be affected by loading because activation of AMP-activated protein kinase can prevent catabolism induced by mechanical injury [150]. Based on these and other data, we hypothesized that dynamic compression within the physiological range will increase glycolytic metabolism to maintain the environment of the PCM. As a first step in evaluating this hypothesis, we conducted the present study to develop and demonstrate methods for targeted quantification of metabolites associated with the central metabolism of SW1353 chondrosarcoma chondrocytes in response to applied dynamic compression in the physiological range. To our knowledge, this is the first application of either targeted or untargeted metabolomics studying chondrocyte mechanotransduction.

The objective of this study was to use targeted and untargeted metabolomics to identify candidate mediators of chondrocyte mechanotransduction. We identified loading-induce changes in ~4000 metabolites in untargeted studies and measured

quantitative changes in 36 targeted metabolites relevant to central metabolism and protein production. From this untargeted metabolomics detection, 54 novel mediators of chondrocyte mechanotransduction were identified. These data define the functional response of chondrocytes to applied loading. Future studies to build on these results will aim to develop a more detailed systems understanding of chondrocyte mechanotransduction.

Materials and Methods

Chondrocyte Culture and Encapsulation. Human SW1353 chondrosarcoma cells were cultured in 5% CO2 in DMEM with 10% fetal bovine serum and antibiotics (10,000 I.U. / mL penicillin and 10,000 μg / mL streptomycin). For encapsulation, cells were trypsinized, counted, and resuspended in media at 11X. Agarose/PBS solution was prepared using low-gelling-temperature agarose (Sigma: Type VII-A A0701) at 1.1X of desired final concentration and placed into a water bath at 40°C. The cell-suspension was added to the agarose with vortexing to distribute the cells throughout the liquid hydrogel. Gels were subsequently cast in an anodized aluminum mold for 5 minutes at 23°C with diameter of 7mm and height of 12.7 mm [113]. Cell-seeded agarose constructs were removed from the molds and cultured in antibiotic free media for 72 hours at 37°C under 5% CO2. These methods have been shown to provide uniform compressive deformations [151] to chondrocytes by modeling the stiffness of the pericellular matrix [62]. The stiffness of the pericellular matrix provides *in vivo* deformations to the relatively less-stiff chondrocytes [152], and the advantage of this approach is that it provides observable

cellular deformations while providing homogeneous, uniaxial unconfined compression as the defined mechanical stimulus[151].

Mechanical Stimulation. Cell-seeded agarose gels were subjected to cyclic compression via a custom made bioreactor for 0, 15, and 30 minutes (Figure 27A). Dynamic unconfined compression was applied between impermeable platens in culture media at a frequency of 1.1 Hz [153] with an average compressive strain of 5% and an amplitude of 1.9% based on the initially measured height of 12.7 ± 0.1 mm. This sampling interval is based on previous observations of changes in central energy metabolism within a 30 minute timescale [154]. Physiological conditions (culture media at 37˚C, 5% CO2) were maintained through the duration of the tests. To assess specificity of the mechanobiological response, unloaded control samples were placed in the bioreactor without deformational loading and analyzed for each time point.

Metabolite Extraction. After each time point samples were removed from the bioreactor, immediately wrapped in sterile foil and frozen in liquid nitrogen. Samples were then placed inside individual wells of a custom-made frozen aluminum mold for pulverization (Figure 18) [113]. From here each sample was crushed using a sterilized stainless steel platen and a ballpeen hammer. Crushed gel particulate was then collected into 2 mL micro-centrifuge tubes. Metabolites were extracted by adding 1 mL of a 70:30 solution of Methanol:Acetone and vortexing every 4-5 minutes for twenty minutes. Samples were extracted further at -20°C overnight. Solid content was pelleted by centrifugation at 13,000 rpm for 10 minutes at 4°C. The supernatant was placed into new

1.6 mL micro-centrifuge tubes where solvent was removed via speed-vac for six hours. The dried samples were then resuspended in 100 µL of a 50:50 Water:Acetonitrile solution for metabolomics analysis.

Untargeted and Targeted LC-MS. Detection of metabolites was performed via HPLC separation with ESI-MS (electrospray mass spectrometry) detection in the Montana State University Mass Spectrometry Core Facility [155-157]. HPLC was performed with an aqueous normal-phase, hydrophilic interaction chromatography (ANP/HILIC) HPLC column. A Cogent Diamond Hydride Type-C column with 4 µm particles and dimensions of 150 mm length and 2.1 mm diameter was used with an Agilent 1290 HPLC system. The column was maintained at 50 °C with a flow rate of 600 µL/min. Chromatography was as follows: solvent consisted of H2O with 0.1% (v/v) formic acid for channel "A" and acetonitrile with 0.1% formic acid for channel "B". Following column equilibration at 95% B, the sample was injected via auto-sampler, and the column was flushed for 2.0 min to waste. From 2.0 min to the end of the run, the column eluent was directed to the MS source. From 2.0 min to 12.5 min, the gradient was linearly ramped from 95% to 25% B. From 12.5 to 13.5 min the column was held isocratically at 25% B, and from 13.5 to 15 minutes the column was re-equilibrated with 95% B. Blank solvent samples were run following each sample.

The mass spectrometer used was an Agilent 6538 Q-TOF with dual-ESI source. Resolution is ~20,000 and accuracy is ~5 ppm. Source parameters were: drying gas 12 L/min, nebulizer 60 psi, capillary voltage 3500 V, capillary exit 120 V. Spectra were collected in positive mode from 50 to 1000 m/z at a rate of 1 Hz. Quality control testing

including mass accuracy calibration of all instruments is performed regularly and documented by the Mass Spectrometry Core Facility staff as part of routine operation.

Metabolites known to be involved in central metabolism [102, 154] were targeted for LC-MS analysis. Using the isotopic distributions of these targeted masses (Agilent Technologies), a list of H+ and Na+ adducts was used to create 20 ppm mass windows for each ion, and pilot data was scanned to determine the range of retention times for each ion based on data from analytical standards (Biolog, Hayward, CA) run by the mass spectrometry core facility for 15 of the 36 targeted metabolites. These standard metabolites were run by Core staff under controlled conditions, and target validation ensured retention times within 0.1 min of core values for samples run on identical instruments under identical conditions. Targeted metabolite intensity was defined as the sum of the intensities of the isotopes of the ions and adducts associated with each metabolite as determined by the Quantitative Analysis package within MassHunter Workstation B.04.00 (Agilent Technologies).

Data Processing. Data analysis involved multiple software packages used to process the raw LC-MS data for feature identification, quantification, and metabolite identification (Supplemental Figure 10). Raw LC-MS scans were converted to mzXML files using Agilent MassHunter and processed in MZmine2 [158] for the untargeted analysis. Unrefined lists of detected metabolites (*i.e.* detected mass values) with corresponding intensities were generated by aligning all LC-MS scans. These unrefined lists resulted in the identification of approximately 25K independent m/z values for positive mode and 18K m/z values for negative mode scans.

Using established methods [159], filtered datasets were generated as follows. Chromatograms were built using centroidal mass detection with a minimum signal level of 1000, minimum timespan of 0.02 seconds, minimum peak height of 1000, and an m/z tolerance of 0.05. Peak deconvolution was performed with a chromatographic threshold of 85%, search minimum in retention time of 0.03 seconds, minimum relative height of 5%, minimum absolute height of 10000, and minimum ratio of top/edge of 1.0. The chromatograms were then normalized by retention times with a retention time tolerance of 0.25 min and a minimum standard intensity of 1000. Chromatograms were aligned and a duplicate peak filter was applied with an m/z tolerance of 0.1 and a retention time difference maximum of 1 minute. These refined lists were used for statistical analysis and candidate metabolite identification. Intensity was quantified via peak height in the total ion intensity chromatogram.

Data Analysis and Candidate Selection. The experimental procedures were repeated for n = 5 independent samples. To assess the biological effects of physiological loading, compressed samples were compared to unloaded controls. The cell-seeded agarose gels that received no mechanical stimulation (0 minute time point extraction) acted as the unloaded controls (UC), while cell-seeded agarose gels that received either 15 or 30 minutes of mechanical stimulation made up the dynamically compressed groups, DC15 and DC30 respectively. Data analysis started with the unrefined lists generated in MZmine2. We defined detected masses as those present in the majority of samples (*i.e.* $\geq$ 3 samples). To minimize false positives associated with multiple comparisons, conservative statistical methods were used to make comparisons between groups.

Comparisons were performed using t-tests [160] and p-value corrections using a standard false discovery rate (FDR) calculation [160]. For metabolites detected in one group (*e.g.* DC15) but not in another, statistical comparisons were enabled by the use of small random values for the non-detected intensities. These small values were < 2% of the minimally detected value and <0.04% of the median value, and were required to calculate the appropriate FDR. Two comparisons were performed: UC vs. DC15 and UC vs. DC30.

Ordination techniques were subsequently used to help identify candidate metabolites from the untargeted data for which statistical significance was not achieved. The point of this analysis was to generate a list of potentially important metabolites for future studies. Data matrices were generated with data binned according to masses and time points. Only masses that were detected in at least three of five time point replicates were analyzed. Principal components analysis was performed using the rda function of the Vegan package in R statistical software [161]. All masses were standardized to unit variance and displayed using the biplot function (scaling=-1). This approach allowed us to visually identify candidate mediators with relatively large magnitudes that were responsible for differentiating between 0, 15, and 30 minutes of loading.

In order to assess metabolite flux over the 30 minute experimental time course, Pearson's correlation coefficients were determined using loading time (0, 15, or 30 minutes) as the independent variable and the intensity of each detected metabolite as the dependent variable. Significant positive correlations indicated metabolite accumulation, and negative correlations indicated metabolite consumption. Candidate mediators were

defined as the twenty largest (*i.e.* accumulated) and twenty smallest (*i.e.* depleted) statistically significant correlations. Targeted metabolite profiles were analyzed by cluster and correlation analyses. Additionally, the median ratios of ATP:ADP, NADP+:NADPH, NAD+:NADH, and GDP:GTP were calculated as a function of time to assess relative changes in energy metabolism.

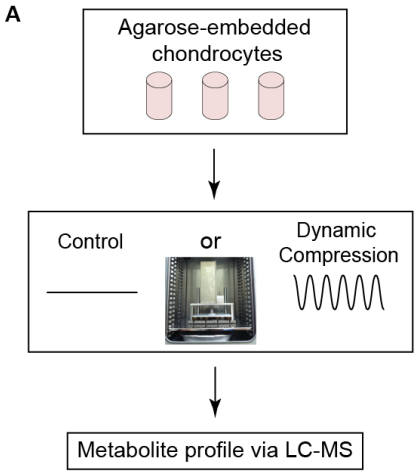

B Candidate Mediators of Mechanotransduction [m/z]

81.0359	220.1650	379.2759	641.0427
96.9614	250.1009	380.9257	653.2354
97.0934	275.0928	388.3028	665.1094
127.0524	287.2730	435.0001	721.4903
145.6061	289.2892	470.1316	730.2875
158.0735	297.1526	510.1599	764.5935
159.0764	304.1410	537.1880	770.6108
188.1398	305.2798	538.1190	778.1822
199.0438	320.2151	538.1869	783.2382
200.0908	332.3151	554.1504	784.2413
204.1270	338.1529	558.2888	881.2040
209.0947	343.1413	603.2831	959.3137
215.1196	376.0413	625.2703	
219.0486	377.2716	631.2563	

C Targeted Metabolites

1,3-bisphosphoglycerate	D-glyceraldehyde 3-phosphate	Glutamine	Oxalacetate
2-phosphoglycerate	dihydroxyacetone phosphate	Glyceraldehyde-3-phosphate	Oxalosuccinate
3-phosphoglycerate	Erythrose-4-phosphate	GTP	Pentose Phosphate
6-P-gluconate	Erythrose-4-phosphate	Hexose-P	P-glucanolactone
Acetyl CoA	FAD	HS-CoA	Phosphoenolpyruvate
ATP	FADH2	Inorganic Phosphate	Pyruvate
ADP	Fructose-1,6,bisphosphate	Isocitric acid	Ribose-5-phosphate
a-ketoglutarate	Fructose-6-Phosphate	L-malate	Ribulose-5-phosphate
Alanine	Fructose-6-phosphate	Malonyl-CoA	Sedoheptulose-7-phosphate
Aspartate	Fumarate	NAD+	Succinate
Cis-aconitate	GDP	NADH	Succinyl CoA
Citrate	Glucose	NADP+	Triose-3-phosphate
D-fructose 1,6-bisphosphate	Glucose-6-Phosphate	NADPH	Uridine Triphosphate
D-fructose-6-P	Glutamate	Nucleic Acids	Xylulose-5-phosphate

Figure 27. (A) Schematic of Experimental Methods. SW1353 Chondrocytes were encapsulated in 4.5% agarose (stiffness ~35 kPa), cultured for 72 hours, and exposed to 0, 15, or 30 minutes of dynamic compression. Metabolites were extracted and analyzed via LC-MS. Inset shows loading apparatus for applying unconfined compression. (B) 59 metabolites were identified as candidate mediators of chondrocyte mechanotransduction in the untargeted studies. These were detected by either significant correlation with time of loading or ordination based on principal components analysis. Underlined values were not detected in database searches and may indicate novel metabolites. (C) List of targeted metabolites.

Compound Identification. Putative compound identifications were made by comparing the metabolite mass to charge (m/z) ratio to previous results using the METLIN and HMDB databases, which contain over 80,000 identifiable metabolites [162, 163] using a mass tolerance of 20 ppm. METLIN parameters were charged masses and adducts of either +1H+ or +1Na+. Compounds with LipidMAPS identifications [164] were designated as human unless detected in a non-human species at the time of database search.

Results

These data provide an initial systems-level view of the cytosolic metabolite profile of human chondrocytes in response to applied compression. We defined 54 novel compounds as candidate mediators (Figure 27B) of chondrocyte mechanotransduction, 40 from correlation analysis of untargeted metabolites and 14 from ordination analysis of targeted metabolites. No identification was possible for 5 of the 54 (11%) mediator masses based on database searches, indicating that these may be novel compounds. The remaining 49 (89%) masses map to a total of 180 metabolites due to isobaric redundancy and structural isomers.

Untargeted Metabolomics. Untargeted studies detected 2438 to 3211 individual metabolites per sample. 1481 metabolites were detected in unloaded samples that were not detected following 15 minutes of loading, whereas 1528 unique metabolites were detected following 15 minutes of loading that were not present in unloaded control samples (Figure 28A). 1574 unique metabolites were detected in unloaded samples that

were not detected following 30 minutes of loading, whereas 1623 metabolites were detected in samples subjected to 30 minutes of dynamic compression that were not detected in unloaded samples (Figure 28B).

Many of the metabolites were significantly regulated in response to dynamic compression. Fifteen minutes of dynamic compression resulted in significant changes in 255 metabolites with 223 metabolites having increased intensity and 32 metabolites having decreased intensity compared with unloaded control samples. Thirty minutes of dynamic compression resulted in significant changes in 787 metabolites with 689 metabolites having increased intensity and 98 metabolites having decreased intensity compared with unloaded control samples. LC-MS analysis of naïve agarose control samples without chondrocytes found <15 metabolites (data not shown), which also served as solvent, reagent, and process controls.

Untargeted metabolite intensity was significantly correlated with time of loading for 254 metabolites (Figure 29). Of the significantly correlated metabolites, 157 were negatively correlated with time indicating cellular consumption and 97 were positively correlated with time indicating accumulation. Identification of these metabolites found peptides, lipids, substrates, and products.

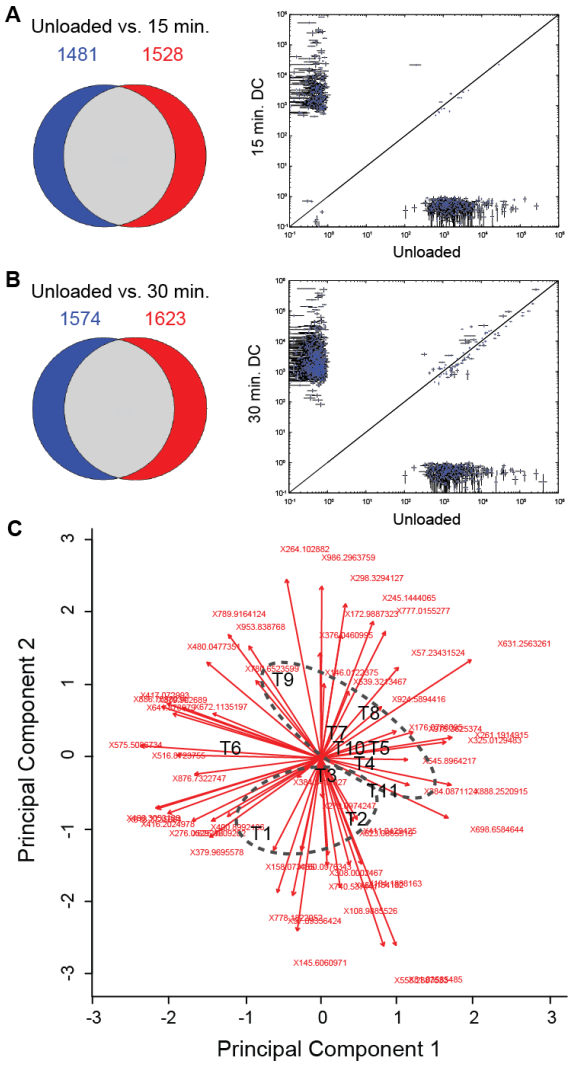

Figure 28. Loading-specific differences in untargeted metabolite expression. Mechanical loading resulted in statistically significant changes in expression of targeted and untargeted metabolites. Left shows Venn diagrams of unique metabolites detected in each group. Right shows quantitative comparisons for metabolites detected in both groups. (A) Unloaded controls versus 15 minutes of dynamic compression (DC). (B) Unloaded controls versus 30 minutes of DC. (C) Principal Components Analysis used for ordination analysis. The first two principal components contained 37.8% of the overall variance for this dataset (3-3-5). The time points are represented as follows: unloaded control: T1-3, DC15: T4-6, and DC30: T7-11. Ellipses represent unloaded controls (T1, T2, and T3) and dynamically compressed samples (≥T4). Principal Component 1 and Principal Component 2 were associated with 22.3% and 15.5% of the total variance among masses.

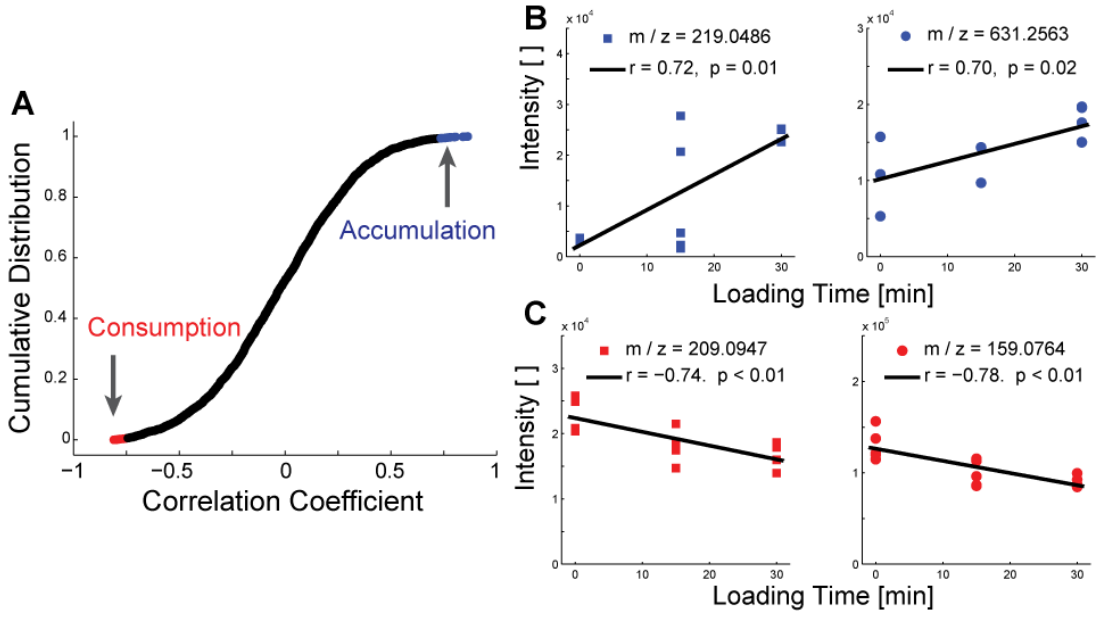

Figure 29. Dynamic compression results in both accumulation and depletion of untargeted metabolites. (A) The cumulative distribution of correlation coefficients of untargeted metabolites were used to identify accumulating (blue) and consumed (red) metabolites. The top and bottom twenty correlations were identified as candidate mediators of chondrocyte mechanotransduction. (B) Accumulation of selected candidate mediators of mechanotransduction. Metabolites were database-matched as gulonic acid (left) and harderoporphyrin (right). (C) Depletion of selected candidate mediators of mechanotransduction, which were database-matched as kynurenine and 4-methylene-L-glutamine.

Targeted Metabolomics. Targeted metabolites related to central energy metabolism exhibited distinct expression patterns with loading time (Figure 30A). Clustering of targeted data resulted in groups of metabolites with increasing intensities with respect to time, intensities peaking at 15 minutes of compression, and decreasing intensities with respect to time. Guanosine tri-phosphate (GTP) was positively correlated with time (Figure 30B, $p = 0.042$). The ratio of NADP+ to NADPH peaked at 15 minutes of loading, as did the ratio of ATP to ADP to a lesser extent (Figure 30C). There were small changes in the ratio of NAD+ to NADH, and the ratio of GDP to GTP

declined substantially with respect to loading time, consistent with the accumulation of GTP (Figure 30B).

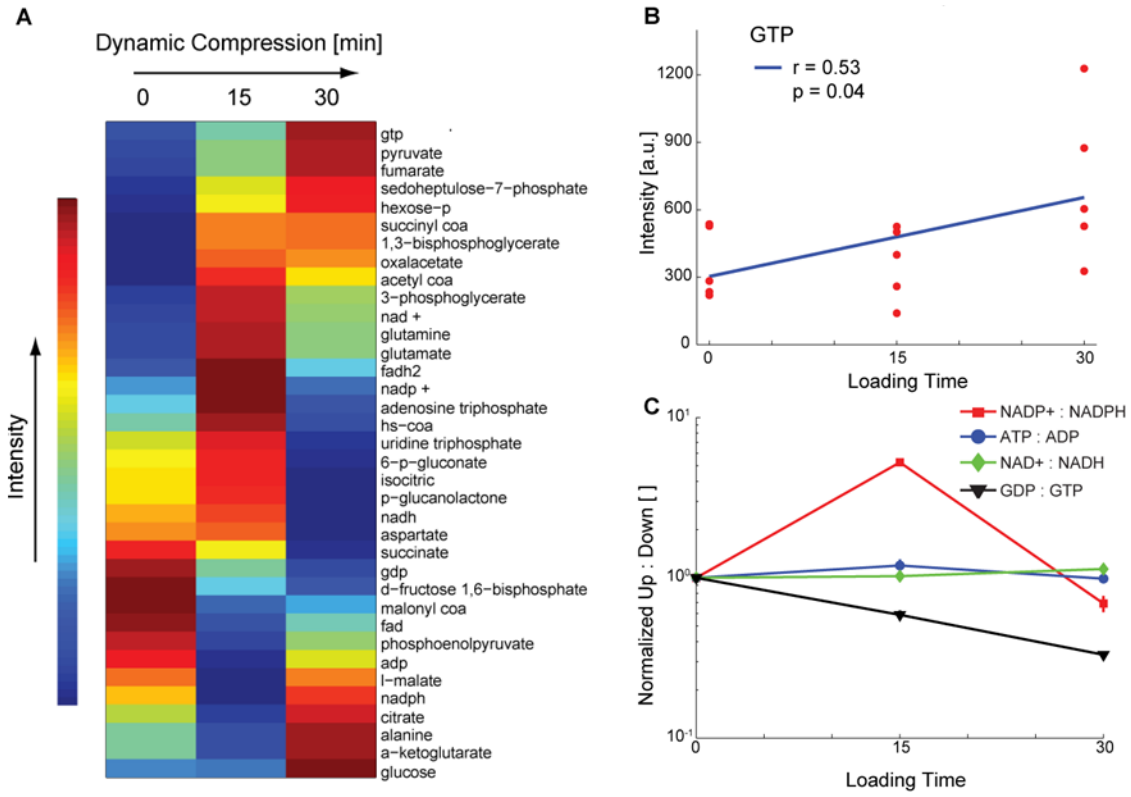

Figure 30. Changes in expression of targeted central-energy-related metabolites over from 0-30 minutes of applied compression. Metabolites associated with central energy metabolism and protein production (*e.g.* amino acids) were targeted for detailed analysis via detection of multiple ionized adducts and ions. (A) Clustered heatmap of co-expressed metabolites. (B) Significant accumulation (correlation) of GTP and marginally-significant depletion of GDP in response to applied compression. (C) Ratios of upstream to downstream mediators of central energy metabolism. The peak in NADP+ to NADPH indicates decreased energy flow toward the pentose phosphate pathway, and the continual decrease in GDP to GPT indicates increased flux through the TCA cycle.

Discussion

The objective of this study was to identify mediators of chondrocyte mechanotransduction using targeted and untargeted metabolomics. SW1353 chondrocytes were embedded in agarose with stiffness in the physiologic range of the human PCM. By providing quantitative measures of presence, absence, and relative abundance of cytosolic metabolites (*i.e.* reactant and product levels for biochemical reactions involved in multiple pathways) these data provide a systems-level view of how the functional chondrocyte fingerprint changes in response to mechanical compression. The significance of this study is that to our knowledge this is the first report of mechanically induced changes in the cellular metabolome. Furthermore, by encapsulating chondrocytes in physiologically-stiff agarose capable of inducing cellular deformations, we were able to identify 54 metabolites mediating chondrocyte mechanotransduction.

The untargeted metabolome is a high-dimensional measure of the functional state of the cell as defined by the individual metabolite levels. The targeted metabolome of central-energy-related metabolites can be used for rigorous hypothesis testing via systems biology. Future studies can utilize these data to map the full mechanisms of chondrocyte mechanotransduction. Below we discuss specific pathways motivated by this initial analysis.

Untargeted experiments found hundreds of metabolites that were statistically different between loading time points (Figure 28). Among these molecules were 54 mediators that have not been previously associated with chondrocyte

mechanotransduction. Database searching of these candidates resulted in the identification of 180 compounds from 49 of the masses: such a non-unique expansion of targets is inevitable due to structural isomers with identical formulae and masses. Molecular mass is a linear Diophantine function of elemental composition, and multiple different molecular formulas can produce the same overall mass [165]. Future work will employ MS / MS analyses to examine these candidate molecules.

These data suggest several specific signaling pathways, many of which have not previously been associated with mechanotransduction. Accumulated molecules of m / z values ~219 and ~631 may include gulonic acid and harderoporphyrin, respectively. The accumulation of gulonic acid may indicate decreased pentose phosphate pathway-related energy metabolism [166]. The accumulation of harderoporphyrin, an intermediate in heme biosynthesis [167], may indicate compression-induced expression of oxidative phosphorylation consistent with the targeted results (see below), although chondrocytes likely reside in a hypoxic environment and have not been demonstrated to produce hemoglobin [168]. Compounds identified from depleted metabolites include kynurenine and 4-methylene-L-glutamine (Figure 29C). Consistent with the presently observed changes in GDP to GTP ratio (Figure 30C) and the known metabolism of pyruvate [166, 169], the depletion of kynurenine and 4-methylene-L-glutamine may represent mechanically-induced re-direction of cellular energy via increased TCA cycle flux.

Human central energy metabolism of glucose involves the pentose phosphate pathway, glycolysis, and the tri-carboxylic acid cycle [102]. The ratio of upstream to downstream metabolites for a particular pathway (*e.g.* glycolysis) can be used as a

surrogate measure of energy flux, under the assumptions of constant enzyme concentration and activity which are reasonable for the short timeframe employed by these experiments. For example, energy flow to the pentose phosphate pathway can be inferred by the ratio of NADP to NADPH with larger ratios indicating decreased flux. Our data show a transient increase in NADP:NADPH at 15 minutes (Figure 30C) which suggests decreased energy flow to the pentose phosphate pathway, which is typically used for nucleic acid production [154]. The ratio of GDP to GTP may represent energy flow to the tri-carboxylic acid cycle. We found a continual decrease in the ratio of GDP:GTP suggesting increased flux through the tri-carboxylic acid cycle, which may represent a re-direction of cellular energy in response to mechanical loading.

GTP, guanosine tri-phosphate, is a substrate required for activation of GTPase signaling pathways. In this study, GTP was significantly upregulated following 30 minutes of dynamic compression (Results and Figure 30B). Previous studies have found early-time (*i.e.* 15 minutes and shorter) activation of the GTPase RhoA [123] which is involved in activation of ROCK to stimulate cytoskeletal remodeling [123] and can also activate the master chondrogenic transcription factor of Sox9 [170]. These data add to a complex picture of chondrocyte mechanotransduction involving directed changes in energy metabolism to maintain and remodel the cytoskeleton. Future studies will build on this work to elucidate both mechanisms and consequences of modifying energy metabolism in response to mechanical loading.

While this study found several candidate mediators of chondrocyte mechanotransduction using targeted and untargeted metabolomics some limitations

apply. First, the temporal resolution of the metabolome was limited to sampling at 15 minute intervals in these initial experiments, and flux inferences assume constant enzyme concentration and activity. Future studies may build on these results by using shorter time intervals, measuring enzyme concentrations and activities, and extending the loading duration. Second, this study quantified and compared the levels of thousands of metabolites. Although we used previously published LC-MS data analysis procedures, the possibility of both false positive and false negative results remains. We controlled the risk of false positive comparisons using a false discovery rate of 0.05 [160]. Third, these studies were performed using SW1353 chondrocytes encapsulated in 4.5% agarose. While the high concentration of agarose modeled the stiffness of the human chondrocyte pericellular environment [47, 62], the *in vivo* chondrocyte pericellular matrix likely contains substantial additional signals for regulating cellular behavior. Additionally, dynamic loading of cartilage can result in a diverse set of mechanical signals including streaming potentials and fluid flow [171, 172] which have been observed previously for lower concentrations of agarose, but have not been measured in the high stiffness *in vitro* system used in this study. Therefore, the pathways and mechanisms reported herein likely represent a subset of mechanically-activated pathways, which represent cell-intrinsic mechanisms of mechanotransduction. Finally, although putative compound identifications were made, a general limitation of metabolomics is the challenge of unique identification, which future studies may address using NMR and MS / MS. Despite these limitations, to our knowledge, this is the first report of the mechanically-

induced metabolome for human chondrocytes, which provides substantial new data describing how chondrocytes respond to mechanical loads.

Conclusions

This study demonstrates the power and challenges associated with high-dimensional data for systems biology and provides both a methodological and data-based foundation for future studies. In untargeted experiments, we found hundreds of statistically-significant changes in metabolites induced by mechanical loading and using advanced statistical methods identified 54 candidate mediators of chondrocyte mechanotransduction. In targeted experiments, we found that mechanical loading induces significant changes in metabolites associated with cellular energy usage. Future studies will identify the mechanisms of these changes and address the cell-type specificity of these responses.

Acknowledgements

We thank Drs. Ross Carlson, Brian Bothner, and Edward Dratz, MSU, for critical insight provided during discussions. The SW1353 cell line was kindly donated by Martin Lotz. Funding was provided by NIH P20GM10339405S1, Montana State University, and the Murdock Charitable Trust.

References

See REFERENCES CITED.

METABOLOMICS

Following the development of the experimental methodology in Chapter 2, the next step in this research was to characterize the metabolite profiles for primary human chondrocytes as a function of dynamic compression. This chapter builds of the foundational groundwork laid in Chapter 2 by using the high-stiffness agarose model to study the *in vitro* response of primary human OA chondrocytes in response to applied, mechanical compression. To my knowledge, this study is the first of its kind in using a systems biology approach along with our novel *in vitro* agarose model for 3D cell encapsulation to study chondrocyte mechanotransduction. This study focuses on studying the metabolomic response of primary human OA chondrocytes in response to short term (<30 minutes) of dynamic compression. By studying the chondrocyte metabolome we can observe significant biological changes in as little as 15 minutes of compression. Metabolomics studies are extremely useful in these short response time studies because the metabolites give insight on functional readout of the cellular state, essentially a snapshot of the physiology of the cell.

The overall objective of this study was to evaluate and define the metabolite profiles for primary human OA chondrocytes as a function of dynamic compression by comparing samples loaded at either 0 minutes (control), 15 minutes, or 30 minutes. Briefly, the methods involve encapsulating primary human OA chondrocytes in physiologically stiff agarose, dynamically stimulating the agarose constructs with physiological loading values, flash-freezing the samples in liquid nitrogen post-loading, and pulverizing them. The metabolites are then extracted and quantified via liquid

chromatography-mass spectrometry (LC-MS) at the MSU Cobre Mass Spectrometry Core Facility. Both untargeted and targeted approaches were used to quantify changes in metabolite levels. To my knowledge, such a study has never been done before and the results from this study provided both a global (untargeted) and a more focused (targeted) understanding of chondrocyte mechanotransduction. Future work may build on this research to use metabolomics as a tool for elucidating potential biomarkers of OA.

MECHANOTRANSDUCTION IN PRIMARY HUMAN OSTEOARTHRITIC CHONDROCYTES IS MEDIATED BY METABOLISM OF ENERGY, LIPIDS, AND AMINO ACIDS

Contribution of Authors and Co-Authors

Author: Donald L. Zignego[1]

Contributions: Acquired, analyzed, and interpreted the data. Drafted and wrote the manuscript.

Co-Author: Carley N. McCutchen[1]

Contributions: Interpreted data and reviewed the manuscript.

Co-Author: Jonathan K. Hilmer[2]

Contributions: Interpreted data and reviewed the manuscript

Corresponding Author: Ronald K. June[1,3]

Contributions: Designed the study, analyzed and interpreted the data, and wrote the manuscript.

[1]Department of Mechanical and Industrial Engineering, Montana State University, Bozeman, MT 59717-3800, USA

[2]Department of Chemistry and Biochemistry, Montana State University, Bozeman, MT 59717-3800, USA

[3]Department of Cell Biology and Neuroscience, Montana State University, Bozeman, MT 59717-3800, USA

Manuscript Information Page

Donald L. Zignego, Carley N. McCutchen, Jonathan K. Hilmer, and Ronald K. June
Arthritis and Rheumatology
Status of Manuscript:
___ Prepared for submission to a peer-reviewed journal
_X_ Officially submitted to a peer-reviewed journal
___ Accepted by a peer-reviewed journal
___ Published in a peer-reviewed journal

Publisher: Arthritis and Rheumatology.
Submitted: July 2015

Abstract

Objective. Chondrocytes are the sole cell type found in articular cartilage and are constantly subjected to mechanical loading *in vivo*. We hypothesized that physiological dynamic compression results in changes in energy metabolism to produce proteins for maintenance of the pericellular and extracellular matrices. The objective of this study was to develop an in-depth understanding for the short term (<30 min.) chondrocyte response to sub-injurious, physiological compression by analyzing metabolomic profiles for human chondrocytes harvested from femoral heads of osteoarthritic donors.

Design. Cell-seeded agarose constructs were randomly assigned to experimental groups, and dynamic compression was applied for 0, 15, or 30 minutes. Following dynamic compression, metabolites were extracted and detected by HPLC-MS. Untargeted analyses examined changes in global metabolomics profiles and targeted analysis examined the expression of specific metabolites related to central energy metabolism.

Results. We identified hundreds of metabolites that were regulated by applied compression, and we report the detection of 16 molecules not found in existing metabolite databases. We observed patient-specific mechanotransduction with aging dependence. Targeted studies found a transient increase in the ratio of NADP+ to NADPH and an initial decrease in the ratio of GDP to GTP, suggesting a flux of energy into the TCA cycle.

Conclusions. To our knowledge, this is the first study to characterize metabolomics profiles of primary chondrocytes in response to applied dynamic compression. These results are consistent with increases in glycolytic energy utilization by mechanically induced signaling, and add substantial new data to a complex picture of how chondrocytes transduce mechanical loads.

Introduction

Osteoarthritis (OA) is the most common joint disorder, affecting more than 40 million individuals in the United States [1, 5]. OA is characterized by the deterioration of the protective, low-friction, load-bearing cartilage that surrounds the joint. The highly specialized chondrocyte plays an important metabolic role in synthesizing, maintaining, and repairing the tissue and is the sole cell type in articular cartilage [37]. At these load-bearing joint surfaces (*e.g.* the femoral head), the articular cartilage, and thus the articular chondrocyte, is subjected to near constant mechanical loading (*e.g.* standing, walking, running, etc.). Chondrocytes and other mammalian cells sense and respond to these mechanical stimuli through biochemical and biological outputs, but the intracellular pathways behind chondrocyte mechanotransduction remain unclear [51, 84, 135].

Mechanical stimulation has both anabolic and catabolic effects on articular chondrocytes [43, 173]. In chondrocytes, anabolic responses promote the synthesis and production of the extracellular matrix (ECM) and the pericellular matrix (PCM) through the secretion of cytokines and protease inhibitors [173]. Catabolic responses involve secretion of proteases (*e.g.* MMP-13) which results in the breakdown of ECM molecules. Dynamic loading has been shown to promote these anabolic responses in chondrocytes whereas static loading has been shown to inhibit them [174, 175]. Dynamic compression has been shown to alter signal transduction including activation of GTPase signaling via the Rho-A and ROCK pathways, Erk-1 and -2, MAPK and SEK, and Smad2 [81, 174, 176, 177].

In addition to signal transduction, chondrocytes can alter their energy metabolism in response to mechanical loading. The enzyme AKT is important in regulating FoxO signaling for energy homeostasis [178], and cyclic loading has been shown to reduce phosphorylation of AKT in OA chondrocytes [93] whereas mechanical stimulation induced AKT phosphorylation in healthy cells [80]. These energy-related signaling responses may affect matrix synthesis because healthy chondrocytes show increases in sulfated glycosaminoglycans (sGAG) in response to mechanical loading in contrast to OA chondrocytes [140]. However, changes in chondrocyte metabolite levels which can mark changes in biosynthetic activity remain to be determined in response to loading.

Previous research suggests that both inflammation and OA alter central energy metabolism, including the balance between glycolysis and oxidative phosphorylation [148]. One potential mechanism of energy-related mechanotransduction involves regulation of AMP-activated protein kinase which can prevent catabolism induced by mechanical injury [150]. Based on these and other data, we hypothesized that physiological dynamic compression increases chondrocyte glycolytic energy flux to promote the anabolic response to maintain the environment of the ECM and PCM. The objective of this study was to use both untargeted (global) and targeted metabolomics to identify candidate mediators of chondrocyte mechanotransduction in primary human OA chondrocytes. This study evaluates our hypothesis using primary human OA chondrocytes subjected to applied dynamic compression following encapsulation in physiologically stiff agarose.

Chondrocyte mechanotransduction happens on both short- and long- timescales. Because early responses have the potential to set the trajectory for longer-term behavior, in this study, we focus on short term (<30 min), loading-induced changes in small molecules (*i.e.* cellular metabolites smaller than ~1000 Da). Building upon previous methodology to encapsulate chondrocytes in agarose similar in stiffness to the human PCM, we profiled the metabolomic responses of primary human OA chondrocytes in response to applied compression at physiological levels [114, 115].

This study identified changes in 1421 untargeted metabolites and 48 metabolites pertinent to central energy metabolites and protein production. Metabolites were identified via database searches (METLIN, and HMDB), and 16 of the 1421 metabolites were not found in database searches, potentially representing novel mediators of chondrocyte mechanotransduction. Future research may build on these results to potentially utilize mechanical loading as a therapeutic strategy for OA.

Materials and Methods

Chondrocyte Culture and Encapsulation. Primary human chondrocytes were harvested from hip cartilage of five Grade IV OA patients undergoing joint replacement surgery (mean age: 63 years, age range: 54-80, mean weight: 80.4 kg, weight range: 56.9-99 kg). The cartilage was digested in Type IV collagenase (2 mg/mL for 12-14 hrs. at 37°C), and then cultured in DMEM with 10% fetal bovine serum and antibiotics (10,000 I.U./mL penicillin and 10000 µg/mL streptomycin) in 5% atmospheric CO_2. Cells were encapsulated using previously optimized methods [116], at a concentration of ~500,000 cells/gel (gel diameter = 7mm, gel height = 12.7mm).

Mechanical Stimulation. From each donor (N = 5), cell-seeded agarose gels were randomly assigned to a loading group (n = 5 biological replicates for each loading group). Loading groups consisted of unloaded controls (*i.e.* 0 minutes of loading), 15, or 30 minutes of dynamic, cyclic compression (Supplemental Figure 13). The rationale for the short loading timescale is that initial early-time responses can set the trajectory for longer-term behavior. The loading protocol followed previously optimized methods [116], in which homogeneous deformations [115] were applied to the cell-seeded gels using a custom built bioreactor emulating physiological loading conditions: frequency of 1.1 Hz [153] and average sinusoidal compressive strains of 5% with an amplitude of 1.9% based on initial gel height.

Metabolite Extraction. Metabolite extraction was performed using identical methods from our previous study [116]. Gels were flash frozen, pulverized, and metabolites were extracted by adding 1 mL of a 70:30 Methanol:Acetone solution and vigorously vortexing the mixture every 5 minutes for 20 minutes. Samples were kept at -20°C overnight for further metabolite extraction. Proteins were removed by centrifugation, the supernatant extracted, and the solvent removed via centrifugation under a vacuum for 6.5 hours. The dried samples were then resuspended in 100 µL of mass spectrometry grade water and acetonitrile (50:50 v/v).

Untargeted and Targeted Metabolomic Profiling. Metabolomics is an experimental technique for characterizing large numbers of small molecules (<1000 Da) in biological samples [96]. Recent studies of joint tissues and fluids have used

metabolomic analysis to examine OA phenotypes, identify candidate biomarkers, and explore the inflammatory responses [179-182]. In this study, metabolites were extracted following dynamic compression and analyzed by nano-liquid chromatography and mass spectrometry (Supplemental Methods, [116]). Untargeted metabolites were detected in positive mode on an Agilent 6538 Q-TOF spectrometer with a resolution of ~20,000 and accuracy of ~5 ppm. For the targeted approach, ~50 metabolites known to be involved in central energy metabolism were analyzed using the Quantitative Analysis package within the Agilent MassHunter Workstation B.04.00 (Agilent Technologies) and a database of the calculated isotopic distributions (including H+ and Na+ adducts) of these targeted masses (Isotope Distribution Calculator, Agilent Technologies).

To assess the effects of physiological loading on chondrocyte biology, three experimental groups were used: unloaded control samples (UC) and samples that received either 15 (DL15) or 30 (DL30) minutes of dynamic compression. Principal components analysis (PCA) was utilized to assess metabolome-scale changes caused by mechanical loading. Pearson's correlation coefficients were used to estimate the flux of metabolite intensities over the timecourse of loading. To assess the differences in intensity distributions (m/z spectra plots for the various loading groups), two-sample Kolmogorov-Smirnov tests were implemented. Targeted metabolite profiles were analyzed by PCA, hierarchical agglomerative cluster analysis and correlation analyses. Additionally, the median ratios of NADP+:NADPH, NAD+:NADH, ATP:ADP, and GDP:GTP were calculated as a function of time to assess relative changes in energy metabolism.

Compound Identification and Enrichment Analysis. To putatively identify compounds, a batch search of all of the untargeted metabolite mass to charge (m/z) values was performed in METLIN and HMDB. Both databases contain over 80,000 identifiable metabolites [162, 163]. Search parameters included using a mass tolerance of 20 ppm, and positively charged molecules with potential $+1H^+$ or $+1Na^+$ adducts. Compounds with LipidMAPS identifications [164] were designated as human and not considered further if detected in a non-human species at the time of database search. Untargeted metabolites were then examined by unsupervised clustering to identify groups of co-regulated metabolites. Clusters of co-regulated metabolites were analyzed for pathway enrichment using IMPaLA [183].

Results

The objective of this study was to characterize the cellular response to applied compression for primary human OA chondrocytes by examining changes in metabolomic profiles. Chondrocytes were harvested from donor joint tissue, grown in tissue culture, embedded in agarose with stiffness similar to the human PCM, and dynamically loaded in tissue culture. Samples were then flash frozen, pulverized, and the metabolites were extracted and analyzed using HPLC-MS. We analyzed untargeted metabolomics profiles to minimize bias from *a priori* selection of relevant pathways which inherently excludes potentially important data. To evaluate our hypothesis, we also analyzed metabolomics profiles of targeted metabolites related to energy metabolism and protein production.

To our knowledge, the present study is the first application of metabolomics to analyze mechanotransduction in primary OA chondrocytes, and these data demonstrate

that applied dynamic compression alters both untargeted and targeted metabolomic responses of primary human OA chondrocytes *in vitro*. Using a systems biology approach, we find key difference between loaded and unloaded OA chondrocytes and identified 70 metabolites as potential mediators for chondrocyte mechanotransduction.

Untargeted Analysis. We detected 4955 metabolites present in at least one of the datasets. We refined the 4955 metabolite list to 1421 metabolites by focusing on metabolites that were present in over half of the samples for each loading group. To determine the effects of dynamic compression on chondrocyte metabolism, unloaded control samples were compared to samples subjected to either 15 or 30 minutes of dynamic compression. Statistical analyses found loading-associated differences that were both shared between human donors (n = 5) and specific to individual donors (examined with 5 replicates per donor).

Unsupervised clustering identified four clusters of interest in the untargeted metabolomic profiles (Figure 31A). These clusters suggest that pathways related to calcium signaling, energy metabolism, redox regulation, amino acid and lipid metabolism are regulated by mechanical loading (Supplemental Information). Comparisons between unloaded control (UC) and DL15 samples revealed changes in 456 metabolites (Figure 31B-C). Of these 456 metabolites, 334 were increased (↑) with dynamic loading and 122 were decreased (↓) in response to loading (Figure 31B-C). Comparisons between UC and DL30 found changes in 705 metabolites, of which 348 increased and 357 decreased, in response to dynamic compression (Figure 31B-C). Finally, we found differences in 512 metabolites between DL15 and DL30 groups. 145 metabolites increased and 367

decreased for 15 minutes of compression compared with 30 minutes of compression (Figure 31B-C).

These differences in mechanically-induced metabolomic profiles are supported by both principal component analysis (PCA) and comparisons of the distributions of metabolites between experimental groups. The log-transformed and normalized metabolite intensity data showed distinct separation in the first 3 principal components between the experimental groups (UC, DL15, and DL30, Figure 31D). The first three principal components contained 99.7% of the overall variance. The first principal component contained 49.4% of the variance, and the second and third principal components contained 31.8% and 18.5% of the total variance, respectively. Kolmogorov-Smirnov two-sample distribution tests revealed significant differences between the distributions of the median metabolite expression levels for the various loading groups (Supplemental Figure 14).

Correlation analysis examined the effects of the duration of dynamic compression (0, 15, or 30 minutes) on metabolite expression levels (Figure 32). There were 249 statistically significant metabolites that correlated with loading time. 119 metabolites were positively correlated (*i.e.* accumulated) and 130 were negatively correlated (*i.e.* depleted) with loading time (Figure 32A). The strongest positively and negatively correlated metabolites were defined as candidate mediators of chondrocyte mechanotransduction.

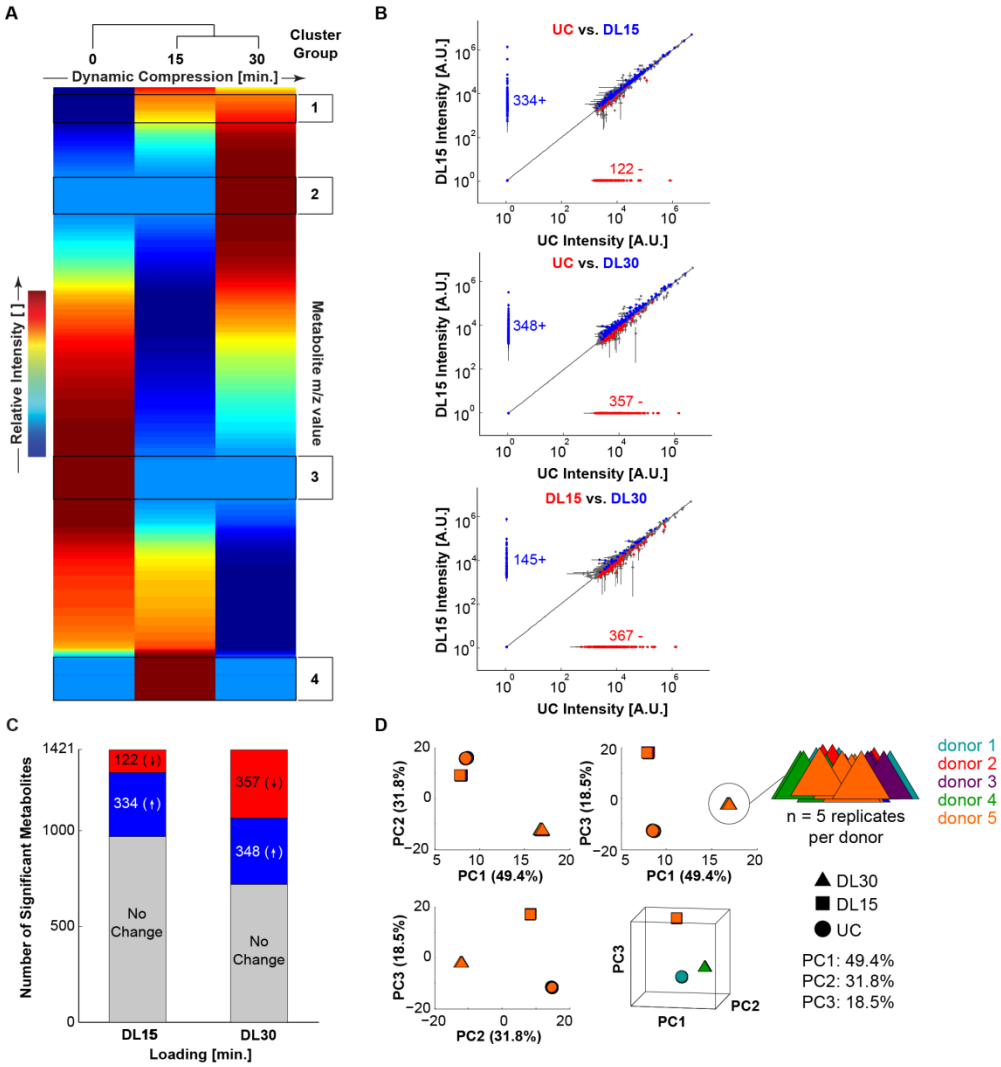

Figure 31. Applied compression resulted in distinct untargeted metabolomic profiles for primary OA chondrocytes. (A) Patterns of metabolite expression displayed via heatmap following hierarchical clustering. Clusters of interest denoted on the right-hand side (see Table 3). for enrichment analysis).Cluster 1: increasing with loading. Cluster 2: on after 30 min. Cluster 3: off with loading. Cluster 4: on at 15 min. (B) Loading-induced up-down regulation plots for UC vs. DL15, UC vs. DL30, and DL15 vs. DL30, respectively. Up regulated metabolites represent molecules that accumulate with respect to mechanical loading, and down regulated metabolites are being depleted with respect to mechanical loading. (C) Of the 1421 metabolites in common to all groups, 334 were upregulated and 122 were downregulated after 15 minutes of compression. 348 were upregulated and 357 were downregulated after 30 minutes of compression. (D) Principal Components Analysis for the untargeted data to assess differences between sample groups. The first three principal components contained 99.7% of the overall variance. For each of the sample groups, UC (●), DL15 (■), and DL30 (▲), there are n = 5 donors each sampled with 5 replicates.

Table 3. Pathways and metabolites altered by mechanical loading. Clusters refer to untargeted clusters identified in Figure 31A.

Pathways	Cluster	Mechanosensitive Metabolites [KEGG ID]
Galactose metabolism	1	C06376;C00159;C00795;C00267;C01132;C00095;C00124;C00137
	4	C00243;C05400;C01235;C05402;C00089
Chondroitin sulfate degradation	1	C02336;C00267;C04053;C00532;C10906;C00379;C01132;C03878;C00221;C01904
	3	C00252;C01083;C00243;C02713;C08240;C08250;C05402;C00089
	4	C00252;C01083;C00243;C08240;C08250;C05402;C00089
Lipid synthesis, transport, and metabolism	1	C00267;C01132;C00588;C01582
	2	C00588;C00157;C00246;C06429
	3	C00350;C00157
	4	C04230;C00157
Glycine, serine, and threonine metabolism	3	C00263;C05519;C06231;C00188
	4	C05519;C00263;C00188

Legend: Cluster 1-increasing with loading. Cluster 2-on after 30 min. Cluster 3-off with loading. Cluster 4-on at 15 min.

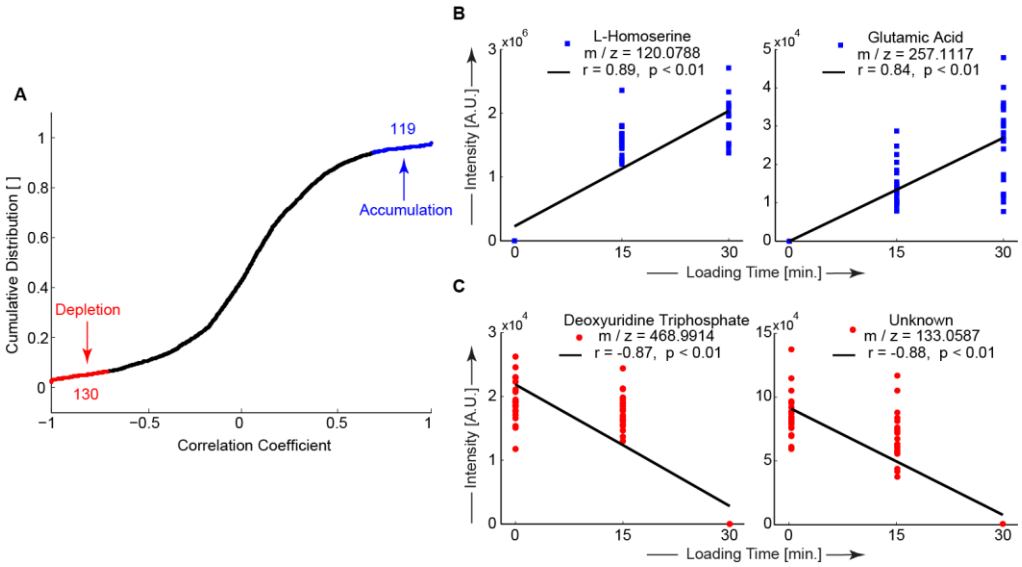

Figure 32. Dynamic compression results in both accumulation and depletion of untargeted metabolites. (A) The cumulative distribution of correlation coefficients of untargeted metabolites was used to identify metabolites that were either accumulating (blue) or being depleted (red). The strongest correlated metabolites were identified as candidate mediators of chondrocyte mechanotransduction. (B and C) Metabolite expression levels versus loading time used for correlation analysis. (B) Accumulation of selected candidate mediators of mechanotransduction which were database-matched as L-homoserine (left) and glutamic acid (right). (C) Depletion of selected candidate mediators of mechanotransduction. Deoxyuridine triphosphate as matched in the METLIN database (left) and a metabolite with m/z = 141.9573 which did not match any database molecules (unknown, right).

The number of significant mechanosensitive metabolites correlated with patient age (Figure 33-4, Table 4, and Supplemental Figure 15). Different donors displayed heterogeneity in their responses to applied compression. For each of the donors, (1-5), both 15 and 30 minutes of dynamic compression resulted in hundreds of statistically significant changes in metabolite expression (Table 4 and Figure 34). These results indicate that there are both shared and patient-specific responses to applied compression that are affected by aging.

Targeted Analysis. By focusing on metabolites common to central energy metabolism and protein production, we examined our hypothesis that that physiological dynamic compression increases chondrocyte glycolytic energy flux to promote the anabolic response to maintain the environment of the ECM and PCM. In this analysis, central energy metabolism focused on glucose metabolism including the pentose phosphate pathway (PPP), glycolysis (Glyc), and the tricarboxylic acid (TCA) cycle. Cluster analysis identified groups of metabolites with similar responses to applied dynamic compression (Figure 35A). PCA on targeted metabolites revealed that central energy metabolites are strongly regulated by applied compression (Figure 35B). Targeted metabolomics profiles from mechanically loaded groups clustered separately from unloaded controls, and the first three principal components contained 94.1% of the overall variance (1^{st} component: 89.1%, 2^{nd} component: 3.5%, and 3^{rd} component: 1.5%).

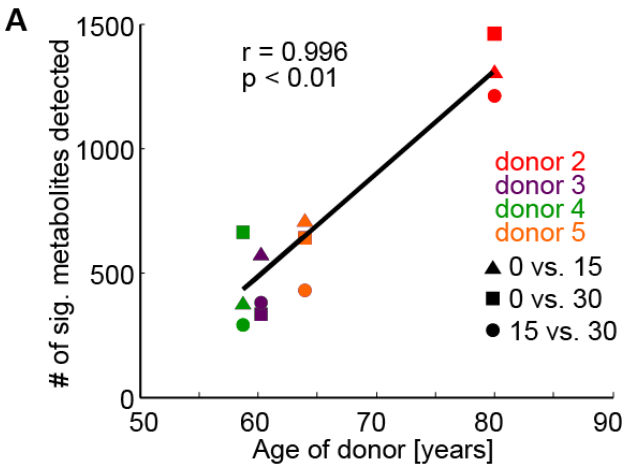

B

Donor	Sex	Age
2	F	80
3	F	60
4	F	59
5	F	64

Figure 33. Aging-related chondrocyte mechanotransduction. We observed a significant correlation ($r = 0.996$, $p < 0.01$) when comparing the number of significant mechanosensitive metabolites with the age of the femoral head donor. (A) Age-correlated increases in the number of significant metabolites. (B) Characteristics of femoral head articular cartilage used in the correlation analysis. Note that Donor 1 was male and is included in
Supplemental Figure 15.

Table 4. Statistically significant changes in metabolites for all five donors. Hundreds of metabolites were both up and down regulated for each of the donors.

Donor Number (age)	0 vs. 15		0 vs. 30	
	Up - regulated	Down - regulated	Up - regulated	Down - regulated
1 (54)	220	171	156	232
2 (80)	152	161	712	706
3 (60)	245	291	185	193
4 (59)	237	167	283	315
5 (64)	256	404	431	167

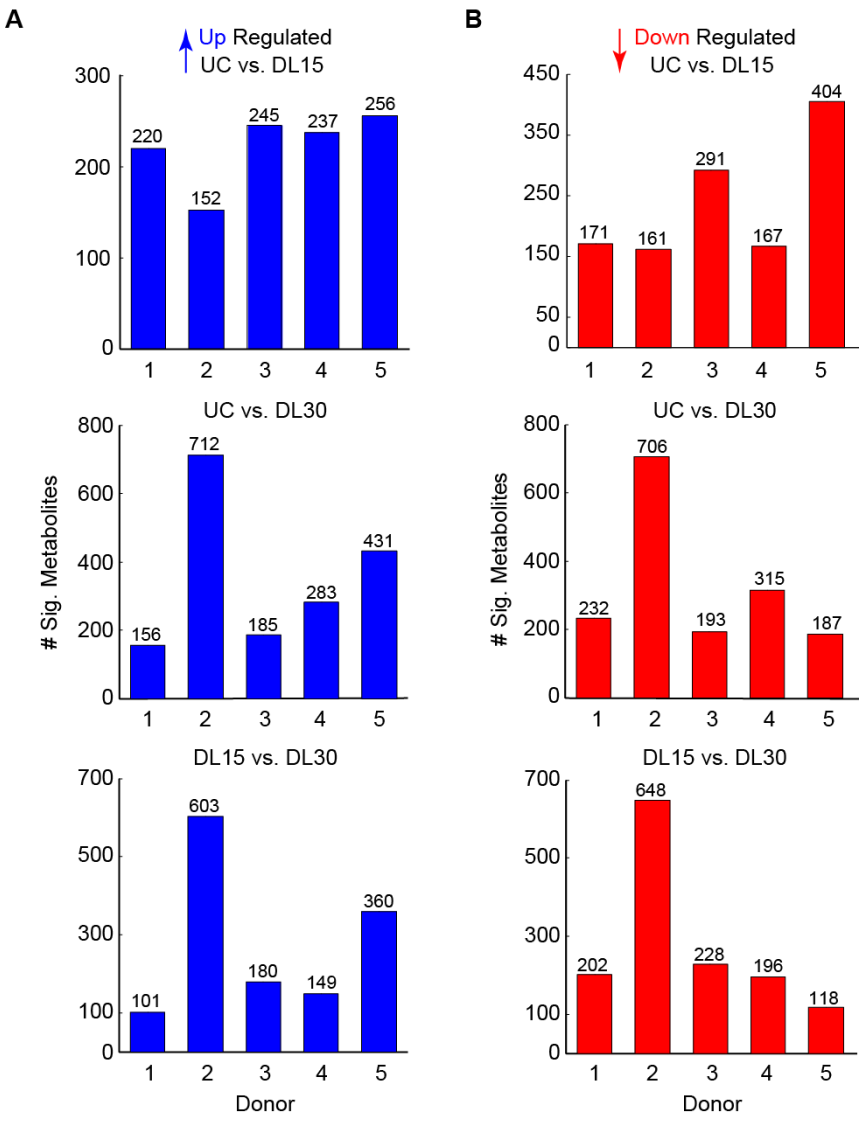

Figure 34. Patient-specific heterogeneity in chondrocyte mechanotransduction
Upon compression chondrocytes from each donor resulted in different numbers of significant mechanically up- (A) or down- (B) regulated metabolites. These differences may stem from variations in both type of end-stage osteoarthritis and patient-specific differences in the cellular response to mechanical loading.

To estimate changes in energy flux through the PPP, Glyc, and the TCA cycle, the median ratios of upstream to downstream expression levels for specific targeted metabolites were analyzed (Figure 35C). The ratio of NADP+ to NADPH decreased after 15 minutes of loading prior to increasing after 30 minutes of loading indicating an initial cessation in energy flow which then increases for the PPP. We observed continual increases in the ratio of ADP to ATP indicating increased glycolytic energy flux consistent with our hypothesis. Finally, we found a substantial decrease in the ratio of GDP to GTP after 15 minutes that was restored after 30 minutes of loading, indicating an initial cessation of TCA-based energy flux that recovers with additional mechanical loading. Both pyruvate and 3-phosphoglycerate were positively correlated with dynamic loading time (Figure 35D, $p < 0.01$). Taken together, these results demonstrate that mechanical loading strongly regulates chondrocyte energy metabolism with upregulation of glycolytic energy flux and transient decreases in energy flow to both the PPP and the TCA cycle that are restored following 30 minutes of loading.

Discussion

Previous studies have found altered mechanotransduction between normal and OA chondrocytes. Kawakita *et al.* found a significant reduction of Akt phosphorylation in diseased (OA) chondrocytes in response to cyclic loading, whereas Niehoff *et al*. found that cyclic loading induced Akt phosphorylation in healthy chondrocytes. Akt is serine/threonine kinase that has been shown to play an important role in a variety of chondrocyte cellular mechanisms, including cell apoptosis [184], cell proliferation and growth [185], and proteoglycan synthesis [186]. Holledge *et al.* found that increased

sulfated glycosaminoglycan production was significantly larger for normal than OA chondrocytes in response to 0.33 Hz oscillatory fluid flow in monolayer. These studies emphasize the differences in cellular phenotypes between normal and OA chondrocytes in response to mechanical stimulation.

We applied dynamic compression to primary chondrocytes and observed both increases and decreases in hundreds of untargeted metabolites. These metabolomic changes represent an altered cellular phenotype resulting from exogenous, dynamic loading. The ability of metabolomic characterization to capture chondrocyte responses to compression is highlighted by our observation that, when comparing between 0, 15, and 30 minutes of loading, 99.7% of the variance is contained in the first 3 principal components (Figure 31D). The importance of compression in regulating chondrocyte behavior is further emphasized by the numerous differences between unloaded and loaded samples (Figure 31-2, and Supplemental Figure 14). These significant differences demonstrate both the importance of mechanical loading to chondrocyte biology and the ability of metabolomics to describe large-scale changes in chondrocyte physiology.

The metabolome is defined as the set of small-molecules found within a biological sample including substrates, co-factors, and other cytosolic molecules that comprise the physiology of cellular biochemistry [95]. The metabolome can be viewed as a collection of state variables describing the cellular phenotype [96]. These measurements provide valuable insight into how chondrocytes sense and respond to applied loading. Future studies may build on this untargeted dataset by creating mathematical models (*e.g.* Hidden Markov Models) between normal and OA cells to

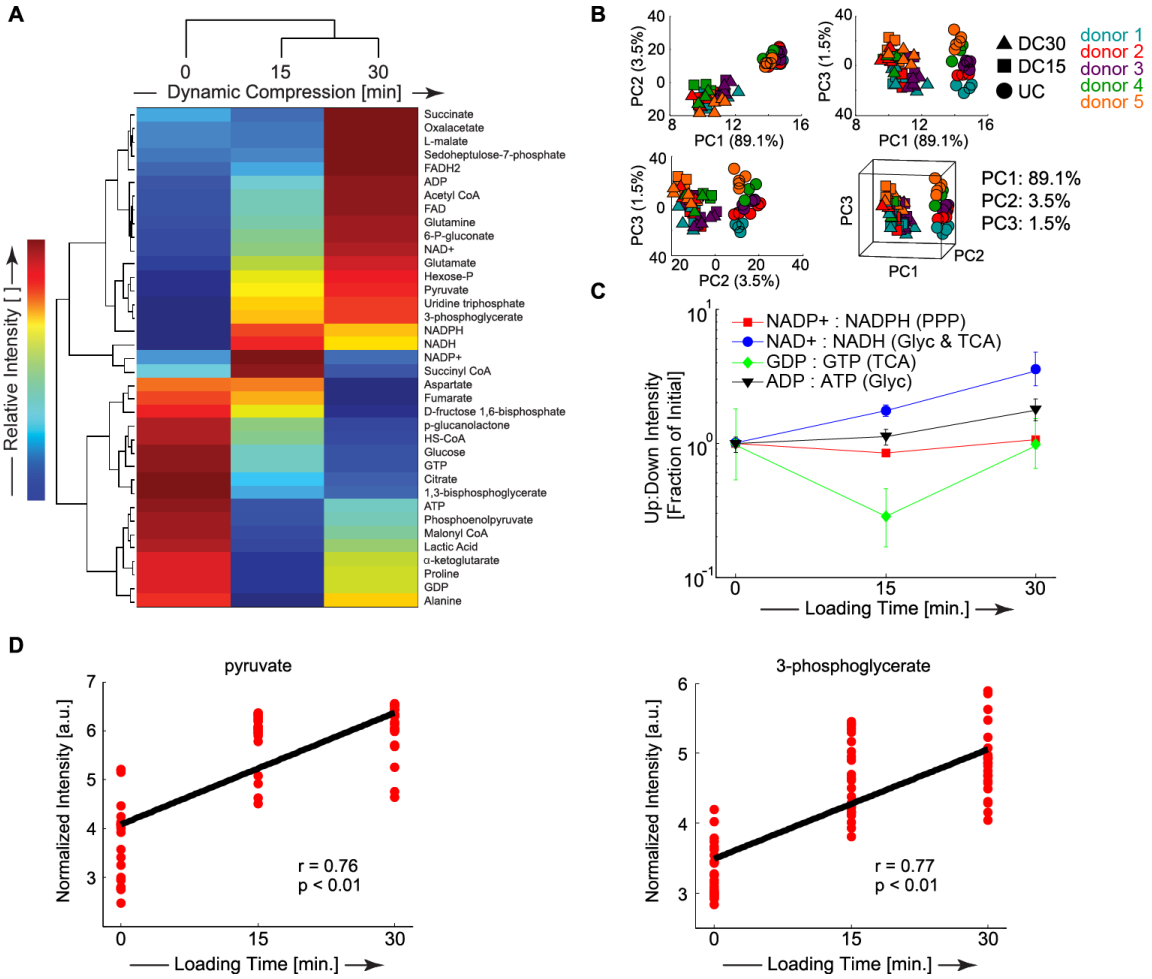

Figure 35. Loading-induced changes in expression of targeted metabolites specific to central-energy-metabolism. Metabolites associated with central energy metabolism and protein production (*e.g.* amino acids) were targeted for detailed analysis via detection of multiple ionized adducts and ions. (A) Hierarchical agglomerative cluster analysis reveals changes in metabolite intensities with respect to increased dynamic loading. (B) Principal Components Analysis for the targeted data was used for comparing differences/separations among sample groups. The first three principal components contained 94.1% of the overall variance. For each of the sample groups, UC(●), DL15(■), and DL30(▲), there were n = 5 donors sampled 5 times. (C) Ratios of upstream to downstream mediators of central energy metabolism. Note error bars are smaller than the symbols and do not display on this plot. PPP = pentose phosphate pathway. Glyc = Glycolysis. TCA = Tricarboxylic Acid Cycle. (D) Significant accumulation of pyruvate and 3-phosphoglycerate in response to applied dynamic compression.

identify candidate pathways for therapeutic intervention. For example, if specific mechanosensitive pathways are found that enable anabolic processes in chondrocytes, mechanical loading (*i.e.* exercise) could potentially be administered as an effective therapeutic method for healing damaged cartilage. Many of the therapeutic strategies available for OA patients today (*e.g.* joint replacement) are extremely expensive, and inaccessible to certain patient populations. Extending these results to determine optimal daily loading of cartilage (*e.g.* exercise) as a therapeutic treatment for OA would be extremely valuable to combat OA and other associated comorbidities simultaneously.

In this study, we identify mechanosensitive pathways using enrichment analysis of clusters of co-regulated metabolites (Figure 31A, Table 3, Supplemental Tables). Dynamic compression notably decreased expression of several metabolites compared with unloaded controls (Figure 31A, Cluster 3), including valine, leucine, and isoleucine biosynthesis. Several other metabolites increase dynamic loading. These metabolites were enriched for ion-channel signaling and glutathione synthesis, which are consistent with prior chondrocyte data [187, 188] and support physiological compression as a mechanism to produce cartilage matrix. Riboflavin metabolism and glycogenoloysis also gradually increased with loading suggesting that cellular energy utilization can be altered by the mechanical environment [189, 190].

Additionally, there was increased expression of metabolites specific to either 15 or 30 minutes of dynamic compression. Fifteen minutes of dynamic compression resulted in glycine, serine, and threonine metabolism (Figure 31A, Cluster 4). Thirty minutes of dynamic compression resulted in upregulation of metabolites enriched for

amino acid and lipid metabolism (Figure 31A, Cluster 2). Metabolites relating to phenylalanine, tyrosine, and tryptophan synthesis were upregulated, in addition to those for arginine and proline metabolism, consistent with the biosynthetic effects of dynamic compression.

Certain pathways were represented in multiple clusters (Table 3). This result may represent differential regulation of distinct pathway components (*e.g.* upstream vs. downstream) or technical limitations. Technical limitations include the inability of the mass spectrometry to distinguish between isomers (*e.g.* changes in phospholipid structure) or between identified masses within 20 ppm database search tolerances. Dynamic compression appeared to increase remodeling of chondroitin sulfate and increase glycine, serine, and threonine metabolism emphasizing the importance of loading to matrix remodeling. Several metabolites related to lipid synthesis, transport, and metabolism were affected suggesting alterations of the cell membrane in response to dynamic compression [191]. Finally, galactose metabolism was upregulated by loading, further suggesting the importance of energy metabolism in defining the chondrocyte response to loading.

Because cartilage is a viscoelastic material, cyclical loading results in internal energy dissipation within the tissue [171, 172]. To date, it is unknown whether or not applied mechanical deformation can alter cellular energy utilization. We hypothesized that physiological dynamic compression will increase glycolytic energy flux to promote the anabolic response in chondrocytes to maintain the environment of the ECM and PCM. This project provides fundamental data for understanding potential mechanical-to-

cellular energy conversion by quantifying relative levels of metabolites targeted to central energy metabolism (Figure 35).

Hierarchical clustering clearly demonstrated that dynamic compression regulates energy-related metabolites, and we found accumulation of key amino acid precursors including pyruvate and 3-phosphoglycerate which may indicate increased glycolytic flux (Figure 35). These glycolytic changes were also marked by the consumption of fructose-1,6-bisphosphate and 1,3-bisphosphoglycerate which may serve to increase pyruvate flux for maximizing protein synthesis. The future application of a stoichiometric matrix model for flux balance analysis will enable full evaluation of our hypothesis by simultaneous analysis of the complete dataset to infer whether observed consumption and accumulation indicate increased or decreased metabolic flux [192]. The significant changes in expression of these specific metabolites in response to dynamic loading may indicate energy utilization towards matrix protein production.

In this study, chondrocytes were harvested from hip replacement patients with Grade IV osteoarthritis. In our analysis, we found a strong correlation between the number of mechanically sensitive metabolites and patient age ($p < 0.01$, $r = 0.996$). These data suggest a relationship between aging and mechanotransduction as measured by the chondrocyte metabolome in response to applied physiological compression. Future studies may build on this work to identify differences in clinical patient populations, by utilizing untargeted LC-MS-based metabolomics as potential mechanism to identify biomarkers in osteoarthritis [193]. The candidate mediators identified in this study (Supplemental Tables) may prove useful as indicators of normal and OA

mechanotransduction. To our knowledge, this is the first time that metabolomics has been used to assess the loading induced differences for primary human OA chondrocytes.

Conclusions

This study demonstrates the power of utilizing high-dimensional metabolomics as a tool for understanding chondrocyte mechanotransduction. In our targeted analysis, we discovered significant correlations with increased mechanical loading and central energy reorganization. Similarly, our untargeted analysis revealed hundreds of significant metabolites, including potential novel mediators for chondrocyte mechanotransduction via energy, lipid, and amino acid metabolism. Finally, we found a positive correlation between the number of mechanically-induced metabolites and patient age, suggesting that metabolomics can characterize aging-dependent changes in chondrocyte mechanotransduction. Metabolomics may yield important biomarker candidates for tracking the progression of OA in clinical populations. Future work will expand on these data to elucidate the mechanosensitive differences between OA and normal human chondrocytes.

Acknowledgements

We acknowledge Drs. Ross Carlson, Brian Bothner, and Edward Dratz, MSU, for critical insight provided during discussions. We thank Timothy Hamerly for generating and sharing the standards data. The SW1353 cell line was kindly donated by Martin Lotz. Funding was provided by NIH P20GM10339405S1, NSF 1342420, Montana State University, and the Murdock Charitable Trust.

References

See REFERENCES CITED.

PHOSPHOPROTEOMICS

To further explore the biological outputs of chondrocytes under applied deformation, this chapter is aimed at evaluating the phosphoproteomic response of primary human OA chondrocytes in response to applied dynamic compression. This chapter builds off of Chapter 3 by using the same *in vitro* model that was developed in Chapter 2, to understand what proteins are phosphorylated when the chondrocytes are exposed to dynamic loading. Again, to my knowledge, this study is the first of its kind, and has yet to be reported to date.

Proteomics is defined as the large-scale study of proteins. In mammalian cells, proteins are coded by genomic DNA sequences (through many complex processes), which is commonly referred to as the central dogma of modern biology. DNA (deoxyribonucleic acid), is a molecule that encodes the genetic instructions used in the development and functioning of all living organisms, and in eukaryotic organisms most of the DNA is stored within the cell nucleus [102]. For production of protein, DNA is transcribed into mRNA (messenger ribonucleic acid), which is a single stranded message containing the genetic code. mRNA is then translated into long strings of amino acids (polypeptides) in the cell's cytoplasm by ribosomes, and eventually fold into complex structures which are known as proteins. Proteins are considered the building blocks and workers of our cells, and each protein serves a unique purpose. After translation (post-translation), proteins can be subjected to an array of chemical alterations, which can affect the protein's function, including the ability to process metabolites. These changes are called post-translational modifications. An important post-translation modification

occurs when a phosphate group is added to an amino acid (most commonly serine and threonine) and is known as protein phosphorylation [103]. Protein phosphorylation modifies the functional activity of a protein and gives insight of specific signaling pathways affected by environmental stimuli, including mechanical loading. Phosphoproteomics is aimed at determining these specific phosphorylated proteins in a cell under some external stimulus.

This Chapter builds off of the methods developed in Chapter 3 to analyze the global phosphoproteomic profiles of chondrocytes in response to mechanical stimulation. This chapter uses identical encapsulation and mechanical stimulation methods as in Chapter 3; however, instead of extracting metabolites, proteins are extracted. Following extraction, proteins are proteolyzed (*i.e.* enzymatically digested), and then the digested proteins (or peptides) are enriched for phosphopeptides using TiO_2 enrichment. Samples are then analyzed using liquid chromatography (LC) and mass spectrometry with fragmentation (MS/MS). The objective of this study is to assess phosphoproteomic changes for primary human OA chondrocytes as a function of dynamic compression from 0-30 minutes. The rationale for this objective is to provide mechanistic insight into the metabolomic data from Chapter 3.

SHOTGUN PHOSPHOPROTEOMICS IDENTIFIES ACTIVATION OF VIMENTIN, ANKYRIN, VAM6/VPS39-LIKE PROTEIN IN PRIMARY HUMAN OSTEOARTHRITIC CHONDROCYTES AFTER MECHANICAL STIMULATION

Contribution of Authors and Co-Authors

Author: Donald L. Zignego[1]

Contributions: Acquired, analyzed, and interpreted the data. Drafted and wrote the manuscript.

Co-Author: Jonathan K. Hilmer[2]

Contributions: Interpreted data and reviewed the manuscript.

Corresponding Author: Ronald K. June[1,3]

Contributions: Designed the study, analyzed and interpreted the data, and wrote the manuscript.

[1]Department of Mechanical and Industrial Engineering, Montana State University, Bozeman, MT 59717-3800, USA

[2]Department of Chemistry and Biochemistry, Montana State University, Bozeman, MT 59717-3800, USA

[3]Department of Cell Biology and Neuroscience, Montana State University, Bozeman, MT 59717-3800, USA

Manuscript Information Page

Donald L. Zignego, Jonathan K. Hilmer, and Ronald K. June
eLife
Status of Manuscript:
_X_ Prepared for submission to a peer-reviewed journal
___ Officially submitted to a peer-reviewed journal
___ Accepted by a peer-reviewed journal
___ Published in a peer-reviewed journal

Publisher: eLife Sciences Publications.
Prepared: July 2015

Abstract

Objective. Articular cartilage is comprised of dense extra cellular matrix (ECM), less dense pericelluar matrix (PCM), water, ions, and the sole cell type found in cartilage, chondrocytes. Chondrocytes are directly responsible for maintaining cartilage homeostasis through a variety of catabolic and anabolic processes. Articular cartilage, and thus chondrocytes, are constantly subjected to mechanical loading *in vivo*. Prior research has shown that chondrocytes have the ability to transduce these mechanical stimuli into biochemical signals; however, many mechanosensitive signaling pathways and processes by which this mechanotransduction occurs remain elusive. In this study we hypothesize that physiological, dynamic compression results specific phosphoproteomic changes that promote matrix synthesis. The objective of this study was to use shotgun proteomics to identify changes in protein phosphorylation to understand mechanotransduction in primary human OA chondrocytes.

Design. Primary human chondrocytes were harvested from the femoral heads of osteoarthritic (OA) donors undergoing total hip replacement (n=5). Physiologically stiff, cell-seeded agarose constructs were randomly assigned to one of three experimental groups: (1) unloaded control samples, and samples loaded for either (2) 15 minutes or (3) 30 minutes of dynamic compression (n=5 samples per experimental group with 5 replicates for each donor). Following dynamic compression, proteins were extracted, digested, peptides enriched for phosphorylation, and detected by HPLC-MS/MS. Untargeted, shotgun analyses examined changes in global phosphoproteomic profiles in response to applied compression.

Results. This study identified over 2000 phosphoproteins in each of loading groups, with 514 phosphoproteins unique to dynamically stimulated samples. We identify novel signaling pathways for each of the loading groups. For loaded samples we identified statistically significant pathways regulated as a result of dynamic compression, including Rho GTPase signaling, hyaluronan synthesis, MAPK signaling, and hedgehog signaling.

Conclusions. To our knowledge, this is the first study to characterize phosphoproteomic profiles of primary human chondrocytes in response to applied dynamic compression. These results complement previous data regarding chondrocyte mechanotransduction, and add significant new data to a developing model of how chondrocytes transduce mechanical loads.

Introduction

Osteoarthritis (OA) is the most common joint disorder worldwide [1-7], and is characterized by the breakdown of the protective articular cartilage the covers the joint surfaces. Articular cartilage is composed primarily of a dense extra cellular matrix (ECM), a less dense pericellular matrix (PCM), and highly specialized cells termed chondrocytes [37]. At these joint surfaces of the body (*e.g.* the hip and knee), the chondrocytes are subjected to repetitive mechanical loading which has been shown to reach magnitudes as high as 10 times an individual's body weight [55]. Cellular mechanotransduction is the process by which cells sense and respond to mechanical stimulation through an array of biological and biochemical outputs [49]. It is well established that chondrocytes [49, 84, 87, 93], and other mammalian cells [133-135, 141] have transduce mechanical inputs into biological signals, but the link between these two processes remains unclear [51].

Chondrocytes are the sole cell type in articular cartilage, and play a critical role in maintaining the homeostasis of the tissue. Cartilage homeostasis is maintained through both anabolic and catabolic chondrocyte metabolism, and it has been shown that the delicate balance between these two processes can be altered with mechanical stimulation [43, 173]. The role of healthy chondrocytes is primarily anabolic in nature. The anabolic program includes protecting, maintaining, and repairing the joint tissue by synthesizing collagen (mostly type II collagen), and proteoglycans [194] through the secretion of cytokines , growth factors, and protease inhibitors [173]. However, in diseased cartilage (*e.g.* OA), the catabolic program dominates, and usually involves the breakdown of ECM

and PCM molecules through the secretion of proteases (*e.g.* matrix metalloproteinase (MMPs)). It has been shown that dynamic loading can promote anabolic responses in chondrocytes, whereas static loading inhibits chondrocyte matrix anabolism [174, 175, 195, 196].

Signaling in chondrocytes has been previously studied, specifically the intercellular pathways involving proliferation [197], cell differentiation and dedifferentiation [198], matrix catabolism (via MMPs and ADAM/ADAM-TS gene expression) [199], and programmed cell death [200]. Proteomics has also been used as a tool for revealing potential biomarkers of OA through analysis of cartilage secreted proteins [201], synovial fluid [202, 203], and serum [204, 205] These studies provide a detailed understanding of various processes in chondrocyte mechanically induced signaling; however many signaling mechanisms remain unclear, including many pathways in which protein phosphorylation is thought to mediate signaling. Previous phosphoproteomic analysis of primary human chondrocytes provided high-dimensional insight into the pathophysiology of degradative diseases in cartilage [194]. However, to our knowledge, few, if any, studies have utilized phosphoproteomics as a tool for elucidating signaling mechanisms of chondrocyte mechanotransduction. In this paper, we seek to expand understanding of chondrocyte mechanotransduction via protein phosphorylation. The objective of this study was to use shotgun proteomics to identify phosphorylated proteins as candidate mediators of chondrocyte mechanotransduction in primary human OA chondrocytes. We hypothesize that physiological dynamic compression results in a phosphoproteomic signature consistent with matrix anabolism.

In the study presented here, we analyze the short term (<30 min) phosphoproteomic changes of primary human OA chondrocytes in response to physiological compression. We have previously demonstrated large-scale metabolomic changes in primary human OA chondrocytes as a result of dynamic compression [206] utilizing cell-seeded agarose hydrogels with stiffness similar to the human PCM [114, 115, 207]. In this study we perform phosphoproteomic profiling of primary chondrocytes following applied compression. Using shotgun proteomics, we identified over 2000 phosphoproteins in each of the loading groups, with 514 phosphoproteins unique to samples subjected to dynamic compression. To our knowledge, such a study has not been reported previously. Future work may build on these results to explore the therapeutic potential of mechanical loading in OA and to identify drug targets for modulating protein phosphorylation to improve cartilage repair strategies.

Materials and Methods

Chondrocyte Culture and Encapsulation. Primary human chondrocytes were harvested, isolated, and encapsulated using previously optimized methods [116, 206]. Briefly, chondrocytes were harvested from five Grade IV OA patients undergoing total hip joint replacement surgery (mean age: 63 years (range: 54-80), and mean mass: 80.4 kg (range: 56.9-99 kg)). Cartilage shavings were digested in Type IV collagenase (2 mg/mL for 12-14 hrs. at 37°C), and cultured in DMEM with 10% fetal bovine serum and 1% antibiotics (10,000 I.U. /mL penicillin and 10000 µg/mL streptomycin) in 5% atmospheric CO_2. Cells were encapsulated at a concentration of ~500,000 cells/gel, and equilibrated in tissue culture conditions for 72 hours.

Mechanical Stimulation. Mechanical stimulation was performed using identical methods from Zignego, *et al.* [116, 206]. Briefly, for each donor (N=5, female), cell-seeded agarose gels were randomly assigned to one of three loading groups: unloaded controls (*i.e.* 0 minutes of loading), 15, or 30 minutes of dynamic, cyclic compression (n = 5 biological replicates for each loading group). Homogenous deformations [115] were applied to cell-seeded gels using previously optimized methods [116, 206], using a custom-built bioreactor emulating physiological loading conditions (3.1-6.9% strain, calculated from initial gel height and a frequency = 1.1 Hz [153]).

Protein Preparation and Extraction. Using methods described previously [116, 206], gels were flash frozen in liquid N_2, pulverized, and stored at -80°C prior to cell lysis. Gels were lysed by sonication and vigorous vortexing in RIPA buffer (50mM Tris-HCL (pH 8.0), 50mM NaCl, 1% NP-40, 0.5% sodium deoxycholate, and 0.1% SDS [208]). Samples were then centrifuged at 21,000 x g at 4°C for 10 minutes. The supernatant was extracted, and the proteins were precipitated using ice-cold acetone overnight at -20°C. Samples were centrifuged the next day at 21,000 x g at 4°C for 10 min, and the acetone supernatant was removed. The purified protein pellet was then re-suspended in 0.5M triethylammonium bicarbonate (TEAB), and all replicates for each loading group from the individual donors were combined (*i.e.* n=5 replicates for the unloaded control samples for donor 1 were combined into one vial, etc…). The combined samples now consisted of one unloaded control sample, one sample at 15 minutes of dynamic compression, and one sample at 30 minutes of dynamic compression for each donor (N=5 donors, n=5 replicates for each loading group).

Proteolysis, TiO2 Phosphopeptide Enrichment, and Graphite Cleanup. Protein concentration was quantified using absorbance at 280 nm (NandDrop 2000c, Thermo Scientific). 400 µg of protein was then reduced for 1 hour at 60°C with 10mM tris (2-carboxyethy) phosphine (TCEP) and cysteine-blocked with 8mM iodoacetamide at room temperature in the dark for 30 minutes prior to proteolysis. Samples were then digested with mass-spectrometry grade trypsin (1:20, Trypsin :Substrate, Promega Gold Trypsin, San Luis Obispo, CA) overnight at 37°C [201]. After digestion, samples were acidified, and solvent was removed using a Speed-Vac concentrator. Digested peptides were resuspended in sample buffer (MS-grade H_20, acetonitrile and TFA, 20:80:0.4 (v/v)), enriched for phosphopeptides, and purified using graphite columns according to the manufacturer's instructions (Pierce TiO_2 Phosphopeptide Enrichment and Clean-up Kit #88301). Enriched samples were then dried a second time using a Speed-Vac concentrator.

Shotgun Phosphoproteomics LC-MS/MS. MS data collection for the prepared peptide samples was performed with nanospray UHPLC-MS in the Montana State University Mass Spectrometry Core Facility [155-157]. The dried peptides were resuspended in 50 µL of mass spectrometry grade water, acetonitrile, and formic acid (98:2:0.1v/v/v) with shaking for 15 minutes, and transferred to auto sampler vials. Aliquots of 5 µL each were sampled via Dionex Ultimate 3000 nano UHPLC, with an Acclaim PepMap100 C18 column used for trapping (100 [MICRO]m x 2cm) and an Acclaim PepMap RSLC C18 (75 µm x 50 cm, C18 2 um 100A) for final peptide separation. The loading pump used 97% H_2O, 3% acetonitrile, with 0.1% formic (v/v).

The analytical/elution pump solvent consisted of H_2O with 0.1% (v/v) formic acid for channel "A" and acetonitrile for channel "B". Chromatography was as follows: for 10 minutes, the sample was loaded onto the trapping column at a flow rate of 10 µL/min. From 10 to 11 minutes, the loading pump flow rate was ramped down to 5 µL/min. At 12 minutes, the loading valve was switched to place the trapping column in-line with the analytical column, and from 12 to 17 minutes the loading pump flow rate was ramped from 5 to 40 µL/min. From 106 to 108 minutes the loading pump was ramped back from 40 to 5 µL/min. The analytical/elution pump was maintained at 500 nL/min for the entire run. From 12 to 90 minutes the analytical pump solvents were ramped from 5% to 30% B. From 90 to 105 minutes the analytical pump solvents were ramped from 30% to 95% B. At 110 minutes, the loading valve was switched to divert the trapping column to waste. From 119 to 120 minutes the analytical pump solvents were ramped from 95% to 5% B, and at 120 minutes each run was completed.

The mass spectrometer was a Bruker maXis Impact with CaptiveSpray ESI source: resolution is ~40,000 and accuracy is better than 1 ppm. Spectra were collected in positive mode from 150 to 2200 m/z at a minimum rate of 2 Hz for both precursor and fragment spectra, and with adaptive acquisition time for highly-abundant ions (16 Hz for >= 25000 counts to 4 Hz for < 2500 counts).

Data Processing. The resulting data files converted with MSConvert (ProteoWizard [209]) to 32-bit .mzML format. These files were then processed with a variety of bioinformatics tools. OpenMS TOPPAS [210] was used to create XTandem workflows to search all of SwissProt and TrEMBL to evaluate all possible matches. Both

fixed (f) and variable (v) modifications were considered in the database search (carbamidomethyl modification of cysteine (f), oxidation of methionine (v), phosphorylation of serine (v), phosphorylation of threonine (v), and phosphorylation of tyrosine (v)), allowing for up to two missed cleavage sites. Precursor tolerance was set to 50 ppm and MS/MS fragmentation tolerance was 0.05 Da [173]. Instrument type was set to ESI-quad-TOF, and peptide charges up to 3+ were permitted. The search database included the reviewed, *Homo sapiens* database (Uniprot/Swissprot) which was modified to contain both targets and "reversed" decoys for FDR (false discovery rate) analysis [211, 212]. The processed data files were then exported into Excel (Microsoft, Redmond, WA), and used for statistical and pathway-over representation analysis using Integrated Molecular Pathway Level Analysis (IMPaLA, http://impala.molgen.mpg.de [213]).

Data Analysis and Candidate Selection. To assess the effects of mechanical loading on chondrocyte protein phosphorylation, three randomly assigned groups of cell-seeded agarose hydrogels were established: unloaded control samples (UC), samples undergoing 15 minutes of dynamic compression (DL15), and samples undergoing 30 minutes of dynamic compression (DL30). Statistical analysis was performed using the combined samples for each loading group, from each donor (n=5 replicates/loading group). We defined detected phosphoproteins as those present in the majority of the replicates. To determine loading induced differences between samples, each dataset was compared against the others to determine (1) unique phosphoproteins to that loading group, and (2) overlapped or shared phosphoproteins between loading groups. Four separate comparisons were made: (1) UC vs. DL15, (2) UC vs. DL30, (3) DL15 vs.

DL30, and (4) UC vs. DL15 vs. DL30. For phosphoproteins identified in all three groups (*i.e.* UC, DL15, and DL30), statistical comparisons were made using Wilcoxon signed rank tests and Kruskal-Wallis one-way analysis of variance.

Results

The objective of this study was to characterize the phosphoproteomic response of primary human OA chondrocytes in response to applied, dynamic compression. In short, chondrocytes were harvested from donor joint tissue (n=5 donors with Grade IV OA), grown in tissue culture, embedded in physiologically stiff agarose (matched to human PCM), and dynamically compressed in tissue culture. Samples were flash frozen, pulverized, and lysed. Proteins were concentrated, purified, and proteolyzed. Digested peptides were then TiO_2 enriched for phosphopeptides, and finally analyzed via shotgun proteomics using HPLC-MS/MS (Figure 36). We analyzed the untargeted (global) phosphoproteomic profiles to minimize bias by the exclusion of important, but unexpected, data (*i.e.* if only a single specific signaling pathway was selected *a priori*). To our knowledge, the present study is the first application of phosphoproteomics to analyze mechanotransduction in primary OA chondrocytes. These data demonstrate that applied dynamic compression alters the phosphoproteomic response of primary human OA chondrocytes *in vitro*.

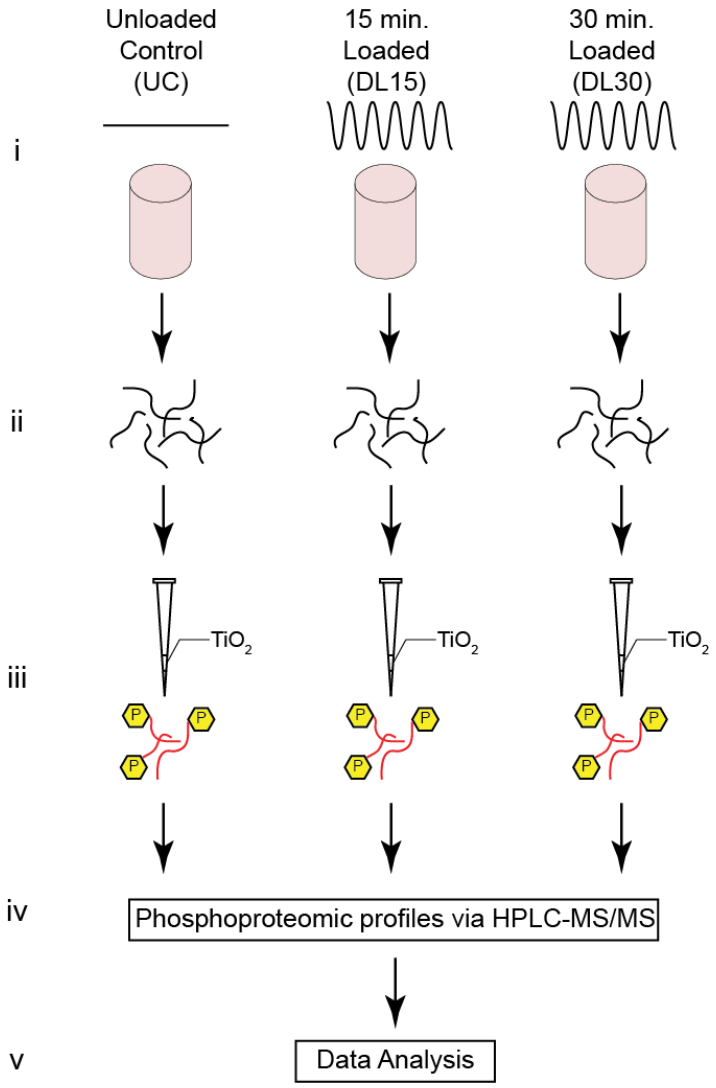

Figure 36. Experimental Design. (A) Schematic for both untargeted experimental methods. (i) Primary human OA chondrocytes are encapsulated in physiologically stiff agarose (4.5% agarose, stiffness ~35 kPa), cultured for 72 hours, and then dynamically compressed in tissue culture for 0, 15, or 30 minutes (Control, DL15, or DL30) at 1.1 Hz. (ii) Proteins are extracted by flash freezing the samples, pulverizing, and lysing the cells followed by overnight enzymatic digestion. (iii) Samples are enriched for phosphopeptides using TiO_2 enrichment, (iv) phosphoproteomic profiles identified via HPLC-MS/MS, and (v) the untargeted data analyzed.

For data processing, each of the individual samples (n=5 replicates per loading group) for each of the loading groups (UC, DL15, and DL30) were processed individually through the TOPPAS pipeline. For UC samples, 13,838 ± 249 (mean ±

SEM) phosphoproteins were identified, which included decoy protein hits. 13,650 ± 525 and 13,088 ± 287 phosphoproteins were identified for DL15 and DL30 samples, respectively. Following false discovery rate (FDR) filtering using the decoy protein hits and combining all replicates from each loading group, we identified 2858, 2246, and 2570 phosphoproteins for UC, DL15, and DL30, respectively. We then further refined these data by focusing only on phosphoproteins that were present in more than half of the samples for each loading group. The final list consisted of 767, 359, and 623 phosphoproteins for UC, DL15, and DL30, respectively. To analyze the effects of dynamic compression on chondrocyte metabolism, we made individual comparisons between unloaded control samples and samples loaded for either 15 or 30 minutes of dynamic compression.

The first comparison between unloaded controls (UC) and DL15 samples revealed 685 phosphoproteins unique to UC, 277 unique to DL15, and 82 phosphoproteins common between the two samples. Of the 82 shared phosphoproteins, 3 of them were significantly ($p<0.05$) up-regulated as a result of mechanical loading, one being proline-rich basic protein 1. For the second comparison, UC was compared against DL30 samples. 658 phosphoproteins were unique to UC, 514 unique to DL30, and 109 common between both samples. Of the 109, 4 were statistically ($p<0.05$) up-regulated and 2 of them statistically down-regulated. For the third comparison (DL15 vs. DL30), 287 phosphoproteins were unique to DL15, 551 unique to DL30, and 72 common between them. Of the 72, one phosphoprotein was down-regulated with increased loading. The final comparison compared UC, DL15, and DL30 together (Figure 37).

612 phosphoproteins were unique to UC, 241 unique to DL15, 273 unique to DL30, and 36 common between all three of them.

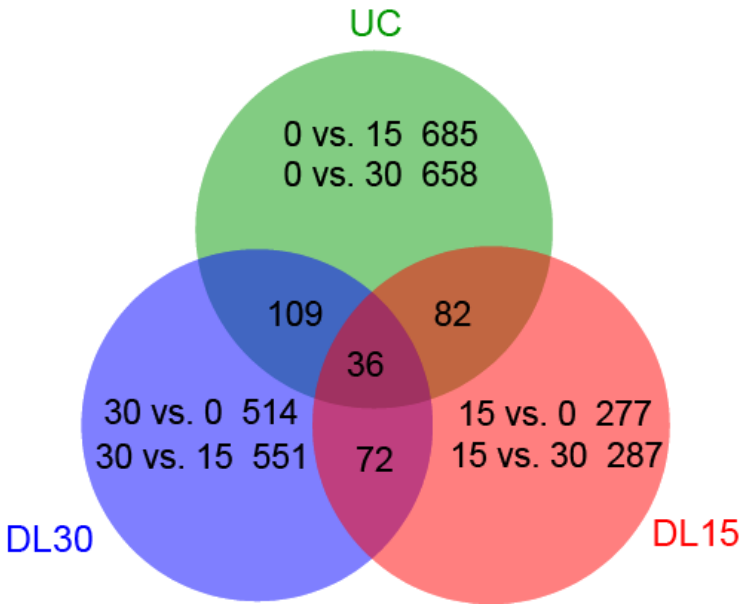

Figure 37. Dynamic compression alters phosphoprotein expression in primary OA chondrocytes. To further explore the effects of dynamic compression on the chondrocyte phosphoproteome, we determined the number of phosphoproteins which were unique to each of the experimental comparisons (UC vs. DL15, UC vs. DL30, DL15 vs. DL30, and UC vs. DL15 vs. DL30). 685 phosphoproteins were identified in control samples (UC) that were not detected in samples subjected to 15 minutes of dynamic compression (DL15), 277 phosphoproteins were identified in DL15 samples that were not detected in UC, and 82 phosphoproteins were common to both samples. 658 phosphoproteins were identified in UC that were not detected in DL30, 514 phosphoproteins were detected in DL30 that were not in UC, and 109 phosphoproteins were common to both samples. 287 phosphoproteins were identified in DL15 that were not detected in DL30, 551 phosphoproteins were detected in DL30 that were not in DL15, and 72 phosphoproteins were common to both samples. 36 phosphoproteins were common to all three samples.

Unsupervised, agglomerative cluster analysis revealed three unique groups of phosphoprotein profiles which were regulated as a result of dynamic compression (Figure 3). Cluster group 1 reveled phosphoproteins which were up-regulated with only 15 minutes of dynamic compression, cluster group 2 revealed phosphoproteins which were

down-regulated as a result of dynamic compression, and cluster group 3 revealed phosphoproteins which were up-regulated only after 30 minutes of dynamic compression. Specific phosphorylated proteins to cluster group 1 included microtubule cross-linking factor 1, unconventional myosin-Va, ankyrin-2, and obscurin. Specific phosphorylated proteins to cluster group 2 included cofilin-1, microtubule-actin crosslinking-factor 1, E3 ubiquitin-protein ligase UBR4, and calreticulin. Phosphorylated proteins from cluster group 3 included vimentin, unconventional myosin-IXb, Titin, Protein AF-9, mediator of RNA polymerase II transcription subunit 13, Zinc-finger protein 592, and Vam6/Vps39-like protein.

The phosphoproteins from each of the comparisons (UC vs. DL15, UC vs. DL30, and DL15 vs. DL30) were used to identify key signaling pathways using the pathway over-representation analysis. We observed hundreds of significant ($p<0.05$) pathways which were identified through the IMPaLA database (Table 5). Significant pathways were determined by comparing the number of overlapping phosphoproteins between specific signaling pathways and phosphoproteins identified in each sample group. For UC vs. DL15, we observed 201 significant ($p<0.05$) signaling pathways which were determined from phosphoproteins unique to UC samples. Specific pathways included collagen formation and biosynthesis ($p<0.01$. 92 significant pathways were identified from phosphoproteins unique to DL15 samples, including Acetyl-CoA biosynthesis ($p=0.0157$) and Hedgehog signaling ($p=0.0386$). Phosphoproteins common to both UC and DL15 resulted in 61 significant signaling pathways, including RhoA activity ($p<0.01$), and Rho GTPase signaling ($p<0.01$).

For the UC vs. DL30 comparison, 215 significant ($p<0.05$) signaling pathways were identified which were unique to UC, 119 unique to DL30, and 71 shared by both UC and DL30. Specific pathways for UC included collagen formation and biosynthesis ($p<0.01$), and extracellular matrix organization ($p=0.0134$). Pathways for DL30 samples included MAPK signaling ($p<0.01$), Rho GTPase signaling ($p<0.01$), hyaluronan biosynthesis ($p=0.0252$), and glucose-6-phosphate dehydrogenase deficiency ($p=0.0473$). Overlapping pathways between UC and DL30 included ECM proteoglycan synthesis ($p=0.0374$), and Erk2 activation ($p=0.0489$).

For DL15 vs. DL30, 80 significant ($p<0.05$) signaling pathways were identified via database searches which were unique to DL15, 100 unique to DL30, and 90 were shared by both DL15 and DL30. Specific pathways to DL15 samples included Hedgehog signaling ($p<0.01$), and calcium signaling ($p=0.0453$). Specific pathways to DL30 samples included MAPK signaling ($p<0.01$), fatty acid activation ($p<0.01$), and Rho GTPase signaling ($p<0.01$). Common pathways between both DL15 and DL30 samples included RhoA activity ($p=0.0168$) and nucleotide sugars metabolism ($p=0.342$).

Table 5. Key signaling pathways determined from pathway over-representation analysis. Comparisons made were UC vs. DL15, UC vs. DL30, and DL15 vs. DL30. The first column of the table represents the comparison being made, and the specific sample group is shown in parenthesis.

Sample Comparison (Exp. Group)	Pathway Name	Pathway Source	# Overlapping Genes	# Genes in Pathway	p-value
UC vs. DL15 (UC)	Collagen formation	Reactome	10	88 (91)	1.45E-03
UC vs. DL15 (UC)	Collagen biosynthesis and modifying enzymes	Reactome	8	65 (68)	2.57E-03
UC vs. DL15 (DL15)	Vitamin B12 Metabolism	Wikipathways	4	50 (51)	7.75E-03
UC vs. DL15 (DL15)	acetyl-CoA biosynthesis from citrate	HumanCyc	1	1 (1)	1.57E-02
UC vs. DL15 (DL15)	Signaling by Hedgehog	Reactome	4	81 (87)	3.86E-02
UC vs. DL15 (UC & DL15)	Regulation of RhoA activity	PID	3	46 (47)	9.51E-04
UC vs. DL15 (UC & DL15)	Signaling by Rho GTPases	Reactome	4	122 (129)	1.72E-03
UC vs. DL30 (UC)	Collagen formation	Reactome	10	88 (91)	1.10E-03
UC vs. DL30 (UC)	Collagen biosynthesis and modifying enzymes	Reactome	8	65 (68)	2.05E-03
UC vs. DL30 (DL30)	p130Cas linkage to MAPK signaling for integrins	Reactome	4	15 (15)	4.35E-04
UC vs. DL30 (DL30)	Rho GTPase cycle	Reactome	10	122 (129)	1.02E-03
UC vs. DL30 (DL30)	Signaling by Rho GTPases	Reactome	10	122 (129)	1.02E-03
UC vs. DL30 (DL30)	Hyaluronan biosynthesis and export	Reactome	1	1 (1)	2.52E-02
UC vs. DL30 (DL30)	MAPK Cascade	Wikipathways	3	29 (29)	3.58E-02
UC vs. DL15 (UC & DL30)	ECM proteoglycans	Reactome	2	55 (56)	3.74E-02
DL15 vs. DL30 (DL15)	Signaling by Hedgehog	Reactome	5	81 (87)	8.68E-03
DL15 vs. DL30 (DL30)	fatty acid activation	HumanCyc	3	8 (9)	9.31E-04
DL15 vs. DL30 (DL30)	Rho GTPase cycle	Reactome	10	122 (129)	1.46E-03
DL15 vs. DL30 (DL30)	Signaling by Rho GTPases	Reactome	10	122 (129)	1.46E-03
DL15 vs. DL30 (DL15 & DL30)	Nucleotide Sugars Metabolism	SMPDB	1	8 (8)	3.42E-02

Discussion

In this study, we demonstrate the ability to successfully extract and analyze phosphoproteins from primary human OA chondrocytes embedded and dynamically stimulated in physiologically stiff agarose. We analyzed the short term (<30 min) phosphoproteomic changes of primary human OA chondrocytes by comparing unloaded control samples (0 min. of loading), to samples subjected to either 15 (DL15) or 30 (DL30) minutes of dynamic compression. These data compliment previous metabolic findings [206], and expand the basic knowledge of chondrocyte signaling pathways as a result of mechanical stimulation. Previous chondrocyte mechanotransduction studies have found proteomic changes as a result of dynamic compression, but little work has been done in analyzing phosphoproteomic alterations.

In mammalian cells, proteins are created from DNA through a number of processes known as the central dogma of molecular biology. Accordingly, DNA is transcribed into mRNA, then mRNA is then translated into proteins in the cytoplasm by ribosomes [102]. Proteins are macromolecules, and considered the building blocks and machines of cells. Following translation, post-translational modifications (*i.e.* phosphorylation) can occur, which have the potential to regulate the function of a specific protein. Protein phosphorylation is a post-translational modification in which a phosphate group is added to a specific protein. To evaluate the effects of dynamic compression on protein phosphorylation profiles, we analyzed 36 phosphoproteins that were shared between all samples (UC, DL15, and DL30) using unsupervised, agglomerative cluster analysis (Figure 38).

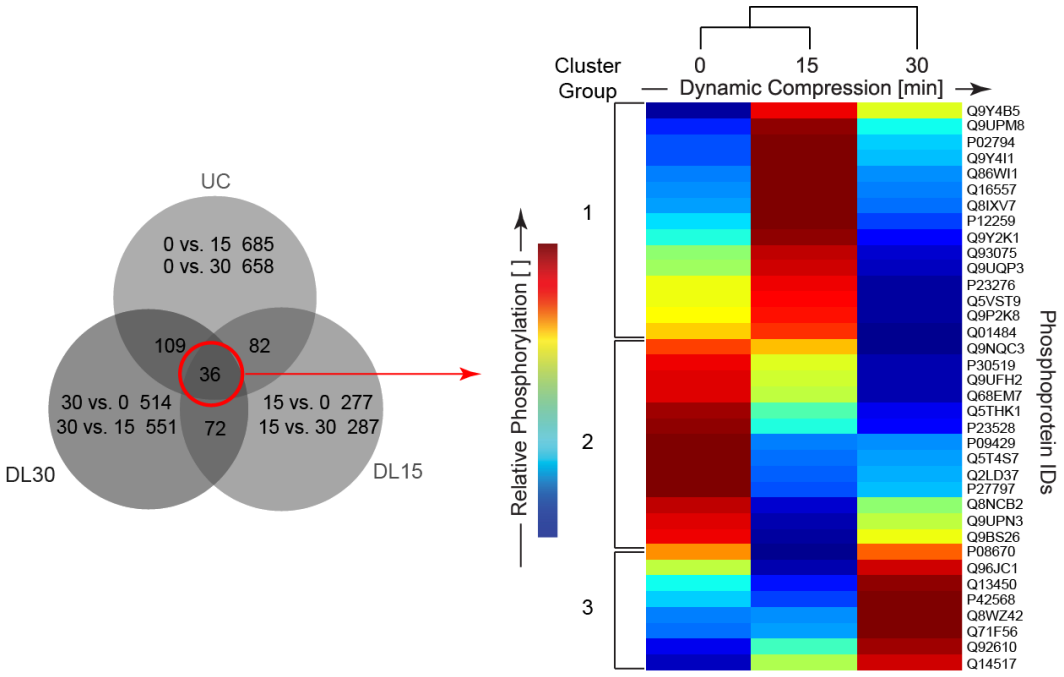

Figure 38. Applied compression resulted in distinct untargeted phosphoproteomic profiles for primary OA chondrocytes. Clustering identified three groups of mechanically-regulated protein phosphorylation. Patterns of overlapped phosphoprotein expression displayed via heatmap following unsupervised, hierarchical clustering on differentially phosphorylated proteins common to the dynamic compression (15 and 30 minutes) and unloaded control groups.

Three unique groups were evident in the cluster analysis. Cluster group 1 reveled phosphoproteins which were up-regulated with 15 minutes of dynamic compression (Figure 3). These phosphorylated proteins were highly phosphorylated after 15 minutes of dynamic compression, and then were dephosphorylated at 30 minutes. Specific phosphorylated proteins to this group included 4 proteins which regulate cytoskeletal dynamics, including ankyrin-2. Ankyrins are adaptor proteins that help mediate attachment of membrane proteins to the cytoskeleton [214]. Ankyrin not only affects chondrocyte cytoskeletal dynamics, but important for maintaining cartilage homeostasis through the single-pass transmembrane protein CD44 which can bind extracellular

hyaluronan providing a potential mechanism for ECM deformation to be transmitted intracellularly[215]. Cluster group 3 also contained phosphorylated proteins that play a role in the arrangement of actin cytoskeletal structures. The actin cytoskeleton is a key component of chondrocyte shape, which has been linked with the matrix synthesis chondrocyte phenotype [216, 217]. Under mechanical deformation in 3D suspension, the actin cytoskeleton is actively remodeled [84, 217, 218], which suggests increased matrix synthesis as a result of as little as 15 minutes of dynamic compression.

Cluster group 2 includes phosphoproteins down-regulated (*i.e.* de-phosphorylated) as a result of mechanical loading, and includes E3 ubiquitin-protein ligase UBR4, and calreticulin. E3 ubiquitin-protein ligase UBR4 is a phosphorylated protein in the ubiquitin-ligase pathway, which may be associated with protein degradation [219]. Given that these data demonstrate de-phosphorylation in response to dynamic loading; this provides a potential protective mechanism for mechanical stimulation which may also increase matrix synthesis. Calreticulin is de-phosphorylated in response to applied compression. Calreticulin is lectin-independent chaperone, which binds and deactivates Ca2+ ions, and ADAMTS. The ADAMTS (a disintegrin and metalloproteinase with thrombospondin motifs) family of peptidases has been shown to inhibit chondrocyte differentiation [220] and promote aggrecan degradation [45]. ADAMTS enzymes are upregulated in OA [221, 222]. Therefore, the observation that Calreticulin is de-phosphorylated in DL15 and DL30 samples, suggests another potential protective mechanism by which mechanical loading may reduce matrix degradation.

Cluster group 3 identified proteins which were highly phosphorylated in response to 30 minutes of mechanical stimulation. This group included a number of actin-associated proteins that were phosphorylated in response to loading, including vimentin. Vimentin is an intermediate filament which is integral to the chondrocyte cytoskeleton. Disruption of vimentin networks in chondrocytes leads to decreased matrix synthesis and cell stiffness [223], as well as OA progression [68]. In this study, vimentin was highly phosphorylated in response to mechanical loading, which may result in increased matrix synthesis as well as other protective mechanisms against OA.

In Cluster group 3, transcriptional regulating proteins (DNA→mRNA) including AF-9, mediator of RNA polymerase II transcription subunit 13, and zinc finger protein 582 were highly phosphorylated in response to mechanical loading. Cam6/Cps39-like protein was also highly phosphorylated in DL30 samples, which is a regulator of TGF-beta activity through activation of SMAD2-dependent gene expression. SMAD2 expression [224] and increased TGF-beta signaling [225] have been shown to affect chondrocyte differentiation and play critical roles in inducing gene expression of cartilage-specific molecules (*i.e.* collagen II). Protein phosphorylation leading to up-regulation of TGF-beta signaling and SMAD expression further strengthen the potential protective mechanisms of mechanical loading against the progression of OA.

To further examine mechanically induced changes in chondrocyte protein phosphorylation, pathway enrichment analysis examined pathway-specific differences between loading groups. In comparisons for UC samples (UC vs. DL15 and UC vs. DL30), collagen biosynthesis and formation were identified as signaling pathways

present in UC samples, and were either in low levels or not detected in loaded samples, and support the 3D agarose culture system used in these experiments. This complements previous [206], where proline levels were down-regulated in response to increased time of dynamic compression. Collagen is synthesized in the chondrocyte's cytoplasm, which incorporates proline and hydroxyproline into the formation of the triple-helix [226], and proline has been shown to be a marker of ECM synthesis [77]. Down-regulation (*i.e.* consumption) of proline in response to mechanical loading, suggests loading-induced collagen synthesis.

Signaling pathways specific to dynamically stimulated samples were identified as those unique to either DL15 or DL30 samples. DL15 samples contained phosphorylated proteins specific to the Hedgehog signaling pathway ($p<0.05$). The hedgehog signaling pathway regulates many fundamental processes in embryonic development, including cell proliferation and differentiation [227], and has also been shown to play an important role in chondrocyte differentiation [228]. Lin *et. al* [228], demonstrated that the hedgehog pathway was upregulated in dedifferentiated in rat chondrocytes, and this phenotype is similar to diseased (OA) chondrocytes [229]. By redifferentiating the dedifferentiated chondrocyte phenotype through activation of the hedgehog signaling pathway, loading may enable OA chondrocytes to recapitulate the normal chondrocyte phenotype, further demonstrating the potential for loading to promote cartilage repair. These data suggest that the hedgehog signaling pathway is activated in as short as 15 minutes. If the hedgehog pathway initiates a healing response of diseased chondrocytes, short duration, mechanical loading may be used as a potential clinical therapy for OA.

DL30 samples contained phosphorylated proteins associated with Rho GTPase signaling, mitogen activated protein kinase (MAPK) signaling, and hyaluronan synthesis. Rho-associated protein kinases (ROCK), from the serine-threonine kinase family, have been previously studied in the chondrocyte mechanotransduction field [84, 123, 170], and rho kinase activation occurs after less than 10 minutes of dynamic compression [123]. Rho kinase plays an important role in actin dynamics which regulate cell shape and size [230]. Cell shape defines the *in vivo* chondrocyte phenotype[37], and reorganization of the actin cytoskeleton is a result of Rho GTPase signaling. In this study, we dynamically stimulated primary human OA chondrocytes in high-stiffness agarose [114], and have previously observed homogenous ellipsoidal deformations induced on the cells which are spherical in the undeformed case [115]. These deformations promote remodeling of the cytoskeleton via the Rho GTPase signaling pathway, which has been linked with increase cartilage matrix production [170]. Increased matrix production is consistent with hyaluronan synthesis, which was identified as a significant ($p<0.05$) pathway in DL30 samples. Hyaluronan has been found to be responsible for organization of proteoglycans in cartilage, and hyaluronan-chondrocyte interactions are important for the production and maintenance of cartilage matrix [231].

The MAPK signaling pathway was also significantly enriched ($p<0.05$) in DL30 samples. The MAPK pathway is present in most eukaryotic cells and controls functions such as cell proliferation, differentiation, survival, and apoptosis [83, 232], and includes protein kinases such as ERK1 and ERK2. Previous studies have found that mechanical compression of articular cartilage induces cell proliferation through activation of the

ERK1/2 pathways [83]. Therefore, if the present data represent MAPK signaling activation for cell proliferation, future studies may explore using applied dynamic compression to expand chondrocytes for cartilage repair.

Conclusions

In summary, this study demonstrates the power of using phosphoproteomics as a tool for understanding the chondrocyte response to short duration (<30 min), dynamic compression. By expanding upon prior metabolomic analysis of primary human OA chondrocytes in response to dynamic compression [206], in this study we were able to identify 514 phosphoproteins unique to dynamically stimulated samples. To our knowledge, this was the first study to successfully identify phosphoproteomic profiles for OA human chondrocytes in response to mechanical loading. This work identified the potential to use mechanical stimulation (*i.e.* short-duration, low-impact exercise) as a therapeutic to promote cartilage repair in OA clinical populations. Future work will expand on this work to elucidate latent biomarkers for OA by comparing phosphoproteomic differences between OA and normal human chondrocytes.

Acknowledgements

We acknowledge Drs. Brian Bothner MSU, for critical insight provided during discussions. We thank Dr. Jonathan Hilmer for assistance and insight provided during LC-MS/MS sample runs and data analysis. Funding was provided by NIH P20GM10339405S1, NSF 1342420, Montana State University, and the Murdock Charitable Trust.

References

See REFERENCES CITED.

IN VIVO MODEL

The final chapter of this dissertation is aimed to provide *in vivo* validation and interpretation of the *in vitro* results obtained in Chapters 3 and 4. This study will use a novel *in vivo* mouse model that allows for *in vivo* quantification of cartilage abundance. Again, this is a novel study, and has never been reported to date.

Mouse models have been used for decades in the scientific community as tools for understanding and treating OA. Current studies utilize a number of different techniques to induce OA in mice, including surgical destabilization of the knee joint [60, 233], injection of proteolytic enzymes [234], and naturally via aging [235]. The caveat for these studies is all of the mice are euthanized for joint dissection and sectioning, and then stained so the deteriorated cartilage can be graded. These grading scales (usually from 0-6) are subject to bias and don't actually quantify the amount of cartilage in the joint [233, 235-237]. This study is unique in that it provides the first ever non-invasive, *in vivo* quantification of the cartilage amount in a mouse model by a genetically encoded reporter. It also carries the benefit of being able to longitudinally monitor each mouse, and their relative amounts of cartilage quantified without having to sacrifice the mouse.

Our working mouse model is defined as follows: A novel transgenic mouse has been generated that expresses firefly luciferase in aggrecan, the most abundant proteoglycan found in cartilage. This bioluminescent signal is identical to how a firefly lights up, hence the name firefly luciferase. These mice have been genetically modified to express Cre-ERT2 in the presence of tamoxifen. When tamoxifen is present, Cre is activated in aggrecan-producing cells (*e.g.* chondrocytes), which excises a stop codon in

the genetic code to initiate transcription of luciferase. When luciferase comes in contact with the substrate luciferin (*i.e.* through an external injection), a bioluminescent signal of light is omitted. The amount of aggrecan in chondrocytes is directly proportionally to the amount of cartilage in the joint. Therefore, the amount of emitted light is directly proportional to the amount of cartilage.

This is an extremely novel study in that it not only validated the *in vitro* results from the metabolomics and phosphoproteomics data sets generated in Chapters 3 and 4, but it also laid the foundational building blocks to allow *in vivo* monitoring of chondrocyte mechanotransduction.

ALTERATIONS IN JOINT METABOLOMICS FOLLOWING SURGICAL DESTABILIZATION AND EXERCISE IN A NOVEL CARTILAGE REPORTER MOUSE MODEL

Contribution of Authors and Co-Authors

Author: Donald L. Zignego[1]

Contributions: Acquired, analyzed, and interpreted the data. Drafted and wrote the manuscript.

Co-Author: Sarah E. Mailhiot[1]

Contributions: Interpreted data and reviewed the manuscript.

Co-Author: Timothy Hamerly[2]

Contributions: Interpreted data and reviewed the manuscript.

Co-Author: Edward E. Schmidt[3]

Contributions: Interpreted data and revised the manuscript.

Corresponding Author: Ronald K. June[1,4]

Contributions: Designed the study, analyzed and interpreted the data, and wrote the manuscript.

[1]Department of Mechanical and Industrial Engineering, Montana State University, Bozeman, MT 59717-3800, USA

[2]Department of Chemistry and Biochemistry, Montana State University, Bozeman, MT 59717-3800, USA.

[3]Department of Microbiology and Immunology, Montana State University, Bozeman, MT 59717-3800, USA.

[2]Department of Cell Biology and Neuroscience, Montana State University, Bozeman, MT 59717-3800, USA

Manuscript Information Page

Donald L. Zignego, Sarah E. Mailhiot, Timothy Hamerly, Edward E. Schmidt, and Ronald K. June
Annals of Biomedical Engineering
Status of Manuscript:
_X_ Prepared for submission to a peer-reviewed journal
___ Officially submitted to a peer-reviewed journal
___ Accepted by a peer-reviewed journal
___ Published in a peer-reviewed journal

Publisher: Annals of Biomedical Engineering, Springer US.
Prepared: July 2015

Abstract

The structure and inaccessibility of synovial joints hinders studies on the dynamic pathophysiology of osteoarthritis (OA). Here we developed advanced methods for quantifying changes in cartilage in a novel post-traumatic model of OA. Using a recently developed mouse model that expresses luciferase in chondrocytes [238], cartilage-specific bioluminescence was quantified by non-invasive *in vivo* imaging. To evaluate the effects of exercise and injury, we established two independent groups of mice (female, 8 weeks old, n=5 per group). Mice that were unexercised and subjected to a sham procedure served as the control group. Mice subjected to intensive forced treadmill exercise and surgical destabilization of the left knee (Ex-des mice) was used to assess osteoarthritic changes. *In vivo* cartilage abundance was quantified bioluminescently over 15 days, after which mice were sacrificed and full-joint metabolomic profiles were determined. Ex-des mice, but not controls, showed progressive cartilage loss over time as determined by decreasing cartilage-specific bioluminescence. Metabolomic profiling detected 496 molecules whose levels differed significantly between groups and 391 of these were identified. These data showed that aliphatic amino acids, arachidonic acid metabolism, and mineral absorption were increased in response to both exercise and injury; the creatine-phosphate biosynthesis pathway was induced by exercise but repressed by injury; and either exercise or injury repressed levels of sugar transport, amino-sugar metabolism, and proline catabolism. The results from this study show the effects of exercise and injury on both cartilage and whole-joint metabolic activity. Future

studies will use these techniques for longitudinal evaluation of murine OA in applications such as disease progression, biomarker development, and candidate drug evaluation.

Introduction

Osteoarthritis (OA) is considered the most prevalent joint disorder in the world and involves the breakdown of the protective, load bearing articular cartilage that covers the joint surface [1-7]. The predominant view is that excessive joint loading causes OA.

Articular cartilage is subjected to repetitious mechanical loading, and contact forces through the joints can be up to 10 times an individual's body weight [55]. Studies indicate there is a delicate balance between healthy and unhealthy joint loading, which can either establish protective mechanisms against OA or result in cartilage deterioration leading to OA [8, 9]. It has been shown that chondrocytes, the sole cell type in articular cartilage, sense and respond to mechanical deformations, but the biological processes describing these mechanisms remain elusive [49, 84, 87, 93, 116]. This study utilized forced exercise via treadmill running after surgical destabilization to model excessive loading in OA.

OA is challenging to study in humans because of (1) the timescale of slow disease progression, and (2) availability of healthy control samples for age-matched comparison. However, mouse models of OA provide the opportunity to study the disease under controlled conditions. While mouse disease may not recapitulate all components of human OA, these models provide a means to study the pathological evolution of OA under controlled conditions [239-241].

Mouse models of OA have been used extensively in predicting the efficacy of pharmacological intervention for OA [242-244], as well as in determining the role mechanical loading on cartilage physiology *in vivo* [60, 222, 245-248]. Experimental OA

in mice can be induced by a variety of methods including surgical destabilization [60, 233], intra-articular chemical injections [241, 249, 250], and applied external loading [251]. Surgical destabilization is the most common, and induces a progression of experimental OA that mimics the pathology of human OA.

The most common methods for quantifying cartilage deterioration in murine OA models include histopathological grading scales [237, 252] and micro-CT imaging [253-255]. One challenge to these studies is longitudinal evaluation to measure progression of the disease over time in the same animal. Current methods for studying the progression of OA require euthanizing animals at specific time points throughout the study, and therefore render longitudinal observations in the same animal impossible. In this study we address this issue by using a transgenic reporter mouse and quantitative non-invasive bioluminescent imaging.

Recently we developed a novel transgenic mouse for non-invasive *in vivo* cartilage quantification [256]. This model includes a tamoxifen-inducible Cre recombinase driven by an IRES (internal ribosomal entry site) within the 3'-untranslated region of the endogenous chondrocyte-specific aggrecan mRNA. In tamoxifen-exposed chondrocytes, Cre removes a "floxed-STOP" cassette from a *ROSA26*-targeted luciferase reporter, resulting in chondrocyte-restricted luciferase expression (Figure 1). *In vivo* imagining is then used to quantify the bioluminescent signal produced in aggrecan-expressing tissues of the mouse (*i.e.* knee, tail, hip, and toes). The objective of this study was to analyze the effects of intensive physical exercise and surgical destabilization (*via* MCL transection and medial meniscectomy) utilizing both longitudinal *in vivo*

bioluminescence imaging of cartilage in transgenic reporter mice and terminal metabolomic profiling of joint tissues.

We observed significant decreases in the bioluminescent signal in the exercised and destabilized mouse joint when compared to the contralateral sham controls, reflecting changes in cartilage and joint health. Furthermore we observed significant differences in metabolite profiles between mouse groups. This study establishes an important model that will be useful for studies of (1) the progression of OA in murine models, (2) specific metabolites as OA biomarkers, and (3) longitudinal studies of therapeutic strategies for OA.

Materials and Methods

Animals. This study was approved by the Montana State University Institutional Animal Care and Use Committee (IACUC). Two separate cages of mice were used as controls or as experimental animals for this study (female, n = 5 mice for each group) (Figure 39A). Mice were housed with *ad libitum* access to food and water in 12 hour light-day cycles. The transgenic reporter mouse has been described previously [238]. Briefly, this line expresses chondrocyte-specific bioluminescence following Cre induction via tamoxifen.

Luciferase Induction, Imaging and Image Processing. Cre-ERT2 activity was induced via subcutaneous scruff injections of tamoxifen (10mg/mL in vegetable oil) serially for 3 days (2 mg/day) (Figure 39B). Following a 5-day rest period, mice were imaged. D-luciferin potassium salt, a substrate required for bioluminescence, was administered via subcutaneous scruff injection (1.5 ml/mouse at 15 mg/mL).

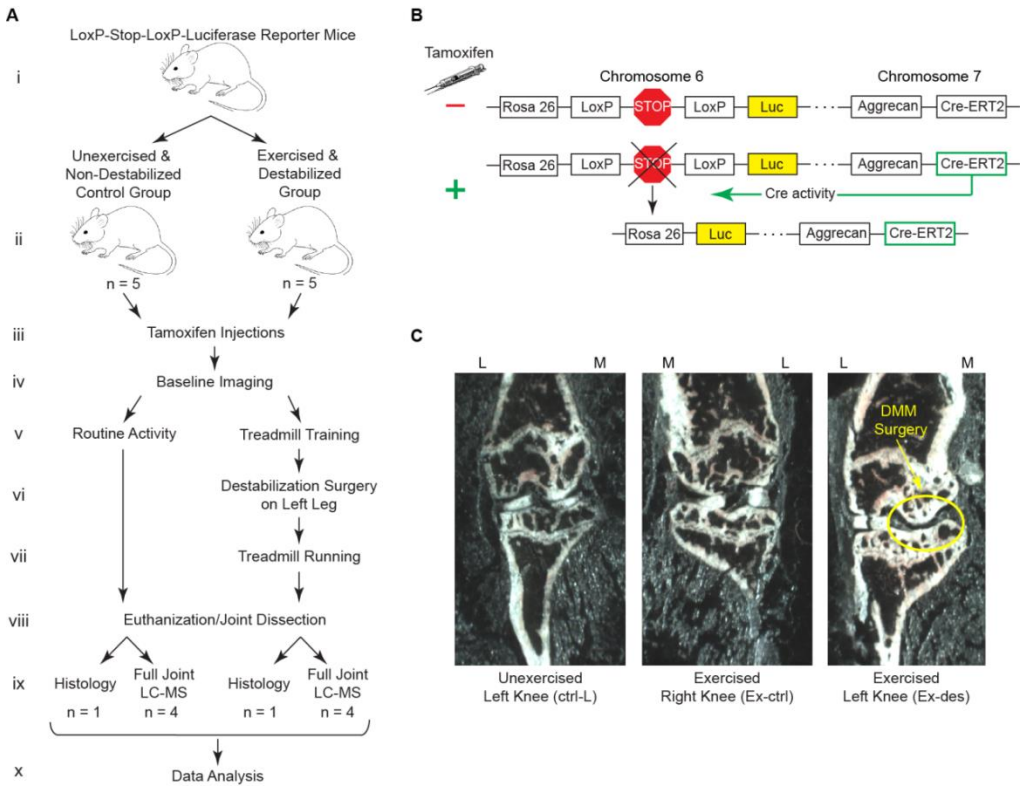

Figure 39. Experimental design and transgenic strategy for mouse with aggrecan-specific bioluminescence. (A) Schematic of the experimental methods for both the exercised and destabilized and unexercised and intact (ctrl) mouse groups. The experimental group consisted of mice subjected to exercise with one knee surgically destabilized (Ex-ctrl, Ex-des). Control mice were not subjected to exercise (ctrl-L, ctrl-R). (i) The transgenic reporter mice are randomly assigned into two experimental groups. (ii) n = 5 female mice are assigned to each experimental group (ctrl or exercised/destabilized), and (iii) are given 3 consecutive days of tamoxifen injections. (iv) Both groups are then imaged to establish baseline intensity values for each mouse, and (v) then exercised/destabilized mice are trained on the treadmill. (vi) Exercised/destabilized mice are then subjected to a destabilization surgery on each of their left hind legs, whereas ctrl mice are used as contralateral sham controls. (vii) Following 96 hours of rest, exercised/destabilized mice are then exposed to vigorous treadmill exercise for 15 consecutive days. (viii) All mice are then euthanized and their joints dissected followed by (ix) either histology (n=1 mouse per group) or full joint LC-MS (n=4 mice per group). Throughout the running protocol ctrl mice resumed routine activity (v-vii). (B) In this mouse model, luciferase expression is induced specifically in aggrecan producing cells (*i.e.* chondrocytes). These mice contain an inducible Cre-recombinase which was inserted into the 5' untranslated region of the endogenous mouse aggrecan transcript. The insert contains an internal ribosomal entry site followed by the tamoxifen-inducible CRE-ERT2 injection. (C) Stereographic images of ctrl Ex-ctrl and Ex-des mouse joints showing the successful destabilization surgery of the left medial (M) side of an Ex-des mouse joint.

After 15 minutes, for luciferin distribution, mice were anesthetized via isoflurane inhalation (2-3% v/v at 2.5 ml/min in oxygen), and imaged using an anterior view with 15 min exposures in no-light conditions (Kodak ImageStation 2000MM). 16-bit TIFF images were analyzed with Matlab. Images were contrasted, inverted, and thresholded before smoothing with a 50 pixel median ball filter [256]. A region of interest (ROI) was selected around each knee, and total pixel intensity was calculated by summing the pixel values in each specific ROI. All mice were imaged serially for 3 days to establish baseline values for bioluminescent intensity.

Treadmill Running and Surgical Destabilization. In order to detect bioluminescent changes in response to exercise, mice were randomized into two groups; unexercised and non-destabilized control mice (n = 5 female), and exercised/destabilized mice (n = 5 female). The exercised/destabilized mice were subjected to extensive treadmill training for 10 consecutive days (maximum speed of 30 cm/s for 20 min at 15° incline) [257]. Following training, these mice had each of their left knees surgically destabilized by MCL transection and medial meniscectomy [233], which we will denote as the "Ex-des" joint (Figure 39C). For surgery, mice were anesthetized via isoflurane inhalation (~3% isoflurane). Following surgery, incisions were sutured, and mice administered analgesics per IACUC protocol (subcutaneous Buprenex at 0.5 mg/kg). Mice were monitored for 7 consecutive days for post-surgical complications. Following 96 hours of recovery, the Ex-des group were run for 15 consecutive days (30 cm/s, 15° incline, 25 min daily). Control mice were handled daily without running as a control. All mice were imaged every other day for 14 days.

Joint Harvest and Metabolite Extraction. Both groups of mice were euthanized by cervical dislocation. To obtain joint-related metabolites, the tibiofemoral joints (n=4, each group) were harvested as follows. Skin was removed from mouse limbs, and muscle was removed from the proximal femur using scissors. Periosteum and other soft tissues were scraped away from the shaft of the femur, and an incision was made along the trochlear groove to access the joint. The patella and associated soft tissue (synovium, fat pad) were removed with scissors, and remaining soft tissue was scraped away from the tibia to the extent possible. The joint was harvested using scissors with a tibial cut immediately below the articular cartilage and a femoral cut which included both condyles and the distal ~80% of the trochlear groove. Joints were flash-frozen in liquid N_2 for 5 minutes and pulverized using a stainless steel platen and a ball peen hammer. Metabolites were then extracted using previously optimized protocols [116, 206]. 1 ml of a 70:30 methanol:acetone solution was added to each pulverized joint in a vial. Vials were vigorously vortexed every 5 min for 20 min, and then stored at -20°C for further metabolite extraction and precipitation of macromolecules. Samples were centrifuged (20,000 x g, 10 min, 4^{o}C), the supernatant was transferred to an Eppendorf tube, and the solvent evaporated using a centrifugal vacuum concentrator for 6 hours. Dried samples were resuspended in 100 µL of 50:50 mass spectrometry grade H_2O:Acetonitrile. Metabolite detection was performed in the Montana State University Mass Spectrometry Core Facility [155-157]. A HILIC HPLC column (Cogent Diamond Hydride Type-C) was used with an Agilent 1290 HPLC system. The column was coupled to an Agilent 6538 Q-TOF dual-ESI source mass spectrometer (~20,000 resolution, and ~5 ppm

accuracy). Mass spectra were collected in positive mode with a mass range of 50-1000 m/z.

Histology. To confirm histological joint changes, knee joints were dissected from the exercised right and left of representative mouse (n=1). The joints were frozen in gelatin and stored at -20° C. Transparent tape (Cryofilm Type 2C, Section-Lab, Hiroshima, Japan [256, 258]) was placed on the front face of the sample and a 20 micron section of tape and sample was cut on a microtome. The samples were stained with 1% Safarin O for 1 min, washed in tap water, stained with 1% Fast Green FCF for 1 min, and washed in tap water. The samples were imaged at 4x and 10x objective magnification (Figure 43).

LC-MS Data Processing. Liquid chromatography-mass spectrometry (LC-MS) data analysis involved an untargeted and targeted strategies. Untargeted analysis was used to examine global changes in the metabolome, whereas the targeted analysis focused on changes in ~40 metabolites involved in central energy metabolism [102, 154].

For the untargeted analysis, data processing followed previously optimized protocols [116, 206]. Briefly, raw HPLC-MS data was converted into .mzXML files (MS-Convert, ProteoWizard), and processed with MZmine2.0 [158]. Datasets were analyzed by filtering chromatograms based on a maximum signal level (1000 m/z with a 15 ppm tolerance), normalized (0.25 min retention time (RT) tolerance), and aligned (mass and RT tolerance of 15ppm). This generated list of metabolites was then used for

statistical analysis and metabolite identification via METLIN (ref -Smith et al., 2005, METLIN: a metabolite mass spectral database).

For the targeted approach, a database of calculated isotopic distributions (including +H and +Na adducts) for the ~40 targeted masses was created using the Quantitative Analysis package within MassHunter Workstation B.04.00 (Agilent Technologies). Retention times were matched to those from standard analytical samples (MSU Mass Spectrometry Core), and a 20 ppm m/z tolerance was used to evaluate the targeted metabolites.

Data Analysis. For the analysis, four analytical groups were established for comparative purposes. Control mice were not subjected to exercise or injury and joints were categorized as control left knees ("ctrl-L") or control right knees ("ctrl-R") to assess differences between stifle joints of the same mouse. Joints from mice that were exposed to exercise and injury were grouped as exercised left knees ("Ex-des") and exercised right knees ("Ex-ctrl"). Ex-des knees were surgically destabilized after training and rested prior to the exercise protocol. To determine the effects of exercise and injury on our murine OA model, we compared both the bioluminescent signal intensities and metabolomic profiles obtained by LC-MS between the experimental groups.

To analyze the bioluminescent data, first, the total pixel intensity was calculated for each ROI for each mouse. Next, the total pixel intensity was normalized to the baseline intensity data for each mouse. Normalized total pixel intensities were then compared among knee joint groups using a non-parametric Kruskal-Wallis one-way

analysis of variance (n=5 knees/group). To determine if the bioluminescent signal decreased with respect to time (increased exercise), correlation analyses were performed.

For the LC-MS data analysis, we defined metabolites as detected masses present in at least half of the samples for each group. To assess differences in metabolite intensities between groups, comparisons were made using Wilcoxon signed rank tests and two-factor Kruskal-Wallis analysis of variance, with multiple-testing corrections using a false discovery rate (FDR) of 0.05 [259]. Four comparisons were made: (1) ctrl-L vs. ctrl-R, (2) Ex-des vs. Ex-ctrl, (3) ctrl-L vs. Ex-des, and (4) ctrl-R vs. Ex-ctrl. Principal components analysis (PCA) was utilized to assess global changes caused by both exercise and injury. To assess differences in metabolite intensity distributions, two-sample Kolmogorov-Smirnov tests were used with a null hypothesis that sample groups result from a population with identical distributions. For all statistical analysis, the significance was set at $p < 0.05$, *a priori*.

To assess the role of injury and exercise on joint health, unsupervised hierarchical agglomerative cluster analysis assessed the patterns of co-regulated metabolites for each sample group. To putatively identify compounds of interest, metabolite m/z values from each group were compared to the METLIN database of known metabolites [163]. Search parameters included m/z values with potential $+1H^+$ or $+1Na^+$ adducts and a 20 ppm mass tolerance. The METLIN database contains over 240,000 identifiable metabolites developed over the past decade [162, 163]. The most significant metabolites from the database searches were searched for pathway-specific over representation, using Integrated Molecular Pathway Level Analysis (IMPaLA, http://impala.molgen.mpg.de

[213]). For the targeted analysis, hierarchical agglomerative cluster analysis was used to identify patterns of energy metabolism between the experimental groups.

Results

The objective of this study was to characterize the effects of forced treadmill running and injury on a novel mouse model by examining changes in metabolomic profiles and bioluminescent intensity. Transgenic mice (n = 5 female mice per group), with cartilage specific bioluminescence, were randomly assigned to one of two groups: the unexercised/non-destabilized control group and the exercised/destabilized group. All mice were imaged over the course of 15 days to evaluate changes in bioluminescence, followed by euthanization, joint dissection, and full joint LC-MS analysis. To evaluate our hypothesis, we analyzed changes in cartilage specific bioluminescence for each mouse and assessed changes in metabolomic profiles between experimental groups.

Bioluminescent Analysis. Bioluminescent signal was evaluated between the four knee groups (ctrl-L, ctrl-R, Ex-des, and Ex-ctrl) by comparing the normalized total pixel intensities. Following day 10 of the exercise protocol, there were significant differences between the control group and the Ex-des joints (Figure 40A,$^{**}p<0.01$, $^{*}p<0.05$). Significant differences were also observed between Ex-des and Ex-ctrl knee groups ($p<0.05$) at days 10 and 12. Analysis of the bioluminescent signal for Ex-des joints showed a significant, negative correlation with time ($p = 0.046$, $r = -0.954$) after one week of exercise, suggesting the onset of cartilage deterioration (Figure 40B&C).

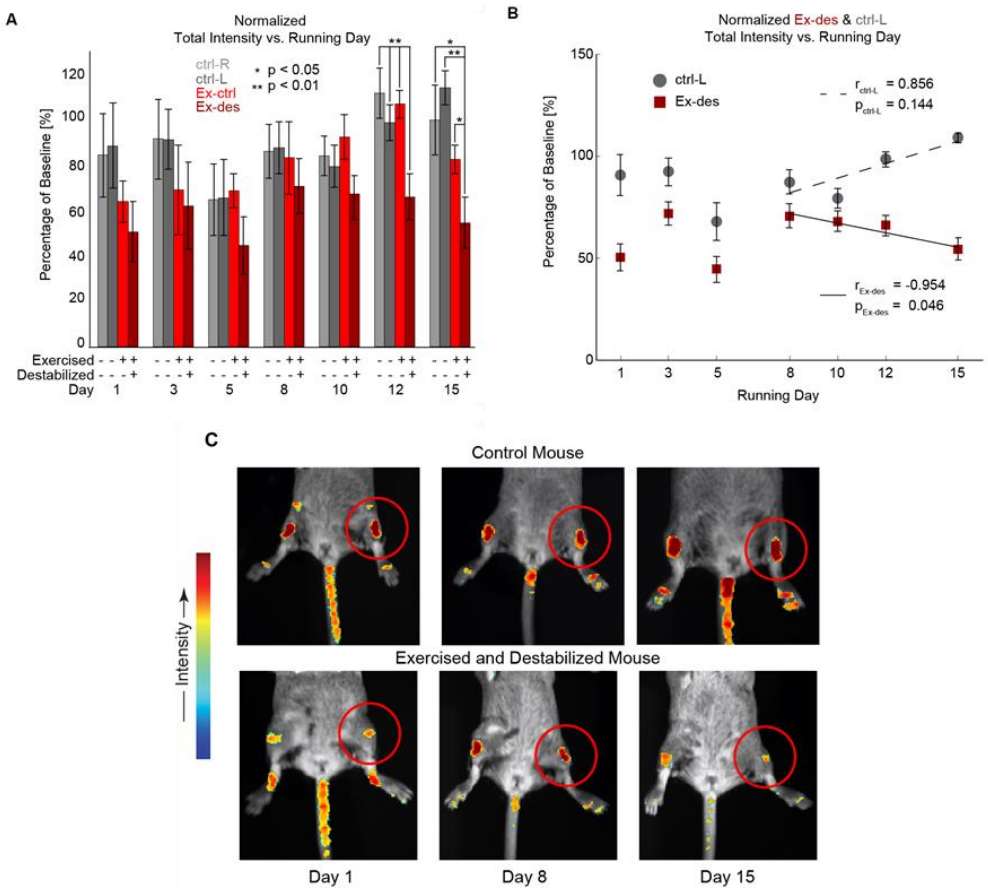

Figure 40. The combination of exercise and joint destabilization resulted in decreased bioluminescence compared with controls. (A) Normalized total signal intensity vs. running day for each of the mouse knee joints (average ± sem). A two-factor Kruskal-Wallis found significant differences on days 12 and 15 comparing Ex-des joints to ctrl-L, ctrl-R, and Ex-ctrl joints (*$p < 0.05$, **$p < 0.01$). (B) Significant decreases ($r = -0.954$, $p = 0.046$) in bioluminescent signal with time were observed in Ex-des joints following day 8 of the running protocol. This decrease indicates a decrease in cartilage health due to either chondrocyte death or loss during the experimental protocol. No differences ($r = 0.856$, $p = 0.144$) were observed for the contralateral sham control joints (ctrl-L). (C) Control mice (top) exhibited stable bioluminescence whereas experimental mice exhibited changes in bioluminescence over the experimental time course. Representative bioluminescence heat maps overlaid with photographs obtained prior to bioluminescence imaging.

Contralateral sham controls showed no significant changes in bioluminescent signal over the course of the experiment ($p = 0.144$, $r = 0.856$, Figure 40B&C).

LC-MS Analysis. Untargeted LC-MS analysis revealed metabolomic differences between the joints of control and experimental mice. Two-sample Kolmogorov-Smirnov distribution tests revealed significant differences between Ex-des and Ex-ctrl spectra distributions ($p < 0.05$), whereas no difference was found between the right and left knees for the control mice ($p = 0.626$, Figure 41A). To identify metabolites differentially regulated by injury and exercise, jointly detected molecule were compared using a false discovery rate of 0.05 and plotted in two-dimensional space (Figure 41B). Right and left joints exhibited similar metabolomic profiles: only 1 metabolite was significantly present in ctrl-R joints that was not found in ctrl-L joints, and 16 metabolites were found in ctrl-L joints that were not found ctrl-R joints (Figure 41B). However, exercise and injury induced changes in hundreds of metabolites: 176 metabolites were present in Ex-ctrl samples that were not found in Ex-des samples, and 280 metabolites were found in Ex-des samples that were not in Ex-ctrl samples (Figure 41B). After resolving the metabolomic profiles onto their principal component axes, we observed differential clustering between sample groups with the Ex-des samples being the most distinct (Figure 41C, Supplementary Figure 2, Supplemental Figure 18). The first three principal components contained 87% of the variance.

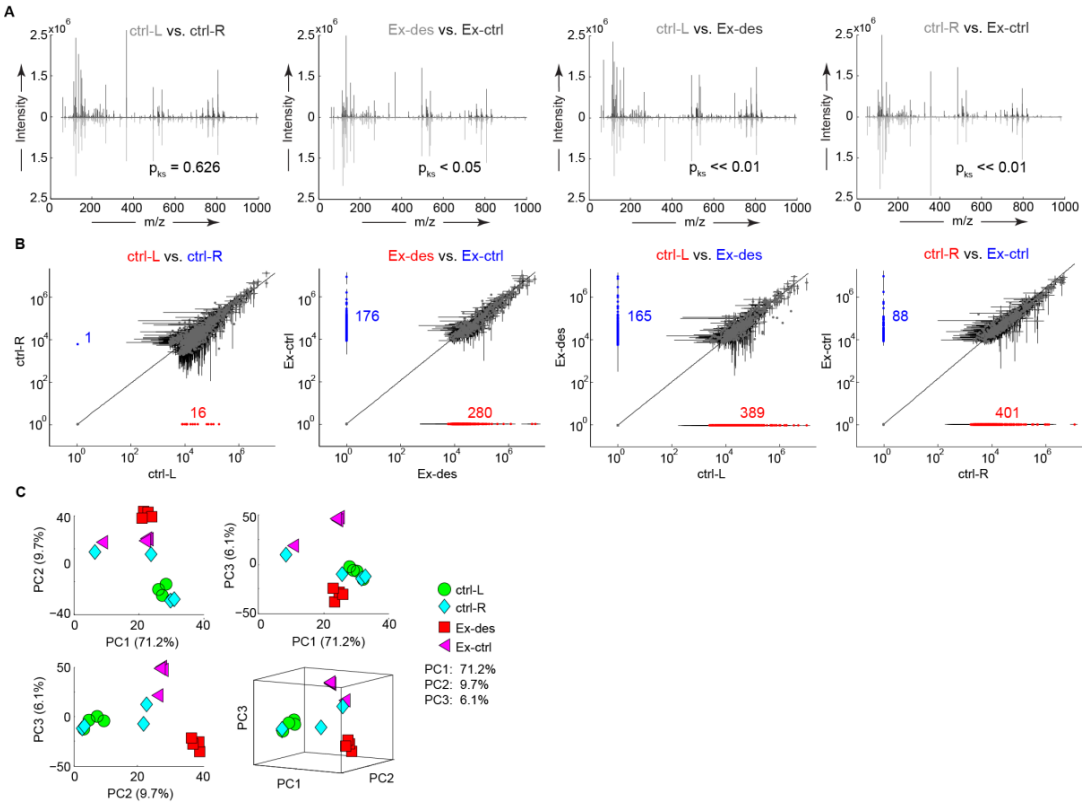

Figure 41. Metabolomic profiling captured joint-wide changes induced by the combination of vigorous treadmill running and joint destabilization. (A) Two-sample Kolmogorov-Smirnov tests reveal statistically significant changes between the distributions of median metabolites for Ex-des vs. Ex-ctrl ($p < 0.05$), ctrl-L vs. Ex-des ($p < 0.001$), and ctrl-R vs. Ex-ctrl ($p < 0.001$) m/z spectra distributions. No differences were observed for ctrl-L vs. ctrl-R ($p = 0.626$) m/z spectra distributions. (B) Exercise and injury induce changes in individual metabolite profiles. Up-down regulation plots for ctrl-L vs. ctrl-R, Ex-des vs. Ex-ctrl, ctrl-L vs. Ex-des, and ctrl-R vs. Ex-ctrl. (C) Principal Components Analysis for the untargeted metabolomic data was used to assess global differences between sample groups. The first three principal components contained 87% of the overall variance, and the first principal component contained 71.2% of the experimental variance indicating that exercise and joint destabilization dramatically alter whole-joint metabolomics. For each of the sample groups ctrl-L (●), ctrl-R (♦), Ex-des (■), and Ex-ctrl (◀), there are n=4 replicates.

In addition to changes in untargeted metabolomic profiles, there were changes in energy-related metabolites as a result of exercise and injury. Expression patterns of metabolites targeted to central energy metabolism were first analyzed through hierarchical agglomerative cluster analysis (Supplemental Figure 17). Cluster analysis identified ctrl-L and ctrl-R samples to have the most similar metabolite distributions, and Ex-des samples were the most distinct.

Untargeted hierarchical agglomerative clustering found distinct groups of metabolites (Figure 42A, Cluster Groups 1-4). Of the 496 metabolites in this group, there were 391 metabolites found in the METLIN database and 105 metabolites that were not identified. Cluster group 1 (Figure 42A & B) revealed metabolites that were up-regulated in exercise joints (Ex-ctrl) and down-regulated in the destabilized joints (Ex-des). Cluster group 2 (Figure 42A &C) revealed metabolites which were highly regulated as a result of injury only (Ex-des only). Cluster group 3 (Figure 42A & D) revealed metabolites that were down-regulated as a result of exercise or injury, and finally cluster group 4 (Figure 42A & E) revealed metabolites which were down-regulated as a result of exercise and injury.

The metabolites from each of the cluster groups were then used to identify key metabolic pathways affected by intensive exercise and injury by using established pathway over-representation analysis [213]. Hundreds of significant ($p < 0.05$) pathways were identified by determining the number of overlapping metabolites between a specific metabolic pathway and metabolites from each of the cluster groups. Cluster group 1 (up in exercise, down in injury) contained metabolites which were significantly overlapped

with the creatine-phosphate biosynthesis pathway ($p = 0.022$). Cluster group 2 (up in exercise and injury) contained metabolites which were significantly overlapped with valine, leucine, and isoleucine biosynthesis ($p<<0.01$), arachidonic acid metabolism ($p << 0.01$), and mineral absorption ($p < 0.01$). Cluster group 3 (down with exercise and/or injury) contained metabolites which were significantly overlapped with the transport of glucose and other sugars ($p << 0.01$) and mineral absorption ($p=0.026$). Finally, the metabolites contained in cluster group 4 (down with exercise and injury) were significantly overlapped amino acid synthesis and interconversion ($p < 0.01$), proline catabolism ($p < 0.01$), and amino sugar metabolism ($p < 0.01$).

Discussion

In the present study, we demonstrate the utility of a novel mouse model to monitor *in vivo* changes in cartilage as a result of an OA model comprising both injury and forced exercise. To observe these changes, bioluminescent imaging was used to quantify cartilage-specific luminescence between two independent groups of mice. Furthermore, whole joint LC-MS-based metabolomics revealed global differences in small molecule abundance between the two mouse groups using established methods [116, 206]. This novel murine model has the potential to advance osteoarthritis research using longitudinal monitoring of OA for repeated measures in the same mouse.

In this study we observed significant changes in bioluminescent signal between mice exposed to exercise and injury compared with control mice. Examining the differences in bioluminescent intensity between the two independent groups of mice, we

observe the development of significant differences beginning on day 12 after surgical destabilization and exercise (Figure 40A, *p<0.05, and **p<0.01).

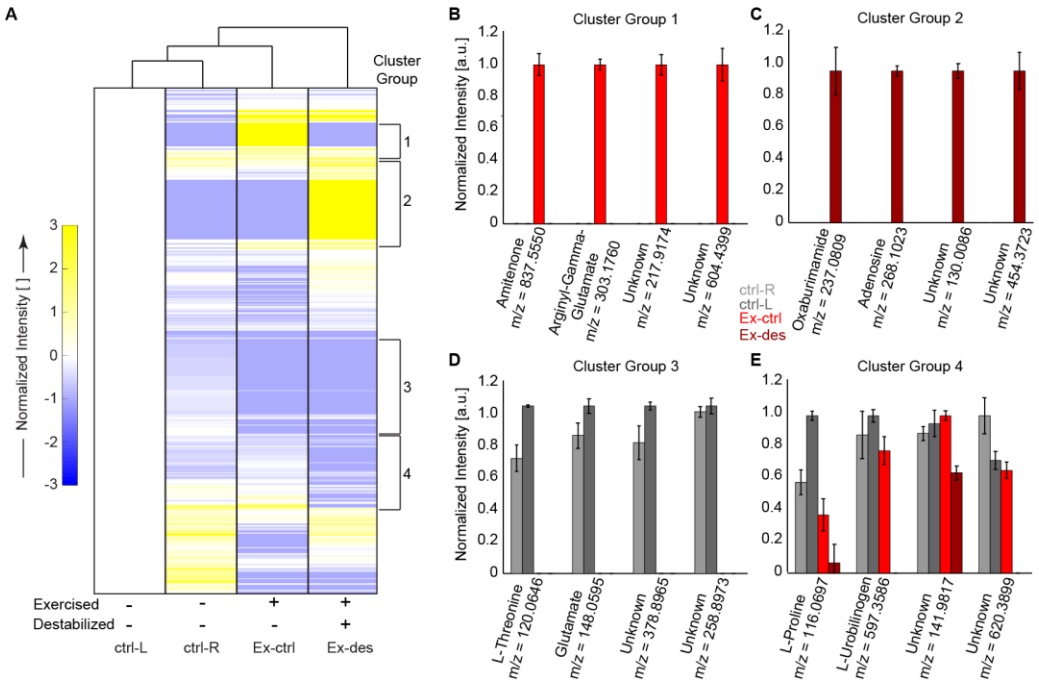

Figure 42. Unsupervised clustering identifies patterns of metabolites differentially regulated by exercise and joint destabilization. (A) Unsupervised clustering revealed 4 distinct clusters (1-4, right hand side) within the experimental groups of ctrl-L, ctrl-R, Ex-des, and Ex-ctrl. (B) Cluster 1 represents metabolites that increase expression in injured joints relative to both negative controls and exercise and destabilized joints. Enriched pathway analysis for cluster 1 included the creatine-phosphate biosynthesis pathway. (C) Cluster 2 involved metabolites with increased expression in joints exposed to both exercise and destabilization. This cluster includes metabolites enriched in valine, leucine, and isoleucine biosynthesis and mineral absorption pathways. (D) Cluster 3 contains metabolites that are down-regulated in both exercised and exercised/destabilized joints. Enriched pathways include glucose/sugar transport and mineral absorption pathways. (E) Cluster 4 represents metabolites that are down-regulated solely in joints subjected to both exercise and destabilization. Enriched pathways include proline and amino sugar metabolism.

The bioluminescent signal represents chondrocyte-specific luciferase expression and changes in this signal have been shown to correlate with histological cartilage changes [238]. In this study, we observed a significant decrease in bioluminescent signal intensity in the joints which were surgically destabilized and subjected to injury (Ex-des, Figure 40B). This decreasing signal results from less chondrocyte-specific bioluminescence and likely represents the progression of OA-like cartilage deterioration (Figure 40A & B). These *in vivo* results were obtained using non-invasive imaging and demonstrate the importance of measuring longitudinal changes in cartilage during the course of experimental OA development. Similar studies in this transgenic mouse line may be used to evaluate candidate therapeutic intervention strategies for OA.

To acquire the luminescence data, all mice were imaged every two days throughout the duration of the running protocol (14 days). The images were then processed in Matlab to quantify the bioluminescent signal. We observed a consistently lower signal in the experimental group when compared to the control group. The lower intensity values are likely a result of ATP depletion following the vigorous treadmill exercise, and terminal metabolomics analyses found the lowest ATP level in the Ex-ctrl group.

There are two chemical reactions required to create a bioluminescent signal using firefly luciferase [260]: in the first reaction, luciferase catalyzes the substrate luciferin in the presence of ATP to produce luciferyl-AMP. In the second reaction, luciferyl-AMP is oxidized, resulting in the production of CO_2, oxyluciferin, AMP, and light [260]. Prior research has shown that the quantity of emitted light is directly proportional to the

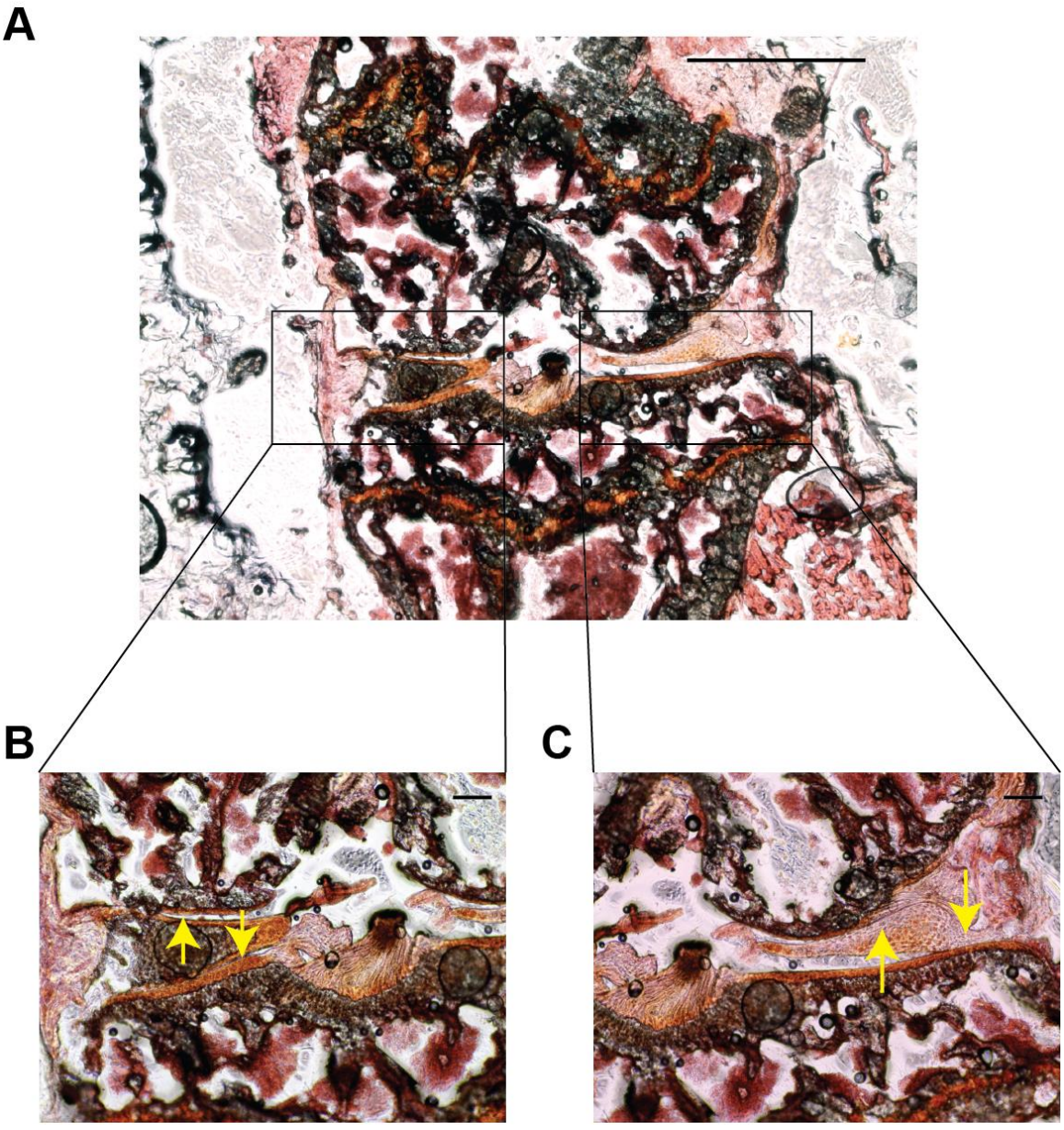

Figure 43. Representative histological images for one mouse from the exercised/destabilized group. (A) Histological images for the left knee (destabilized, Ex-des) highlighting the (B) lateral and (C) medial menisci. (B) The lateral side of the joint contains relatively uniform cartilage thickness and the presence of the lateral meniscus. (C) The medial side of the joint shows a lack of medial meniscus and thinned articular cartilage where the meniscus is removed. Scale bar in (A) is 200 µm; scale bar in (B) and (C) is 50 µm.

quantity of ATP present in the reaction [261]. Therefore, decreased joint ATP levels following exercise may explain the decreased signal in the experimental mice compared to the control mice. Following the treadmill exercise, the experimental mice were given 10 minutes of rest prior to imaging. These data suggest that 10 minutes may be insufficient to restore ATP reserves in the mouse joint.

To further examine joint-related molecular changes following forced exercise and destabilization, metabolomic profiles for each mouse joint were analyzed using LC-MS, following whole-joint dissection at the conclusion of the experiment. We observed significant differences in global metabolite expression between control and experimental mice (Figure 41). The distinct metabolomic profiles represent biological changes between groups as a direct result of forced treadmill running and injury. As expected, we found few differences between ctrl-L and ctrl-R joints (Figure 41A & B). However, we observe substantive and significant differences when comparing destabilized and exercised joints to controls (*e.g.* Ex-des vs. Ex-ctrl, ctrl-L vs. Ex-des, and ctrl-R vs. Ex-ctrl). The differences in metabolomic profiles for the Ex-des and Ex-ctrl joints are a direct result of the destabilization surgery. Ex-des-specific metabolomic changes are therefore the results of the combination of mechanical joint destabilization and surgical incision.

Prior results have demonstrated that the destabilization surgery results in OA-like changes in both the destabilized and contralateral joints [60, 233]. These differences are clearly described by untargeted metabolomic profiling (*e.g.* Figure 41A & B). In this study, the observed differences in metabolomic profiles between ctrl-L and Ex-des are a

result of the combination of treadmill exercise and the destabilization surgery. Using the ctrl-L joint to compare between an intact joint and our induced OA joint, we found changes induced by exercise alone (ctrl-R vs. Ex-ctrl, Figure 41A & B).

Mechanical stimulation has been shown to alter chondrocyte metabolism [43, 84, 116, 173-175, 195, 206, 262, 263], and these data provide additional insight into mechanotransduction at the whole-joint level. We identified metabolites of interest using hierarchical agglomerative cluster analysis. Clusters were used to define metabolites of interest (Figure 42). The first cluster (Figure 42) identifies metabolites which were highly expressed in exercise (Ex-ctrl) and down-regulated in the remaining groups (ctrl-L, ctrl-R, and Ex-des). These metabolites represent mediators of exercise in joint physiology. Pathway analysis revealed enrichment of metabolites in the creatine-phosphate biosynthesis pathway, which is stimulated during periods of high energy demands in the cells. This observation is consistent with the high levels of energy requirements were needed as a result of forced treadmill running.

Additional clusters (2 and 4, Figure 42) identify key metabolites that are either highly expressed or depleted only in joints subjected to both surgical injury and exercise (Ex-des). These metabolites are unique to the destabilized joint, demonstrating substantial alterations in metabolic pathways likely due to the progression of OA in the joint. The pathway analysis for cluster group 2 revealed enrichment in the biosynthesis of the amino acids valine, leucine and isoleucine, which shares common metabolites with pyruvate metabolism. In order for valine, leucine, and isoleucine to be synthesized, pyruvate flux must be elevated, suggesting increased glycolytic metabolism. This

observation suggests a shift of energy utilization toward matrix synthesis OA joint of the mouse (Ex-des) which may be an attempt at repair.

Similarly, the cluster of metabolites depleted in exercise and destabilized joints (Ex-des, 4, Figure 42) contained metabolites enriched in proline catabolism, suggesting the consumption of proline by the chondrocytes to synthesize matrix proteins. Proline contributes more than 20% of the total amino acid residues in type II collagen [264]. These results agree with previous findings using low-strain stimulation of primary human OA chondrocytes [206], and future studies will examine injury and low-dose loading separately to deconvolute this important *in vivo* observation.

The 3rd cluster identifies metabolites that were depleted as a result of injury and/or exercise. These metabolites may represent metabolites that are consumed due to either vigorous exercise or injury, and pathway enrichment analysis identified decreases in glucose transport and mineral absorption. Future studies may elucidate the role of this consumption in the progression of experimental OA which may yield novel targets for therapeutic intervention.

Conclusions

In summary, non-invasive cartilage quantification methods in a novel transgenic reporter mouse found a decrease in *in vivo* bioluminescent signal for mice exposed to injury and forced treadmill running, indicating changes in cartilage and the likely onset of experimental post-traumatic OA. These results were further confirmed through whole joint metabolomic profiling, where injury and exercise caused many metabolomic changes. Extension of these methods may link molecular changes with macroscale

pathology and help identify candidate metabolomic biomarkers in the mouse. The combination of this unique mouse model and high dimensional metabolomics analysis provides an important tool for *in vivo* and longitudinal monitoring of disease progression in murine OA models.

Acknowledgements

We thank Drs. Brian Bothner, and Edward Dratz, Montana State University, for critical insight provided during discussions, and J. Kundert Montana State University for assistance with animal experiments. Funding was provided by NIH P20GM10339405S1, Montana State University, and the Murdock Charitable Trust.

References

See REFERENCES CITED.

CONCLUSION

The overall goal of this research was to develop a comprehensive understanding of the cellular response of the chondrocyte to applied, dynamic compression. To my knowledge, the experiments performed in the various chapters of this dissertation had never been previously done, and considerably advanced the scientific knowledge of chondrocyte mechanobiology. This research generated well-controlled datasets of the intracellular response to mechanical loading and tested our hypothesis that dynamic compression induces matrix synthesis in the context of OA using a number of novel techniques. To test our hypothesis and meet our objectives, this research was portioned into three parts: (1) the methods development, (2) mechanistic data sets, and (3) *in vivo* validation.

The objective of Chapter 2, or the methods development section, was to develop novel *in vitro* methods for studying chondrocyte mechanotransduction. Most of the current research in the chondrocyte mechanotransduction field utilizes agarose gels for cellular encapsulation with much lower stiffness than the physiological environment that chondrocytes reside in our cartilage. This Chapter focused on developing methods for encapsulating chondrocytes in a more effective, philological environment. By better representing the physiological environment of the chondrocytes, biological studies will more effectively represent *in vivo* conditions. In this Chapter we developed and optimized methods for encapsulating chondrocytes in high stiffness agarose (agarose stiffness was matched to the human PCM stiffness). To validate our method we confirmed (1) the spatial homogeneity in physiologically stiff agarose under applied

compression, (2) viability of the cells following 72 hours of encapsulation, and (3) capability of extracting and analyzing inter/extracellular metabolites. These methods were the first of their kind, and not only laid the essential building blocks for my research, but potentially changed the way chondrocyte mechanotransduction studies will be performed in the future.

Following the *in vitro* methods development in Chapter 2, Chapters 3 and 4 were designed to generate well-defined, mechanistic data sets of the chondrocytes response to applied, dynamic compression. Both chapters utilized mechanically stimulated chondrocytes, encapsulated in physiologically stiff agarose, which were harvested from 5 patients with grade IV OA. The objective for these chapters were to analyze metabolomic and phosphoproteomic changes in chondrocytes in direct response to short-duration mechanical compression (0, 15, and 30 minute stimulation), respectively. Chapter 3 was designed to quantify changes in the metabolome for primary human chondrocytes in response to physiological, dynamic compression utilizing both global/untargeted and targeted approaches. Chapter 4 was designed nearly identical to Chapter 3, however, phosphoproteins were analyzed.

The results from Chapter 3 demonstrate the power of utilizing high-dimensional metabolomics as a tool for understanding chondrocyte mechanotransduction. In our targeted analysis (analysis of metabolites associated with central energy metabolism), we discovered significant correlations with increased mechanical loading and central energy reorganization, including key amino acid precursors for protein synthesis. Similarly, our untargeted analysis revealed hundreds of significant metabolites, which were putatively

identified through database searches. We also observed many metabolites which were not found in database searches, which have the potential to be novel mediators for chondrocyte mechanotransduction. Finally, we found a significant, positive correlation between the number of mechanically-induced metabolites and patient age. This was an accidental finding, but none the less suggests the potential of using metabolomics as a tool to characterize aging-dependent changes in chondrocyte mechanotransduction. Metabolomics has huge potential to reveal important biomarker candidates for tracking the progression of OA in clinical populations. This was the first ever application of metabolomics to study mechanotransduction of chondrocytes encapsulated in physiologically stiff agarose. Future work may build off of this work to elucidate the mechanosensitive differences between OA and normal human chondrocytes.

The results from Chapter 4 compliment the results from Chapter 3 and demonstrates the power of using phosphoproteomics as a tool for understanding the chondrocyte response to short duration (<30 min), dynamic compression. We expanded off of previous work, where we analyzed the metabolomic changes of primary human OA chondrocytes as a result of dynamic compression, and were able to identify 514 phosphoproteins unique to dynamically stimulated samples. To our knowledge, this was the first ever chondrocyte mechanotransduction study to successfully identify phosphoproteomic profiles for late OA human chondrocytes. This work identified the potential to use mechanical stimulation (i.e. short-duration, low-impact exercise) as a potential therapeutic to promote cartilage repair in OA clinical populations. Future work

will expand on this work to elucidate latent biomarkers for OA by comparing phosphoproteomic differences between OA and normal human chondrocytes.

The final Chapter of this dissertation was designed to validate the *in vitro* results in Chapters 3 and 4 using a novel, *in vivo* model. The objective of this chapter was to quantify changes in cartilage in response to *in vivo* dynamic, mechanical loading on cartilage reporter mice. This Chapter was highly crucial in that it helped validate the *in vitro* results by comparing metabolites with macro-scale imaging obtained in the context of an exercise-induced mouse loading model. This study was unique in that we utilized novel, transgenic mice that express cartilage specific bioluminescence to quantify cartilage *in vivo* without mouse euthanization. Currently, cartilage quantification changes in mouse models of OA are studied utilizing histopathological grading scales or micro-CT imaging. While these techniques have aided in important findings, they lack the ability to monitor longitudinal cartilage changes *in vivo*. On the contrary, our murine model allows for longitudinal monitoring of cartilage and the progression of OA using the same mouse. In this Chapter we developed methods for quantifying *in vivo* changes in cartilage utilizing a novel, post traumatic model of OA involving surgical destabilization and forced exercise via treadmill running. Using these novel methods we analyzed the effects of forced treadmill running (FTR) and injury by comparing an unexercised/uninjured control group of mice to mice that were exposed to both exercise and injury. Our results suggest that our non-invasive cartilage quantification methods in a novel transgenic reporter mouse found a decrease in *in vivo* bioluminescent signal for mice exposed to injury and FTR. The decreased bioluminescent signal correlated well

with histological scoring for decreasing cartilage thickness, suggesting that the changes in cartilage are most likely due to the onset of experimental, post-traumatic OA. These results were further confirmed through whole joint LC-MS analysis, where injury and exercise caused many significant, metabolomic changes. Future work may build on these methods to link molecular changes with macroscale pathology and help identify potential metabolomic biomarkers in the mouse. The results from this Chapter also suggest the extension of using this unique mouse model as a promising tool in the scientific field for *in vivo*, longitudinal monitoring in murine OA progression.

All of the studies performed in this dissertation were extremely novel, and to our knowledge, had not been previously reported. This research considerably advanced the scientific knowledge of chondrocyte mechanobiology and laid many fundamental building blocks for future work in this field, specifically in understanding how mechanotransduction plays a role in OA. This work dramatically expanded the fundamental knowledge and understanding of chondrocyte mechanotransduction identified the potential to utilize mechanical loading as a therapeutic in preventing or treating OA.

REFERENCES CITED

[1] Cicuttini, F. M., Wluka, A. E., Urquhart, D., Tanamas, S. K., and Wang, Y., 2011, "Epidemiology should not be forgotten in osteoarthritis imaging," Osteoarthritis Cartilage, 19(9), pp. 1165-1166.

[2] Cobb, J. P., 2011, "Osteoarthritis excess mortality. Painful limping and early death," BMJ, 342, p. d2137.

[3] Goekoop, R. J., Kloppenburg, M., Kroon, H. M., Dirkse, L. E. V., Huizinga, T. W. J., Westendorp, R. G. J., and Gussekloo, J., 2011, "Determinants of absence of osteoarthritis in old age," Scandinavian Journal of Rheumatology, 40(1).

[4] Hayashi, D., Guermazi, A., and Hunter, D. J., 2011, "Response to Letter to the Editor: 'Epidemiology should not be forgotten in osteoarthritis imaging'," Osteoarthritis and cartilage / OARS, Osteoarthritis Research Society, 19(9), p. 1167.

[5] Woolf, A. D., Erwin, J., and March, L., 2012, "The need to address the burden of musculoskeletal conditions," Best Practice & Research in Clinical Rheumatology, 26(2).

[6] Woolf, A. D., and Pfleger, B., 2003, "Burden of major musculoskeletal conditions," Bulletin of the World Health Organization, 81(9), pp. 646-656.

[7] Zhang, Y., and Jordan, J. M., 2010, "Epidemiology of osteoarthritis," Clin Geriatr Med, 26(3), pp. 355-369.

[8] Harada, Y., Tomita, N., Nakajima, M., Ikeuchi, K., and Wakitani, S., 2005, "Effect of low loading and joint immobilization for spontaneous repair of osteochondral defect in the knees of weightless (tail suspension) rats," Journal of Orthopaedic Science, 10(5), pp. 508-514.

[9] Bougault, C., Paumier, A., Aubert-Foucher, E., and Mallein-Gerin, F., 2008, "Molecular analysis of chondrocytes cultured in agarose in response to dynamic compression," BMC Biotechnol., 8, p. 10.

[10] Biology, B., 2015, "Types of Synovial Joints," https://www.boundless.com/biology/textbooks/boundless-biology-textbook/the-musculoskeletal-system-38/joints-and-skeletal-movement-217/types-of-synovial-joints-822-12066/.

[11] Zhang, Y., and Jordan, J. M., 2010, "Epidemiology of Osteoarthritis," Clinics in Geriatric Medicine, 26(3).

[12] KELLGREN, J. H., and LAWRENCE, J. S., 1957, "Radiological assessment of osteo-arthrosis," Ann Rheum Dis, 16(4), pp. 494-502.

[13] www.Radiopaedia.org, 2015, "Kellgren and Lawrence system for classification of osteoarthritis of knee," http://radiopaedia.org/articles/kellgren-and-lawrence-system-for-classification-of-osteoarthritis-of-knee.

[14] Lawrence, R. C., Felson, D. T., Helmick, C. G., Arnold, L. M., Choi, H., Deyo, R. A., Gabriel, S., Hirsch, R., Hochberg, M. C., Hunder, G. G., Jordan, J. M., Katz, J. N., Kremers, H. M., Wolfe, F., and Workgroup, N. A. D., 2008, "Estimates of the prevalence of arthritis and other rheumatic conditions in the United States. Part II," Arthritis Rheum, 58(1), pp. 26-35.

[15] Dillon, C. F., Rasch, E. K., Gu, Q., and Hirsch, R., 2006, "Prevalence of knee osteoarthritis in the United States: arthritis data from the Third National Health and Nutrition Examination Survey 1991-94," J Rheumatol, 33(11), pp. 2271-2279.

[16] Felson, D. T., Naimark, A., Anderson, J., Kazis, L., Castelli, W., and Meenan, R. F., 1987, "The prevalence of knee osteoarthritis in the elderly. The Framingham Osteoarthritis Study," Arthritis Rheum, 30(8), pp. 914-918.

[17] Jordan, J. M., Helmick, C. G., Renner, J. B., Luta, G., Dragomir, A. D., Woodard, J., Fang, F., Schwartz, T. A., Abbate, L. M., Callahan, L. F., Kalsbeek, W. D., and Hochberg, M. C., 2007, "Prevalence of knee symptoms and radiographic and symptomatic knee osteoarthritis in African Americans and Caucasians: the Johnston County Osteoarthritis Project," J Rheumatol, 34(1), pp. 172-180.

[18] Murphy, L., and Helmick, C. G., 2012, "The impact of osteoarthritis in the United States: a population-health perspective: A population-based review of the fourth most common cause of hospitalization in U.S. adults," Orthop Nurs, 31(2), pp. 85-91.

[19] Srikanth, V. K., Fryer, J. L., Zhai, G., Winzenberg, T. M., Hosmer, D., and Jones, G., 2005, "A meta-analysis of sex differences prevalence, incidence and severity of osteoarthritis," Osteoarthritis Cartilage, 13(9), pp. 769-781.

[20] Wluka, A. E., Davis, S. R., Bailey, M., Stuckey, S. L., and Cicuttini, F. M., 2001, "Users of oestrogen replacement therapy have more knee cartilage than non-users," Ann Rheum Dis, 60(4), pp. 332-336.

[21] Loughlin, J., 2005, "The genetic epidemiology of human primary osteoarthritis: current status," Expert Rev Mol Med, 7(9), pp. 1-12.

[22] Spector, T. D., Cicuttini, F., Baker, J., Loughlin, J., and Hart, D., 1996, "Genetic influences on osteoarthritis in women: a twin study," BMJ, 312(7036), pp. 940-943.

[23] Palotie, A., Väisänen, P., Ott, J., Ryhänen, L., Elima, K., Vikkula, M., Cheah, K., Vuorio, E., and Peltonen, L., 1989, "Predisposition to familial osteoarthrosis linked to type II collagen gene," Lancet, 1(8644), pp. 924-927.

[24] Valdes, A. M., Evangelou, E., Kerkhof, H. J., Tamm, A., Doherty, S. A., Kisand, K., Kerna, I., Uitterlinden, A., Hofman, A., Rivadeneira, F., Cooper, C., Dennison, E. M., Zhang, W., Muir, K. R., Ioannidis, J. P., Wheeler, M., Maciewicz, R. A., van Meurs, J. B., Arden, N. K., Spector, T. D., and Doherty, M., 2011, "The GDF5 rs143383 polymorphism is associated with osteoarthritis of the knee with genome-wide statistical significance," Ann Rheum Dis, 70(5), pp. 873-875.

[25] Evangelou, E., Valdes, A. M., Kerkhof, H. J., Styrkarsdottir, U., Zhu, Y., Meulenbelt, I., Lories, R. J., Karassa, F. B., Tylzanowski, P., Bos, S. D., Akune, T., Arden, N. K., Carr, A., Chapman, K., Cupples, L. A., Dai, J., Deloukas, P., Doherty, M., Doherty, S., Engstrom, G., Gonzalez, A., Halldorsson, B. V., Hammond, C. L., Hart, D. J., Helgadottir, H., Hofman, A., Ikegawa, S., Ingvarsson, T., Jiang, Q., Jonsson, H., Kaprio, J., Kawaguchi, H., Kisand, K., Kloppenburg, M., Kujala, U. M., Lohmander, L. S., Loughlin, J., Luyten, F. P., Mabuchi, A., McCaskie, A., Nakajima, M., Nilsson, P. M., Nishida, N., Ollier, W. E., Panoutsopoulou, K., van de Putte, T., Ralston, S. H., Rivadeneira, F., Saarela, J., Schulte-Merker, S., Shi, D., Slagboom, P. E., Sudo, A., Tamm, A., Thorleifsson, G., Thorsteinsdottir, U., Tsezou, A., Wallis, G. A., Wilkinson, J. M., Yoshimura, N., Zeggini, E., Zhai, G., Zhang, F., Jonsdottir, I., Uitterlinden, A. G., Felson, D. T., van Meurs, J. B., Stefansson, K., Ioannidis, J. P., Spector, T. D., Consortium, a., and (TreatOA), T. R. i. E. A. T. f. O., 2011, "Meta-analysis of genome-wide association studies confirms a susceptibility locus for knee osteoarthritis on chromosome 7q22," Ann Rheum Dis, 70(2), pp. 349-355.

[26] Felson, D. T., Zhang, Y., Anthony, J. M., Naimark, A., and Anderson, J. J., 1992, "Weight loss reduces the risk for symptomatic knee osteoarthritis in women. The Framingham Study," Ann Intern Med, 116(7), pp. 535-539.

[27] Messier, S. P., Loeser, R. F., Miller, G. D., Morgan, T. M., Rejeski, W. J., Sevick, M. A., Ettinger, W. H., Pahor, M., and Williamson, J. D., 2004, "Exercise and dietary weight loss in overweight and obese older adults with knee osteoarthritis: the Arthritis, Diet, and Activity Promotion Trial," Arthritis Rheum, 50(5), pp. 1501-1510.

[28] Puranen, J., Ala-Ketola, L., Peltokallio, P., and Saarela, J., 1975, "Running and primary osteoarthritis of the hip," Br Med J, 2(5968), pp. 424-425.

[29] Kujala, U. M., Kettunen, J., Paananen, H., Aalto, T., Battié, M. C., Impivaara, O., Videman, T., and Sarna, S., 1995, "Knee osteoarthritis in former runners, soccer players, weight lifters, and shooters," Arthritis Rheum, 38(4), pp. 539-546.

[30] Lane, N. E., Michel, B., Bjorkengren, A., Oehlert, J., Shi, H., Bloch, D. A., and Fries, J. F., 1993, "The risk of osteoarthritis with running and aging: a 5-year longitudinal study," J Rheumatol, 20(3), pp. 461-468.

[31] 2015, "Total Knee Replacement Cost," http://www.kneereplacementcost.com/.

[32] Control, C. f. D., May 16th, 2104, "Osteoarthritis," http://www.cdc.gov/arthritis/basics/osteoarthritis.htm.

[33] Newton, P. M., Mow, V. C., Gardner, T. R., Buckwalter, J. A., and Albright, J. P., 1997, "Winner of the 1996 Cabaud Award. The effect of lifelong exercise on canine articular cartilage," Am J Sports Med, 25(3), pp. 282-287.

[34] Goekoop, R. J., Kloppenburg, M., Kroon, H. M., Dirkse, L. E., Huizinga, T. W., Westendorp, R. G., and Gussekloo, J., 2011, "Determinants of absence of osteoarthritis in old age," Scand J Rheumatol, 40(1), pp. 68-73.

[35] Stockwell, R. A., "Biology of Cartilage Cells."

[36] Pearle, A. D., Warren, R. F., and Rodeo, S. A., 2005, "Basic science of articular cartilage and osteoarthritis," Clin Sports Med, 24(1), pp. 1-12.

[37] Sophia Fox, A. J., Bedi, A., and Rodeo, S. A., 2009, "The basic science of articular cartilage: structure, composition, and function," Sports Health, 1(6), pp. 461-468.

[38] Alford, J. W., and Cole, B. J., 2005, "Cartilage restoration, part 1: basic science, historical perspective, patient evaluation, and treatment options," Am J Sports Med, 33(2), pp. 295-306.

[39] Campbell, N. A., Reece, J. B., and Mitchell, L. G., 1999, Biology Fifth Edition, Benjamin/Cummings, Menlo Park, CA.

[40] Jenniskens, Y. M., Koevoet, W., de Bart, A. C., Weinans, H., Jahr, H., Verhaar, J. A., DeGroot, J., and van Osch, G. J., 2006, "Biochemical and functional modulation of the cartilage collagen network by IGF1, TGFbeta2 and FGF2," Osteoarthritis Cartilage, 14(11), pp. 1136-1146.

[41] van den Berg, W. B., and van Riel, P. L., 2005, "Uncoupling of inflammation and destruction in rheumatoid arthritis: myth or reality?," Arthritis Rheum, 52(4), pp. 995-999.

[42] Fernandes, J. C., Martel-Pelletier, J., and Pelletier, J. P., 2002, "The role of cytokines in osteoarthritis pathophysiology," Biorheology, 39(1-2), pp. 237-246.

[43] Farnsworth, N. L., Antunez, L. R., and Bryant, S. J., 2013, "Dynamic compressive loading differentially regulates chondrocyte anabolic and catabolic activity with age," Biotechnol Bioeng.

[44] Loeser, R. F., 2006, "Molecular mechanisms of cartilage destruction: mechanics, inflammatory mediators, and aging collide," Arthritis Rheum, 54(5), pp. 1357-1360.

[45] Troeberg, L., and Nagase, H., 2012, "Proteases involved in cartilage matrix degradation in osteoarthritis," Biochim Biophys Acta, 1824(1), pp. 133-145.

[46] Archer, C. W., and Francis-West, P., 2003, "The chondrocyte," Int J Biochem Cell Biol, 35(4), pp. 401-404.

[47] Darling, E. M., Wilusz, R. E., Bolognesi, M. P., Zauscher, S., and Guilak, F., 2010, "Spatial mapping of the biomechanical properties of the pericellular matrix of articular cartilage measured in situ via atomic force microscopy," Biophysical journal, 98(12), pp. 2848-2856.

[48] Alexopoulos, L. G., Setton, L. A., and Guilak, F., 2005, "The biomechanical role of the chondrocyte pericellular matrix in articular cartilage," Acta Biomater, 1(3), pp. 317-325.

[49] Vincent, T. L., 2013, "Targeting mechanotransduction pathways in osteoarthritis: a focus on the pericellular matrix," Curr Opin Pharmacol.

[50] Garcia, M., and Knight, M. M., 2010, "Cyclic Loading Opens Hemichannels to Release ATP as Part of a Chondrocyte Mechanotransduction Pathway," Journal of Orthopaedic Research, 28(4), pp. 510-515.

[51] Jaalouk, D. E., and Lammerding, J., 2009, "Mechanotransduction gone awry," Nat Rev Mol Cell Biol, 10(1), pp. 63-73.

[52] Choi, J. B., Youn, I., Cao, L., Leddy, H. A., Gilchrist, C. L., Setton, L. A., and Guilak, F., 2007, "Zonal changes in the three-dimensional morphology of the chondron under compression: the relationship among cellular, pericellular, and extracellular deformation in articular cartilage," Journal of biomechanics, 40(12), pp. 2596-2603.

[53] Guilak, F., 2000, "The deformation behavior and viscoelastic properties of chondrocytes in articular cartilage," Biorheology, 37(1-2), pp. 27-44.

[54] Liu, F., Kozanek, M., Hosseini, A., Van de Velde, S. K., Gill, T. J., Rubash, H. E., and Li, G., 2010, "In vivo tibiofemoral cartilage deformation during the stance phase of gait," Journal of biomechanics, 43(4), pp. 658-665.

[55] Guilak, F., 2011, "Biomechanical factors in osteoarthritis," Best Practice & Research in Clinical Rheumatology, 25(6), pp. 815-823.

[56] Morrell, K. C., Hodge, W. A., Krebs, D. E., and Mann, R. W., 2005, "Corroboration of in vivo cartilage pressures with implications for synovial joint tribology and osteoarthritis causation," Proc Natl Acad Sci U S A, 102(41), pp. 14819-14824.

[57] Buckwalter, J. A., Mow, V. C., and Ratcliffe, A., 1994, "Restoration of Injured or Degenerated Articular Cartilage," J Am Acad Orthop Surg, 2(4), pp. 192-201.

[58] Ytterberg, S. R., Mahowald, M. L., and Krug, H. E., 1994, "Exercise for arthritis," Baillieres Clin Rheumatol, 8(1), pp. 161-189.

[59] Oliveria, S. A., Felson, D. T., Cirillo, P. A., Reed, J. I., and Walker, A. M., 1999, "Body weight, body mass index, and incident symptomatic osteoarthritis of the hand, hip, and knee," Epidemiology, 10(2), pp. 161-166.

[60] Glasson, S. S., Blanchet, T. J., and Morris, E. A., 2007, "The surgical destabilization of the medial meniscus (DMM) model of osteoarthritis in the 129/SvEv mouse," Osteoarthritis and cartilage / OARS, Osteoarthritis Research Society, 15(9), pp. 1061-1069.

[61] Clements, K. M., Price, J. S., Chambers, M. G., Visco, D. M., Poole, A. R., and Mason, R. M., 2003, "Gene deletion of either interleukin-1beta, interleukin-1beta-converting enzyme, inducible nitric oxide synthase, or stromelysin 1 accelerates the development of knee osteoarthritis in mice after surgical transection of the medial collateral ligament and partial medial meniscectomy," Arthritis Rheum, 48(12), pp. 3452-3463.

[62] Wilusz, R. E., Zauscher, S., and Guilak, F., 2013, "Micromechanical Mapping of Early Osteoarthritic Changes in the Pericellular Matrix of Human Articular Cartilage," Osteoarthritis and cartilage / OARS, Osteoarthritis Research Society.

[63] Armstrong, C. G., and Mow, V. C., 1982, "Variations in the intrinsic mechanical properties of human articular cartilage with age, degeneration, and water content," J Bone Joint Surg Am, 64(1), pp. 88-94.

[64] Setton, L. A., Elliott, D. M., and Mow, V. C., 1999, "Altered mechanics of cartilage with osteoarthritis: human osteoarthritis and an experimental model of joint degeneration," Osteoarthritis Cartilage, 7(1), pp. 2-14.

[65] Stolz, M., Gottardi, R., Raiteri, R., Miot, S., Martin, I., Imer, R., Staufer, U., Raducanu, A., Düggelin, M., Baschong, W., Daniels, A. U., Friederich, N. F., Aszodi, A., and Aebi, U., 2009, "Early detection of aging cartilage and osteoarthritis in mice and patient samples using atomic force microscopy," Nat Nanotechnol, 4(3), pp. 186-192.

[66] Desrochers, J., Amrein, M. A., and Matyas, J. R., 2010, "Structural and functional changes of the articular surface in a post-traumatic model of early osteoarthritis measured by atomic force microscopy," J Biomech, 43(16), pp. 3091-3098.

[67] Kisiday, J. D., Lee, J. H., Siparsky, P. N., Frisbie, D. D., Flannery, C. R., Sandy, J. D., and Grodzinsky, A. J., 2009, "Catabolic responses of chondrocyte-seeded peptide hydrogel to dynamic compression," Annals of biomedical engineering, 37(7), pp. 1368-1375.

[68] Haudenschild, D. R., Chen, J., Pang, N., Steklov, N., Grogan, S. P., Lotz, M. K., and D'Lima, D. D., 2011, "Vimentin contributes to changes in chondrocyte stiffness in osteoarthritis," Journal of orthopaedic research : official publication of the Orthopaedic Research Society, 29(1), pp. 20-25.

[69] Knight, M. M., Toyoda, T., Lee, D. A., and Bader, D. L., 2006, "Mechanical compression and hydrostatic pressure induce reversible changes in actin cytoskeletal organisation in chondrocytes in agarose," Journal of Biomechanics, 39(8).

[70] Vaughan, N. M., Grainger, J., Bader, D. L., and Knight, M. M., 2010, "The potential of pulsed low intensity ultrasound to stimulate chondrocytes matrix synthesis in agarose and monolayer cultures," Med Biol Eng Comput, 48(12), pp. 1215-1222.

[71] Normand, V., Lootens, D. L., Amici, E., Plucknett, K. P., and Aymard, P., 2000, "New insight into agarose gel mechanical properties," Biomacromolecules, 1(4).

[72] Filatov, D., Bjorklund, S., Johansson, E., and Thelander, L., 1996, "Induction of the mouse ribonucleotide reductase R1 and R2 genes in response to DNA damage by UV light," Journal of Biological Chemistry, 271(39), pp. 23698-23704.

[73] Alexopoulos, L. G., Williams, G. M., Upton, M. L., Setton, L. A., and Guilak, F., 2005, "Osteoarthritic changes in the biphasic mechanical properties of the chondrocyte pericellular matrix in articular cartilage," J Biomech, 38(3), pp. 509-517.

[74] Buckwalter, J. A., and Mankin, H. J., 1998, "Articular cartilage: tissue design and chondrocyte-matrix interactions," Instructional course lectures, 47.

[75] Buschmann, M. D., Kim, Y. J., Wong, M., Frank, E., Hunziker, E. B., and Grodzinsky, A. J., 1999, "Stimulation of aggrecan synthesis in cartilage explants by cyclic loading is localized to regions of high interstitial fluid flow," Archives of biochemistry and biophysics, 366(1), pp. 1-7.

[76] Fitzgerald, J. B., Jin, M., Chai, D. H., Siparsky, P., Fanning, P., and Grodzinsky, A. J., 2008, "Shear- and compression-induced chondrocyte transcription requires MAPK activation in cartilage explants," The Journal of biological chemistry, 283(11), pp. 6735-6743.

[77] Jin, M., Frank, E. H., Quinn, T. M., Hunziker, E. B., and Grodzinsky, A. J., 2001, "Tissue shear deformation stimulates proteoglycan and protein biosynthesis in bovine cartilage explants," Arch Biochem Biophys, 395(1), pp. 41-48.

[78] Bougault, C., Paumier, A., Aubert-Foucher, E., and Mallein-Gerin, F., 2008, "Molecular analysis of chondrocytes cultured in agarose in response to dynamic compression," BMC biotechnology, 8, p. 71.

[79] Fanning, P. J., Emkey, G., Smith, R. J., Grodzinsky, A. J., Szasz, N., and Trippel, S. B., 2003, "Mechanical regulation of mitogen-activated protein kinase signaling in articular cartilage," The Journal of biological chemistry, 278(51), pp. 50940-50948.

[80] Niehoff, A., Offermann, M., Dargel, J., Schmidt, A., Bruggemann, G. P., and Bloch, W., 2008, "Dynamic and static mechanical compression affects Akt phosphorylation in porcine patellofemoral joint cartilage," Journal of orthopaedic research : official publication of the Orthopaedic Research Society, 26(5), pp. 616-623.

[81] De Croos, J. N., Jang, B., Dhaliwal, S. S., Grynpas, M. D., Pilliar, R. M., and Kandel, R. A., 2007, "Membrane type-1 matrix metalloproteinase is induced following cyclic compression of in vitro grown bovine chondrocytes," Osteoarthritis and cartilage / OARS, Osteoarthritis Research Society, 15(11), pp. 1301-1310.

[82] Li, K. W., Wang, A. S., and Sah, R. L., 2003, "Microenvironment regulation of extracellular signal-regulated kinase activity in chondrocytes: effects of culture configuration, interleukin-1, and compressive stress," Arthritis and rheumatism, 48(3), pp. 689-699.

[83] Ryan, J. A., Eisner, E. A., DuRaine, G., You, Z., and Reddi, A. H., 2009, "Mechanical compression of articular cartilage induces chondrocyte proliferation and inhibits proteoglycan synthesis by activation of the ERK pathway: implications for tissue engineering and regenerative medicine," Journal of tissue engineering and regenerative medicine, 3(2), pp. 107-116.

[84] Haudenschild, D. R., D'Lima, D. D., and Lotz, M. K., 2008, "Dynamic compression of chondrocytes induces a Rho kinase-dependent reorganization of the actin cytoskeleton," Biorheology, 45(3-4).

[85] Bougault, C., Aubert-Foucher, E., Paumier, A., Perrier-Groult, E., Huot, L., Hot, D., Duterque-Coquillaud, M., and Mallein-Gerin, F., 2012, "Dynamic Compression of Chondrocyte-Agarose Constructs Reveals New Candidate Mechanosensitive Genes," PLoS One, 7(5), p. 11.

[86] Nebelung, S., Gavenis, K., Lüring, C., Zhou, B., Mueller-Rath, R., Stoffel, M., Tingart, M., and Rath, B., 2012, "Simultaneous anabolic and catabolic responses of human chondrocytes seeded in collagen hydrogels to long-term continuous dynamic compression.," Ann Anat.

[87] Neu, C. P., Khalafi, A., Komvopoulos, K., Schmid, T. M., and Reddi, A. H., 2007, "Mechanotransduction of bovine articular cartilage superficial zone protein by transforming growth factor beta signaling," Arthritis and rheumatism, 56(11), pp. 3706-3714.

[88] Zanetti, N. C., and Solursh, M., 1984, "Induction of chondrogenesis in limb mesenchymal cultures by disruption of the actin cytoskeleton," J Cell Biol, 99(1 Pt 1), pp. 115-123.

[89] Woods, A., Wang, G., and Beier, F., 2007, "Regulation of chondrocyte differentiation by the actin cytoskeleton and adhesive interactions," J Cell Physiol, 213(1), pp. 1-8.

[90] Alexopoulos, L. G., Williams, G. M., Upton, M. L., Setton, L. A., and Guilak, F., 2005, "Osteoarthritic changes in the biphasic mechanical properties of the chondrocyte pericellular matrix in articular cartilage," Journal of Biomechanics, 38(3), pp. 509-517.

[91] Buckwalter, J. A., and Martin, J. A., 2006, "Osteoarthritis," Advanced Drug Delivery Reviews, 58(2), pp. 150-167.

[92] Fukui, N., Ikeda, Y., Ohnuki, T., Tanaka, N., Hikita, A., Mitomi, H., Mori, T., Juji, T., Katsuragawa, Y., Yamamoto, S., Sawabe, M., Yamane, S., Suzuki, R., Sandell, L. J., and Ochi, T., 2008, "Regional differences in chondrocyte metabolism in osteoarthritis: a detailed analysis by laser capture microdissection," Arthritis Rheum, 58(1), pp. 154-163.

[93] Kawakita, K., Nishiyama, T., Fujishiro, T., Hayashi, S., Kanzaki, N., Hashimoto, S., Takebe, K., Iwasa, K., Sakata, S., Nishida, K., Kuroda, R., and Kurosaka, M., 2012, "Akt phosphorylation in human chondrocytes is regulated by p53R2 in response to mechanical stress," Osteoarthritis and cartilage / OARS, Osteoarthritis Research Society, 20(12), pp. 1603-1609.

[94] Adams, S. B., Setton, L. A., and Nettles, D. L., 2013, "The role of metabolomics in osteoarthritis research," J Am Acad Orthop Surg, 21(1), pp. 63-64.

[95] Oliver, S. G., Winson, M. K., Kell, D. B., and Baganz, F., 1998, "Systematic functional analysis of the yeast genome," Trends in biotechnology, 16(9), pp. 373-378.

[96] Patti, G. J., Yanes, O., and Siuzdak, G., 2012, "Innovation: Metabolomics: the apogee of the omics trilogy," Nat Rev Mol Cell Biol, 13(4), pp. 263-269.

[97] Smith, C. A., Want, E. J., O'Maille, G., Abagyan, R., and Siuzdak, G., 2006, "XCMS: processing mass spectrometry data for metabolite profiling using nonlinear peak alignment, matching, and identification," Anal Chem, 78(3), pp. 779-787.

[98] Spectrometry, S. C. f. M. a. M., 2015, "What is Mass Spectrometry?," http://masspec.scripps.edu/mshistory/whatisms_toc.php.

[99] Snyder, L. R., Kirkland, J. J., and Dolan, J. W., 2009, Introduction to Modern Liquid Chromatography, Wiley-Blackwell,, Hoboken, NJ.

[100] Corp., W., 2015, "HPLC - High Performance Liquid Chromatography," http://www.waters.com/waters/en_US/HPLC---High-Performance-Liquid-Chromatography-Beginner%27s-Guide/nav.htm?locale=en_US&cid=10048919.

[101] Wilkins, M., 2009, "Proteomics data mining," Expert Rev Proteomics, 6(6), pp. 599-603.

[102] Alberts, B., Johnson, A., Lewis, J., Raff, M., Roberts, K., and Walter, P., 2002, Molecular Biology of the Cell, Garland Science, New York, NY.

[103] Olsen, J. V., Blagoev, B., Gnad, F., Macek, B., Kumar, C., Mortensen, P., and Mann, M., 2006, "Global, in vivo, and site-specific phosphorylation dynamics in signaling networks," Cell, 127(3), pp. 635-648.

[104] Health, N. I. o., 2014, "All About the Human Genome Project," http://www.genome.gov/.

[105] O'Farrell, P. H., 1975, "High resolution two-dimensional electrophoresis of proteins," J Biol Chem, 250(10), pp. 4007-4021.

[106] Ruiz-Romero, C., Calamia, V., Mateos, J., Carreira, V., Martínez-Gomariz, M., Fernández, M., and Blanco, F. J., 2009, "Mitochondrial dysregulation of osteoarthritic human articular chondrocytes analyzed by proteomics: a decrease in mitochondrial superoxide dismutase points to a redox imbalance," Mol Cell Proteomics, 8(1), pp. 172-189.

[107] Rawlings, N. D., and Barrett, A. J., 1994, "Families of serine peptidases," Methods Enzymol, 244, pp. 19-61.

[108] Wells, J. M., and McLuckey, S. A., 2005, "Collision-induced dissociation (CID) of peptides and proteins," Methods Enzymol, 402, pp. 148-185.

[109] Blackstock, W. P., and Weir, M. P., 1999, "Proteomics: quantitative and physical mapping of cellular proteins," Trends Biotechnol, 17(3), pp. 121-127.

[110] Pappin, D. J., Hojrup, P., and Bleasby, A. J., 1993, "Rapid identification of proteins by peptide-mass fingerprinting," Curr Biol, 3(6), pp. 327-332.

[111] James, P., Quadroni, M., Carafoli, E., and Gonnet, G., 1993, "Protein identification by mass profile fingerprinting," Biochem Biophys Res Commun, 195(1), pp. 58-64.

[112] Yates, J. R., Speicher, S., Griffin, P. R., and Hunkapiller, T., 1993, "Peptide mass maps: a highly informative approach to protein identification," Anal Biochem, 214(2), pp. 397-408.

[113] Jutila, A. A., 2013, "Development and Validation of a System for Studying Chondrocyte Mechanotransduction wtih Preliminary Metabolomic Results," MSME, Montana State University, Bozeman, MT.

[114] Jutila, A. A., Zignego, D. L., Schell, W. J., and June, R. K., 2014, "Encapsulation of Chondrocytes in High-Stiffness Agarose Microenvironments for In Vitro Modeling of Osteoarthritis Mechanotransduction," Annals of biomedical engineering.

[115] Zignego, D. L., Jutila, A. A., Gelbke, M. K., Gannon, D. M., and June, R. K., 2013, "The mechanical microenvironment of high concentration agarose for applying deformation to primary chondrocytes," Journal of biomechanics.

[116] Jutila, A. A., Zignego, D. L., Hwang, B. K., Hilmer, J. K., Hamerly, T., Minor, C. A., Walk, S. T., and June, R. K., 2014, "Candidate mediators of chondrocyte mechanotransduction via targeted and untargeted metabolomic measurements," Arch Biochem Biophys, 545, pp. 116-123.

[117] Knight, M. M., Ghori, S. A., Lee, D. A., and Bader, D. L., 1998, "Measurement of the deformation of isolated chondrocytes in agarose subjected to cyclic compression," Med Eng Phys, 20(9), pp. 684-688.

[118] Lee, D. A., and Knight, M. M., 2004, "Mechanical loading of chondrocytes embedded in 3D constructs: in vitro methods for assessment of morphological and metabolic response to compressive strain," Methods Mol Med, 100, pp. 307-324.

[119] Bougault, C., Aubert-Foucher, E., Paumier, A., Perrier-Groult, E., Huot, L., Hot, D., Duterque-Coquillaud, M., and Mallein-Gerin, F., 2012, "Dynamic compression of chondrocyte-agarose constructs reveals new candidate mechanosensitive genes.," PLoS One, 7(5), p. e36964.

[120] Lee, D. A., Knight, M. M., Bolton, J. F., Idowu, B. D., Kayser, M. V., and Bader, D. L., 2000, "Chondrocyte deformation within compressed agarose constructs at the cellular and sub-cellular levels," J Biomech, 33(1), pp. 81-95.

[121] Bougault, C., Paumier, A., Aubert-Foucher, E., and Mallein-Gerin, F., 2009, "Investigating conversion of mechanical force into biochemical signaling in three-dimensional chondrocyte cultures," Nat Protoc, 4(6), pp. 928-938.

[122] Kim, Y. J., Bonassar, L. J., and Grodzinsky, A. J., 1995, "The role of cartilage streaming potential, fluid flow and pressure in the stimulation of chondrocyte biosynthesis during dynamic compression," J Biomech, 28(9), pp. 1055-1066.

[123] Haudenschild, D. R., Nguyen, B., Chen, J., D'Lima, D. D., and Lotz, M. K., 2008, "Rho kinase-dependent CCL20 induced by dynamic compression of human chondrocytes," Arthritis Rheum, 58(9), pp. 2735-2742.

[124] Lee, D. A., Brand, J., Salter, D., Akanji, O. O., and Chowdhury, T. T., 2011, "Quantification of mRNA using real-time PCR and Western blot analysis of MAPK events in chondrocyte/agarose constructs," Methods Mol Biol, 695, pp. 77-97.

[125] Muir, H., 1995, "The chondrocyte, architect of cartilage. Biomechanics, structure, function and molecular biology of cartilage matrix macromolecules," Bioessays, 17(12), pp. 1039-1048.

[126] Garcia, M., and Knight, M. M., 2010, "Cyclic loading opens hemichannels to release ATP as part of a chondrocyte mechanotransduction pathway," Journal of orthopaedic research : official publication of the Orthopaedic Research Society, 28(4), pp. 510-515.

[127] McLeod, M. A., Wilusz, R. E., and Guilak, F., 2013, "Depth-dependent anisotropy of the micromechanical properties of the extracellular and pericellular matrices of articular cartilage evaluated via atomic force microscopy," J Biomech, 46(3), pp. 586-592.

[128] Normand, V., Lootens, D. L., Amici, E., Plucknett, K. P., and Aymard, P., 2000, "New insight into agarose gel mechanical properties," Biomacromolecules, 1(4), pp. 730-738.

[129] Geers, M. G. D., DeBorst, R., and Brekelmans, W. A. M., 1996, "Computing strain fields from discrete displacement fields in 2D-solids," International Journal of Solids and Structures, 33(29), pp. 4293-4307.

[130] Neu, C. P., Hull, M. L., and Walton, J. H., 2005, "Heterogeneous three-dimensional strain fields during unconfined cyclic compression in bovine articular cartilage explants," Journal of Orthopaedic Research, 23(6), pp. 1390-1398.

[131] Chan, D. D., Toribio, D., and Neu, C. P., 2012, "Displacement smoothing for the precise MRI-based measurement of strain in soft biological tissues," Comput Methods Biomech Biomed Engin.

[132] Ohlendorf, C., Tomford, W. W., and Mankin, H. J., 1996, "Chondrocyte survival in cryopreserved osteochondral articular cartilage," J Orthop Res, 14(3), pp. 413-416.

[133] Ward, C. W., Prosser, B. L., and Lederer, W. J., 2013, "Mechanical stretch induced activation of ROS/RNS signaling in striated muscle," Antioxid Redox Signal.

[134] Ko, F. C., Dragomir, C., Plumb, D. A., Goldring, S. R., Wright, T. M., Goldring, M. B., and van der Meulen, M. C., 2013, "In vivo cyclic compression causes cartilage degeneration and subchondral bone changes in mouse tibiae," Arthritis and rheumatism, 65(6), pp. 1569-1578.

[135] Grygorczyk, R., Furuya, K., and Sokabe, M., 2013, "Imaging and characterization of stretch-induced ATP release from alveolar A549 cells," J Physiol, 591(Pt 5), pp. 1195-1215.

[136] Niehoff, A., Muller, M., Bruggemann, L., Savage, T., Zaucke, F., Eckstein, F., Muller-Lung, U., and Bruggemann, G. P., 2011, "Deformational behaviour of knee cartilage and changes in serum cartilage oligomeric matrix protein (COMP) after running and drop landing," Osteoarthritis and cartilage / OARS, Osteoarthritis Research Society, 19(8), pp. 1003-1010.

[137] Coleman, J. L., Widmyer, M. R., Leddy, H. A., Utturkar, G. M., Spritzer, C. E., Moorman, C. T., 3rd, Guilak, F., and DeFrate, L. E., 2013, "Diurnal variations in articular cartilage thickness and strain in the human knee," Journal of biomechanics, 46(3), pp. 541-547.

[138] Haudenschild, D. R., D'Lima, D. D., and Lotz, M. K., 2008, "Dynamic compression of chondrocytes induces a Rho kinase-dependent reorganization of the actin cytoskeleton," Biorheology, 45(3-4), pp. 219-228.

[139] Adatia, A., Rainsford, K. D., and Kean, W. F., 2012, "Osteoarthritis of the knee and hip. Part I: aetiology and pathogenesis as a basis for pharmacotherapy," The Journal of pharmacy and pharmacology, 64(5), pp. 617-625.

[140] Holledge, M. M., Millward-Sadler, S. J., Nuki, G., and Salter, D. M., 2008, "Mechanical regulation of proteoglycan synthesis in normal and osteoarthritic human articular chondrocytes--roles for alpha5 and alphaVbeta5 integrins," Biorheology, 45(3-4), pp. 275-288.

[141] Fogh, J., 1986, "Human tumor lines for cancer research," Cancer investigation, 4(2), pp. 157-184.

[142] Mansfield, J., Yu, J., Attenburrow, D., Moger, J., Tirlapur, U., Urban, J., Cui, Z., and Winlove, P., 2009, "The elastin network: its relationship with collagen and cells in articular cartilage as visualized by multiphoton microscopy," Journal of anatomy, 215(6), pp. 682-691.

[143] Hansen, U., Allen, J. M., White, R., Moscibrocki, C., Bruckner, P., Bateman, J. F., and Fitzgerald, J., 2012, "WARP interacts with collagen VI-containing microfibrils in the pericellular matrix of human chondrocytes," PloS one, 7(12), p. e52793.

[144] Macdonald, D. W., Squires, R. S., Avery, S. A., Adams, J., Baker, M., Cunningham, C. R., Heimann, N. B., Kooyman, D. L., and Seegmiller, R. E., 2013, "Structural variations in articular cartilage matrix are associated with early-onset osteoarthritis in the spondyloepiphyseal dysplasia congenita (sedc) mouse," International journal of molecular sciences, 14(8), pp. 16515-16531.

[145] Knight, M. M., Toyoda, T., Lee, D. A., and Bader, D. L., 2006, "Mechanical compression and hydrostatic pressure induce reversible changes in actin cytoskeletal organisation in chondrocytes in agarose," Journal of biomechanics, 39(8).

[146] Campbell, J. J., Blain, E. J., Chowdhury, T. T., and Knight, M. M., 2007, "Loading alters actin dynamics and up-regulates cofilin gene expression in chondrocytes," Biochem Biophys Res Commun, 361(2), pp. 329-334.

[147] Chen, J., Irianto, J., Inamdar, S., Pravincumar, P., Lee, D. A., Bader, D. L., and Knight, M. M., 2012, "Cell mechanics, structure, and function are regulated by the stiffness of the three-dimensional microenvironment," Biophys J, 103(6), pp. 1188-1197.

[148] Nishida, T., Kubota, S., Aoyama, E., and Takigawa, M., 2013, "Impaired glycolytic metabolism causes chondrocyte hypertrophy-like changes via promotion of phospho-Smad1/5/8 translocation into nucleus," Osteoarthritis and cartilage / OARS, Osteoarthritis Research Society, 21(5), pp. 700-709.

[149] O'Neill, L. A., and Hardie, D. G., 2013, "Metabolism of inflammation limited by AMPK and pseudo-starvation," Nature, 493(7432), pp. 346-355.

[150] Petursson, F., Husa, M., June, R., Lotz, M., Terkeltaub, R., and Liu-Bryan, R., 2013, "Linked decreases in liver kinase B1 and AMP-activated protein kinase activity modulate matrix catabolic responses to biomechanical injury in chondrocytes," Arthritis Res Ther, 15(4), p. R77.

[151] Zignego, D. L., Jutila, A. A., Gelbke, M. K., Gannon, D. M., and June, R. K., 2013, "The mechanical microenvironment of high concentration agarose for applying deformation to primary chondrocytes," Journal of biomechanics, In Press.

[152] Darling, E. M., Zauscher, S., and Guilak, F., 2006, "Viscoelastic properties of zonal articular chondrocytes measured by atomic force microscopy," Osteoarthritis and cartilage / OARS, Osteoarthritis Research Society, 14(6), pp. 571-579.

[153] Umberger, B. R., and Martin, P. E., 2007, "Mechanical power and efficiency of level walking with different stride rates," J Exp Biol, 210(Pt 18), pp. 3255-3265.

[154] Munger, J., Bennett, B. D., Parikh, A., Feng, X. J., McArdle, J., Rabitz, H. A., Shenk, T., and Rabinowitz, J. D., 2008, "Systems-level metabolic flux profiling identifies fatty acid synthesis as a target for antiviral therapy," Nature biotechnology, 26(10), pp. 1179-1186.

[155] Heinemann, J., Hamerly, T., Maaty, W. S., Movahed, N., Steffens, J. D., Reeves, B. D., Hilmer, J. K., Therien, J., Grieco, P. A., Peters, J. W., and Bothner, B., 2013, "Expanding the paradigm of thiol redox in the thermophilic root of life," Biochim Biophys Acta.

[156] Ortmann, A. C., Brumfield, S. K., Walther, J., McInnerney, K., Brouns, S. J., van de Werken, H. J., Bothner, B., Douglas, T., van de Oost, J., and Young, M. J., 2008, "Transcriptome analysis of infection of the archaeon Sulfolobus solfataricus with Sulfolobus turreted icosahedral virus," J Virol, 82(10), pp. 4874-4883.

[157] Secor, P. R., Jennings, L. K., James, G. A., Kirker, K. R., Pulcini, E. D., McInnerney, K., Gerlach, R., Livinghouse, T., Hilmer, J. K., Bothner, B., Fleckman, P., Olerud, J. E., and Stewart, P. S., 2012, "Phevalin (aureusimine B) production by Staphylococcus aureus biofilm and impacts on human keratinocyte gene expression," PLoS One, 7(7), p. e40973.

[158] Pluskal, T., Castillo, S., Villar-Briones, A., and Oresic, M., 2010, "MZmine 2: modular framework for processing, visualizing, and analyzing mass spectrometry-based molecular profile data," BMC Bioinformatics, 11, p. 395.

[159] Katajamaa, M., and Oresic, M., 2005, "Processing methods for differential analysis of LC/MS profile data," BMC Bioinformatics, 6, p. 179.

[160] Benjamini, Y., Drai, D., Elmer, G., Kafkafi, N., and Golani, I., 2001, "Controlling the false discovery rate in behavior genetics research," Behav Brain Res, 125(1-2), pp. 279-284.

[161] Team, R. C., 2013, "R: A language and environment for statistical computing.," R Foundation for Statistical Computing, Vienna, Austria.

[162] Wishart, D. S., Jewison, T., Guo, A. C., Wilson, M., Knox, C., Liu, Y., Djoumbou, Y., Mandal, R., Aziat, F., Dong, E., Bouatra, S., Sinelnikov, I., Arndt, D., Xia, J., Liu, P., Yallou, F., Bjorndahl, T., Perez-Pineiro, R., Eisner, R., Allen, F., Neveu, V., Greiner, R., and Scalbert, A., 2013, "HMDB 3.0--The Human Metabolome Database in 2013," Nucleic acids research, 41(Database issue), pp. D801-807.

[163] Zhu, Z. J., Schultz, A. W., Wang, J., Johnson, C. H., Yannone, S. M., Patti, G. J., and Siuzdak, G., 2013, "Liquid chromatography quadrupole time-of-flight mass spectrometry characterization of metabolites guided by the METLIN database," Nature protocols, 8(3), pp. 451-460.

[164] Fahy, E., Subramaniam, S., Murphy, R. C., Nishijima, M., Raetz, C. R., Shimizu, T., Spener, F., van Meer, G., Wakelam, M. J., and Dennis, E. A., 2009, "Update of the LIPID MAPS comprehensive classification system for lipids," Journal of lipid research, 50 Suppl, pp. S9-14.

[165] Kind, T., and Fiehn, O., 2007, "Seven Golden Rules for heuristic filtering of molecular formulas obtained by accurate mass spectrometry," BMC Bioinformatics, 8, p. 105.

[166] Kanehisa, M., 2013, "Molecular network analysis of diseases and drugs in KEGG," Methods in molecular biology, 939, pp. 263-275.

[167] Schmitt, C., Gouya, L., Malonova, E., Lamoril, J., Camadro, J. M., Flamme, M., Rose, C., Lyoumi, S., Da Silva, V., Boileau, C., Grandchamp, B., Beaumont, C., Deybach, J. C., and Puy, H., 2005, "Mutations in human CPO gene predict clinical expression of either hepatic hereditary coproporphyria or erythropoietic harderoporphyria," Human molecular genetics, 14(20), pp. 3089-3098.

[168] Rajpurohit, R., Koch, C. J., Tao, Z., Teixeira, C. M., and Shapiro, I. M., 1996, "Adaptation of chondrocytes to low oxygen tension: relationship between hypoxia and cellular metabolism," Journal of cellular physiology, 168(2), pp. 424-432.

[169] Wang, W., Mazurkewich, S., Kimber, M. S., and Seah, S. Y., 2010, "Structural and kinetic characterization of 4-hydroxy-4-methyl-2-oxoglutarate/4-carboxy-4-hydroxy-2-oxoadipate aldolase, a protocatechuate degradation enzyme evolutionarily convergent with the HpaI and DmpG pyruvate aldolases," The Journal of biological chemistry, 285(47), pp. 36608-36615.

[170] Haudenschild, D. R., Chen, J., Pang, N., Lotz, M. K., and D'Lima, D. D., 2010, "Rho kinase-dependent activation of SOX9 in chondrocytes," Arthritis Rheum, 62(1), pp. 191-200.

[171] Grodzinsky, A. J., Lipshitz, H., and Glimcher, M. J., 1978, "Electromechanical properties of articular cartilage during compression and stress relaxation," Nature, 275(5679), pp. 448-450.

[172] Mow, V. C., Kuei, S. C., Lai, W. M., and Armstrong, C. G., 1980, "Biphasic creep and stress relaxation of articular cartilage in compression? Theory and experiments," Journal of biomechanical engineering, 102(1), pp. 73-84.

[173] Ruiz-Romero, C., Carreira, V., Rego, I., Remeseiro, S., López-Armada, M. J., and Blanco, F. J., 2008, "Proteomic analysis of human osteoarthritic chondrocytes reveals protein changes in stress and glycolysis," Proteomics, 8(3), pp. 495-507.

[174] Bougault, C., Aubert-Foucher, E., Paumier, A., Perrier-Groult, E., Huot, L., Hot, D., Duterque-Coquillaud, M., and Mallein-Gerin, F., 2012, "Dynamic compression of chondrocyte-agarose constructs reveals new candidate mechanosensitive genes," PloS one, 7(5), p. e36964.

[175] Buschmann, M. D., Gluzband, Y. A., Grodzinsky, A. J., and Hunziker, E. B., 1995, "Mechanical compression modulates matrix biosynthesis in chondrocyte/agarose culture," J Cell Sci, 108 (Pt 4), pp. 1497-1508.

[176] Haudenschild, D. R., Chen, J., Pang, N., Lotz, M. K., and D'Lima, D. D., 2010, "Rho Kinase-Dependent Activation of SOX9 in Chondrocytes," Arthritis and rheumatism, 62(1).

[177] Fitzgerald, J. B., Jin, M., Chai, D. H., Siparsky, P., Fanning, P., and Grodzinsky, A. J., 2008, "Shear- and compression-induced chondrocyte transcription requires MAPK activation in cartilage explants," Journal of Biological Chemistry, 283(11).

[178] Lehtinen, M. K., Yuan, Z., Boag, P. R., Yang, Y., Villen, J., Becker, E. B., DiBacco, S., de la Iglesia, N., Gygi, S., Blackwell, T. K., and Bonni, A., 2006, "A conserved MST-FOXO signaling pathway mediates oxidative-stress responses and extends life span," Cell, 125(5), pp. 987-1001.

[179] Zhang, W., Likhodii, S., Zhang, Y., Aref-Eshghi, E., Harper, P. E., Randell, E., Green, R., Martin, G., Furey, A., Sun, G., Rahman, P., and Zhai, G., 2014, "Classification of osteoarthritis phenotypes by metabolomics analysis," BMJ Open, 4(11), p. e006286.

[180] Mickiewicz, B., Heard, B. J., Chau, J. K., Chung, M., Hart, D. A., Shrive, N. G., Frank, C. B., and Vogel, H. J., 2015, "Metabolic profiling of synovial fluid in a unilateral ovine model of anterior cruciate ligament reconstruction of the knee suggests biomarkers for early osteoarthritis," Journal of orthopaedic research : official publication of the Orthopaedic Research Society, 33(1), pp. 71-77.

[181] Attur, M., Dave, M., Abramson, S. B., and Amin, A., 2012, "Activation of diverse eicosanoid pathways in osteoarthritic cartilage: a lipidomic and genomic analysis," Bull NYU Hosp Jt Dis, 70(2), pp. 99-108.

[182] Mickiewicz, B., Kelly, J. J., Ludwig, T. E., Weljie, A. M., Wiley, J. P., Schmidt, T. A., and Vogel, H. J., 2015, "Metabolic analysis of knee synovial fluid as a potential diagnostic approach for osteoarthritis," Journal of orthopaedic research : official publication of the Orthopaedic Research Society.

[183] Cavill, R., Kamburov, A., Ellis, J. K., Athersuch, T. J., Blagrove, M. S., Herwig, R., Ebbels, T. M., and Keun, H. C., 2011, "Consensus-phenotype integration of transcriptomic and metabolomic data implies a role for metabolism in the chemosensitivity of tumour cells," PLoS Comput Biol, 7(3), p. e1001113.

[184] Oh, C. D., and Chun, J. S., 2003, "Signaling mechanisms leading to the regulation of differentiation and apoptosis of articular chondrocytes by insulin-like growth factor-1," J Biol Chem, 278(38), pp. 36563-36571.

[185] Priore, R., Dailey, L., and Basilico, C., 2006, "Downregulation of Akt activity contributes to the growth arrest induced by FGF in chondrocytes," Journal of cellular physiology, 207(3), pp. 800-808.

[186] Starkman, B. G., Cravero, J. D., Delcarlo, M., and Loeser, R. F., 2005, "IGF-I stimulation of proteoglycan synthesis by chondrocytes requires activation of the PI 3-kinase pathway but not ERK MAPK," The Biochemical journal, 389(Pt 3), pp. 723-729.

[187] O'Conor, C. J., Leddy, H. A., Benefield, H. C., Liedtke, W. B., and Guilak, F., 2014, "TRPV4-mediated mechanotransduction regulates the metabolic response of chondrocytes to dynamic loading," Proc Natl Acad Sci U S A, 111(4), pp. 1316-1321.

[188] Knight, M. M., Roberts, S. R., Lee, D. A., and Bader, D. L., 2003, "Live cell imaging using confocal microscopy induces intracellular calcium transients and cell death," Am J Physiol Cell Physiol, 284(4), pp. C1083-1089.

[189] Lakshmi, A. V., 1998, "Riboflavin metabolism--relevance to human nutrition," Indian J Med Res, 108, pp. 182-190.

[190] Terkeltaub, R., Yang, B., Lotz, M., and Liu-Bryan, R., 2011, "Chondrocyte AMP-activated protein kinase activity suppresses matrix degradation responses to proinflammatory cytokines interleukin-1beta and tumor necrosis factor alpha," Arthritis and rheumatism, 63(7), pp. 1928-1937.

[191] Anishkin, A., Loukin, S. H., Teng, J., and Kung, C., 2014, "Feeling the hidden mechanical forces in lipid bilayer is an original sense," Proc Natl Acad Sci U S A, 111(22), pp. 7898-7905.

[192] Stephanopoulos, G. N., Aristidou, A. A., and Nielsen, J., 1998, Metabolic Engineering: Principles and Methodologies, Academic Press.

[193] Adams, S. B., Jr., Setton, L. A., Kensicki, E., Bolognesi, M. P., Toth, A. P., and Nettles, D. L., 2012, "Global metabolic profiling of human osteoarthritic synovium," Osteoarthritis and cartilage / OARS, Osteoarthritis Research Society, 20(1), pp. 64-67.

[194] Melas, I. N., Chairakaki, A. D., Chatzopoulou, E. I., Messinis, D. E., Katopodi, T., Pliaka, V., Samara, S., Mitsos, A., Dailiana, Z., Kollia, P., and Alexopoulos, L. G., 2014, "Modeling of signaling pathways in chondrocytes based on phosphoproteomic and cytokine release data," Osteoarthritis Cartilage, 22(3), pp. 509-518.

[195] Sah, R. L. Y., Kim, Y. J., Doong, J. Y. H., Grodzinsky, A. J., Plaas, A. H. K., and Sandy, J. D., 1989, "BIOSYNTHETIC RESPONSE OF CARTILAGE EXPLANTS TO DYNAMIC COMPRESSION," Journal of Orthopaedic Research, 7(5), pp. 619-636.

[196] Jones, I. L., Klämfeldt, A., and Sandström, T., 1982, "The effect of continuous mechanical pressure upon the turnover of articular cartilage proteoglycans in vitro," Clin Orthop Relat Res(165), pp. 283-289.

[197] Hayashi, S., Nishiyama, T., Miura, Y., Fujishiro, T., Kanzaki, N., Hashimoto, S., Matsumoto, T., Kurosaka, M., and Kuroda, R., 2011, "DcR3 induces cell proliferation through MAPK signaling in chondrocytes of osteoarthritis," Osteoarthritis Cartilage, 19(7), pp. 903-910.

[198] Nishihara, A., Fujii, M., Sampath, T. K., Miyazono, K., and Reddi, A. H., 2003, "Bone morphogenetic protein signaling in articular chondrocyte differentiation," Biochem Biophys Res Commun, 301(2), pp. 617-622.

[199] Koshy, P. J., Lundy, C. J., Rowan, A. D., Porter, S., Edwards, D. R., Hogan, A., Clark, I. M., and Cawston, T. E., 2002, "The modulation of matrix metalloproteinase and ADAM gene expression in human chondrocytes by interleukin-1 and oncostatin M: a time-course study using real-time quantitative reverse transcription-polymerase chain reaction," Arthritis Rheum, 46(4), pp. 961-967.

[200] Notoya, K., Jovanovic, D. V., Reboul, P., Martel-Pelletier, J., Mineau, F., and Pelletier, J. P., 2000, "The induction of cell death in human osteoarthritis chondrocytes by nitric oxide is related to the production of prostaglandin E2 via the induction of cyclooxygenase-2," J Immunol, 165(6), pp. 3402-3410.

[201] Lourido, L., Calamia, V., Mateos, J., Fernández-Puente, P., Fernández-Tajes, J., Blanco, F. J., and Ruiz-Romero, C., 2014, "Quantitative proteomic profiling of human articular cartilage degradation in osteoarthritis," J Proteome Res, 13(12), pp. 6096-6106.

[202] Mateos, J., Lourido, L., Fernández-Puente, P., Calamia, V., Fernández-López, C., Oreiro, N., Ruiz-Romero, C., and Blanco, F. J., 2012, "Differential protein profiling of synovial fluid from rheumatoid arthritis and osteoarthritis patients using LC-MALDI TOF/TOF," J Proteomics, 75(10), pp. 2869-2878.

[203] Liao, H., Wu, J., Kuhn, E., Chin, W., Chang, B., Jones, M. D., O'Neil, S., Clauser, K. R., Karl, J., Hasler, F., Roubenoff, R., Zolg, W., and Guild, B. C., 2004, "Use of mass spectrometry to identify protein biomarkers of disease severity in the synovial fluid and serum of patients with rheumatoid arthritis," Arthritis Rheum, 50(12), pp. 3792-3803.

[204] Fernández-Costa, C., Calamia, V., Fernández-Puente, P., Capelo-Martínez, J. L., Ruiz-Romero, C., and Blanco, F. J., 2012, "Sequential depletion of human serum for the search of osteoarthritis biomarkers," Proteome Sci, 10(1), p. 55.

[205] Fernández-Puente, P., Mateos, J., Fernández-Costa, C., Oreiro, N., Fernández-López, C., Ruiz-Romero, C., and Blanco, F. J., 2011, "Identification of a panel of novel serum osteoarthritis biomarkers," J Proteome Res, 10(11), pp. 5095-5101.

[206] Zignego, D. L., Hilmer, J. K., Minor, C. A., Gelbke, M. K., and June, R. K., 2015, "Candidate Mediators of Osteoarthritic Human Chondrocyte Mechanotransduction via Targeted and Untargeted Metabolomic Measurements," Osteoarthritis and Cartilage. In review.

[207] Darling, E. M., Wilusz, R. E., Bolognesi, M. P., Zauscher, S., and Guilak, F., 2010, "Spatial Mapping of the Biomechanical Properties of the Pericellular Matrix of Articular Cartilage Measured In Situ via Atomic Force Microscopy," Biophysical Journal, 98(12), pp. 2848-2856.

[208] Ikeda, D., Ageta, H., Tsuchida, K., and Yamada, H., 2013, "iTRAQ-based proteomics reveals novel biomarkers of osteoarthritis," Biomarkers, 18(7), pp. 565-572.

[209] Kessner, D., Chambers, M., Burke, R., Agus, D., and Mallick, P., 2008, "ProteoWizard: open source software for rapid proteomics tools development," Bioinformatics, 24(21), pp. 2534-2536.

[210] Kenar, E., Franken, H., Forcisi, S., Wörmann, K., Häring, H. U., Lehmann, R., Schmitt-Kopplin, P., Zell, A., and Kohlbacher, O., 2014, "Automated label-free quantification of metabolites from liquid chromatography-mass spectrometry data," Mol Cell Proteomics, 13(1), pp. 348-359.

[211] Moore, R. E., Young, M. K., and Lee, T. D., 2002, "Qscore: an algorithm for evaluating SEQUEST database search results," J Am Soc Mass Spectrom, 13(4), pp. 378-386.

[212] Käll, L., Storey, J. D., MacCoss, M. J., and Noble, W. S., 2008, "Assigning significance to peptides identified by tandem mass spectrometry using decoy databases," J Proteome Res, 7(1), pp. 29-34.

[213] Kamburov, A., Cavill, R., Ebbels, T. M., Herwig, R., and Keun, H. C., 2011, "Integrated pathway-level analysis of transcriptomics and metabolomics data with IMPaLA," Bioinformatics, 27(20), pp. 2917-2918.

[214] Bennett, V., and Baines, A. J., 2001, "Spectrin and ankyrin-based pathways: metazoan inventions for integrating cells into tissues," Physiol Rev, 81(3), pp. 1353-1392.

[215] Knudson, W., and Loeser, R. F., 2002, "CD44 and integrin matrix receptors participate in cartilage homeostasis," Cell Mol Life Sci, 59(1), pp. 36-44.

[216] Daniels, K., and Solursh, M., 1991, "Modulation of chondrogenesis by the cytoskeleton and extracellular matrix," J Cell Sci, 100 (Pt 2), pp. 249-254.

[217] Haudenschild, D. R., Chen, J., Steklov, N., Lotz, M. K., and D'Lima, D. D., 2009, "Characterization of the chondrocyte actin cytoskeleton in living three-dimensional culture: response to anabolic and catabolic stimuli," Mol Cell Biomech, 6(3), pp. 135-144.

[218] Knight, M. M., Toyoda, T., Lee, D. A., and Bader, D. L., 2006, "Mechanical compression and hydrostatic pressure induce reversible changes in actin cytoskeletal organisation in chondrocytes in agarose," J Biomech, 39(8), pp. 1547-1551.

[219] Pickart, C. M., and Eddins, M. J., 2004, "Ubiquitin: structures, functions, mechanisms," Biochim Biophys Acta, 1695(1-3), pp. 55-72.

[220] Bai, X. H., Wang, D. W., Luan, Y., Yu, X. P., and Liu, C. J., 2009, "Regulation of chondrocyte differentiation by ADAMTS-12 metalloproteinase depends on its enzymatic activity," Cell Mol Life Sci, 66(4), pp. 667-680.

[221] Stanton, H., Rogerson, F. M., East, C. J., Golub, S. B., Lawlor, K. E., Meeker, C. T., Little, C. B., Last, K., Farmer, P. J., Campbell, I. K., Fourie, A. M., and Fosang, A. J., 2005, "ADAMTS5 is the major aggrecanase in mouse cartilage in vivo and in vitro," Nature, 434(7033), pp. 648-652.

[222] Glasson, S. S., Askew, R., Sheppard, B., Carito, B., Blanchet, T., Ma, H. L., Flannery, C. R., Peluso, D., Kanki, K., Yang, Z., Majumdar, M. K., and Morris, E. A., 2005, "Deletion of active ADAMTS5 prevents cartilage degradation in a murine model of osteoarthritis," Nature, 434(7033), pp. 644-648.

[223] Blain, E. J., Gilbert, S. J., Hayes, A. J., and Duance, V. C., 2006, "Disassembly of the vimentin cytoskeleton disrupts articular cartilage chondrocyte homeostasis," Matrix Biol, 25(7), pp. 398-408.

[224] Hellingman, C. A., Davidson, E. N., Koevoet, W., Vitters, E. L., van den Berg, W. B., van Osch, G. J., and van der Kraan, P. M., 2011, "Smad signaling determines chondrogenic differentiation of bone-marrow-derived mesenchymal stem cells: inhibition of Smad1/5/8P prevents terminal differentiation and calcification," Tissue Eng Part A, 17(7-8), pp. 1157-1167.

[225] Li, T. F., O'Keefe, R. J., and Chen, D., 2005, "TGF-beta signaling in chondrocytes," Front Biosci, 10, pp. 681-688.

[226] Brodsky, B., and Persikov, A. V., 2005, "Molecular structure of the collagen triple helix," Adv Protein Chem, 70, pp. 301-339.

[227] Rubin, L. L., and de Sauvage, F. J., 2006, "Targeting the Hedgehog pathway in cancer," Nat Rev Drug Discov, 5(12), pp. 1026-1033.

[228] Lin, L., Shen, Q., Xue, T., Duan, X., Fu, X., and Yu, C., 2014, "Sonic hedgehog improves redifferentiation of dedifferentiated chondrocytes for articular cartilage repair," PLoS One, 9(2), p. e88550.

[229] Aigner, T., Zhu, Y., Chansky, H. H., Matsen, F. A., Maloney, W. J., and Sandell, L. J., 1999, "Reexpression of type IIA procollagen by adult articular chondrocytes in osteoarthritic cartilage," Arthritis Rheum, 42(7), pp. 1443-1450.

[230] Ridley, A. J., 2001, "Rho family proteins: coordinating cell responses," Trends Cell Biol, 11(12), pp. 471-477.

[231] Aguiar, D. J., Knudson, W., and Knudson, C. B., 1999, "Internalization of the hyaluronan receptor CD44 by chondrocytes," Exp Cell Res, 252(2), pp. 292-302.

[232] Kolch, W., 2000, "Meaningful relationships: the regulation of the Ras/Raf/MEK/ERK pathway by protein interactions," Biochem J, 351 Pt 2, pp. 289-305.

[233] Kamekura, S., Hoshi, K., Shimoaka, T., Chung, U., Chikuda, H., Yamada, T., Uchida, M., Ogata, N., Seichi, A., Nakamura, K., and Kawaguchi, H., 2005, "Osteoarthritis development in novel experimental mouse models induced by knee joint instability," Osteoarthritis and cartilage / OARS, Osteoarthritis Research Society, 13(7), pp. 632-641.

[234] van Lent, P. L., Blom, A. B., Schelbergen, R. F., Sloetjes, A., Lafeber, F. P., Lems, W. F., Cats, H., Vogl, T., Roth, J., and van den Berg, W. B., 2012, "Active involvement of alarmins S100A8 and S100A9 in the regulation of synovial activation and joint destruction during mouse and human osteoarthritis," Arthritis Rheum, 64(5), pp. 1466-1476.

[235] Mahr, S., Menard, J., Krenn, V., and Muller, B., 2003, "Sexual dimorphism in the osteoarthritis of STR/ort mice may be linked to articular cytokines," Ann Rheum Dis, 62(12), pp. 1234-1237.

[236] Bomsta, B. D., Bridgewater, L. C., and Seegmiller, R. E., 2006, "Premature osteoarthritis in the Disproportionate micromelia (Dmm) mouse," Osteoarthritis Cartilage, 14(5), pp. 477-485.

[237] Glasson, S. S., Chambers, M. G., Van Den Berg, W. B., and Little, C. B., 2010, "The OARSI histopathology initiative - recommendations for histological assessments of osteoarthritis in the mouse," Osteoarthritis and cartilage / OARS, Osteoarthritis Research Society, 18 Suppl 3, pp. S17-23.

[238] Mailhiot, S., Zignego, D., Prigge, J., Wardwell, E., Schmidt, E., and June, R., 2015, "Non-invasive quantification of cartilage using a novel in vivo bioluminescent reporter mouse,"PLOS ONE.

[239] Kim, B. J., Kim, D. W., Kim, S. H., Cho, J. H., Lee, H. J., Park, D. Y., Park, S. R., Choi, B. H., and Min, B. H., 2013, "Establishment of a reliable and reproducible murine osteoarthritis model," Osteoarthritis and cartilage / OARS, Osteoarthritis Research Society, 21(12), pp. 2013-2020.

[240] Little, C. B., and Zaki, S., 2012, "What constitutes an "animal model of osteoarthritis"--the need for consensus?," Osteoarthritis and cartilage / OARS, Osteoarthritis Research Society, 20(4), pp. 261-267.

[241] Bendele, A. M., 2001, "Animal models of osteoarthritis," J Musculoskelet Neuronal Interact, 1(4), pp. 363-376.

[242] Bendele, A. M., Bendele, R. A., Hulman, J. F., and Swann, B. P., 1996, "[Beneficial effects of treatment with diacerhein in guinea pigs with osteoarthritis]," Rev Prat, 46(6 Spec No), pp. S35-S39.

[243] Smith, G. N., Myers, S. L., Brandt, K. D., Mickler, E. A., and Albrecht, M. E., 1999, "Diacerhein treatment reduces the severity of osteoarthritis in the canine cruciate-deficiency model of osteoarthritis," Arthritis and rheumatism, 42(3), pp. 545-554.

[244] Kobayashi, K., Amiel, M., Harwood, F. L., Healey, R. M., Sonoda, M., Moriya, H., and Amiel, D., 2000, "The long-term effects of hyaluronan during development of osteoarthritis following partial meniscectomy in a rabbit model," Osteoarthritis and cartilage / OARS, Osteoarthritis Research Society, 8(5), pp. 359-365.

[245] Sanchez-Adams, J., Leddy, H. A., McNulty, A. L., O'Conor, C. J., and Guilak, F., 2014, "The mechanobiology of articular cartilage: bearing the burden of osteoarthritis," Curr Rheumatol Rep, 16(10), p. 451.

[246] Kuroki, K., Cook, C. R., and Cook, J. L., 2011, "Subchondral bone changes in three different canine models of osteoarthritis," Osteoarthritis and cartilage / OARS, Osteoarthritis Research Society, 19(9), pp. 1142-1149.

[247] Little, C. B., Barai, A., Burkhardt, D., Smith, S. M., Fosang, A. J., Werb, Z., Shah, M., and Thompson, E. W., 2009, "Matrix metalloproteinase 13-deficient mice are resistant to osteoarthritic cartilage erosion but not chondrocyte hypertrophy or osteophyte development," Arthritis and rheumatism, 60(12), pp. 3723-3733.

[248] Clark, A. L., Votta, B. J., Kumar, S., Liedtke, W., and Guilak, F., 2010, "Chondroprotective role of the osmotically sensitive ion channel transient receptor potential vanilloid 4: age- and sex-dependent progression of osteoarthritis in Trpv4-deficient mice," Arthritis and rheumatism, 62(10), pp. 2973-2983.

[249] van Osch, G. J., van der Kraan, P. M., and van den Berg, W. B., 1994, "Site-specific cartilage changes in murine degenerative knee joint disease induced by iodoacetate and collagenase," Journal of orthopaedic research : official publication of the Orthopaedic Research Society, 12(2), pp. 168-175.

[250] van der Kraan, P. M., Vitters, E. L., van Beuningen, H. M., van de Putte, L. B., and van den Berg, W. B., 1990, "Degenerative knee joint lesions in mice after a single intra-articular collagenase injection. A new model of osteoarthritis," Journal of experimental pathology, 71(1), pp. 19-31.

[251] Christiansen, B. A., Anderson, M. J., Lee, C. A., Williams, J. C., Yik, J. H., and Haudenschild, D. R., 2012, "Musculoskeletal changes following non-invasive knee injury using a novel mouse model of post-traumatic osteoarthritis," Osteoarthritis and cartilage / OARS, Osteoarthritis Research Society, 20(7), pp. 773-782.

[252] Pritzker, K. P., Gay, S., Jimenez, S. A., Ostergaard, K., Pelletier, J. P., Revell, P. A., Salter, D., and van den Berg, W. B., 2006, "Osteoarthritis cartilage histopathology: grading and staging," Osteoarthritis and cartilage / OARS, Osteoarthritis Research Society, 14(1), pp. 13-29.

[253] Palmer, A. W., Guldberg, R. E., and Levenston, M. E., 2006, "Analysis of cartilage matrix fixed charge density and three-dimensional morphology via contrast-enhanced microcomputed tomography," Proceedings of the National Academy of Sciences of the United States of America, 103(51), pp. 19255-19260.

[254] Siebelt, M., Waarsing, J. H., Kops, N., Piscaer, T. M., Verhaar, J. A., Oei, E. H., and Weinans, H., 2011, "Quantifying osteoarthritic cartilage changes accurately using in vivo microCT arthrography in three etiologically distinct rat models," Journal of orthopaedic research : official publication of the Orthopaedic Research Society, 29(11), pp. 1788-1794.

[255] Ruan, M. Z., Dawson, B., Jiang, M. M., Gannon, F., Heggeness, M., and Lee, B. H., 2013, "Quantitative imaging of murine osteoarthritic cartilage by phase-contrast micro-computed tomography," Arthritis and rheumatism, 65(2), pp. 388-396.

[256] Mailhiot, S. E., Zignego, D. L., Prigge, J. R., Wardwell, E. R., Schmidt, E. E., and June, R. K., 2015, "Non-invasive quantification of cartilage using a novel in vivo bioluminescent reporter mouse," PLoS One, In Press.

[257] Kotwal, N., Li, J., Sandy, J., Plaas, A., and Sumner, D. R., 2012, "Initial application of EPIC-muCT to assess mouse articular cartilage morphology and composition: effects of aging and treadmill running," Osteoarthritis and cartilage / OARS, Osteoarthritis Research Society, 20(8), pp. 887-895.

[258] Ushiku, C., Adams, D. J., Jiang, X., Wang, L., and Rowe, D. W., 2010, "Long bone fracture repair in mice harboring GFP reporters for cells within the osteoblastic lineage," Journal of orthopaedic research : official publication of the Orthopaedic Research Society, 28(10), pp. 1338-1347.

[259] Benjamini, Y., and Yekutieli, D., 2001, "The control of the false discovery rate in multiple testing under dependency," Ann Stat, 29(4), pp. 1165-1188.

[260] de Wet, J. R., Wood, K. V., DeLuca, M., Helinski, D. R., and Subramani, S., 1987, "Firefly luciferase gene: structure and expression in mammalian cells," Mol Cell Biol, 7(2), pp. 725-737.

[261] DeLuca, M., and McElroy, W. D., 1984, "Two kinetically distinguishable ATP sites in firefly luciferase," Biochem Biophys Res Commun, 123(2), pp. 764-770.

[262] Buschmann, M. D., Kim, Y. J., Wong, M., Frank, E., Hunziker, E. B., and Grodzinsky, A. J., 1999, "Stimulation of aggrecan synthesis in cartilage explants by cyclic loading is localized to regions of high interstitial fluid flow," Archives of Biochemistry and Biophysics, 366(1), pp. 1-7.

[263] Haudenschild, D. R., Chen, J., Pang, N., Lotz, M. K., and D'Lima, D. D., 2010, "Rho Kinase-Dependent Activation of SOX9 in Chondrocytes," Arthritis and Rheumatism, 62(1).

[264] Smith, R. J., and Phang, J. M., 1978, "Proline metabolism in cartilage: the importance of proline biosynthesis," Metabolism, 27(6), pp. 685-694.

[265] Harris, M. D., Anderson, A. E., Henak, C. R., Ellis, B. J., Peters, C. L., and Weiss, J. A., 2012, "Finite element prediction of cartilage contact stresses in normal human hips," J Orthop Res, 30(7), pp. 1133-1139.

[266] Alexopoulos, L. G., Haider, M. A., Vail, T. P., and Guilak, F., 2003, "Alterations in the mechanical properties of the human chondrocyte pericellular matrix with osteoarthritis," J Biomech Eng, 125(3), pp. 323-333.

[267] Wilusz, R. E., Defrate, L. E., and Guilak, F., 2012, "A biomechanical role for perlecan in the pericellular matrix of articular cartilage," Matrix Biol, 31(6), pp. 320-327.

[268] Engler, A. J., Sen, S., Sweeney, H. L., and Discher, D. E., 2006, "Matrix elasticity directs stem cell lineage specification," Cell, 126(4), pp. 677-689.

[269] Eisenberg, J. L., Safi, A., Wei, X., Espinosa, H. D., Budinger, G. S., Takawira, D., Hopkinson, S. B., and Jones, J. C., 2011, "Substrate stiffness regulates extracellular matrix deposition by alveolar epithelial cells," Research and reports in biology, 2011(2), pp. 1-12.

[270] Yeh, Y. T., Hur, S. S., Chang, J., Wang, K. C., Chiu, J. J., Li, Y. S., and Chien, S., 2012, "Matrix stiffness regulates endothelial cell proliferation through septin 9," PLoS One, 7(10), p. e46889.

[271] Candiello, J., Singh, S. S., Task, K., Kumta, P. N., and Banerjee, I., 2013, "Early differentiation patterning of mouse embryonic stem cells in response to variations in alginate substrate stiffness," Journal of biological engineering, 7(1), p. 9.

[272] Thomasy, S. M., Morgan, J. T., Wood, J. A., Murphy, C. J., and Russell, P., 2013, "Substratum stiffness and latrunculin B modulate the gene expression of the mechanotransducers YAP and TAZ in human trabecular meshwork cells," Experimental eye research, 113, pp. 66-73.

[273] Mauck, R. L., Soltz, M. A., Wang, C. C., Wong, D. D., Chao, P. H., Valhmu, W. B., Hung, C. T., and Ateshian, G. A., 2000, "Functional tissue engineering of articular cartilage through dynamic loading of chondrocyte-seeded agarose gels," J Biomech Eng, 122(3), pp. 252-260.

[274] Huang, C. Y., Soltz, M. A., Kopacz, M., Mow, V. C., and Ateshian, G. A., 2003, "Experimental verification of the roles of intrinsic matrix viscoelasticity and tension-compression nonlinearity in the biphasic response of cartilage," J Biomech Eng, 125(1), pp. 84-93.

[275] June, R. K., Mejia, K. L., Barone, J. R., and Fyhrie, D. P., 2009, "Cartilage stress-relaxation is affected by both the charge concentration and valence of solution cations," Osteoarthritis Cartilage, 17(5), pp. 669-676.

[276] June, R. K., and Fyhrie, D. P., 2013, "A comparison of cartilage stress-relaxation models in unconfined compression: QLV and stretched exponential in combination with fluid flow," Computer methods in biomechanics and biomedical engineering, 16(5), pp. 565-576.

[277] June, R. K., Neu, C. P., Barone, J. R., and Fyhrie, D. P., 2011, "Polymer Mechanics as a Model for Short-Term and Flow-Independent Cartilage Viscoelasticity," Materials science & engineering. C, Materials for biological applications, 31(4), pp. 781-788.

[278] de Gennes, P.-G., 2002, "Relaxation Anomalies in Linear Polymer Melts," Macromolecules, 35(9), pp. 3785-3786.

[279] June, R. K., Ly, S., and Fyhrie, D. P., 2009, "Cartilage stress-relaxation proceeds slower at higher compressive strains," Arch Biochem Biophys, 483(1), pp. 75-80.

[280] June, R. K., and Fyhrie, D. P., 2009, "Enzymatic digestion of articular cartilage results in viscoelasticity changes that are consistent with polymer dynamics mechanisms," Biomedical engineering online, 8, p. 32.

[281] Bracewell, R., 1999, The Fourier Transform and Its Applications, McGraw-Hill.

[282] Zignego, D. L., Jutila, A. A., Gelbke, M. K., Gannon, D. M., and June, R. K., 2014, "The mechanical microenvironment of high concentration agarose for applying deformation to primary chondrocytes," J Biomech, 47(9), pp. 2143-2148.

[283] Lima, E. G., Tan, A. R., Tai, T., Bian, L., Ateshian, G. A., Cook, J. L., and Hung, C. T., 2008, "Physiologic deformational loading does not counteract the catabolic effects of interleukin-1 in long-term culture of chondrocyte-seeded agarose constructs," J Biomech, 41(15), pp. 3253-3259.

[284] Ng, K. W., Lima, E. G., Bian, L., O'Conor, C. J., Jayabalan, P. S., Stoker, A. M., Kuroki, K., Cook, C. R., Ateshian, G. A., Cook, J. L., and Hung, C. T., 2010, "Passaged adult chondrocytes can form engineered cartilage with functional mechanical properties: a canine model," Tissue engineering. Part A, 16(3), pp. 1041-1051.

[285] Ng, K. W., O'Conor, C. J., Kugler, L. E., Cook, J. L., Ateshian, G. A., and Hung, C. T., 2011, "Transient supplementation of anabolic growth factors rapidly stimulates matrix synthesis in engineered cartilage," Ann Biomed Eng, 39(10), pp. 2491-2500.

[286] Blanco, F. J., and Ruiz-Romero, C., 2012, "Osteoarthritis: Metabolomic characterization of metabolic phenotypes in OA," Nature reviews. Rheumatology, 8(3), pp. 130-132.

[287] Wishart, D. S., Tzur, D., Knox, C., Eisner, R., Guo, A. C., Young, N., Cheng, D., Jewell, K., Arndt, D., Sawhney, S., Fung, C., Nikolai, L., Lewis, M., Coutouly, M. A., Forsythe, I., Tang, P., Shrivastava, S., Jeroncic, K., Stothard, P., Amegbey, G., Block, D., Hau, D. D., Wagner, J., Miniaci, J., Clements, M., Gebremedhin, M., Guo, N., Zhang, Y., Duggan, G. E., Macinnis, G. D., Weljie, A. M., Dowlatabadi, R., Bamforth, F., Clive, D., Greiner, R., Li, L., Marrie, T., Sykes, B. D., Vogel, H. J., and Querengesser, L., 2007, "HMDB: the Human Metabolome Database," Nucleic acids research, 35(Database issue), pp. D521-526.

[288] Doi, M., and Edwards, S. F., 1988, The Theory of Polymer Dynamics, Oxford University Press, Oxford, UK.

[289] Jimenez-Barbero, J., Bouffar-Roupe, C., Rochas, C., and Perez, S., 1989, "Modelling studies of solvent effects on the conformational stability of agarobiose and neoagarobiose and their relationship to agarose," International journal of biological macromolecules, 11(5), pp. 265-272.

[290] Erickson, I. E., Huang, A. H., Chung, C., Li, R. T., Burdick, J. A., and Mauck, R. L., 2009, "Differential maturation and structure-function relationships in mesenchymal stem cell- and chondrocyte-seeded hydrogels," Tissue engineering. Part A, 15(5), pp. 1041-1052.

[291] Knight, M. M., McGlashan, S. R., Garcia, M., Jensen, C. G., and Poole, C. A., 2009, "Articular chondrocytes express connexin 43 hemichannels and P2 receptors - a putative mechanoreceptor complex involving the primary cilium?," Journal of anatomy, 214(2), pp. 275-283.

[292] Tan, A. R., Dong, E. Y., Ateshian, G. A., and Hung, C. T., 2010, "Response of engineered cartilage to mechanical insult depends on construct maturity," Osteoarthritis Cartilage, 18(12), pp. 1577-1585.

[293] Sysi-Aho, M., Katajamaa, M., Yetukuri, L., and Oresic, M., 2007, "Normalization method for metabolomics data using optimal selection of multiple internal standards," BMC bioinformatics, 8, p. 93.

[294] Dieterle, F., Ross, A., Schlotterbeck, G., and Senn, H., 2006, "Probabilistic quotient normalization as robust method to account for dilution of complex biological mixtures. Application in 1H NMR metabonomics," Anal Chem, 78(13), pp. 4281-4290.

[295] Veselkov, K. A., Vingara, L. K., Masson, P., Robinette, S. L., Want, E., Li, J. V., Barton, R. H., Boursier-Neyret, C., Walther, B., Ebbels, T. M., Pelczer, I., Holmes, E., Lindon, J. C., and Nicholson, J. K., 2011, "Optimized preprocessing of ultra-performance liquid chromatography/mass spectrometry urinary metabolic profiles for improved information recovery," Anal Chem, 83(15), pp. 5864-5872.

APPENDICES

APPENDIX A

ENCAPSULATION OF CHONDROCYTES IN HIGH-STIFFNESS AGAROSE MICROENVIRONMENTS FOR *IN VITRO* MODELING OF OSTEOARTHRITIS MECHANOTRANSDUCTION

ENCAPSULATION OF CHONDROCYTES IN HIGH-STIFFNESS AGAROSE MICROENVIRONMENTS FOR *IN VITRO* MODELING OF OSTEOARTHRITIS MECHANOTRANSDUCTION

Contribution of Authors and Co-Authors

Author: Aaron A. Jutila[1,*]

Contributions: Acquired, analyzed, and interpreted the data. Drafted and wrote the manuscript.

Co-Author: Donald L. Zignego[1,*]

Contributions: Acquired, analyzed, and interpreted the data. Drafted and wrote the manuscript.

Co-Author: William J. Schell[1]

Contributions: Acquired samples and reviewed the manuscript.

Corresponding Author: Ronald K. June[1,2]

Contributions: Designed the study, analyzed and interpreted the data, and wrote the manuscript.

[1] Department of Mechanical and Industrial Engineering, Montana State University, Bozeman, MT 59717-3800, USA

[2] Department of Cell Biology and Neuroscience, Montana State University, Bozeman, MT 59717-3800, USA

[*] Authors made equal contributions to this work.

Manuscript Information Page

*Aaron A. Jutila, *Donald L. Zignego, William J. Schell, and Ronald K. June
Annals of Biomedical Engineering
Status of Manuscript:
___ Prepared for submission to a peer-reviewed journal
___ Officially submitted to a peer-reviewed journal
___ Accepted by a peer-reviewed journal
_X_ Published in a peer-reviewed journal

Publisher: Springer US
Issue: May 2015, Vol. 43, Issue 5, Pages 1132-1144

Abstract

In articular cartilage, chondrocytes reside within a gel-like pericellular matrix (PCM). This matrix provides a mechanical link through which joint loads are transmitted to chondrocytes. The stiffness of the PCM decreases in the most common degenerative joint disease, osteoarthritis. To develop a system for modeling the stiffness of both the healthy and osteoarthritic PCM, we determined the concentration-stiffness relationships for agarose. We extended these results to encapsulate chondrocytes in agarose of physiological stiffness. Finally, we assessed the relevance of stiffness for chondrocyte mechanotransduction by examining the biological response to mechanical loading for cells encapsulated in low- and high- stiffness gels. We achieved agarose equilibrium stiffness values as large as 51.3 kPa. At 4.0% agarose, we found equilibrium moduli of 34.3 ± 1.65 kPa, and at 4.5% agarose, we found equilibrium moduli of 35.7 ± 0.95 kPa. Cyclical tests found complex moduli of ~100-300 kPa. Viability was >96% for all studies. We observed distinct metabolomic responses in >500 functional small molecules describing changes in cell physiology, between primary human chondrocytes encapsulated in 2.0% and 4.5% agarose indicating that the gel stiffness affects cellular mechanotransduction. These data demonstrate both the feasibility of modeling the chondrocyte pericellular matrix stiffness and the importance of the physiological pericellular stiffness for understanding chondrocyte mechanotransduction.

Key Terms: Osteoarthritis; Mechanotransduction; Biomechanics; 3D cell culture; Biomaterials, Substrate Stiffness

Introduction

Articular cartilage is the smooth, load-bearing tissue which lines the surfaces of bones in joints such as the knee and the hip. As a result of normal human activity (*e.g.* walking), cartilage experiences mechanical loading which varies with both time and spatial position in the joint.[265] The hierarchy of cartilage structure includes a dense hydrated extracellular matrix (ECM) which encapsulates a pericellular matrix (PCM) that directly surrounds articular chondrocytes.[125] The PCM transmits tissue-level deformations to the cells of cartilage termed chondrocytes.

The stiffness of the PCM is a relevant environmental input since it applies external loads to chondrocytes and can direct their biological behavior via cellular mechanotransduction. For example, exogenous loading has been shown to change Superficial Zone Protein expression,[87] RhoA activation,[123] and induce transcription of ECM genes.[76] Dynamic compression of cell seeded agarose constructs can promote Smad2 phosphorylation as an early response to mechanical stimuli.[119] To obtain a deeper understanding of chondrocyte mechanotransduction, which is necessary for designing improved therapeutic strategies for joint disease, advanced *in vitro* models are needed which simulate the varying stiffness of the chondrocyte PCM during osteoarthritis progression.

While several studies have examined *in vitro* chondrocyte responses to applied loading, the stiffness of the hydrogel responsible for applying these loads has received little emphasis. *In vitro* model stiffness is important because *in vivo c*hondrocytes are linked to their extracellular environment by the PCM which provides information

regarding the extracellular biomechanical and biochemical microenvironment. Previous studies have found the stiffness of the PCM for human chondrocytes to be in the range of 25-200 kPa.[47, 127, 266] Importantly, the PCM stiffness appears to decline in osteoarthritic tissue,[266] which may be a patho-mechanical signaling mechanism in the most common degenerative joint disease osteoarthritis (OA).[267]

Furthermore, several studies demonstrate the importance of substrate stiffness as a relevant environmental variable for cellular mechanotransduction in other cell types.[268-272] Thus *in vitro* models which mimic the stiffness of the chondrocyte PCM modeling may provide an improved understanding of how chondrocytes sense and respond to mechanical loads. Here we defined the concentration-stiffness relationships for agarose as an *in vitro* substrate for chondrocyte mechanotransduction studies. We extended these results to determine if chondrocytes can be encapsulated within agarose of physiological stiffness. Finally, we assessed the relevance of stiffness for chondrocyte mechanotransduction by examining the biological response to mechanical loading for cells encapsulated in low- and high- stiffness gels.

We found concentration-dependent agarose stiffness (equilibrium, dynamic, and complex) of ~20-300 kPa for agarose ranging between 3 and 5% (weight / volume, w/v). Building upon previous methods,[121, 124] we were able to encapsulate chondrocytes in high-stiffness agarose with high viability (>96%). Agarose stiffness affected chondrocyte biology as demonstrated by distinct metabolomics differences between chondrocytes encapsulated in 2.0% and 4.5% agarose. These data show that agarose can be used as a 3D culture medium for mimicking the stiffness of the cartilage PCM.

Furthermore, by changing the concentration of agarose, it is possible to model disease-dependent changes in the *in vitro* stiffness as seen in human osteoarthritis.[266] To our knowledge, this is the first successful demonstration of chondrocyte encapsulation in agarose >3%.

Materials and Methods

Agarose Constructs. Agarose constructs were prepared using low-gelling-temperature agarose (Sigma: Type VII-A A0701) which was selected because of previous success for mechanotransduction studies.[120, 121] Concentrations of 2-5% (w / v) agarose were dissolved in PBS at 1.1X strength at 40°C. After ~5 minutes, dissolved agarose was diluted to 1X with 40°C PBS. This procedure is readily applied to encapsulating cells based on the methods of Lee *et al* and Bougalt *et al.*[120, 121] The final agarose solution was cast in anodized aluminum molds at 23°C. These molds produced cylindrical samples with heights of 12.7 ± 0.1 mm and diameters of 7.0 ± 0.1 mm as measured using digital calipers on >20 independent samples. This sample geometry was selected to provide uniaxial deformations consistent with spatially homogeneous mechanical strain fields[122] for applying well-defined mechanical stimuli to embedded cells.

Mechanical Testing. Samples were tested on a custom-built bioreactor capable of applying displacement-controlled loading with sub-micron precision (Supplementary Figures 1-3). Because most previous studies have characterized the response for gels of concentration ≤3% for this study, the agarose concentration was 3-5%.[147, 273] Prior to

testing, samples were equilibrated in PBS at 37°C for 30 minutes. Samples were placed in polysulfone loading cups, and the compression platens were lowered until sample contact was achieved as demonstrated by a load change of 0.089 N, the smallest possible preload and consistent with previous methodology.[274] The sample was then allowed to relax to an equilibrium state. Based on pilot studies (n = 3), complete preload relaxation was achieved in < 10 minutes. Therefore, we used a preload time of 10 minutes in this study. Two mechanical tests were performed in unconfined compression: stepwise stress-relaxation and cyclical loading with n = 5 samples for each experiment from multiple agarose castings.

Stepwise stress-relaxation tests were performed to measure dynamic and equilibrium stiffness values for agarose gels at various concentrations. For these tests, samples were subjected to four consecutive steps of 4% nominal compressive Lagrangian strain. Each strain step was maintained for 90 minutes at 37°C in tissue culture conditions (humidified 5% CO_2 atmosphere). Load data was sampled at 1000 Hz for the duration of the test. Average stress was calculated by normalizing the load data by the sample cross sectional area.

Dynamic stiffness was calculated by performing linear regression on the strain versus peak stress data for each sample, and equilibrium stiffness was calculated similarly for the equilibrium stress data. The transient response for each strain step of each sample was analyzed using three measures.[275] First, a model-independent parameter termed $\widehat{D}$ was used to quantify the dynamics of stress-relaxation for each strain step. $\widehat{D}$ was calculated by quantifying the area under normalized stress-relaxation curves.

Second, the stretched exponential model ($y = \exp(-\left(\frac{t}{\tau_{SE}}\right)^{\beta})$ [276, 277] was fit to the normalized stress-relaxation data to determine the parameters τ_{SE} and β. This model has been linked mechanistically to fundamental polymer physics[278] and successfully used to model cartilage viscoelastic behavior.[279, 280]

Cyclical loading tests were performed to assess the complex stiffness and phase lag of agarose gels. In these experiments, samples were subjected to a 5% prestrain for 2 hours followed by 100 cycles of sinusoidal compression from 3.1 to 6.9% based on the initially measured height. Samples were tested at 0.55, 1.1, and 5.5 Hz. These frequencies were selected to bound the preferred stride rates for humans.[153] Load and displacement values were sampled simultaneously at 100 Hz to ensure sampling above the Nyquist limit.[281] Average stresses were calculated as described above. Cyclical loading data were analyzed to determine the complex modulus (*i.e.* stiffness) defined as the amplitude of the stress divided by the amplitude of the strain and the phase lag of the stress relative to the strain.

Chondrocyte Encapsulation. To assess the potential for using agarose of varying stiffness to model the chondrocyte pericellular matrix, cells were embedded in agarose of varying concentrations. Human SW1353 chondrosarcoma cells were cultured at 5% CO_2 in DMEM with 10% fetal bovine serum and antibiotics (10,000 I.U. / mL penicillin and 10000 ug / mL streptomycin). For encapsulation, cells were trypsinized, counted, and resuspended in media at 11X. Agarose was prepared as described above. The cell-suspension was added to the agarose during vortexing to distribute the cells throughout

the liquid hydrogel. Gels were subsequently cast as described above for 5 minutes at 23°C. Cell-seeded agarose constructs were removed from the molds and placed in tissue culture for 24 and 72 hours prior to viability analysis to examine a relevant timeframe for molecular biology experiments.

Viability Assays. To assess feasibility of the encapsulation process, we assessed chondrocyte viability using standard methods.[132] Cells were incubated in 8 μM calcein-AM and 75 μM propidium iodide. Following incubation, constructs were examined by confocal microscopy for calcein-AM fluorescence (excitation: 496 nm emission: 516 nm) indicating live cells via intracellular thioesterase activity and propidium iodide fluorescence (excitation: 536 nm emission: 617 nm) defining dead cells via DNA binding indicative of compromised plasma membranes. Confocal images were acquired from 6 positions within each hydrogel to assess potential spatial variability in cell viability.[282] Images were thresholded, and the number of viable and dead cells were quantified.

Chondrocyte Mechanotransduction and Metabolomics. Following successful encapsulation of SW1353 chondrocytes in high-concentration agarose, we expanded to study primary human osteoarthritic chondrocytes. Discarded joint replacement tissue (Bridger Orthopedics, informed consent obtained under IRB-approved human subjects exemption) was used to harvest primary human chondrocytes from a single donor via collagenase digestion. Primary chondrocytes were passaged once and embedded in high-stiffness agarose (4.5% w/v) and low-stiffness agarose (2% w/v) using previously

optimized methods.[282] The rationale for these gel concentrations is that 4.5% provides stiffness that approaches physiological. The concentration of the low-stiffness samples was based on a literature survey which found 2% to be commonly used. [283-285]

Cell-seeded agarose gels were then randomly assigned to a loading group (n = 5 replicates. 0 minutes, 15 minutes or 30 minutes of dynamic loading) and dynamically stimulated in tissue culture with applied compression from 4.5-5.5% nominal strain. Metabolites were extracted, and detection of metabolites was performed via HPLC-MS (Mass Spectrometry Core Facility, Montana State University) using previously validated methods.[116] Immediately following mechanical stimulation, samples were flash-frozen, pulverized, and immersed in 1 mL of 70:30 Methanol:Acetone. Samples were vortexed every 4-5 minutes for 20 minutes and further extracted overnight at -20˚C. Solids were pelleted at 13,000xg for 10 min at 4˚C. Supernatant was placed in a new tube, and solvent was evaporated by speedvac. After 6 hours, metabolites were resuspended in 50:50 water:acetonitrile. Metabolomic characterization was performed using hydrophilic interaction chromatography coupled to an Agilent 6538 Q-TOF mass spectrometer with electrospray ionization and positive mode spectral collection. The rationale for performing metabolomics characterization is that metabolites represent a high-dimensional fingerprint describing the actual state of the cell at a given instant in time. Prior studies have found substantial changes in chondrocyte metabolomics in response to loading and OA.[116, 286]

Statistical Analysis. Mechanical testing data was analyzed using Multivariate Analysis of Variance (MANOVA). The first MANOVA model examined the effects of

agarose concentration on both the dynamic and equilibrium stiffness. The second MANOVA model utilized repeated measures to examine the effects of gel concentration, compression level, and stress-relaxation model on the peak stress, equilibrium stress, $\widehat{D}$, stress-relaxation model parameters, and fit quality measures. The third MANOVA examined the effects of loading frequency and gel concentration on the complex modulus and phase lag. The final MANOVA examined the effects of gel concentration and spatial position on cell viability. Bonferroni *post hoc* tests were used to ascertain specific differences with an *a priori* significance level of $\alpha = 0.05$.

For an aggregate comparison between experimental groups, distributions of metabolites were compared using the Kolmogorov-Smirnov test. Expression of individual metabolites was compared using T-tests to assess differences between low and high-stiffness agarose gels with corrections for multiple comparisons. Comparisons were performed using a false discovery rate (FDR) of $p = 0.05$.[259] For each of the two concentrations of agarose gels, two comparisons were made: unloaded control (UC) vs. 15 minutes of dynamic loading 15 (DL15) and unloaded controls vs. 30 minutes of dynamic loading (DL30). For both 15 and 30 minutes of loading, chondrocyte metabolomics responses in 2.0% and 4.5% were compared to assess using the Kolmogorov-Smirnov test the effect of gel stiffness on chondrocyte mechanotransduction. Statistical models and tests were performed in both MiniTab (MANOVA) and MATLAB (metabolomics data). Metabolites of interest were searched against available databases to identify putative molecules associated with metabolomic features.[163, 287]

Results

Stepwise Stress-Relaxation. Agarose stiffness as measured by the dynamic and equilibrium moduli from stepwise stress-relaxation tests was a function of agarose concentration from 3-5%. Agarose samples demonstrated viscoelasticity via time-dependent stress relaxation while held at a constant strain (Supplemental Figure 1A). 5% agarose reached higher peak and equilibrium loads than 3% agarose under the same strain. Increasing gel concentration increased mechanical stiffness (Dynamic: $p < 0.0001$ Equilibrium: $p < 0.0001$, $n = 25$).

We achieved agarose equilibrium stiffness as large as 51.3 kPa and dynamic stiffness as large as 90.7 kPa with 5% agarose gels, and as expected lower agarose concentrations resulted in lower stiffness (Supplemental Figure 1B-C, Supplemental Table 1). At 4.5% agarose, we found equilibrium stiffness of 35.7 ± 0.95 kPa (mean ± standard error of the mean). Dynamic stiffness was approximately twice as large as corresponding equilibrium stiffness (Supplemental Figure 1C, Supplemental Table 1), with 3.0% dynamic stiffness of 39.4 ± 4.5 kPa 5.0% yielding 78.4 ± 3.2 kPa.

The stretched exponential fit the stepwise stress-relaxation data ($R^2 = 0.90 \pm 0.03$). Stretched Exponential parameter τ_{SE} decreased with agarose gel concentration ($p < 0.0001$), while β remained relatively constant with gel concentration (Supplemental Figure 2A-B). Model independent parameter $\widehat{D}$ was not affected by concentration ($p = 0.442$) with an overall average of 8.24 ± .05 sec.

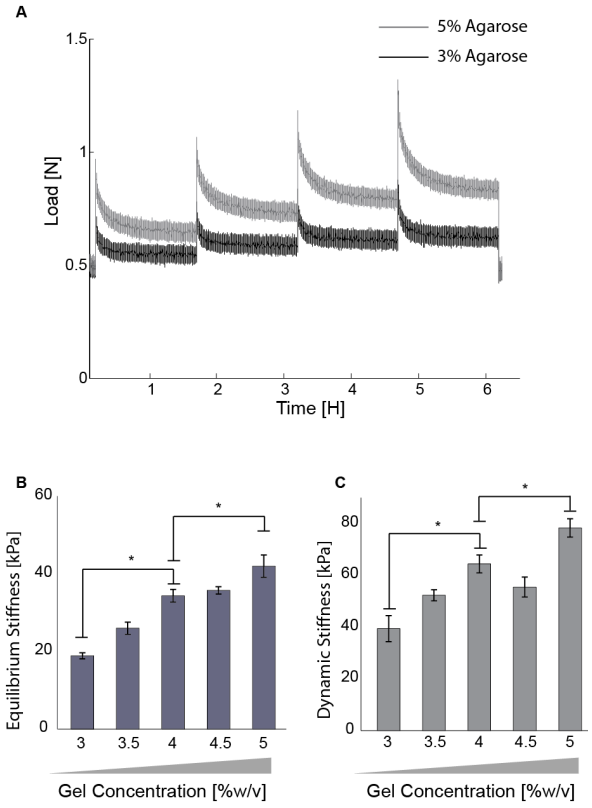

Supplemental Figure 1. Agarose stiffness was concentration dependent as determined in stress-relaxation experiments. (A). Representative stress-relaxation load curves for 3 and 5% (w / v) agarose. (B). Equilibrium modulus as a function of agarose concentration. (C). Dynamic modulus as a function of agarose concentration. * Indicates significant planned comparison ($p < 0.05$). Both Equilibrium and Dynamic Stiffness expressed strong dependence on concentration (both $p<0.0001$ for main effects).

Supplemental Table 1. Stiffness values from mechanical testing experiments. Repeated stress-relaxation (SR) tests were used to measure stiffness as defined by the equilibrium and dynamic moduli. Complex stiffnesses were defined from the complex modulus determined at 1.1 Hz which mimics the preferred stride rate of human walking [Umberger *et al* 2007]. Data are mean ± standard error in kPa.

Agarose [%w/v]	**Stiffness [kPa]**		
	Equilibrium, SR	Dynamic, SR	Complex, 1.1 Hz
3	18.9 ± 0.8	39.4 ± 4.5	147.6 ± 7.7
3.5	26.0 ± 1.6	52.3 ± 1.9	151.4 ± 8.0
4	34.3 ± 1.7	64.4 ± 3.1	119.1 ± 13.6
4.5	35.7 ± 1.0	55.5 ± 3.5	216.5 ± 26.6
5	42.0 ± 2.9	78.4 ± 3.2	226.1 ± 18.7

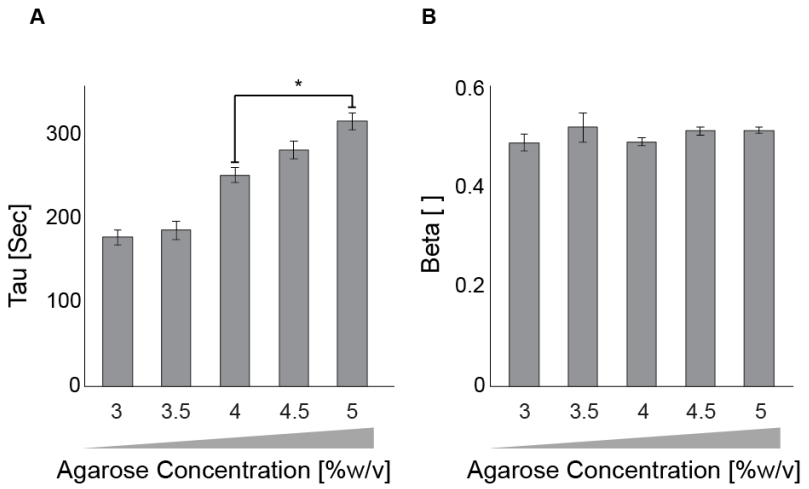

Supplemental Figure 2. Concentration-dependent dynamics of agarose stress-relaxation. The dynamics of agarose stress-relaxation were modeled using the stretched exponential model. (A) The relaxation time constant, τ_{SE} increased with agarose concentration expressing a strong dependence on gel concentration (main effect: $p<0.0001$). (B) There were no significant effects of gel concentration on the stretching parameter Beta ($p=0.834$).

Cyclical Loading. Sinusoidal applied strain induced sinusoidal stress profiles for all gel concentrations at all frequencies suggesting linear elastic material behavior (Supplemental Figure 3A). Cyclical tests found complex moduli of ~100-300 kPa (Supplemental Figure 3B, Supplemental Table 1). Low-concentration gels had similar complex stiffness between 3-4% agarose, while the complex stiffness of 4-5% agarose was larger. For a normal walking rate (~1.1 Hz), 4.5% agarose gels yielded complex moduli values of 216.5 ± 26.6 kPa.

The phase lag between stress and strain is a measure of the energy absorption within a viscoelastic material. Phase lag decreased with increasing frequency (Supplemental Figure 3C). Loading frequency significantly impacted phase lag ($p <$

0.0001), but agarose concentration had no effects (p = 0.934). The concentration-averaged phase lag at 1.1 Hz was 0.11 ± 0.002 s.

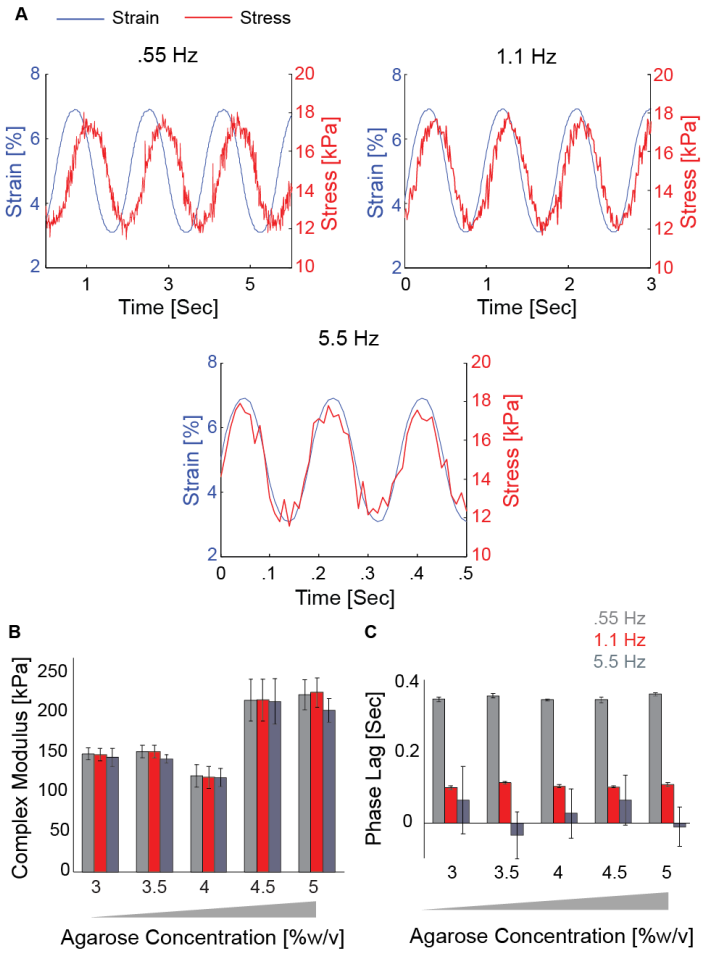

Supplemental Figure 3. Complex agarose stiffness as high as ~225 kPa from cyclical loading experiments. (A) Representative stress and strain profiles as a function of time for applied compression frequencies of 0.55, 1.0, and 5.5 Hz. (B) Complex modulus values were a function of agarose concentration (Main Effect: p<0.0001). (C) Phase lag data, indicating energy dissipation within the agarose, were determined to be function of frequency (p<0.0001) and not a function of agarose concentration (p=0.934).

Chondrocyte Viability in 3D Constructs. To assess the relevance of using high-concentration agarose as an *in vitro* model to mimic the stiffness of the human pericellular matrix, viability was assessed using confocal microscopy for 3-5% agarose.

We found high viability both 24 and 72 hours following encapsulation (Supplemental Figure 4A). Imaging revealed high viability which was not location-specific ($p = 0.496$) indicating that the methods resulted in an even spatial distribution of cells. Viability rates for all agarose gel concentrations were >96% both 24 and 72 h following encapsulation.

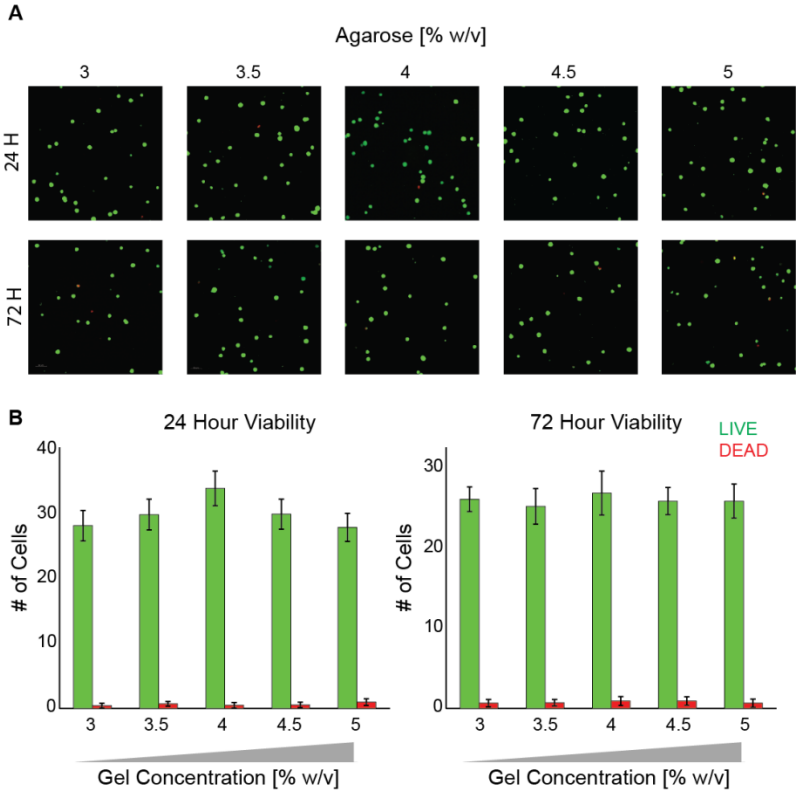

Supplemental Figure 4. Encapsulation of SW1353 chondrocytes in high-stiffness agarose gels resulted in high viability. Gels were incubated with Calcein-AM and propidium iodide to assess viability via fluorescent microscopy (A) Representative images. (B) Viability >96% was observed in all gel concentrations both 24 and 72 hours after encapsulation. There were no significant differences in viability rates between agarose concentration, spatial position within the gel, or time point.

Metabolomics. Changes in agarose concentration, and therefore gel stiffness, resulted in metabolomics changes following mechanical loading. After both 15 and 30

minutes of dynamic compression, distributions of metabolites harvested from low stiffness 2%- and high stiffness 4.5%-agarose were distinct as determined by a non-parametric, two-sample Kolmogorov-Smirnov (15 minutes: $p = 0.032$ and 30 minutes: $p = 0.021$, Supplemental Figure 5A-B).

Agarose concentration differentially regulated the profiles of mechanosensitive metabolites. For 15 minutes of dynamic compression, 204 metabolites (FDR corrected p-value < 0.05) were significantly upregulated and 101 metabolites were significantly down-regulated in 4.5% agarose compared with 2.0% agarose (Supplemental Figure 5C). For 30 minutes of dynamic compression, 212 metabolites were significantly upregulated and 99 were significantly down-regulated in 4.5% compared with 2.0% agarose (Supplemental Figure 5D).

Individual metabolite expression in response to applied dynamic compression was also affected by agarose stiffness. Loading of primary human chondrocytes in both 2% and 4.5% agarose gels resulted in both up- and down- regulation of several metabolites (Supplemental Figure 5E-F). In the 2% low-stiffness gels 15 minutes of dynamic compression resulted in up-regulation of 47 unique metabolites and down-regulation of 56 unique metabolites. In contrast, for the 4.5% high-stiffness gels, 15 minutes of dynamic compression resulted in up-regulation of 108 unique metabolites and down-regulation of 97 unique metabolites. Similar results were seen in response to 30 minutes of dynamic compression (Supplemental Figure 5F). Metabolites targeted to central energy metabolism were differentially regulated by mechanical loading in 4.5% and 2% agarose (Supplemental Table 2). We found 97 metabolites of interest, as defined by

differential response to loading between 4.5% and 2% agarose gels (Supplemental Table 3) which resulted in database identification of many putative compounds relevant to chondrocyte mechanotransduction.

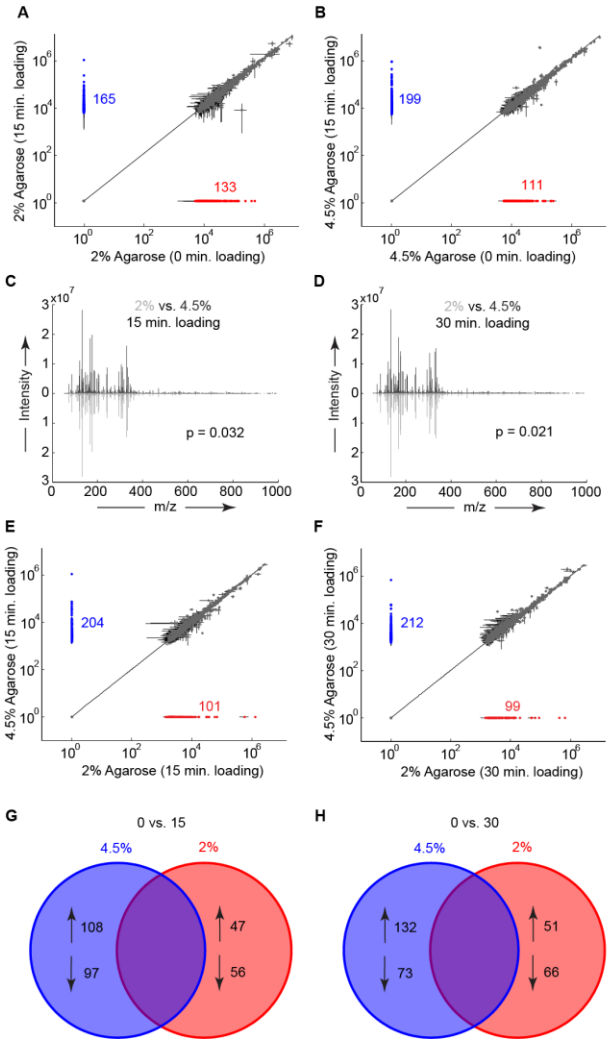

Supplemental Figure 5. Primary human chondrocyte mechanotransduction is affected by agarose concentration. Primary human chondrocytes were harvested from joint replacement tissue, passaged once in culture, and encapsulated in either 2% or 4.5% agarose prior to applied dynamic compression and metabolomics analysis. Summary results comparing unloaded and 15 minutes of loading for (A) 2% agarose and (B) 4.5% agarose. (C) Representative mass spectra after 15 minutes of loading for 2% (bottom) agarose and 4.5% (top) agarose gels. A two-sample Kolmogorov-Smirnov test revels a statically significant difference between the two mass spectra distributions ($p = 0.032$).

(D) Representative mass spectra after 30 minutes of loading for 2% (bottom) agarose and 4.5% (top) agarose gels, with statistically significant mass spectra distributions (two-sample Kolmogorov-Smirnov test, $p = 0.021$). (E) After 15 minutes of loading, 204 metabolites were significantly upregulated (FDR corrected, $p < 0.05$) in high-stiffness 4.5% gels, and 101 metabolites were upregulated in low-stiffness gels (F) After 30 minutes of loading 212 and 99 metabolites were upregulated in the high and low-stiffness gels, respectively. (G) 4.5% agarose resulted in increased numbers of unique mechanosensitive metabolites after 15 minutes of loading and (H) 30 minutes of loading.

Supplemental Table 2. Mechanically-induced changes in metabolites targeted to central energy metabolism depended on agarose concentration. We observed more changes in central energy metabolites in 4.5% gels than 2% gels. In each agarose concentration, distinct metabolites accumulated and were depleted following 15 minutes of dynamic compression. Phosphoglucanolactone decreased and pyruvate accumulated in both gel concentrations. m/z represents detected mass, and RT represents the retention time in minutes.

m/z	RT [min]	Metabolite Name	Observation
277.0319	6.11	6-P-gluconate	↑ in 4.5%
111.0053	8.46	pyruvate	↑ in 4.5%
291.0476	6.06	sedoheptulose-7-phosphate	↑ in 4.5%
444.0321	5.84	GDP	↑ in 4.5%
523.9985	6.92	GTP	↓ in 4.5%
119.0343	5.50	succinate	↓ in 4.5%
154.9951	7.45	oxaloacetate	↓ in 4.5%
215.0148	2.71	citrate	↓ in 4.5%
259.0213	6.37	p-glucanoalactone	↓ in 4.5%
135.0273	3.47	L-malate	↓ in 4.5%
136.9845	6.27	fumarate	↓ in 4.5%
111.0053	8.45	pyruvate	↑ in 2%
91.0388	2.58	lactic acid	↑ in 2%
786.1644	6.04	FAD	↓ in 2%
259.0213	6.37	p-glucanoalactone	↓ in 2%
215.0148	2.67	citrate	↓ in 2%

KEY		
	↑ in 4.5%	↑ in 2%
	↓ in 4.5%	↓ in 2%

Supplemental Table 3. Untargeted metabolites of interest following 15 minutes of dynamic compression in either 4.5% or 2% agarose. Several metabolites were differentially regulated between agarose concentrations following compression. m/z represents detected mass, and RT represents the retention time in minutes. These detected masses were used to identify putative molecules using database searches.

m/z	RT [min]	Observation
137.08084	8.09	↑ in 4.5%
141.07072	8.36	↑ in 4.5%
163.05245	5.78	↑ in 4.5%
211.10299	8.47	↑ in 4.5%
256.12723	7.94	↑ in 4.5%
263.14452	10.48	↑ in 4.5%
283.09727	2.71	↑ in 4.5%
289.08812	2.75	↑ in 4.5%
291.06743	2.71	↑ in 4.5%
316.18734	8.34	↑ in 4.5%
332.11198	6.59	↑ in 4.5%
350.06474	5.61	↑ in 4.5%
365.27303	11.47	↑ in 4.5%
367.12609	2.51	↑ in 4.5%
483.26462	8.35	↑ in 4.5%
496.33422	6.39	↑ in 4.5%
671.21398	5.60	↑ in 4.5%
754.52638	5.65	↑ in 4.5%
154.08382	5.59	↓ in 4.5%
206.05397	8.88	↓ in 4.5%
250.09049	6.19	↓ in 4.5%
258.10844	8.45	↓ in 4.5%
263.14460	9.10	↓ in 4.5%
269.08677	2.96	↓ in 4.5%
276.04639	6.54	↓ in 4.5%
283.10171	2.71	↓ in 4.5%
306.10092	2.57	↓ in 4.5%
311.12921	2.64	↓ in 4.5%
312.17139	8.48	↓ in 4.5%
314.08337	2.74	↓ in 4.5%
314.10655	2.49	↓ in 4.5%
319.11918	3.27	↓ in 4.5%
319.14839	8.03	↓ in 4.5%
353.11473	2.57	↓ in 4.5%
355.11317	2.54	↓ in 4.5%
361.10664	3.08	↓ in 4.5%
369.06443	6.61	↓ in 4.5%
378.14547	2.48	↓ in 4.5%
379.11824	3.49	↓ in 4.5%
393.20667	3.26	↓ in 4.5%
427.09147	7.42	↓ in 4.5%
428.09458	7.43	↓ in 4.5%
449.07337	7.41	↓ in 4.5%
464.12472	3.51	↓ in 4.5%
537.18981	8.46	↓ in 4.5%
673.23737	8.48	↓ in 4.5%
959.31243	3.96	↓ in 4.5%

KEY		
	↑ in 4.5%	↑ in 2%
	↓ in 4.5%	↓ in 2%

m/z	RT [min]	Observation
186.0346	6.48	↑ in 2%
227.1094	8.79	↑ in 2%
254.1334	3.52	↑ in 2%
255.1326	8.48	↑ in 2%
257.0735	2.78	↑ in 2%
264.0744	2.64	↑ in 2%
276.9984	2.92	↑ in 2%
281.0945	8.46	↑ in 2%
283.1003	2.66	↑ in 2%
291.0676	2.64	↑ in 2%
293.0819	2.67	↑ in 2%
307.0982	2.50	↑ in 2%
316.1876	8.37	↑ in 2%
325.1586	8.80	↑ in 2%
327.1247	5.51	↑ in 2%
349.0567	2.55	↑ in 2%
350.2307	8.16	↑ in 2%
351.2324	8.16	↑ in 2%
359.0387	6.05	↑ in 2%
384.1130	2.62	↑ in 2%
397.1263	5.64	↑ in 2%
404.0614	6.10	↑ in 2%
406.1677	2.55	↑ in 2%
429.0746	5.63	↑ in 2%
479.2364	8.42	↑ in 2%
483.2663	8.39	↑ in 2%
505.2536	8.31	↑ in 2%
521.2117	8.39	↑ in 2%
585.1268	3.32	↑ in 2%
138.09062	8.52	↓ in 2%
159.09076	3.34	↓ in 2%
165.07411	3.01	↓ in 2%
202.06991	6.65	↓ in 2%
258.10851	8.46	↓ in 2%
260.07247	6.51	↓ in 2%
261.10929	4.08	↓ in 2%
270.14686	3.46	↓ in 2%
303.12273	5.83	↓ in 2%
312.17153	8.52	↓ in 2%
351.15742	8.40	↓ in 2%
361.10828	3.09	↓ in 2%
362.30227	3.41	↓ in 2%
379.11859	3.49	↓ in 2%
383.11378	2.75	↓ in 2%
427.09152	7.43	↓ in 2%
428.09424	7.45	↓ in 2%
449.07386	7.42	↓ in 2%
451.12837	2.68	↓ in 2%
455.05226	3.02	↓ in 2%
673.23789	8.50	↓ in 2%

Discussion

The objectives of this study were to (1) determine the a range of agarose gel concentrations necessary to mimic the physiological stiffness of both OA pericellular matrix (PCM) and healthy PCM, (2) assess the feasibility of encapsulating human chondrocytes in physiologically stiff agarose, and (3) determine the effect of gel stiffness on chondrocyte mechanotransduction. We measured various viscoelastic properties as a function of agarose gel concentration which can aid in designing future studies of chondrocyte mechanotransduction. We assessed viability for all gel concentrations at 24 and 72 hours following encapsulation. Chondrocytes encapsulated in high-stiffness 4.5% agarose gels demonstrated metabolomic responses to mechanical compression that were markedly different than compression-induced changes observed for chondrocytes in lower-stiffness 2.0% agarose, which demonstrates the importance of using high-stiffness substrates to model healthy human pericellular matrix in mechanotransduction studies.

In articular cartilage, chondrocytes reside within a pericellular matrix defining their immediate surroundings and providing biochemical and mechanical signals. One biomechanical cue for chondrocytes is PCM stiffness. Previous studies have found the range of PCM stiffness for human PCM to be 17-200 kPa.[47, 127, 266] Osteoarthritic PCM appears to have a lower stiffness than healthy PCM.[73] In this study, viscoelastic stiffness measures tended to increase with agarose concentration, and we found dynamic, equilibrium, and complex moduli of 55.5, 35.7, and 216.5 kPa, respectively for 4.5% agarose (Supplemental Table 4). These data suggest that modeling osteoarthritis-induced changes in chondrocyte PCM stiffness is feasible using variable-concentration agarose.

Agarose of ≤3% w/v may simulate osteoarthritic PCM, and agarose of ≥4.5% may simulate the mechanical microenvironment of the healthy chondrocyte.

Supplemental Table 4. PCM and agarose stiffness measurements. Darling *et al* 2010 used AFM at low- and high- force to characterize the stiffness of 3 μm fresh-frozen sections of human PCM. Alexopolous *et al* used micropipetting to characterize the stiffness of extracted human normal and OA chondrons. This study performed macroscale tests on cylinders of agarose. 4.5% was selected as the most-stiff concentration feasible for cell encapsulation.

Measurement	**Stiffness [kPa]**
Darling et al 2010 (AFM on PCM)	17 +/- 14 (low force)
	104 +/- 51 (high force)
Alexopoulos et al (Micropipette on PCM)	66.5 +/- 23.3 (normal)
	41.3 +/- 21.1 (OA)
This study 4.5% agarose (Macroscale)	216.5 +/- 26.6 (complex)
	55.5 +/- 3.5 (dynamic)
	35.7 +/- 1.0 (equilibrium)

These viscoelastic data provide insight into the macroscale mechanics of agarose. We observed differences in in dynamic, equilibrium, and complex stiffness at 4.5% agarose (Supplemental Figure 1B-C and Supplemental Figure 3B). These data may indicate an overlap concentration at 4.5% w/v defining distinct physical regimes of polymeric behavior.[288] Furthermore, the stretched exponential time constant was strongly dependent on gel concentration ($p < 0.0001$, $n = 100$) while we saw no changes in the stretching factor β ($p = 0.834$), which suggests that the distribution of relaxation dynamics is similar between gel concentrations as expected for a monodisperse preparation of agarose.[278] Finally, for this range of loading frequencies, there were no effects on complex modulus. These data suggest that the complex modulus of agarose is an intrinsic material property, dependent on gel concentration, but independent of loading

frequency. Future studies may evaluate the role of viscoelastic properties in chondrocyte mechanotransduction.

For studies encapsulating chondrocytes and other cells, *in vitro* models must maintain cellular viability. Agarose is a linear polysaccharide with a monomeric unit of agarobiose which is a dissacharide linked by both α- and β- glycosidic bonds with similar structure to cartilage glycosaminoglycans chondroitin- and keratin- sulfate [289]. Consistent with previous studies,[290-292] we found viability greater than 96% for all gel concentrations tested in this study. This indicates that chondrocytes can be successfully encapsulated in agarose gels of variable stiffness. Importantly, we are interested in cytosolic mechanisms of chondrocyte mechanotransduction independent of potential biochemical cues provided by the PCM. As such, these studies were conducted 3 days after encapsulation prior to the observation of substantial pericellular matrix formation. Stiffness is only one mechanical measure of the pericellular matrix. *In vivo* mechanotransduction is likely guided by a combination of mechanical and biochemical cues, and this approach represents an experimental model of a single variable (*i.e.* stiffness) in a complex system. Future studies should combine mechanical and biochemical cues to further our understanding of chondrocyte mechanotransduction.

The metabolome defines a functional fingerprint of cellular physiology via quantification of the abundance of large numbers of small biological molecules (e.g. peptides, oligonucleic acids, substrates, etc.).[163] In this study, we successfully detected thousands of metabolites in both low- and high- stiffness gels seeded with primary human osteoarthritic chondrocytes. We found differences in the distributions of

compression-induced metabolites between the 4.5% high stiffness and the 2.0% lower stiffness agarose gels (Supplemental Figure 5A-B). Furthermore, we found several compression-induced metabolites that were unique to either the high- or the low-stiffness gels (Supplemental Figure 5C-F). In conjunction with the stiffness results (Supplemental Figure 1), these metabolomic data demonstrate the ability of dynamic compression to regulate chondrocyte mechanobiology in a manner dependent on substrate stiffness. These stiffness-dependent changes may result from chondrocyte compression in the 4.5% agarose gels that is not observed in the 2.0% agarose gels.[282] These data demonstrate the feasibility of modeling mechanical changes in the chondrocyte pericellular matrix stiffness which occur in osteoarthritis (Supplemental Figure 6).[73]

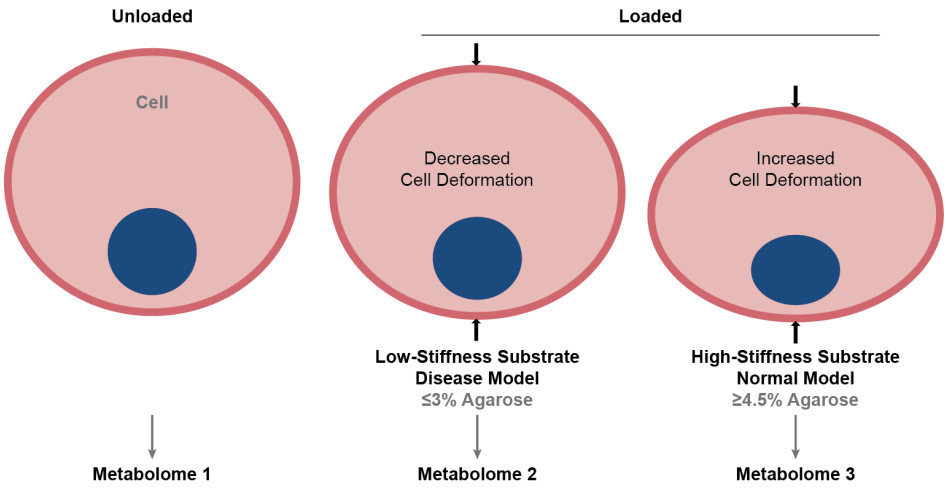

Supplemental Figure 6. Model for studying mechanotransduction in joint disease. Previous studies have found differences in pericellular matrix stiffness between osteoarthritic (OA) and normal studies [37]. The data and methods presented herein suggest that agarose can be used to model both the normal and the OA pericellular matrix. Agarose concentrations of 4.5% and higher would model the stiffness of healthy pericellular matrix (PCM) and agarose concentrations of 3% and lower would model the decreased stiffness of the OA PCM.

The metabolomic responses induced by 15 minutes of dynamic compression were distinct between 4.5% and 2% agarose gels. For metabolites targeted to central energy metabolism, only phosphoglucanoalactone and pyruvate were similarly regulated. The observed accumulation of pyruvate may indicate direction of energy metabolism toward matrix synthesis, as pyruvate is a precursor to the synthesis of many proteins. In general, 4.5% gels exhibited greater regulation of energy-related metabolites than 2% gels (11 changed in 4.5% vs. 4 changed in 2%). Several untargeted metabolites were differentially regulated by 4.5% and 2% gels following compression (Supplemental Table 3).

Conclusions

These data demonstrate the feasibility of encapsulating chondrocytes in agarose of both physiological and pathological stiffness. Because the stiffness of the pericellular matrix is affected by osteoarthritis, these results provide a foundation for both improving the physiological relevance of *in vitro* culture systems and applying relevant mechanical stimulation to chondrocytes. The advantage of the agarose system is that cells can be manipulated with modern tools of molecular biology (e.g. viral transduction) prior to encapsulation within a microenvironment of physiological stiffness. These results establish the basis for future studies should encapsulate healthy and OA chondrocytes in low- and high- stiffness agarose using these methods. Continuation of this work may yield insight into how healthy and OA chondrocytes respond to mechanical loads which may inform therapeutic strategies for cartilage repair in OA.

Acknowledgements

This work was funded by NIH P20 GM103394, NSF EEC-1342420, and funds from the Vice President for Research at Montana State University. To view the database search data in Supplementary Tables 1 and 2, email the corresponding author at rjune@me.montana.edu.

References

See REFERENCES CITED.

APPENDIX B

SUPPLEMENTAL MATERIAL FOR CHAPTER 2
DEVELOPMENT OF EXPIRIMENTAL METHODOLOGY

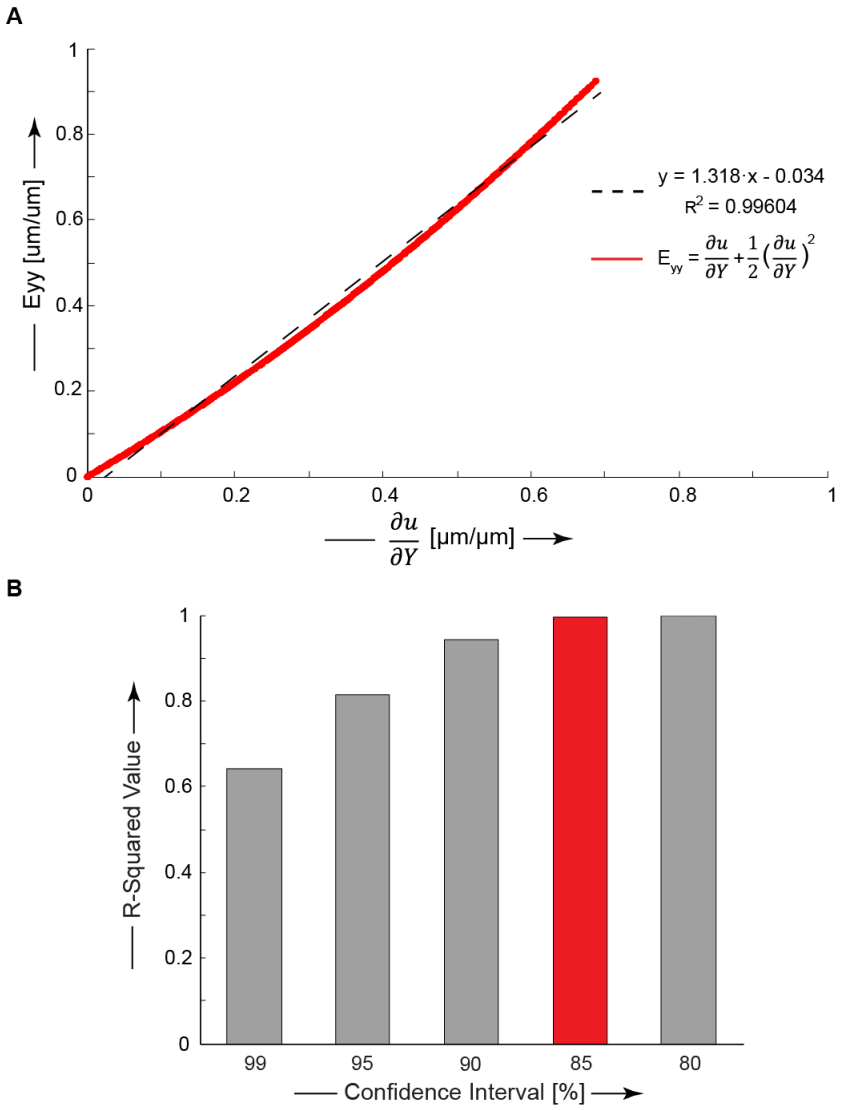

Supplemental Figure 7. Pilot study to determine confidence interval for bead displacements. To determine the largest confidence interval of bead displacements required to mitigate errors in displacement tracking (*e.g.* missed observations due to obstruction by a neighboring bead), the coefficient of determination (R2) was determined for the linear regression between the analytical relationship between finite strain and deformation gradient ($\frac{du}{dY}$) (panel A). The 85% confidence interval was selected to utilize the largest confidence interval for experimentally-measured bead displacements that provide the theoretically predicted R2 value.

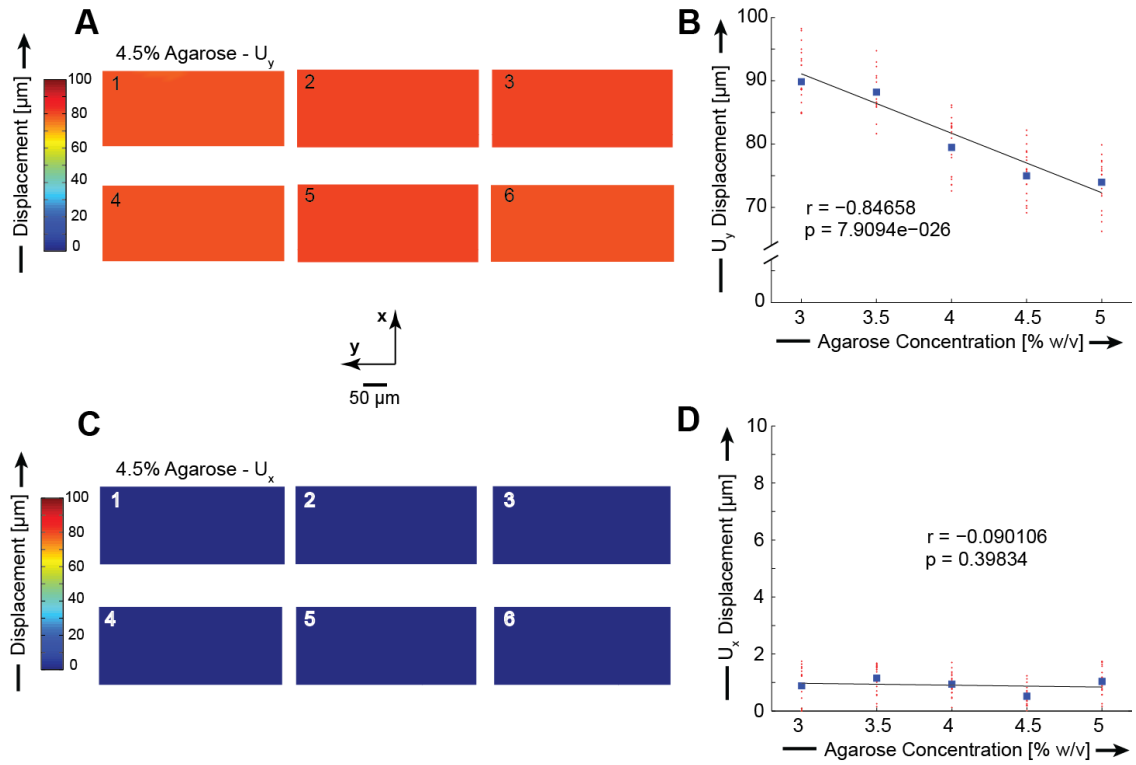

Supplemental Figure 8. Concentration-dependent displacement fields within 4.5% agarose hydrogels. Uy Displacements were calculated from bead positions within the hydrogels following application of a validated 2D filter [Chan et al 2012]. Average axial (Uy) displacement values (A and B) were 89.89 ± 1.05 µm, 88.20 ± 0.78 µm, 79.89 ± 1.06 µm, 74.99 ± 0.94 µm, and 73.98 ± 0.90 µm for 3, 3.5, 4, 4.5, and 5% agarose (w/v), respectively. Across all agarose concentrations, the precision in axial displacement was 1.17%. Average transverse (Ux) displacement values (C and D) were below the 5 µm pixel size (*i.e.* ~1.00 µm) for all agarose concentrations. Results are shown as mean ± SEM. The precision of displacement measurements between all locations was 5.3% of the mean value for 4.5% gels. Blue dots in Figures B & D represent the average displacement values. Red dots are data points from all positions and concentrations. Compression applied in the positive y-direction.

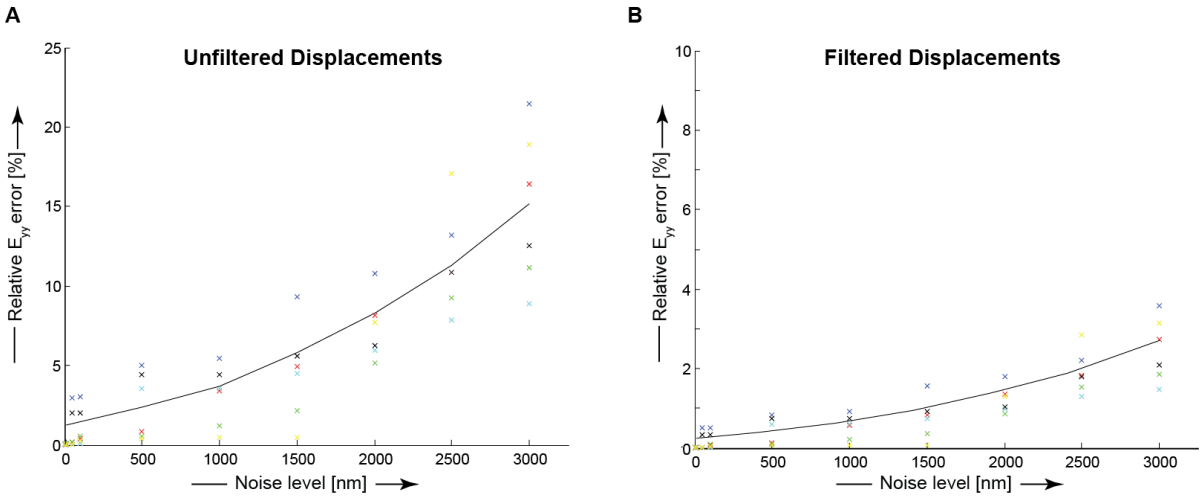

Supplemental Figure 9. Propagation of displacement errors for axial strain (Eyy) calculation. Random noise of varying amplitude from 0-3000 nm was added to the raw displacement data. Without the filtering, error propagation was substantial (A). The addition of a validated filter [131] resulted in minimal error propagation (B). The precision of the displacement measurements was ~700-1000 nm (Supplemental Table 5) indicating ~1% propagated error for calculating Eyy. Note the vertical scale has been magnified in panel B to visualize the data.

Supplemental Table 5. Average Exx, Eyy, and Exy strains ± SEM for each gel concentration. Note that the average strains were taken from 6 unique locations in 3 separate gels (total of 18 total data points).

Gel Conc. [%w/v]	Exx Strain (mm/mm)	Eyy Strain (mm/mm)	Exy Strain (mm/mm)
3	0.01 ± 0.00	2.01 ± 0.08	0.20 ± 0.02
3.5	0.00 ± 0.00	1.65 ± 0.11	0.21 ± 0.03
4	0.01 ± 0.00	1.33 ± 0.10	0.19 ± 0.03
4.5	0.01 ± 0.00	1.11 ± 0.08	0.18 ± 0.02
5	0.00 ± 0.00	0.98 ± 0.07	0.14 ± 0.02

Supplemental Table 6. Cell viability after 24 and 72 hours for primary human chondrocytes. Results are shown as mean ± sem.

Gel Conc. [%w/v]	% Live cells (24 hour)	% Dead cells (24 hour)	% Live cells (72 hour)	% Dead cells (72 hour)
3	98.5 ± 0.5	1.5 ± 0.5	97.6 ± 0.8	2.4 ± 0.8
3.5	97.8 ± 0.5	2.2 ± 0.5	97.3 ± 0.7	2.7 ± 0.7
4	98.7 ± 0.4	1.3 ± 0.4	96.9 ± 0.8	3.1 ± 0.8
4.5	98.2 ± 0.6	1.8 ± 0.6	96.2 ± 0.9	3.8 ± 0.9
5	97.5 ± 0.8	2.5 ± 0.8	97.8 ± 0.8	2.2 ± 0.8

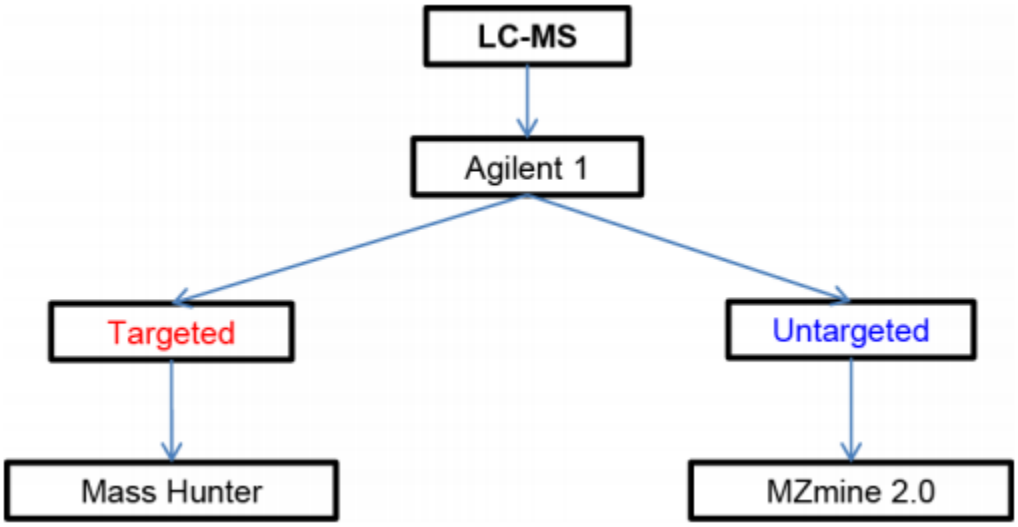

Supplemental Figure 10. Analysis workflow for quantifying metabolite intensities following LC-MS analysis.

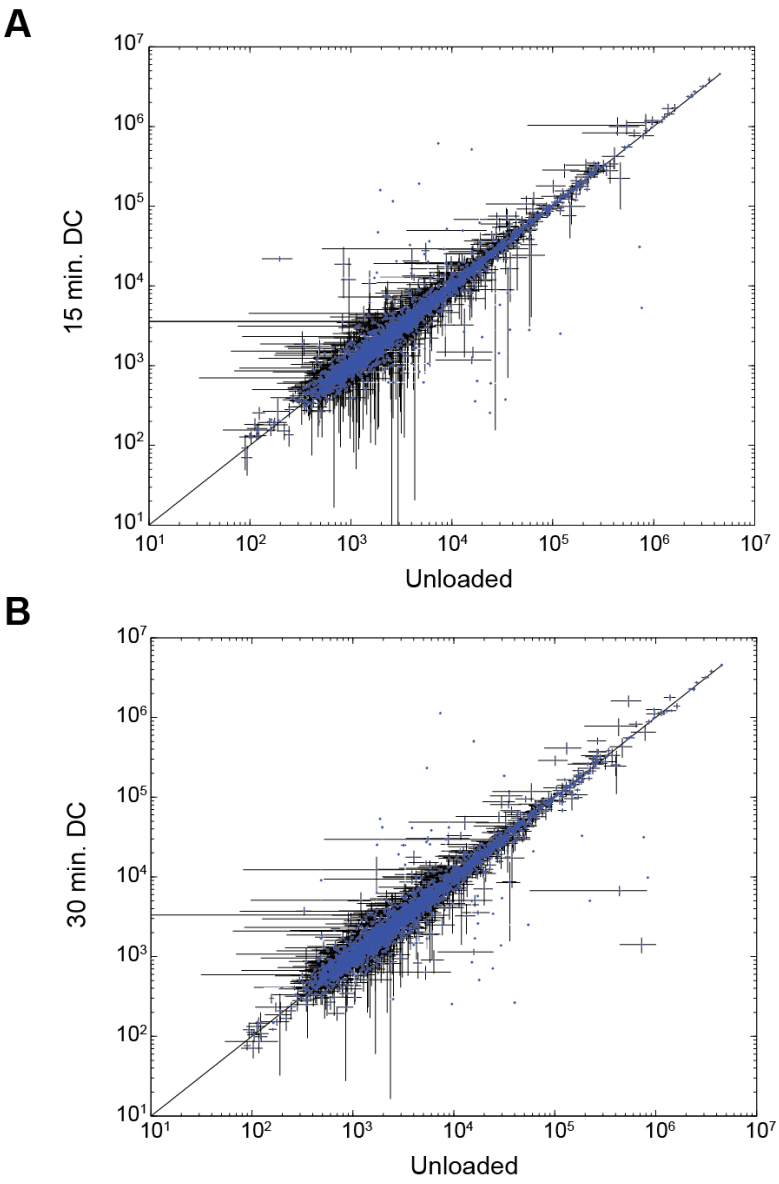

Supplemental Figure 11. Scatter plots of untargeted metabolites. Comparing unloaded controls to both 15 minutes of loading (A) and 30 minutes of loading (B), we observe clusters of metabolites that are either induced or suppressed by mechanical loading.

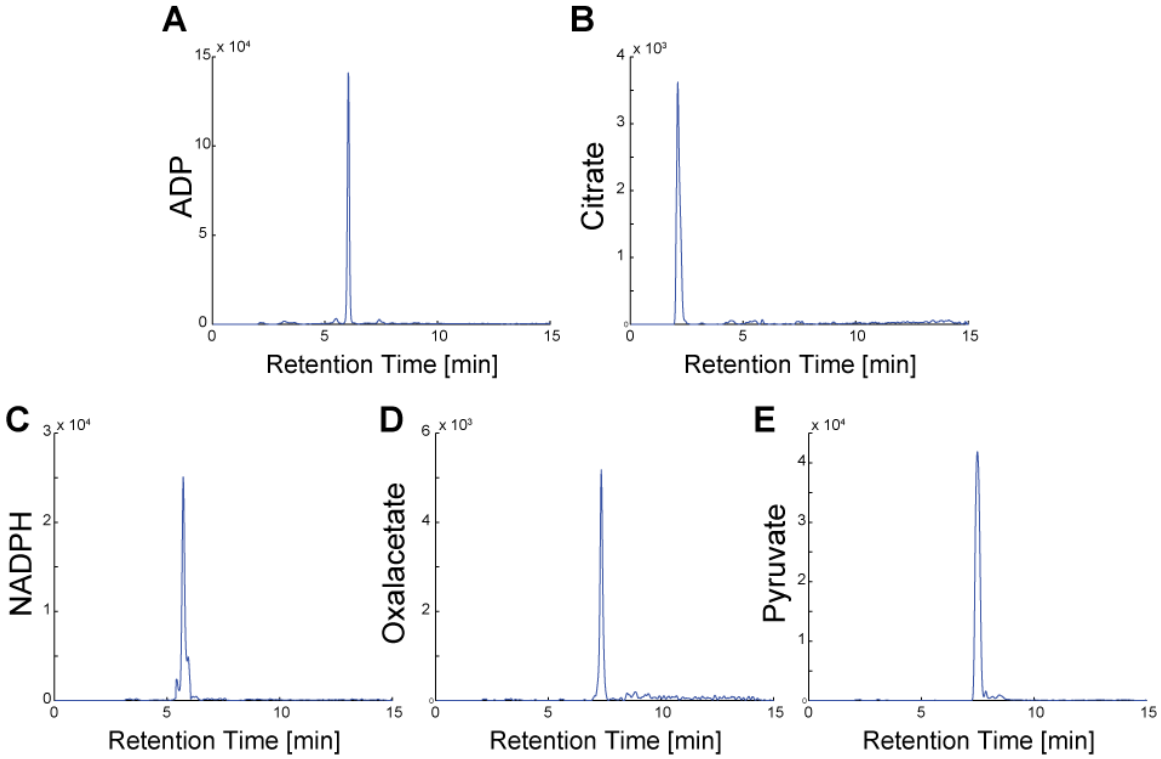

Supplemental Figure 12. Representative chromatograms of targeted metabolites. Representative chromatograms are shown for the extracted ion intensity of targeted metabolites of median intensity. Intensity is summed over all ions and adducts. (A) ADP (B) Citrate (C) NADPH (D) Oxaloacetate (E) Pyruvate.

APPENDIX C

SUPPLEMENTAL MATERIAL FOR CHAPTER 3
METABOLOMICS

Supplemental Materials and Methods

Untargeted and Targeted Metabolomic Profiling. Metabolomics is an experimental technique for characterizing large numbers of small molecules (<1000 Da) in biological samples [96]. Recent studies of joint tissues and fluids have used metabolomic analysis to examine OA phenotypes, identify candidate biomarkers, and explore the inflammatory responses [179-182]. Metabolite detection was performed in the Montana State University Mass Spectrometry Core Facility [155-157] via HPLC-MS. An aqueous normal-phase, hydrophilic interaction chromatography (ANP/HILIC) HPLC column was used (Cogent Diamond Hydride Type-C) with 4 μm particles, 150 mm length, and 2.1 mm diameter. The column was used with an Agilent 1290 HPLC system. Chromatography was performed using previously developed methods [116]. Buffer A consisted of H_2O with 0.1% (v/v) formic acid and buffer B consisted of acetonitrile with 0.1% formic acid. The sample was injected (4 μL per injection) via an autosampler following column equilibration at 95% B. The column as flushed for 2.0 min, and then from 2.0 min until the end of the run, the eluant was directed to the mass spectrometer (MS). For each run, the gradient was linearly ramped from 95% B at 2 minutes to 25% B at 12.5 minutes. . The column was then held isocratically at 25% B from 12.5 min to 13.5 min prior to re-equilibration at 95% B from 13.5 min to 15 min. Following each run, blank solvent samples were run to ensure complete washing of the column and fluidics. Metabolites were detected using an Agilent 6538 Q-TOF dual-ESI source mass spectrometer with a resolution of ~20,000 and accuracy of ~5 ppm. The spectra were collected in positive mode for a mass range of 50 m/z to 1000 m/z at a frequency of 1 Hz.

Data Processing. Data analysis involved both an untargeted and targeted approach (Supplemental Figure 13). For the untargeted approach, raw HPLC-MS data was converted into .mzXML files using MS Convert (ProteoWizard), and then processed using MZmine2.0 [158]. In MZmine2.0 the datasets were then filtered using established methods [116, 158] as follows: the chromatograms were generated using a minimum signal level of 1000 m/z with m/z tolerance of 15 ppm, and a minimum time span of 0.1 minutes. Chromatograms were then normalized using a retention time tolerance of 0.25 min and a minimum standard intensity of 1000 m /z, with a tolerance of 15 ppm. Following chromatogram normalization, chromatograms were then aligned using the retention time tolerance, and a mass tolerance of 15 ppm. The generated lists were then used for statistical analysis and metabolite identification.

For the targeted approach, ~50 metabolites known to be involved in central energy metabolism [102, 154] were analyzed. Using the Quantitative Analysis package within MassHunter Workstation B.04.00 (Agilent Technologies), a database of the calculated isotopic distributions (including H+ and Na+ adducts) of these targeted masses (Isotope Distribution Calculator, Agilent Technologies) was created. To identify these targeted metabolites, retention times were used with matched values to those from standard analytical samples determined and maintained by the MSU Mass Spectrometry Core. A 20 ppm window for each m/z value was used to evaluate each of the targeted metabolites.

Data Analysis and Candidate Selection. To assess the effects of physiological loading on chondrocyte biology, unloaded control samples were compared against

dynamically compressed samples. Three groups of cell-seeded agarose hydrogels were established for comparative purposes. Samples that did not undergo dynamic compression served as the unloaded control samples (UC), and then samples that received either 15 (DL15) or 30 (DL30) minutes of dynamic compression comprised the loaded samples. Statistical analysis was performed both on individual donors and pooling the data from all the donors together. We defined detected masses as those present in the majority of samples and replicates. To determine statistically significant differences between unloaded samples and loaded samples comparisons were made using t-tests [160] with p-value corrections using standard false discovery rate (FDR) calculations [259] to minimize false positives associated with multiple comparison testing. Three comparisons were made: (1) between individual donors and (2) between groups within the pooled data: UC vs. DL15, UC vs. DL30, and DL15 vs. DL30.

Principal components analysis (PCA) was utilized to assess metabolome-scale changes caused by mechanical loading. HPLC-MS data were normalized using both variance-stabilizing logarithmic transformation [293] and median fold change normalization [294, 295]. Median fold change normalization has been shown to be a robust method in normalizing HPLC-MS data with dilution and concentration-induced variations [295]. This technique normalizes each of the intensities by the median of the fold changes of peak intensities (Equation 1).

$$MFC_j = median(\frac{x_{ij}}{x_{rv}}) \quad (1)$$

where x_{ij} are the individual intensity values and x_{rv} is the reference variable for normalizing the intensity values. The choice of the reference variable (*i.e.* median) is not

critical for this normalization technique and is usually chosen to be the median profile value [295]. To account for heteroscedastic noise in the data, a logarithmic-based transformation was used to help stabilize the variance by transforming the peak intensity variance from a multiplicative error into an additive error.

Pearson's correlation coefficients were used to estimate the flux of metabolite intensities over the time course of loading. For the correlation analysis, the duration of dynamic loading (0, 15, or 30 minutes) was chosen as the independent variable and the dependent variable was chosen to be the intensity values for each detected metabolite. Metabolite accumulations with increased loading were identified by positive correlations values, and negative correlations were indicative of metabolite depletion. Candidate mediators were defined as the top 25 (*i.e.* accumulated) and bottom 25 (*i.e.* depleted) statistically significant correlations. Data are presented as mean +/- standard error of the mean.

To assess the differences in intensity distributions (m/z spectra plots for the various loading groups), two-sample Kolmogorov-Smirnov tests were implemented. Kolmogorov-Smirnov tests are a non-parametric test for the equality of distributions between two samples. Mass values were the independent variables and detected metabolite intensities were the dependent variables for distribution analysis. Three sample distribution comparisons were made: UC vs. DL15, UC vs. DL30, and DL15 vs. DL30.

Targeted metabolite profiles were analyzed by PCA, hierarchical agglomerative cluster analysis and correlation analyses. Additionally, the median ratios of NADP+:NADPH, NAD+:NADH, ATP:ADP, and GDP:GTP were calculated as a function of time to assess relative changes in energy metabolism.

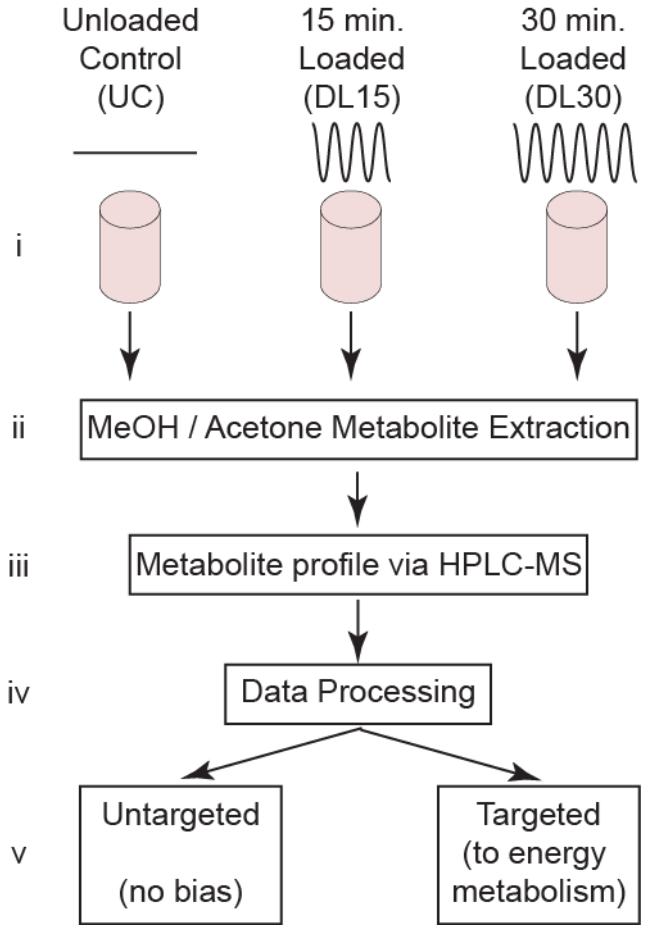

Supplemental Figure 13. Experimental design. (A) Schematic for both targeted and untargeted experimental methods. (i) Primary human OA chondrocytes are encapsulated in physiologically stiff agarose (4.5% agarose, stiffness ~35 kPa), cultured for 72 hours, and then compressed in tissue culture for 0, 15, or 30 minutes (Control, DL15, or DL30). (ii) Metabolites are extracted following freezing and pulverization. (iii) Metabolite profiles are identified using HPLC-MS, and (iv) the data is processed using Agilent software prior to (v) untargeted and targeted analyses.

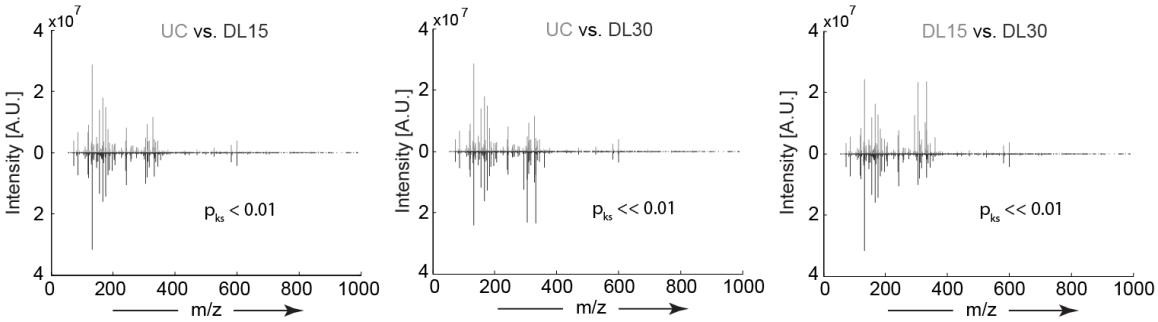

Supplemental Figure 14. Statistically significant differences (two-sample Kolmogorov-Smirnov tests) in m/z spectra distributions for UC vs. DL15 ($p_{ks} < 0.01$), UC vs. DL30 ($p_{ks} << 0.01$), and DL15 vs. DL30 ($p_{ks} << 0.01$), respectively.

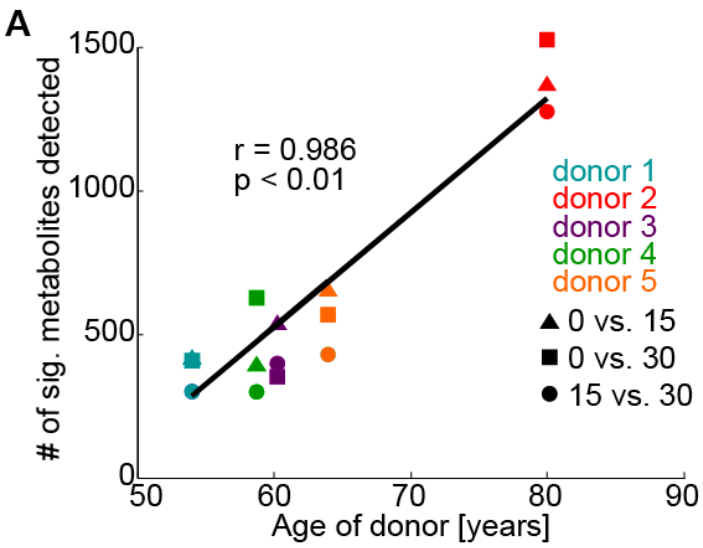

B

Donor	Sex	Age
1	M	54
2	F	80
3	F	60
4	F	59
5	F	64

Supplemental Figure 15. (A) Age-correlated increases in the number of significant metabolites for donors 1 - 5. (B) Characteristics of femoral head articular cartilage for all donors used in this study. All patients had Grade IV osteoarthritis at the time of joint replacement.

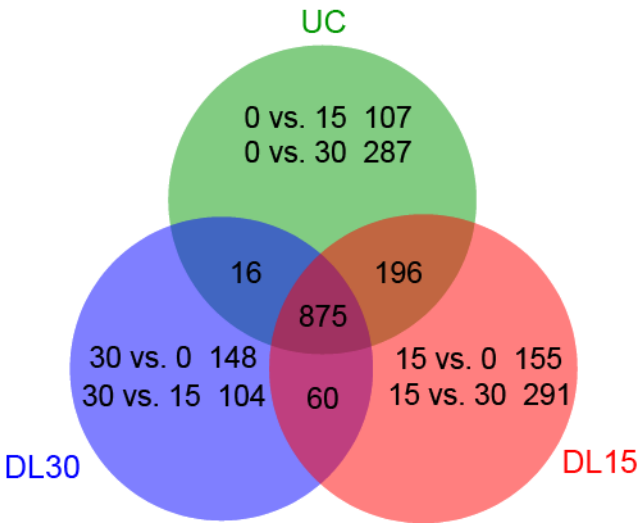

Supplemental Figure 16. To further explore the effects of dynamic compression on the chondrocyte metabolome, we determined the number of metabolites unique to each experimental group (UC, DL15, and DL30). 107 metabolites were detected in the unloaded control samples (UC) that were not detected in the samples subjected to 15 minutes of dynamic loading (DL15), and 155 metabolites were detected in DL15 that were not detected in UC. 287 metabolites were detected in UC that were not detected in samples subjected to 30 minutes of dynamic loading (DL30), whereas 148 metabolites were detected in DL30 that were not in UC. 291 metabolites were detected in DL15 that were not detected in DL30, whereas 104 metabolites were detected in DL30 that were not in DL15 samples.

Supplemental Table 7. Candidate mediators of chondrocyte mechanotransduction from the targeted metabolite analysis.

m/z	RT	Metabolite Name	Observation
664.1164	5.6318	NAD+	↑ w/ loading
147.0764	6.4786	Glutamine	↑ w/ loading
810.1620	5.5304	FADH2	↑ w/ loading
810.1330	5.5775	Acetyl CoA	↑ w/ loading
277.0319	6.0896	6-P-Gluconate	↑ w/ loading
119.0343	5.5587	Succinate	↑ w/ loading
291.0476	6.0405	Sedoheptulose-7-Phosophate	↑ w/ loading
170.0913	8.7273	Glutamate	↑ w/ loading
283.0189	5.4653	Hexose-P	↑ w/ loading
111.0053	8.9530	Pyruvate	↑ w/ loading
208.9821	7.3474	3-phosphoglycerate	↑ w/ loading
768.0803	5.5285	NADPH	↑ w/ loading
790.1044	5.6345	HS-CoA	↓ w/ loading
529.9850	5.9012	ATP	↓ w/ loading
259.0213	6.3640	p-glucanolactone	↓ w/ loading
203.0508	2.7622	Glucose	↓ w/ loading
444.0321	5.8544	GDP	↓ w/ loading
167.9818	6.0890	Phosphoenolpyruvate	↓ w/ loading
112.0369	8.4078	Alanine	↓ w/ loading
156.0751	8.1884	Aspartate	↓ w/ loading
215.0148	2.5620	Citrate	↓ w/ loading
116.0700	8.3419	Proline	↓ w/ loading

Supplemental Table 8. Up-regulated candidate mediators of chondrocyte mechanotransduction from the untargeted metabolite analysis.

m/z	RT	Condition	Compound
84.9592	**8.9222**	**↑ w/ loading**	**Unknown**
111.0433	3.0974	↑ w/ loading	3R-Hydroxybutan-2-one
120.0788	**5.5073**	**↑ w/ loading**	**Unknown**
129.0541	3.0800	↑ w/ loading	Ascorbic acid
138.0713	3.5688	↑ w/ loading	Unknown
143.0746	**3.3049**	**↑ w/ loading**	**Unknown**
147.1252	**6.4780**	**↑ w/ loading**	**Unknown**
156.1286	**8.0259**	**↑ w/ loading**	**Unknown**
163.0577	5.7755	↑ w/ loading	2-Dehydro-3-deoxy-L-rhamnonate
164.9203	**5.7195**	**↑ w/ loading**	**Unknown**
176.0903	10.3790	↑ w/ loading	N-Guanylhistamine
182.1348	**3.4106**	**↑ w/ loading**	**Unknown**
186.0340	6.4681	↑ w/ loading	Syringic acid
208.0134	5.6282	↑ w/ loading	Quinoclamin
218.1365	6.0933	↑ w/ loading	O-propanoyl-carnitine
257.1117	3.4792	↑ w/ loading	Dihydrothymine
328.1359	5.4860	↑ w/ loading	3-Methyladipic acid
350.0643	5.6207	↑ w/ loading	O-Desmethyloxotolrestat
382.0866	5.5249	↑ w/ loading	Mesosulfuran-Methyl
404.1211	7.9940	↑ w/ loading	Tryptamine
426.0650	**7.3623**	**↑ w/ loading**	**Unknown**
639.2869	8.4505	↑ w/ loading	1,1-Dimethoxyethane
650.0662	**5.9640**	**↑ w/ loading**	**Unknown**
911.1567	**6.4476**	**↑ w/ loading**	**Unknown**

Supplemental Table 9. Down-regulated candidate mediators of chondrocyte mechanotransduction from the untargeted metabolite analysis.

m/z	RT	Condition	Compound
113.0651	**8.2841**	**↓ w/ loading**	**Unknown**
122.0699	**9.3803**	**↓ w/ loading**	**Unknown**
125.9847	9.1663	↓ w/ loading	Taurine
133.0587	**9.3807**	**↓ w/ loading**	**Unknown**
141.9573	**3.1275**	**↓ w/ loading**	**Unknown**
143.0569	8.1949	↓ w/ loading	2-Methyl-5-vinylpyrazine
144.0463	9.3821	↓ w/ loading	2-Propionyl-2-thiazoline
162.0889	2.4060	↓ w/ loading	1-Indolizidinone
177.0410	2.8854	↓ w/ loading	5-Dehydro-4-deoxy-D-glucuronate
184.0590	2.7111	↓ w/ loading	5-Methoxy-3-hydroxyanthranilate
204.0545	**5.5727**	**↓ w/ loading**	**Unknown**
259.0252	6.3637	↓ w/ loading	2-Keto-3-deoxy-6-phosphogluconic acid
319.1379	8.1488	↓ w/ loading	12S-HHT
326.1550	8.2630	↓ w/ loading	alpha-Ethyl-alpha,beta-diphenyl-2-pyridineethanol
369.0816	2.7279	↓ w/ loading	Methyl 6-O-galloyl-beta-D-glucopyranoside
400.9953	**3.2679**	**↓ w/ loading**	**Unknown**
408.0922	3.4148	↓ w/ loading	Zeanoside C
438.1920	2.5692	↓ w/ loading	Fluphenazine
468.9914	3.0655	↓ w/ loading	Cromoglicic acid
505.9194	6.0645	↓ w/ loading	dCTP
535.1237	6.4521	↓ w/ loading	(R)-Isobyakangelicin 3'-glucoside
542.1715	**5.0268**	**↓ w/ loading**	**Unknown**
564.2168	**9.2873**	**↓ w/ loading**	**Unknown**
663.1087	6.3861	↓ w/ loading	Nelumboside

APPENDIX D

SUPPLEMENTAL MATERIAL FOR CHAPTER 5
IN VIVO MODEL

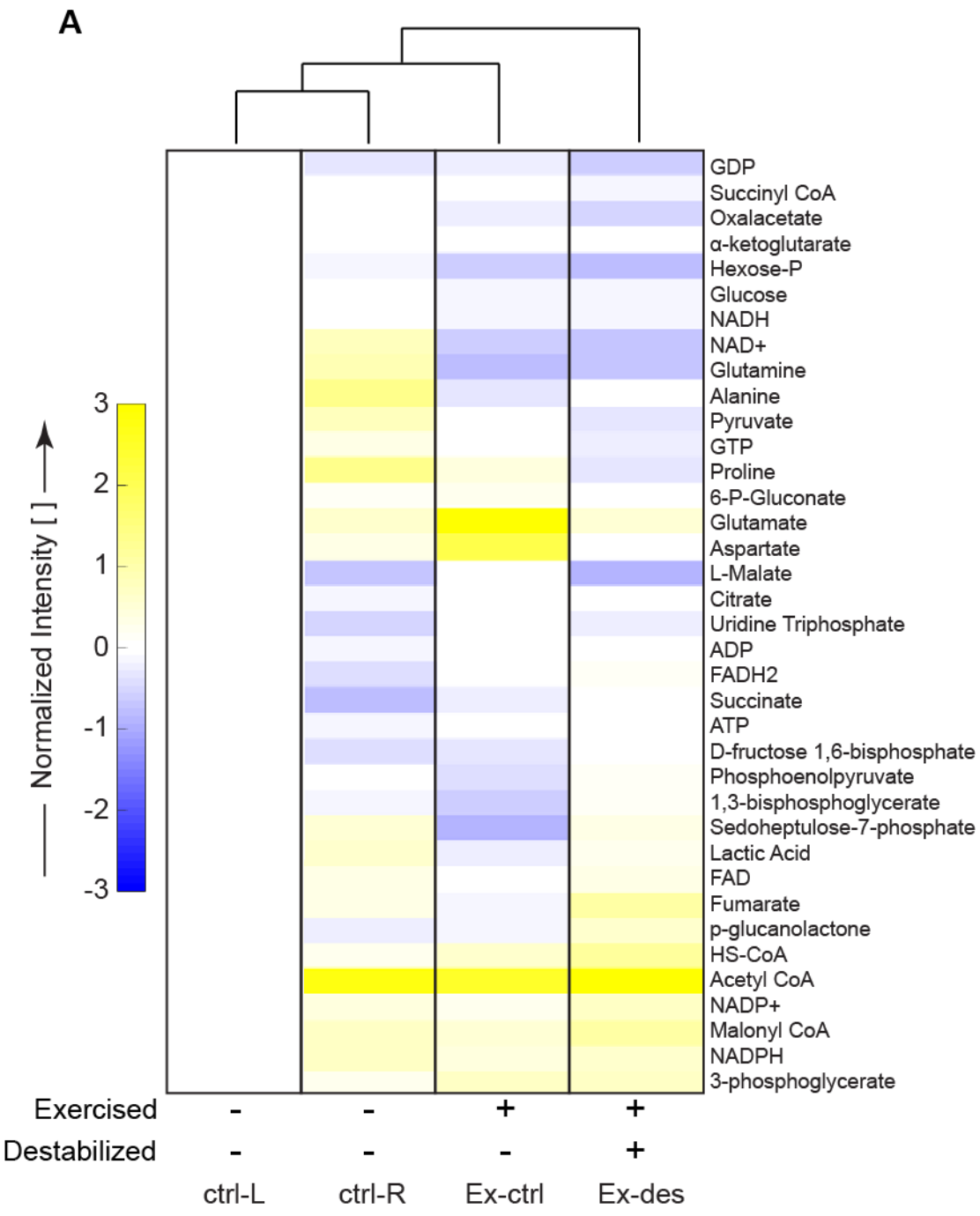

Supplemental Figure 17. Patterns of distinct metabolite distribution for 37 targeted metabolites common to central energy metabolism. Unsupervised agglomerative clustering reveals changes in metabolite intensities for each of the sample groups (ctrl-L, ctrl-R, Ex-des, and Ex-ctrl).

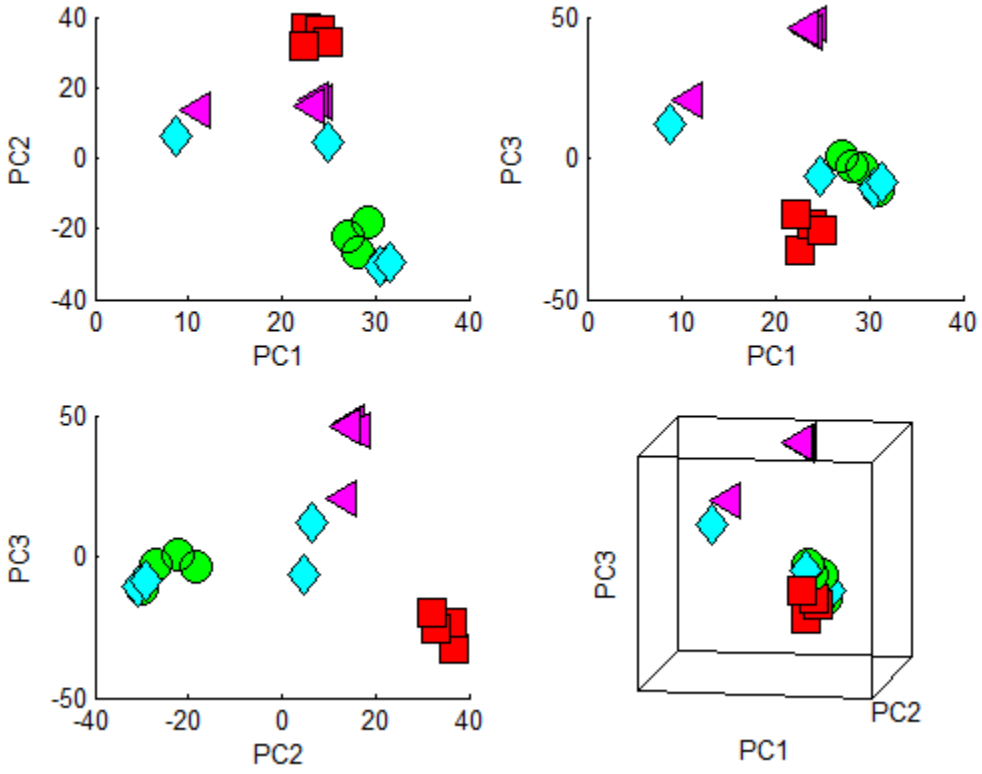

Supplemental Figure 18. Untargeted Principal Components Analysis. The first three principal components contained 87% of the overall variance. For each of the sample groups ctrl-L (●), ctrl-R (♦), Ex-des (■), and Ex-ctrl (◀), there are n=4 replicates.